Analysis of Dynamic Characteristics and their Sensitivities for Anisotropy Mistuned Bladed Disks with Friction Contact Interfaces

Adam Koscso

Submitted for the degree of Doctor of Philosophy

University of Sussex

April 2022

Declaration

I hereby declare that this thesis has not been and will not be submitted in whole or in part to another University for the award of any other degree.

Signature:

Adam Koscso

UNIVERSITY OF SUSSEX

Adam Koscso

Analysis of Dynamic Characteristics and Their Sensitivities for Anisotropy Mistuned Bladed Disks with Contact Interfaces

Acknowledgements

First and foremost, I would like to express my greatest gratitude to my supervisor Dr. Evgeny Petrov. His expertise, dedication and endless guidance helped to this thesis to materialize.

I am thankful for MTU Aero Engines AG, for the financial support. The MTU scholarship allowed me to invest all my efforts into the PhD studies.

I am honored to be able to be involved in the very supporting research environment of the University of Sussex. The valuable recommendations during the reviews from Prof. Julian Dunne and from Prof. Martin Rose helped me guiding during the research process.

Thank you for my post-graduate research colleagues, Dr. Rahul Rajasekharan Nair, Thomas Irps, Daniel Payne, Yeru Shang and Harri Koivisto for guiding me with valuable tips, thank you for the fascinating technical discussions. The atmosphere of the Thermo-fluid Mechanics Research Centre would not have been the same without you.

The project behind the PhD thesis was supported by many brilliant colleagues of MTU Aero Engines. Thank you for Dr. Andreas Hartung for leading the project and for the frequent and valuable feedback on the progress. During the years of project duration the colleagues Dr. Guido Dhondt, Dr. Hans-Peter Hackenberg, Dr. Alexander Buck and Jorge Orlando Rivera Roldan had valuable inputs, which all elevated the quality of the PhD work.

My eternal gratitude goes to my loving and always fully supporting parents. Thank you for showing me the value in hard work, the importance in setting goals and the joy in following my curiosity. I consider myself lucky that from my sister I could learn a lot a about life, probably a lot more than what she thinks she thought me.

I am forever thankful for the trust, love and support of my wife, Gretel Huerta de los Santos. Your patience is one of the key ingredients of this PhD thesis.

Abstract

In the modern jet engines single-crystal materials are used for turbine stages to withstand the high pressures, temperatures and to have sufficient creep resistance. Single crystal materials are inherently anisotropic, and their properties are dependent on the crystal orientation. The current technology of blade manufacturing by controlled solidification of the blades produces significant scatter in the crystal orientation. The mistuning introduced in bladed disks by blade material orientation scatter and by inevitable differences between blade-disk, shroud and dampers' contact interfaces, can lead to the increase of vibratory amplitudes and stress localization. This work aims to quantify the effect blade-to-blade anisotropy orientation on the vibratory characteristics of bladed disks.

In the thesis the effects of the anisotropy mistuning on the modal properties and forced response have been studied using high-fidelity FE models together with detailed modelling of nonlinear interaction at friction contact interfaces at blade-disk root joints, blade-shroud and under-platform damper contacts.

For the analysis of the sensitivity of natural frequencies and mode shapes with respect to the material anisotropy orientation in blades, efficient methods have been developed and implemented.

An efficient framework for the calculation of the linear and nonlinear forced response and their sensitivities for anisotropy mistuned bladed disks with friction joints has been developed and implemented.

The sensitivity calculations for the modal properties, linear and nonlinear forced response have been validated by finite difference method. The calculated nonlinear forced response functions have been validated against measurement data from rotating test rigs. The efficient modeling strategies were explored and studied to address the common issues that occur during the nonlinear forced response analysis of large mistuned bladed disk models.

The effects of the material anisotropy mistuning in bladed disks on natural frequencies, mode shapes and on linear and nonlinear forced response amplitudes for several modes have been studied. For the nonlinear forced response, the effect of anisotropy mistuning has been studied for varying excitation levels and damping levels. The characteristics of the sensitivities of modal properties and nonlinear forced response amplitudes to the anisotropy angles have been studied for several industrial mistuned bladed disks.

Preface

The work from this thesis has been published or is accepted for publication in the following papers:

- Koscso, A., Dhondt, G. and Petrov, E.P., 2018, *"High-fidelity sensitivity analysis of modal properties of mistuned bladed disks regarding material anisotropy."* Journal of Engineering for Gas Turbines And Power, 141 (2). 021036 1-11. ISSN 0742-4795

- Koscso, A., Rajasekharan, R., and Petrov, E. P., 2018. *"Sensitivity and uncertainity of modal characteristics and forced response of bladed disks mistuned by material anisotropy"*. In Proceedings of the 15th ISUAAAT, Oxford, UK. Paper No. ISUAAAT15-092.

- Koscso, A. and Petrov, E. P. (2019), *"Sensitivity and forced response analysis of anisotropy-mistuned bladed disks with nonlinear contact interfaces"*. Journal of Engineering for Gas Turbines and Power, 141 (10). a101025. ISSN 0742-4795

- Koscso, A, Petrov, EP. *"Blade Root Joint Modelling and Analysis of Effects of Their Geometry Variability on the Nonlinear Forced Response of Tuned and Mistuned Bladed Disks."* Proceedings of the ASME Turbo Expo 2020: Turbomachinery Technical Conference and Exposition. Volume 11: Structures and Dynamics: Structural Mechanics, Vibration, and Damping; Supercritical CO2. Virtual, Online. September 21–25, 2020. V011T30A024. ASME

Contents

List of Tables

List of Figures

Nomenclature

Abbreviations

AM Algebraic method

CS Coordinate system

DOF Degree-of-freedom

EO Engine order

FE Finite element

MDOF Multi-degree-of-freedom

FRF Forced response function

MAC Modal assurance criterion

MM Modal method

ND Nodal diameter

MPC Multi-point constraint

ROM Reduced order model

SPC Single-point constraint

SNM Subset of nominal modes

UPD Under-platform damper

Symbols

α Primary anisotropy angle for single crystals

β Secondary anisotropy angle for single crystals

$\boldsymbol{B}$ Strain-displacement matrix

$\boldsymbol{C}$ Damping matrix

$\boldsymbol{C}$ Material elasticity matrix

c_{jk} Coefficient of series expansion for modal method of mode shape calculation

Δ Finite difference step

$\boldsymbol{\epsilon}$ Strain tensor

$\boldsymbol{k}^e$ Finite element stiffness matrix

E Young's modulus

$\boldsymbol{F}(\boldsymbol{X})$ Vector of multiharmonics nonlinear contact forces in frequency domain

$\boldsymbol{A}_0$ Flexibility matrix

$\widetilde{\boldsymbol{A}}(\omega)$ Forced response function matrix

γ General parameter describing crystal orientation

G Shear modulus

$\delta\boldsymbol{\omega}$ Infinitesimal rotation

$\boldsymbol{J}$ Jacobian matrix

$\boldsymbol{K}$ Global stiffness matrix

λ_j Eigenvalue of j-th mode

ν Poisson's ratio

ν_j Modal damping of j-th mode

ω Excitation frequency

ω_0 Reference frequency

$\widetilde{\omega}_v$ Skew-symmetric matrix of the rotation vector components

$\boldsymbol{P}$ Vector of harmonic excitation in frequency domain

Φ All calculated mode shapes

ϕ_j Mode shape of j-th mode

$\boldsymbol{p}(t)$ Vector of harmonic excitation

$\boldsymbol{R}$ Rotation matrix

r_j Residual vector for j-th mode for modal method of mode shape calculation

$\boldsymbol{\sigma}$ Cauchy stress tensor

$\boldsymbol{S}$ Material compliance matrix

s Regularization coefficient for algebraic method of mode shape calculation

$\boldsymbol{T}$ Stress transformation matrix

$\boldsymbol{v}$ Rotation vector

V^e Finite element volume

$\boldsymbol{X}$ Vector of harmonic forced response in frequency domain

$\boldsymbol{f}(\boldsymbol{x}(t))$ Vector of nonlinear friction forces

$\boldsymbol{x}(t)$ Vector of harmonic forced response

ζ Circular anisotropy angle for single crystals

Chapter 1

Introduction

The modern jet engines both in the aerospace and energy sector face high safety, environmental and economical challenges. In order to meet the requirements of the most up-to-date standards, engineers and manufacturers are constantly searching for solutions to increase efficiency, reduce weight, manufacturing and maintenance costs. Nevertheless, the highest priority for any engine development program is to meet the high regulatory safety requirements. Therefore, the structural integrity will always be the most important design requirement of any gas turbine.

The high cycle fatigue resistance of the blades is dependent on the static and dynamic stresses. In general, the static stresses of the bladed disks can easily be evaluated. For linear and linearized bladed disks, the evaluation of the dynamic stresses is also done through commonly known approaches. On the other hand, the calculation of the vibration amplitudes and stresses for bladed disks with friction contact interfaces, is a complex task.

The bladed disks, such as the fan, compressor and turbine stages, experience periodic excitation during the operation of the jet engine. Generally, the airfoils in the flow path are the most affected by vibrations. Therefore, the dynamic assessment of the bladed disks is essential for the safe operation of the engine on the whole operation range.

For the accurate calculation of the forced response amplitudes of the turbine bladed disks, the damping of the dynamic system needs to be assessed. The materials used in blades and disks of the turbine stages have low material damping. Apart from aero-damping, the major source of the energy dissipated is the frictional forces appearing on the dry friction contact interfaces. For modern turbine bladed disks, the contact interfaces are located on the blade roots, on under-platform dampers (UPD) and between the outer shrouds of the blades. Under centrifugal forces the contact interfaces are pressed against each other. As vibration amplitudes of the blades around resonances increase, the friction joints may start to slip and under certain conditions they can partially or fully separate. The increased energy dissipation through the friction forces and the change of dynamic stiffness due to the change in the contact status needs to be considered for the forced response calculation.

For the study of the dynamic characteristics, including natural frequencies, mode shapes and forced response, the effect of several design parameters needs to be assessed. The dynamic properties of bladed disks depend on design variables such as material properties, airfoil geometry and properties of contact interfaces. Generally, the computational assessment of the dynamic behavior is done by modeling only a sector of the bladed disk and applying cyclic symmetric condition on its boundaries. Analyses with cyclic symmetric conditions allow for a high discretization and the computational effort is significantly reduced compared to the calculations for 360° model of bladed disk. On the other hand, for the cyclic symmetric bladed disk model, all sectors in the bladed disk assembly are considered to be identical. This means that the design parameters for every blade are modeled to be identical.

In reality, despite the high manufacturing standards of the aviation industry, the blade sectors are not identical. No manufacturing process is perfect, therefore there will always be some variation in geometry and material. The blade-to-blade differences during engine operation can increase mainly through wear of the contact interfaces, resulting in varying contact conditions.

The small differences from one blade to another, called mistuning or detuning, has been shown to lead to significant increase of maximum vibratory amplitudes compared to amplitudes of the bladed disk with identical blades. According to Whitehead's [99], the maximum amplification can be analytically derived, and it is proportional to the number of blades in the bladed disk. The distribution of the maximum forced response amplitudes and the dynamic stresses along the circumference of the bladed disk is significantly influenced by mistuning. Experimental results have shown, the distribution of the forced response magnitudes can not only change from one bladed disk assembly to another, but also from run to run [33]. This is considered to be caused by the change in the contact conditions from one run to another as the bladed disk stage is loaded and unloaded. Mistuning may cause the concentration of energy for only a few blades resulting in high vibratory stresses that lead to reduced fatigue life of the bladed disk. The research in the field of the dynamic behavior of the mistuned bladed disks have been in a focus point since the 1960s and thus resulted in hundreds of scientific publications.

One of the sources of mistuning appeared in the field of turbomachinery as more advanced materials have been applied for the turbine stages of the jet engine. Such materials are nickel base superalloys: directionally solidified and single crystal materials. The turbine stages downstream of the combustion chamber need to be able to withstand very high temperatures and pressures. The single crystal materials that are formed of only one type of columnar grain can eliminate the grain boundaries and therefore reduce the risk of the crack initiation and propagation. Moreover, using single crystal materials increase the creep resistance of the material, which is essential for turbine stages operating in high temperature conditions.

The nickel-based superalloys that single crystal blades are generally made of are orthotropic materials. The principal directions of the anisotropy depend on the orientation of the single crystals. During blade casting the crystal orientation is carefully controlled, making sure that one of the principal material direction does not significantly deviate from stacking axis. The orientation of the other principal material directions are generally not controlled. This can result in significant variation in crystal orientation from one blade to another, resulting in anisotropy mistuned bladed disks.

This research is looking for the answers of one paramount question: how does the blade-to-blade anisotropy orientation variation affect the dynamic characteristics of bladed disks?

This research question can be divided into subquestions along the dynamic parameters under investigation, the methods used to investigate them and with additional complexities:

- Dynamic characteristics of linear structures are described in the form of the modal properties. In this work it is studied, how the anisotropy mistuning influences the natural frequencies and mode shapes. How do the natural frequencies for mistuned bladed disks change when compared to the nominal (e.g. tuned) bladed disk? What kind of changes are expected in the blade mode shapes for anisotropy mistuned bladed disks.

- By solving the equation of motion, the forced response of the mistuned bladed disk is calculated. The linear forced response can be calculated by the modal superposition method when an equivalent overall modal damping is approximated. Considering the forced response of mistuned bladed disks, the quantification of the scatter in the individual blade resonance frequencies and maximum forced response amplitudes is of interest. The ratio between the maximum forced response amplitude around the resonance over all blades and mean maximum or tuned forced response amplitudes give the value of amplification factor. Additionally, the mistuning can also result in alteration in the operational deflection shape, which in turn may result in changes in limiting location for vibratory stresses.

- The turbine bladed disks are inherently nonlinear structures and on the dry friction contact interfaces nonlinear damping forces appear. In order to assess the forced response amplitudes, the friction forces on the contact joints need to be resolved. For such nonlinear forced response analyses work witch significantly more physical and numerical parameters, e.g. number of mode shapes, number of harmonics, number of contact elements used in the analysis or the values for friction coefficient and contact stiffness. This work is looking for the effect of such parameters and assesses when converged solutions are obtained. Moreover, the effect of anisotropy mistuning on the nonlinear forced response is investigated. Similarly to the analyses for the linear forced response, the major interest lies in the value of amplification factors, change and scatter of resonance frequencies.

- For the previously mentioned dynamic characteristics there can be several ways to quantify the effect of the blade-to-blade anisotropy orientation variation. This piece of research work is aiming to show several possibilities (e.g. Monte Carlo simulation, use of sensitivities) for studying the influence of the anisotropy mistuning on the modal and dynamic properties.

- When the research question was posed, the use of sensitivities was formulated as an efficient way of quantifying the influence of the input parameters on the output parameters of interest. In case of the anisotropy mistuned bladed disks, the crystal orientation of the blades can be described with the anisotropy angles, and they are the stochastic input parameters for the study. The output parameters can be the modal properties and the linear and nonlinear forced response. The sensitivities with respect to the design variables can provide important information about the solution for the parameters of interest for the mistuned the bladed disks. The local sensitivities show which parameters are influencing the solution more and how robust the obtained solution is. Sensitivities are also used for optimization methods, as they provide additional information about the gradient of the solution. Other major application field of the sensitivities is the response surface type methods that can substitute the dynamic system with a mathematical description. The response surface models, such as the gradient based polynomial chaos, can be used to obtain statistical properties and global sensitivities of the anisotropy mistuned bladed disk [63].

Chapter 2

Literature review

The following literature review is written considering the posed research question. This chapter gives an overview of previous works that are related to the current field of study. As this work fits into a long historic research effort, the covered topics needs to include the vibratory characteristics of mistuned bladed disks, works on dynamic characteristics for single crystal bladed disks, methods for model reduction and nonlinear forced response analysis, methods for calculations for eigenvector sensitivities and practical applications for the nonlinear forced response methods for bladed disks with friction joints and for their sensitivity analyses.

The effects of mistuning on the dynamic behavior of the bladed disks have been studied since the 1960s. The significant research interest resulted in hundreds of scientific publications. In the early days research was done with simple single degree-of-freedom systems. As computational capabilities started to increase, more detailed models were used to analyze the effect of mistuning on forced response amplitudes. The most recent computer codes allow for the calculation of nonlinear forced response and its sensitivities for high-fidelity mistuned bladed disks. This tremendous advancement has been achieved thanks to the hard work of a large scientific community. Mentioning every publication is a challenge on its own, here the most relevant and most important studies are reviewed.

2.1 Fundamentals of the dynamic behavior of tuned and mistuned bladed disks

During the early research on the bladed disk assemblies in the 1960s and 1970s the fundamentals of the dynamic behavior have been described. At that point the applied mechanics knowledge had a very good understanding of the vibration characteristics of the blades and the blades could also be analyzed by analytical and experimental means. One of the most important work from this time originates from Ewins 1973 [20]. In this research paper it has been found that it is not sufficient to analyze the blades alone as cantilever beams, but the whole bladed disk assembly has to be analyzed. The vibration characteristics of bladed disks result from the interaction of the disk and the individual blades, which results in more complex system than the individual blades. This means that bladed disks have many more natural frequencies than the individual blades. Through the interaction of the blade and disk modes and mode families are identified [21] , where for each blade mode several disk modes with different nodal diameter pattern appear. The number of maximum nodal diameter modes is dependent on the number of blades in the bladed disk. In case of the tuned dynamic systems for each mode only one nodal diameter component exists, and the highest possible number of nodal diameters equal to $N/2$ or $(N-1)/2$ if N the number of blades in a bladed disk is even or odd respectively.

The main interest of the structural engineers lies in identifying critical resonances. In order to find the rotation speed of the resonances, the source of excitation is identified. Due to the obstructions in the flow field the force varies with the angular position, therefore the blades experience a fluctuating load proportional to $\cos(i\Omega t)$, where i is the engine order and Ω is the rotational speed. For jet engines, the major source of excitations are with the engine order of the number of blades and their higher harmonics of the stators upstream and downstream. The critical rotor speeds, at which resonances occur, can be identified where the radial lines of the engine order excitation cross the nodal diameter lines of each mode, see Fig. 2.1. The bladed disks rotate during the gas turbine engine operation and the rotation speed affects the natural frequencies. In order to analyze the effects of rotation speed and determine the rotation speeds at which the resonance vibrations excited by different engine orders of the aerodynamic forces occur, the Campbell diagram is used, see 2.1.

The Fig. 2.2 shows an example for the natural frequency-nodal diameter plot for a tuned, with the exploitation of the cyclic symmetric conditions. One can see, that with more and more nodal diameters in the mode shapes, the natural frequency is increasing and asymptotically approaching the natural frequency of the cantilever blade. In [21] this is accounted to be due to the fact that with an increasing number of nodal diameter the disk is getting stiffer at the roots of the blades.

When in the bladed disk model also mistuning or detuning is included, then in the modal analysis the segments cannot be considered identical. The variation from blade to

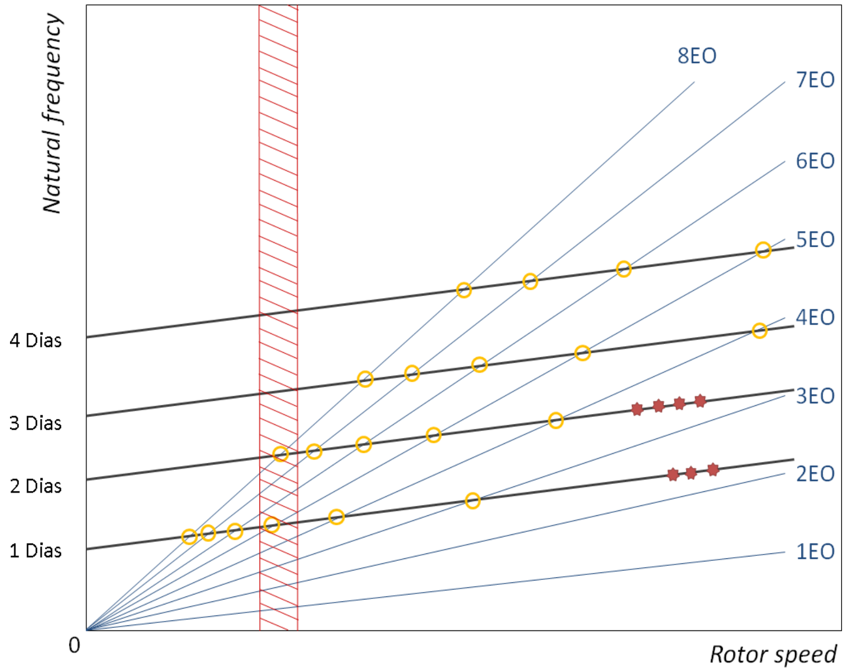

Figure 2.1: A Campbell diagram showing resonance conditions for a mistuned bladed disk [46]

blade makes the double natural frequencies at a certain nodal diameter for a given mode shape family split, except for the 0 nodal diameter and $N/2$ in case the number of blades is even.

One another important conclusion have been drawn in the paper [21], namely that due to the mistuning in the bladed disk assembly, the mode shapes are not perfect nodal diameters anymore and every mode shape consists of several more nodal diameters as well. This results in the fact, that a mode shape with the i^{th} nodal diameter can also be excited with other engine order excitations, not only with the i^{th} engine order. Therefore, on Campbell diagram, Fig. 2.1, every engine order crossing with the nodal diameter lines is subjected to resonance condition, which are denoted with yellow circles. On this diagram a selected rotor speed region is selected that is mostly of interest of the structural engineers, as in that given range two natural frequencies are located relative near to each other. The red dots at the higher rotor speed range represent possible flutter conditions [95], which is an unstable, self-excited vibration of the blades that can lead to severe damage in case of fans [58].

The effect of mistuning on the vibration characteristics have been investigated since the 1960s at a great extent. The variation of the structural properties from one blade to another has been in the focus of the dynamic research of the turbomachines.

In order to simulate the forced response of the mistuned bladed disks, with direct

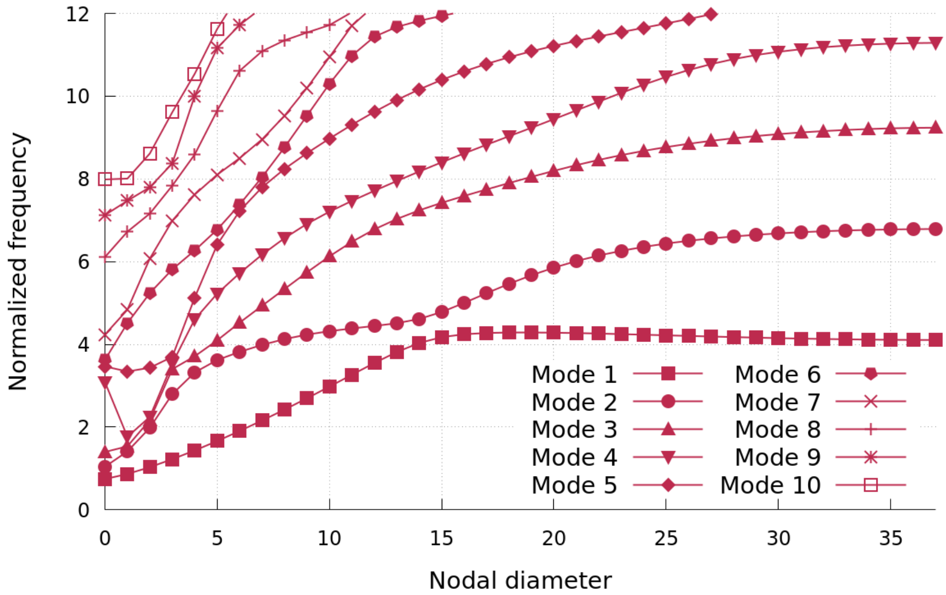

Figure 2.2: Natural frequencies collected into families plotted against the number of nodal diameters

blade-to-blade variations takes enormous computational effort. In order to come around this obstacle several different methods were developed in the past. Historically it has started off with the simplest dynamic models that consisted of a very limited degrees of freedom lumped parameter mass-spring models (LPM). The foundation of the physics of the mistuned bladed disks have been laid down in the years before 1990 with such significant papers as [22],[21] and [97]. The developments until this date have been concluded in the survey of D. J. Ewins [1]. The publication states the main questions that have been thoroughly investigated and some are still under investigation, while other questions have been somewhat reformulated throughout the years.

- How the mistuning will influence the vibration characteristics of the bladed disk assembly?
- "What will be the variation in blade vibration levels if their individual properties vary by x%?"
- If there is blade to blade variation introduced, how much worse the vibration will be in comparison with the tuned case?
- If the vibration is localized, which blade will have the largest amplitude?
- Is there an optimal pattern of the mistuning that can reduce vibration the most and offer a robust solution?

- What are the extremes of the effect of mistuning?
- What are the methods that allow fast computation for a given mistuning pattern and the methods for discovering wide range of mistuning patterns?

Most of the questions appeared as direct or indirect questions in [1], however some of them have been formulated later in accordance with development of the research in the field.

A more recent survey has also been published in 2006 by Castanier and Pierre [15]. The publication sums up the fundamental background of the dynamic behavior. It recaps the most important developments, such as reduced order models, the analysis with respect to mistuning sensitivity and the research related to uncertainty and reliability assessment.

2.2 Methods for the calculation of nonlinear forced response

The turbine bladed disk assemblies consists of several parts: blades, disk, retainer and under-platform dampers. In service, nonlinear forces occur on the friction contact interfaces, at blade root, shroud, under-platform dampers, etc., that make the forced response strongly nonlinear. Therefore, linear models are insufficient to calculate accurate forced response amplitudes for bladed disks with friction contact interfaces. Apart from the aerodynamic damping, the friction forces that appear on the contact surfaces are the main source of damping. Therefore, it is necessary to assess the energy dissipation through the nonlinear friction forces to obtain correct forced response amplitudes.

Efficient calculation of the nonlinear forced response is carried out in frequency domain using the multiharmonic balance method [76, 51, 26]. The principal assumption of the multiharmonic balance method is that multi-degree-of-freedom system is excited by a harmonic forcing and therefore the steady state solution is searched for a harmonic form. A comprehensive review on the calculation of the nonlinear forced response with friction contact interfaces using the multiharmonic balance method can be found in [49].

The simulations for the investigation of the dynamic properties are conventionally carried out with the use of finite element models. The calculations for modal properties and forced response are very efficient with cyclic symmetric models even when very fine meshes are applied. the modeling of mistuning is not possible with simple cyclic symmetric conditions. The computation efforts significantly increase when the full mistuned bladed disk is modeled. Such 360° models can be used for linear static and modal analysis, however a nonlinear static or nonlinear forced response analysis would result in significantly higher computational efforts. As a remedy in the early 2000s a variety of reduced order methods appear. These methods work with real size finite element models, however still capable of reducing the size of the system of linear equations without losing precision in the results.

One of the first publications on reduced order method, namely the component mode synthesis was written by Irretier [39]. The method later used in several works including for example [14],where it has been proven that the method can capture the forced response with some reasonable decrease in accuracy.

The other classical recipe for using reduction in the finite element models is called subset of nominal modes (SNM), developed by Yang and Griffin [102]. Running simulations with SNM requires significant amount of input data, therefore it is difficult to use.

Further development of SNM has been presented in the later years from the same group at the Carnegie Mellon University by Feiner et. al. [24]. They have presented the Fundamental Mistuning Model (FMM), which is based on the tuned natural frequencies and the blade-alone frequency deviations, given that an isolated family of modes is under investigation. It has been worked out to be a method that is easier to use, therefore more user-friendly.

In 2002 Petrov et. al. presented [80], where a model reduction is based on the sector model and the modification introduced in the frequency response function (FRF). The method provides an efficient and accurate forced response calculation.

In the publication of [78], a technique has been presented for multiharmonic vibration analysis of mistuned bladed disks. The analysis is based on a former method with nonlinear contact calculations, and the mistuning is modeled with the random scatter of underplatform damper parameters, shroud gap and blade frequency.

The publication of Bhartiya et. al. in 2011 [10] discussed the comparison of the Modified Modal Domain Analysis (MMDA) and the Subset of Nominal Modes (SNM) method, which is a method based on Frequency Mistuning. It has been concluded that MMDA delivers better results for region of isolated modes and overlapping modes, in cases of mistuning caused by blade-to-blade geometry differences.

The component mode mistuning (CMM) was developed for running reduced order model calculations with damping mistuning in [41] by Joshi and Epureanu. Statistical methods were used in order to find correlation between the damping variation and amplification factor distribution.

In the work of Hohl et. al. [36] the Component Mode Synthesis (CMS) and the Wave Based Substructuring (WBS) has been utilized to achieve a reduced order method. Their method could be applied with the help of Monte Carlo simulation for finding the best and worst patterns of a bladed disks with respect to forced response. This paper is one of the examples of a more overall publication taking from the developments of chapters regarding statistical methods in Section 2.4.2 method and optimization in Section 2.4.3.

Turbine blades are designed with high-cycle fatigue in consideration, because of which, accurate calculation of vibration amplitudes is necessary. The accuracy of the calculation can be influenced by the computational parameters and by the mechanical parameters of the contact interfaces.

Regarding the contact surface modeling parameters of tuned bladed disks with friction joints at the blade-disk root significant studies have been done, e.g. [77, 94, 37, 7, 67]. These studies cover many different kinds of parameters, such as number of modes, number of nodes, time harmonics included.

Moreover, significant studies have been done on the physical parameters for the modeling of the friction contact interactions, such as number of contact elements, static pre-load and contact stiffness coefficient.

Such parametric studies can be done very efficiently and fast for tuned bladed disks by considering cyclic symmetric conditions and modeling the bladed disk with only one sector. With the current computational capabilities, the analysis of such systems can be carried out for models with very high fidelity.

For realistic mistuned bladed disks with millions of degrees of freedom considered as a full model, such as anisotropy-mistuned bladed disks [47], a very good understanding of how the modeling of the contact interfaces influence the nonlinear forced response. Due to the increased computational effort, only as many nonlinear contact elements, harmonics and mode shapes are advised to be used as necessary.

According to the previous studies, static pre-load can have significant effect on the nonlinear forced response. Generally, a preliminary static calculation is carried out in order to obtain pressure values that are applied to the contact elements. The work from Zucca et al. [104] investigated the coupling the static equation with the dynamic equation that allows for the changes in the static pressures due to the changes in contact conditions as vibration amplitudes change. In [101], it has been shown that considering non-uniformity on the contact interfaces leads to changes in the forced response.

Some of the sources of the change in the contact conditions and the in pre-load are level of static loading, the geometry uncertainty on the macro-scale, variation in assembly procedures. One non-rotating application, the flange joints on the outside of jet engines, when contact stresses have a high influence on the forced response was studied in [93]. A contact model has been developed in [4] for different contact geometries using non-spherical contact surfaces. The analysis of the static displacements for bladed disks with small root geometry variations has been analyzed in [87].

Given that the applied modeling strategies can influence the forced response amplitudes, it is essential to have them validated. For the validation of the nonlinear forced response against experimental data, only a handful of publications can be found. The experimental evaluation of the forced response levels for blade-root geometry has been presented in [17, 25]. The calculation of the nonlinear forced response for bladed disks with friction dampers and with blade-disk interface has been validated experimentally in [40]. A comprehensive validation campaign was carried out by Hartung et. al. in [32]. The comparison of the numerically and experimentally obtained forced response frequencies and levels was done for bladed disks with root and shroud damping and with additional underplatform dampers.

2.3 Influence of material anisotropy angle on the modal properties and the forced response

In section earlier there have been several ways mentioned how the mistuning could be introduced. If we are only looking at the later simulations with realistic, full-scale finite element models of the bladed disks, we could see several schemes for introducing blade-to-blade variations. For example direct frequency variation [24], perturbation in the stiffness matrix [60], variation in the contact parameters [72], Young modulus discrepancy [9], in the values of the frequency response function [80] or with damping variations [41]. The orientation of the single crystals have been published on a limited extent, this chapter shall give an overview on the available literature.

During the evolution of the turbomachines a search for more resistant materials have been carried out, as the operating conditions in the turbines include high gas loads and extreme temperatures [89]. In order to extend the cyclic lives, increase the creep resistance and reduce oxidation, the casting method gradually developed from the conventional casting (CC) processes.

In the recent decades, directionally solidified (DS) and single crystal (SC) alloys have been most widely used instead of polycrystalline alloys for the material of the blades in turbomachinery applications. The SC alloys are typically used in jet engines while DS alloys are used in gas turbines.

The evolution of the Ni-based superalloys for the application of the single crystal blades have been described in detail in the survey paper of [13]. The advances in the alloy composition, the manufacturing processes is followed up for the first three generation of superalloys. The study includes recent developments and outlook for future developments. Since then the latest generation is called the 6^{th} generation. A few examples of first- and second-generation superalloys are CMSX-6, MC 2, SRR 99, PWA 1480 [16], PWA 1484, René N and SC2000.

In the single crystal materials the elements that strengthens the grain boundaries are suppressed, therefore the grain boundaries can be eliminated. This feature helps to eliminate the possibility of grain boundary separation related fatigue failures.

On the other hand, in case of the single crystal materials all crystals are oriented in the same direction, therefore the linear material behavior is anisotropic. The crystals have face centered cubic (FCC) crystal structure in the commonly applied nickel-based alloys. This crystal structure introduces an additional symmetry; therefore the single crystals are orthotropic with 3 independent material elasticity constants [30].

Most of the publications have a discussion on how the high cycle fatigue is influenced by applying the new superalloys. High cycle fatigue is one of the major failure modes of turbine bladed disks, therefore it is of engineering interest.

In 2002 Arakere and Swanson published the paper [6] in which the dependence of the crystal orientation on the fatigue life in case of high cycle fatigue has been investigated. Due to the orthotropic material behavior of the nickel based superalloys, in the paper a new fatigue failure criterion is presented considering the slip systems in single crystal materials [61]. Simulations were run with 297 different crystal orientation configuration and evaluating the critical failure parameter on all slip systems at a critical point on the blade model. It has been concluded that an optimum orientation can be found and therefore the blade's resistance against fatigue crack growth can be increased by solely the control of the single crystal orientation.

A publication from Hou et. al. has analyzed the effect of the influence of the crystal orientation of the crystals on the fatigue life of the turbine blades [38]. In this study a single blade has been investigated using finite element method. During the analysis centrifugal and thermal load has been applied and the von Mises and maximum resolved shear stress, moreover the fatigue life has been calculated. The analyses have been carried out with several crystal orientation and the dependence of the calculated stresses and fatigue life has been plotted against the independent angles of primary and secondary angles. With limiting the deviation of the primary angle to 15°and there has been a 5% range observer for the stress values by varying the two angles. The variation of the angles had a greater effect on the fatigue life, reaching the 20% range given the varying the angles. There has been only a limited number of angles investigated, therefore the numerical values are not necessarily showing the limits of the range that can be achieved by varying the crystal orientation.

There could be more papers with [35] or [62] mentioned in detail analyzing the fatigue life of the nickel based superalloys, however at this point the focus of the literature review mainly focuses on the research of dynamics of the single crystal blades.

One of the first studies regarding the dynamic behavior of the blades with single crystal blade materials have been published in 1987 by Moss and Smith [59], which focuses on the space shuttle application of NASA. The limited scope study using finite element analysis, analytical and experimental methods, concluded that no greater than 5 percent change has been reported for the modal properties. Utilizing the Campbell diagram, the it is being reported that one of the engine order interferences could be avoided with using the SC instead of DS blades.

In the work of Manetti et. al. 2009 [57] the influence of the crystal orientation on the turbine buckets have been investigated for a second-generation superalloy. The analyses have been carried out for a gas turbine bucket with second generation single crystal superalloy. Experimental natural frequency measurements have been carried out for 12 specimen and were compared with natural frequencies calculated with finite element software. During this comparison the anisotropic material definition in finite element model with different crystal orientations have been validated. In order to analyze the effect of the crystal orientation on the natural frequencies a design of experiment approach has been used. With using 20 design points with different primary and secondary angles, a response surface has been created. This allows a good prediction for the natural frequency values between the design of experiment points. It has been concluded that the influence of the crystal orientation on the first 10 free-free modes of the turbine buckets is smaller than 4%, moreover the natural frequencies are more sensitive to the change in the primary angles then to the change in the secondary angles.

In the work of Kaneko 2011 [42] it has been verified that the directionally solidified blades can be considered as transverse isotropic materials even if the number of columnar grains is small. In the publication the SC blades are modeled as simple rectangular plates and the effect of the three Euler angles describing the crystal orientations is analyzed for first 10 modes. It could be seen that for a given mode not all angles have that same influence, and the extent of the influence could be categorized by mode shape type. The relationship between the material elastic constants in the direction of blade chord and blade height and angles describing the crystal orientation have been examined with the help of first order second method published in [44] by Kaneko et. al. in 2006. Using standard distribution for describing the crystal orientation distribution, it could be concluded that the standard deviation of the frequency due to the deviation caused by the elastic constants is almost doubled for the DS and SC blade compared with the CC blades.

The effect of the crystal orientation of the single crystal blades on the static stresses were investigated in the 2011 paper of Savage [91]. In this publication the generally used terms of the primary and secondary angles are explained for single crystal blades. The analytic demonstration of the stress transformation is presented. It has been illustrated how the elastic constants of the single crystal blades change due to the crystal orientation. This method is implemented in several commercial FE software and in CalculiX [19] by the linear anisotropic material implementation. One segment of the bladed disk without shrouds has been investigated with the help of the FE analysis. There have been 81 calculations carried out with different Eulerian angles defining crystal orientation. Because the simulations are using cyclic symmetric conditions on the two sides of the model in tangential direction, all blades have the same crystal orientation. The static simulation is calculated with friction contact definitions created on the disk, that is modeled by linear isotropic material law, and blade interfaces. The analysis focuses on the maximum principal stresses on the contact interfaces. A 1-5% change in the stresses is reported by discovering creating response surfaces for the given angles. Savage considers the variation of stresses important in exploiting for increased fatigue life, however a more comprehensive investigation should show how the rest of the blade would behave to different crystal orientation settings.

In the more recent 2015 publication from Kaneko et al.[43], the resonant response and random response of the DS blades have been investigated for a more realistic bladed disk model. According to the knowledge of the author of this review, this is the only publication, which analyzes the effect anisotropic material orientation directly on the dynamic behavior for bladed disks. During their study the first the unshrouded blade alone frequency and its sensitivity with respect to anisotropy angles were calculated, with these the response surface was evaluated with respect to lattice growing direction. In order to use less computational effort, the Fundamental Mistuning Model (FMM) [24] has been utilized for the calculation of the forced response. With the help of Monte Carlo simulations and 10,000 random variables the response surface has been calculated, which showed convex shape for with respect to the angle variations. Any variation from the initial crystal orientation when the crystal coordinate system coincides with the blade coordinate system, caused an increase of the natural frequencies for the first and second mode shapes. An important new result is that the resonant frequency range increases for the DS blades, compared to CC blades. The forced response for both of kind of reached its peak when the standard deviation of material constants was a point that caused 1% standard deviation for the blade alone natural frequencies.

2.4 Sensitivity and statistical methods for the dynamic properties of bladed disks

For the calculated modal properties and forced response amplitudes, it is of particular interest to carry out sensitivity studies. The overview of the methods for carrying out the sensitivity analyses is shown here. Moreover, the sensitivities are beneficial inputs for statistical, optimization and robustness assessments.

2.4.1 Numerical methods for sensitivity of mode shapes

For the calculation of the sensitivity of the forced response amplitudes, first the sensitivity of the modal properties needs to be available. Obtaining the derivative of the eigenvalues with respect to the design parameters is a straight-forward procedure. However, the sensitivity of the mode shapes cannot be solved directly, because coefficient matrix of the governing equations of the sensitivity of eigenvector problem is singular. In order to overcome this issue, several different strategies have been developed. First, Fox and Kapoor [27] developed a modal superposition method for obtaining the sensitivity of mode shapes. The drawback of the method presented is, that it can only be used for small systems, as the method requires all eigenvectors of the system for the sensitivity calculation. This method has been improved in [56] and [98], where not all eigenvectors are required. In [103] a method is presented for the calculation of the sensitivity of eigenvectors of free-free systems. This methodology is using the transformation with the eigenvalue shift. These improved methods account for the truncated modes in a form of a residual term.

One of the early methods developed by Nelson [64], requires the knowledge of the eigenpair, the eigenvalues and eigenvectors, for the mode for which the derivatives are calculated for. This algebraic approach modifies the rank of the original eigensystem (n-1) to rank (n), which is then solved for a vector that together with the eigenvector gives the first-order derivative of the eigenvector for systems with distinct eigenvalues.

The development of the algebraic methods has been started by Lee and Jung [52], who developed a method for calculating the sensitivity of eigenvectors for system with distinct eigenvalues. The method applies an additional constraint on the length of the eigenvectors and making the matrix equation solvable.

For the calculation of the derivative of the eigenvectors iterative methods have been developed as well e.g. [90].

In [2] the status of the research on the sensitivity analysis has been surveyed in the middle of the 1980s.

For axis-symmetric dynamic systems, that have repeated eigenvalues, several methods have been developed in [66, 53, 54, 55, 100, 65].

For non-conservative, asymmetric damped systems, the left and the right eigenvectors are distinct. For the calculation of the distinct and complex left and right eigenvectors methods in [3] and in [29] have been developed.

2.4.2 Application of statistical methods

The blade-to-blade parameters causing the mistuning in the bladed disks are inherent distributed in a random manner. The controlling of these parameters is not always possible as, for example, the conditions on the contact interfaces can change from one run to another [31]. Given the variations of the mistuning parameters a search has been performed in order to gain a better understanding of the statistical distribution of the dynamic response of the bladed disk assemblies.

The work of Myhre et. al. [60] uses a ROM for assessing the statistical distribution of the forced response of the mistuned bladed disk for mistuning. The mistuning is modeled with the introduction of perturbation in the stiffness matrix of the system. For which perturbation parameter normal probability distribution has been applied. In order to assess several data points and approximate the statistical distribution of the response, the most common and simple simulation technique is the Monte Carlo simulation. The dataset of the maximum amplitude of the whole bladed disk has been approximated with Weibull (type III) parameter distribution, that the authors found to be the most appropriate.

In [72] Petrov has proposed a method where no sampling such as Monte Carlo is necessary. The developed approach can calculate the statistical characteristics of the forced response with respect to distribution of the friction contact interfaces. The uncertainty ranges, the coefficients of variance and the probability density functions are calculated analytically and with the analytical derivation of the sensitivity of the of forced response with respect to the design parameters. It has been shown on a realistic bladed disk finite element model that the uncertainty of the forced response is contained within 10%. One exception from this is the resonant conditions, where the slip-stick transition occurs on the contact interfaces and the uncertainty significantly increases.

The nonlinear forced response of mistuned bladed disks considering nonlinear contact interfaces and geometrically nonlinear effects has been calculated in [11] by Capiez-Lernout et. al. Using a reduced order method the stochastic nonlinear equations are solved with the help of Monte Carlo simulation in time domain. The confidence region of the amplification factor has been evaluated for both linear and nonlinear mistuned cases. It has been concluded, the nonlinear models have a higher confidence range and more sensitive to parameter variations.

2.4.3 Optimization problems for finding extreme amplification factors and patterns

While the statistical results can help to understand the outcome of the dynamic behavior in a probabilistic basis, engineers are also interested in the worst and best scenarios. Therefore, there has been research carried out for finding the best and worst mistuning patterns in a bladed disk. This can either be carried out with a large sample of design variables such as Monte Carlo simulation, or as an optimization problem. If an optimization method is applied, one shall calculate the sensitivity of the response function with respect to the design variables, which gradient information is essential in order to carry out the optimization search.

The first theoretical prediction of the largest amplification factor was published by Whitehead in 1966 [99]. It has the very elegant form of $\frac{1}{2}(1+\sqrt{N})$ where N is the number of blades in a stage. In the early research several other limits were calculated for the vibration levels of the blades with the help of simple mass-spring models in [22], [23] and [8].

One of the first optimization method applied for the mistuned bladed disk was published by Petrov, Vitali and Haftka in 2000 [81]. By selecting the amplitude of the vibration and the individual blade mistuning to be objective function and design variable respectively, the optimization process is carried out. A robust method is presented that utilizes both the response surface and gradient information for finding the best and worst mistuning patterns.

Optimization process was carried out in [75] with the use of detailed, realistic finite element models. For the design parameters the frequency deviation of the single sectors was chosen, and the sensitivities of the displacements calculated with respect to those design variables. The paper has shown a superior solution for finding the worst mistuning pattern, in comparison with the random statistical search. Petrov and Ewins could find a response amplification factor of 5.02 during this work.

In breakthrough publication [73] of Petrov a new phenomenon has been revealed. Until that point mistuning has only been reported for increasing the amplitudes of the forced response, and for stabilizing the unstable flutter vibrations. In the work it has been proven that the distortion in the mode shapes can cause an increase of the overall damping of the mistuned bladed disk system. The simulations including and excluding aero-effects have been conducted for a large sample of patterns, that were either randomly assembled or rearranged given an initial mistuning pattern. The probability density functions have proved, the aero-effects are reducing the amplification factors. This work also includes a sensitivity-based optimization for the search of the optimum pattern, for which the initial pattern where the search is started from is decisive. With the optimum search approach a maximum of 3.2 times lower amplification factor has been found. During this research it has been proven that the minimums of the objective functions can provide a robust solution.

The work of Beirow et. al. [9] has continued on the research with and without aeroelastic effects. With the help of the SNM reduced order method several Young modulus based mistuning patterns were investigated. Using the finite element model of a compressor blisk they could find the highest amplification factor of 2.82 and the lowest of 0.52.

Analyses for frequency mistuned linear bladed disks were done in [96]. The presented approach calculates the first and second derivative of the forced response function with respect to the frequency mistuning parameter. The sensitivities then applied in optimizing algorithm for finding best and worst mistuning patterns. The work assessed the effect of linearized damping on the amplification factor for the worst and best mistuning patterns.

As it could be seen there were different amplification factors calculated for different mistuning cases, therefore, the maximum amplification caused by mistuning is dependent on the bladed disk, the type of mistuning was introduced, moreover on the method with which the calculations have been carried out.

2.4.4 Investigations regarding damping assessment and contact conditions

One of the challenges in assessing the forced response of the complex dynamic systems, such as bladed disk assemblies, is the good prediction of the damping caused by the energy dissipation on the contact interfaces. A review has been published by Griffin in 1990 [28] on the modeling aspects of the friction dampers in order to reduce the vibrations of the compressor and turbine stages.

In 2003 Petrov and Ewins [76] have derived an analytical formulation for the friction contact interactions for calculating forced response. Given that an analytical ansatz has been implemented, it provides fast, accurate and stable computations.

The paper of Petrov [71] the method was used for assessing the probability density function of the forced response with respect to the contact parameters.

A year later in 2009 Petrov released a study [84] on the sensitivity analysis of the bladed disks at the resonance condition. The results in that publication have been collected with several different kind of bladed disk assemblies.

Krack et. al. have reported [48] an optimization method with additional robustness analysis of uncertainty of the contact parameters of a tuned bladed disk. The proposed technique utilizes analytically derived sensitivity calculations for assessing the uncertainty of the forced response with respect to varying parameters.

2.4.5 Conclusions

This literature review highlighted the basic differences in the dynamic properties for the tuned and mistuned bladed disks. Most of the analyses for this research was done for anisotropy mistuned bladed disks, while some, mainly the parametric studies, were done for tuned bladed disks.

After reviewing the work on the static and dynamic characteristics for turbine blades and bladed disks made of directionally solidified and single crystal materials opportunities for new research arise. The previous works already covered the effect of anisotropy orientation variation on static and modal properties. In the work of Kaneko [43] the forced response of anisotropy mistuned bladed disks were studied for the first time.

For anisotropy mistuned bladed disks, there is potential in further analyzing the effect of crystal orientation variation on modal properties and linear forced response. As for the nonlinear forced response, which was not done for anisotropy mistuned bladed disk at the beginning of the research, considering damping through friction forces leads to new research findings. Moreover, the literature review showed that at the time of the beginning of the research work, no sensitivity studies has been done in which the design parameter the crystal orientation was.

In order to accomplish the previously described new research, already existing methods can be applied, and some methods can be modified for the calculations for anisotropy mistuned bladed disks.

The forced response calculation for bladed disks with friction contact joints is a challenging task, which is generally solved in the frequency domain. The two major challenges appear in the form of large number of DOFs in the system, which result in extreme calculation times moreover, the exact description of the contact status and friction forces in time domain. Among the methods presented in the previous sections, in this work the high-accuracy model reduction [85] is used. The method for the nonlinear forced response calculation, which is selected for this work is described in reference [76].

For the sensitivity calculation of the linear and nonlinear forced response the already available method described in [71] is used. In order to calculate the sensitivity for the forced response the sensitivity of modal properties with respect to anisotropy angles need to be obtained first. To this end the already available methods based on modal superposition and algebraic bordering methods are implemented in a modified form.

Chapter 3

Methods of the nonlinear forced response and its sensitivities with respect to material anisotropy angles

In this chapter the methods used for the modeling of anisotropic material behavior of the single crystal blades are presented. The discussion also extends to the methods used for the calculation of the linear and nonlinear forced response of tuned and mistuned bladed disks. Regarding the sensitivities, the methods used for the calculations of the sensitivity of modal properties, flexibility matrix and forced response are presented.

3.1 Modeling of the material properties of single crystal blades

For the modeling of the linear elastic behavior of single crystal blades anisotropic material models are used. The crystals of the modern nickel-base superalloy blades are organized in a face centered cubic crystal structure. This symmetric structure results in a material that is a subset of orthotropic materials: cubic material. The material has the 3 independent material constants, unlike a general anisotropic material that has 21 independent constants. The three independent material constants defined in the material coordinate system (CS) are the Young's modulus E_0, the shear modulus G_0 and the Poissions's ration ν_0.

The compliance matrix in the stress-strain relation $\boldsymbol{\epsilon} = \boldsymbol{S}\boldsymbol{\sigma}$, using the Voigt notation, for a nickel base superalloy is defined in the material CS as Eq. (3.1). Where the constants are: $S_{33} = 1/E_0$, $S_{13} = -\nu_0/E_0$ and $S_{44} = 1/G_0$.

$$\boldsymbol{S} = \begin{bmatrix} S_{33} & S_{13} & S_{13} & 0 & 0 & 0 \\ S_{13} & S_{33} & S_{13} & 0 & 0 & 0 \\ S_{13} & S_{13} & S_{33} & 0 & 0 & 0 \\ 0 & 0 & 0 & S_{44} & 0 & 0 \\ 0 & 0 & 0 & 0 & S_{44} & 0 \\ 0 & 0 & 0 & 0 & 0 & S_{44} \end{bmatrix} \tag{3.1}$$

The elasticity matrix is defined as the inverse of the of the compliance matrix, from $\boldsymbol{\sigma} = \boldsymbol{S}^{-1}\boldsymbol{\epsilon} = \boldsymbol{C}\boldsymbol{\epsilon}$. The elasticity matrix can be defined in a different coordinate system as $\boldsymbol{C}^*$, by multiplying the elasticity matrix with stress transformation matrix from the left and right as

$$\boldsymbol{C}^* = \boldsymbol{T}\,\boldsymbol{C}\,\boldsymbol{T}^T. \tag{3.2}$$

where $\boldsymbol{T}$ is the stress transformation matrix between two coordinate systems, $\boldsymbol{T}^T$ the transpose of the stress transformation matrix and $\boldsymbol{C}$ is the elasticity matrix in the initial CS, in other words the material CS. In order to be able to specify the stress transformation matrix, the coordinate transformation matrix needs to be specified between the two coordinate systems [30]. The stress transformation matrix between coordinate systems for which the rotation matrix is in the form

$$\boldsymbol{R} = \begin{bmatrix} l_1 & l_2 & l_3 \\ m_1 & m_2 & m_3 \\ n_1 & n_2 & n_3 \end{bmatrix} \tag{3.3}$$

can be written as

$$\boldsymbol{T} = \begin{bmatrix} l_1^2 & m_1^2 & n_1^2 & 2l_1m_1 & 2l_1n_1 & 2m_1n_1 \\ l_2^2 & m_2^2 & n_2^2 & 2l_2m_2 & 2l_2n_2 & 2m_2n_2 \\ l_3^2 & m_3^2 & n_3^2 & 2l_3m_3 & 2l_3n_3 & 2m_3n_3 \\ l_1l_2 & m_1m_2 & n_1n_2 & l_1m_2+m_1l_2 & l_1n_2+n_1l_2 & m_1n_2+n_1m_2 \\ l_1l_3 & m_1m_3 & n_1n_3 & l_1m_3+m_1l_3 & l_1n_3+n_1l_3 & m_1n_3+n_1m_3 \\ l_2l_3 & m_2m_3 & n_2n_3 & l_2m_3+m_2l_3 & l_2n_3+n_2l_3 & m_2n_3+n_2m_3 \end{bmatrix} \tag{3.4}$$

For the description of the material properties of single crystal blades in a bladed disk assembly, three coordinate systems need to be defined. The material CS defined with the material axes [100][010] and [001] in Fig. 3.1a. This coordinate system is used for the description of the material constants, E_0, G_0 and ν_0.

For single crystal blades, the material CS is generally not coinciding with the CS of the blade, denoted with x', y' and z' in Fig. 3.1a. The z' axis is the stacking axis of each

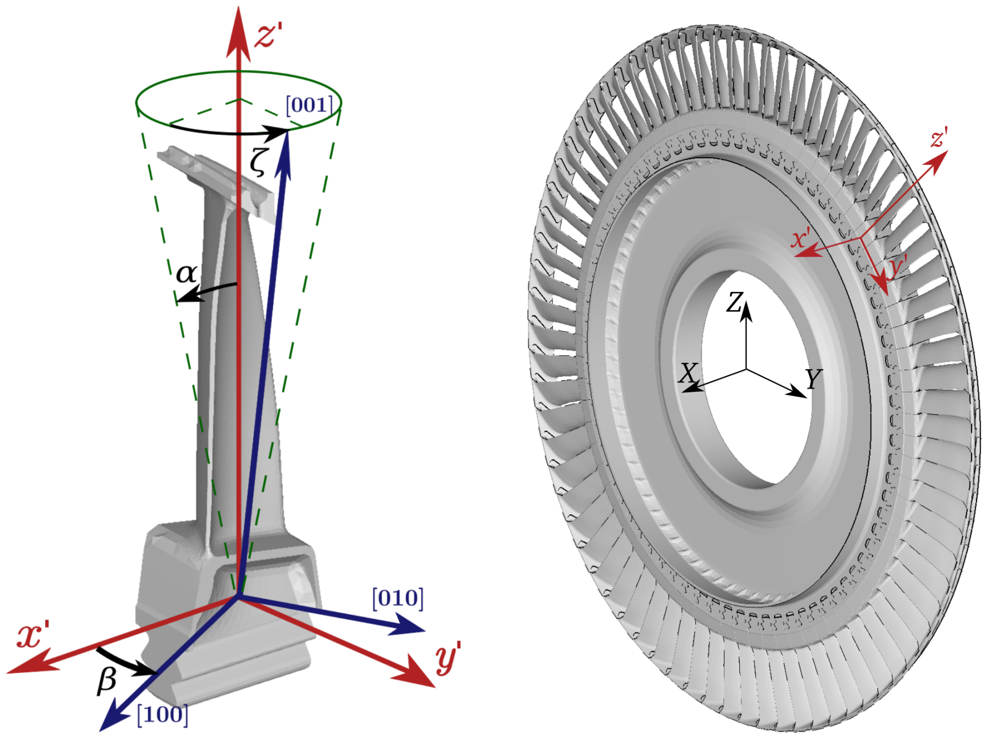

(a) Definition of the material and blade CS (b) Blade CS in the global CS

Figure 3.1: Definition of the material and blade coordinate system

blade and x' is parallel to the machine's axis. The deviation of the material CS system with respect to blade CS is described by the material anisotropy angles, α, β and ζ.

In the current practice, the description of the material anisotropy is defined by the material anisotropy angles $\Gamma = \{\alpha, \beta, \zeta\}$ that are defined in the local coordinate system of each blade in the following way: The primary angle, the deviation of [001] axis with respect to is z' axis, is represented by α. The secondary angle β is defined as the smaller angle between x' axis and [100] or x' axis and [010]. The third angle ζ defines the position of the [001] axis on a circle defined parallel to the $x' - y'$ plane. The angle ζ can take any value between $-180°$ and $180°$.

After the casting process, the anisotropy angles of the single crystal blades are measured by the manufacturer using the Laue method [5, 50]. After years of single crystal blade production a MTU has collected a large sample of anisotropy angles, which allows for fitting a statistical evaluation to the anisotropy parameters. For each of the anisotropy angles, α, β and ζ, a commonly known statistical distribution is fitted. Using pseudo random sampling from the distributions of the crystal orientation angles random anisotropy mistuning patterns can be created. The type and the parameters cannot be published due to confidentiality agreements with the sponsor company.

For the finite element (FE) description an anisotropy mistuned bladed disk, it is important to be able to describe the anisotropy orientation for every blade in the global CS of the FE model. The origin of the global Cartesian coordinate system is placed such that the x axis coincides the axis of rotation. In order to be able to calculate the finite element matrices, all anisotropic material properties need to be calculated for global coordinate system.

In order to be able to define the material properties for each blade in an anisotropy mistuned bladed disk in the global CS, coordinate transformation needs to be defined from the material CS to the global CS. The rotation matrix defining the crystal orientation of the blade material with respect to the CS of the blade is defined by $\boldsymbol{R}_M$. The matrix $\boldsymbol{R}_M$ can be described by rotating with the anisotropy angles of α, β and ζ:

$$\boldsymbol{R}_M(\boldsymbol{\Gamma}) = \boldsymbol{R}_\zeta \boldsymbol{R}_{\beta^*} \boldsymbol{R}_\alpha \tag{3.5}$$

where $\beta* = \beta - \zeta$. The rotation matrix $\boldsymbol{R}_\alpha$ rotates about y' axis and $\boldsymbol{R}_{\beta*}$, $\boldsymbol{R}_\zeta$ rotate about z' axis.

For the rotation between the stacking axis of the specific blade and the global CS the rotation matrix $\boldsymbol{R}_B$ is defined. Arriving to the rotation matrix $\boldsymbol{R}_G(\boldsymbol{\Gamma})$ which, describes the blade material crystal orientation in the global CS depending on the location of the blade taking the form:

$$\boldsymbol{R}_G(\boldsymbol{\Gamma}) = \boldsymbol{R}_B \boldsymbol{R}_M(\boldsymbol{\Gamma}) \tag{3.6}$$

The transformation of the elasticity tensor for linear-elastic materials can be executed from the CS attached to every blade to the global CS with the help of the stress transformation matrix $\boldsymbol{T}$ as:

$$\boldsymbol{C}^*(\boldsymbol{R}_M, \boldsymbol{R}_B) = \boldsymbol{T}(\boldsymbol{R}_M, \boldsymbol{R}_B)\, \boldsymbol{C}\, \boldsymbol{T}^T(\boldsymbol{R}_M, \boldsymbol{R}_B) \tag{3.7}$$

The stress transformation matrix $\boldsymbol{T}$ is dependent on the rotation matrices $\boldsymbol{R}_M$ and $\boldsymbol{R}_B$.

The element stiffness matrix can be calculated using the element stiffness formulation for 3D isoparametric elements:

$$\boldsymbol{k}^e = \int\limits_{V^e} \boldsymbol{B}^T\, \boldsymbol{C}^*\, \boldsymbol{B}\, dV \tag{3.8}$$

Where $\boldsymbol{k}^e$ is the finite element stiffness matrix, $\boldsymbol{C}^*$ is the elasticity matrix defined in the global coordinate system, $\boldsymbol{B}$ is the strain-displacement matrix and V^e is the volume of the element. The global stiffness matrix $\boldsymbol{K}$ can be assembled by adding the expanded element stiffness matrices together, after which the finite element calculations for the whole structure can be carried out.

$$\boldsymbol{K} = \bigcup_e \boldsymbol{k}^e \tag{3.9}$$

3.2 Modal properties of bladed disks

The natural frequencies and the modes shapes describe the dynamic behavior of the linear structures. In this section the modal properties are described for tuned and mistuned bladed disks.

For tuned bladed disks it is sufficient to model only one sector of the structure. For blade disks this is generally sector with one blade with the corresponding disk sector. For bladed disks with intentional mistuning, e.g. A and B pattern mistuning of low- and high-frequency airfoils [92], two airfoils are included in a cyclic symmetric sector. Applying cyclically symmetric conditions on the left and right boundaries of the blade disk sector significantly reduces the computational effort of the calculations.

When modal properties of mistuned bladed disks are obtained, no cyclic symmetric conditions are applied and the full bladed disk is modeled. This modeling allows the introduction of blade-to-blade variation. Such variation can be changes in geometry, material properties or contact parameters.

The interest of the studies was the sensitivities of the modal parameters with respect to anisotropy angles for mistuned bladed disks. The method for the sensitivity calculation of mistuned bladed disks are presented here.

The modal properties are the model input for linear and nonlinear forced response calculations. For the calculation of the sensitivity of forced response, first the sensitivity of the modal characteristics need to be calculated.

3.2.1 Modal properties of tuned bladed disks with cyclic symmetric conditions

For the calculation of the mode shapes of the cyclic symmetric bladed disks CalculiX is used [18]. The cyclic symmetric condition is applied such that an N_{ND} nodal diameter (ND) mode shape has N_{ND} complete sinusoidal waves along the circumference of the bladed disk. The maximum value of nodal diameters for bladed disks with N blades is

$$N_{ND,max} = \begin{cases} N/2 & \text{for } \textit{even } N \\ (N-1)/2 & \text{for } \textit{odd } N \end{cases} \tag{3.10}$$

The boundary condition of the cyclic symmetry can be expressed [?] as

$$\boldsymbol{\phi}_B = \boldsymbol{\phi}_A \cdot e^{i\frac{2\pi N_{ND}}{N}} \tag{3.11}$$

for point A and point B along the circumference of the cyclic symmetric structure. Point A is the left and B is on the right boundaries and the phase shift for the modal displacements between them is $\frac{2\pi N_{ND}}{N}$.

Because of the complex boundary conditions on the boundaries of the fundamental sector, the resulting eigenproblem will also be complex. Therefore, the calculated the resulting eigenvalues will be duplicate and the eigenvectors for the eigenvalue pairs are complex conjugates.

3.2.2 Modal properties of mistuned bladed disks

For anisotropy mistuned bladed disks, the full FE model allows for applying different crystal orientation for each blade. As described in section 3.1, for each single crystal blade in the bladed disk the crystal orientation can be defined by a set of anisotropy angles $\Gamma = \{\alpha, \beta, \zeta\}$. Therefore, for a mistuned bladed disk the anisotropy mistuning pattern can be defined by $3 \cdot N$ number of anisotropy parameters.

The eigenvalue problem for asymmetric systems, such as anisotropy mistuned bladed disks, can be written in the form

$$\boldsymbol{K}\boldsymbol{\phi}_j = \lambda_j \boldsymbol{M}\boldsymbol{\phi}_j \tag{3.12}$$

Where, the stiffness matrix $\boldsymbol{K}$, the eigenvalues λ_j and the mode shapes, $\boldsymbol{\phi}_j$, are dependent on the anisotropy angles, but the mass matrix $\boldsymbol{M}$, for anisotropy mistuned bladed disks, is not, and the subscript j is the mode number. The geometric stiffening effects of the centrifugal forces of a rotating bladed disk assembly can be considered in the stiffness matrix $\boldsymbol{K}$.

It is worth noting that for a mistuned system all eigenvalues and mode shapes are real and distinct. Moreover, for each mode shape family there are N number of mode shapes. This means that for example for a bladed disks with 75 blades, there will be 75 mode shapes from the first mode family. If the modes of interest are from the higher mode shape families, it takes significant calculation effort to obtain hundreds of modes.

For solving the equation (3.12) and obtaining natural frequencies and mode shapes, the open-source FE solve of CalculiX is used: CalculiX CrunchiX (ccx).

3.3 Sensitivity of modal characteristics

The eigenvalue problem of the multi-degree-of-freedom (MDOF) dynamic system can be written in the form:

$$\boldsymbol{K}(\gamma)\boldsymbol{\phi}_j = \lambda_j \boldsymbol{M}\boldsymbol{\phi}_j \tag{3.13}$$

Where, the stiffness matrix $\boldsymbol{K}(\gamma)$, the eigenvalues λ_j and the mode shapes, $\boldsymbol{\phi}_j$, are dependent on the anisotropy angles, but the mass matrix $\boldsymbol{M}$ is not, and the subscript j is the mode number. Here, γ is introduced as a general parameter that can be any parameter describing the crystal orientation of the anisotropic material.

Assuming mass-normalized eigenvectors, $\boldsymbol{\phi}_j$, the equation describing the sensitivity of the eigenvalues for a MDOF dynamic system takes the form [27] :

$$\frac{\partial \lambda_j}{\partial \gamma} = \boldsymbol{\phi}_j^T \left(\frac{\partial \boldsymbol{K}}{\partial \gamma} - \lambda_j \frac{\partial \boldsymbol{M}}{\partial \gamma} \right) \boldsymbol{\phi}_j \tag{3.14}$$

Since the mass matrix is not dependent on γ for the applications considered in this work, this expression becomes:

$$\frac{\partial \lambda_j}{\partial \gamma} = \boldsymbol{\phi}_j^T \frac{\partial \boldsymbol{K}}{\partial \gamma} \boldsymbol{\phi}_j \tag{3.15}$$

The derivative of the stiffness matrix in Eq. (3.15), with respect to the anisotropy angle for linear calculations can be calculated using an analytic method. The sensitivity of the stiffness matrix on the element level can be expressed with the modified equation of the element stiffness formulation of a three-dimensional isoparametric finite element as:

$$\frac{\partial \boldsymbol{k}^e}{\partial \gamma} = \int_{V^e} \boldsymbol{B}^T \frac{\partial \boldsymbol{C}^*}{\partial \gamma} \boldsymbol{B}\, dV \tag{3.16}$$

Where $\boldsymbol{k}^e$ is the finite element stiffness matrix, $\boldsymbol{C}^*$ is the elasticity matrix defined in the global coordinate system, $\boldsymbol{B}$ is the strain-displacement matrix and V^e is the volume of the finite element. In order to carry out the calculation described in Eq.(3.16) the derivative of the elasticity matrix is calculated.

The methodologies for the calculation of the sensitivity of mode characteristics have been implemented in the open-source finite element software CalculiX. The calculation of the derivative of the stiffness matrix is done using the finite difference scheme as

$$\frac{\partial \boldsymbol{k}^e(\gamma)}{\partial \gamma} \approx \frac{\boldsymbol{k}^e(\gamma + \Delta\gamma) - \boldsymbol{k}^e(\gamma)}{\Delta\gamma} \tag{3.17}$$

where, $\Delta\gamma$ is the finite difference step. For the application of the formula, two evaluations are necessary for each sensitivity calculation. One with unperturbed rotation vector components and one with a perturbed rotation vector component.

3.3.1 Enhanced modal method

In order to express the sensitivity of mode shapes, a series expansion formulation is traditionally used e.g. see Ref. [2]

$$\frac{\partial \boldsymbol{\phi}_j}{\partial \gamma} = \sum_{k=1}^{m} c_{jk}\boldsymbol{\phi}_k = \boldsymbol{\Phi}\boldsymbol{c}_j \tag{3.18}$$

The formulation in Eq. (3.18) considers only a subset of mode shapes m in the expansion of the derivative of the mode shapes. In order to increase the precision and the speed of convergence, an enhanced method is proposed [82]. This approach accounts for the mode shapes that are not included in the expansion, in the form of a residual vector $\boldsymbol{r}_j$.

$$\frac{\partial \boldsymbol{\phi}_j}{\partial \gamma} = \boldsymbol{\Phi}\boldsymbol{c}_j + \boldsymbol{r}_j \tag{3.19}$$

The coefficients of the first term on the right hand side of Eq. (3.19), $\boldsymbol{c}_j$, can be derived by first substituting Eq. (3.18) into the total derivative of Eq. (3.13) with respect to the general anisotropy parameter γ:

$$\left(\boldsymbol{K} - \lambda_j \boldsymbol{M}\right)\boldsymbol{\Phi}\boldsymbol{c}_j = \boldsymbol{f}_j \tag{3.20}$$

where the right hand side for a general case is:

$$\boldsymbol{f}_j = -\left(\frac{\partial \boldsymbol{K}}{\partial \gamma} - \lambda_j \frac{\partial \boldsymbol{M}}{\partial \gamma} - \frac{\partial \lambda_j}{\partial \gamma}\boldsymbol{M}\right)\boldsymbol{\phi}_j \tag{3.21}$$

Then the components c_{jk} of the vector of the sensitivity expansion coefficients for j-th mode shape $\boldsymbol{c}_j$ are obtained for $k \neq j$ by multiplying Eq. (3.20) with the k^{th} mass-normalized mode shape $\boldsymbol{\phi}_k^T$ from the left. The coefficient c_{jj} is calculated by differentiating the normalization condition: $\boldsymbol{\phi}_j^T \boldsymbol{M} \boldsymbol{\phi}_j = 1$, which for a general case gives:

$$c_{jj} = -0.5\boldsymbol{\phi}_j^T \frac{\partial \boldsymbol{M}}{\partial \gamma}\boldsymbol{\phi}_j \tag{3.22}$$

For the sensitivity analysis to material anisotropy orientation, considered in this paper, the dependence of the mass matrix on the anisotropy orientation can be neglected. Therefore, Eq. (3.21) takes the following form:

$$\boldsymbol{f}_j = -\left(\frac{\partial \boldsymbol{K}}{\partial \gamma} - \frac{\partial \lambda_j}{\partial \gamma}\boldsymbol{M}\right)\boldsymbol{\phi}_j \tag{3.23}$$

The coefficients of the mode shape sensitivity expansion, considering that the mass matrix is not dependent on γ, result in:

$$c_{jk} = \begin{cases} \frac{\boldsymbol{\phi}_k^T \boldsymbol{f}_j}{\lambda_k - \lambda_j} & \text{if } k \neq j \\ 0 & \text{if } k = j \end{cases} \tag{3.24}$$

The residual vector in Eq. (3.19) teaks into account the contribution of the modes which are truncated in Eq. (3.18)

$$\boldsymbol{r}_j = \sum_{k=m+1}^{N} \frac{\boldsymbol{\phi}_k^T \boldsymbol{f}_j}{\lambda_k - \lambda_j} \boldsymbol{\phi}_k \tag{3.25}$$

where N is the total number of modes in a considered structure (which is equal to the total number of DOFs in the finite element model). In order to be able to calculate the residual vector, here some value λ_0 is substituted instead of λ_j. This value is chosen to be very close to, but different from λ_j to avoid division by 0.

The expression $\boldsymbol{r}_j$ can be divided into two terms as:

$$\boldsymbol{r}_j \approx \sum_{k=1}^{N} \frac{\boldsymbol{\phi}_k^T \boldsymbol{f}_j}{\lambda_k - \lambda_0} \boldsymbol{\phi}_k - \sum_{k=1}^{m} \frac{\boldsymbol{\phi}_k^T \boldsymbol{f}_j}{\lambda_k - \lambda_0} \boldsymbol{\phi}_k = \boldsymbol{r}_j^0 - \sum_{k=1}^{m} c_{jk}^r \boldsymbol{\phi}_k \tag{3.26}$$

The former term can be reformulated as a system of linear equations and therefore solved with a linear equation solver.

$$(\boldsymbol{K} - \lambda_0 \boldsymbol{M})\, \boldsymbol{r}_j^0 = \boldsymbol{f}_j \tag{3.27}$$

Substitution of Eq.(3.26) in Eq. (3.19) gives us the enhanced expression for the mode shape sensitivities:

$$\frac{\partial \boldsymbol{\phi}_j}{\partial \gamma} = \boldsymbol{\Phi} \boldsymbol{c}_j + \boldsymbol{r}_j^0 - \boldsymbol{\Phi} \boldsymbol{c}_j^r = \boldsymbol{\Phi} \boldsymbol{c}_j^* + \boldsymbol{r}_j^0 \tag{3.28}$$

The coefficients of the sensitivity of mode shapes using enhanced formulation in Eq. (3.28) can be calculated as:

$$c_{jk}^* = \begin{cases} \frac{\lambda_j - \lambda_0}{(\lambda_k - \lambda_j)(\lambda_k - \lambda_0)} \boldsymbol{\phi}_k^T \boldsymbol{f}_j & \text{if } k \neq j \\ -\frac{\boldsymbol{\phi}_k^T \boldsymbol{f}_j}{\lambda_k - \lambda_0} & \text{if } k = j \end{cases} \tag{3.29}$$

3.3.2 Algebraic method

For the introduction of the algebraic method [83], the sensitivity eigenvalue problem, together with the derivative of the equation for the mass normalized mode shapes, can be rewritten in the following form:

$$\begin{bmatrix} \boldsymbol{K} - \lambda_j \boldsymbol{M} & -\boldsymbol{M}\boldsymbol{\phi}_j \\ -\boldsymbol{\phi}_j^T \boldsymbol{M} & 0 \end{bmatrix} \begin{bmatrix} \partial \boldsymbol{\phi}_j / \partial \gamma \\ \partial \lambda_j / \partial \gamma \end{bmatrix} = \begin{bmatrix} -((\partial \boldsymbol{K}/\partial\gamma) - \lambda_j (\partial \boldsymbol{M}/\partial \gamma))\boldsymbol{\phi}_j \\ 0 \end{bmatrix} \tag{3.30}$$

This system of equations in Eq. (3.30) can be written in a compact form:

$$\begin{bmatrix} \boldsymbol{A} & \boldsymbol{b} \\ \boldsymbol{b}^T & 0 \end{bmatrix} \begin{bmatrix} \partial \boldsymbol{\phi}_j / \partial \gamma \\ \partial \lambda_j / \partial \gamma \end{bmatrix} = \begin{bmatrix} \boldsymbol{c} \\ 0 \end{bmatrix} \tag{3.31}$$

where, $\boldsymbol{A} = \boldsymbol{K} - \lambda_j \boldsymbol{M}$, $\boldsymbol{b} = -\boldsymbol{M}\boldsymbol{\phi}_j$ and $\boldsymbol{c} = -((\partial \boldsymbol{K}/\partial\gamma) - \lambda_j(\partial \boldsymbol{M}/\partial\gamma))\boldsymbol{\phi}_j$. Using the notations in Eq. (3.31) the sensitivity of the eigenvalues in Eq. (3.14) can be expressed as

$$\partial \lambda_j / \partial \gamma = -\boldsymbol{\phi}_j^T \boldsymbol{c} \tag{3.32}$$

By definition, the matrix $\boldsymbol{A}$ is singular. Here, bordering algorithm [45] is used for solving the singular system of equations. The matrix $\boldsymbol{A}$ is regularized by adding the regularization coefficient s to one of the entries on the principal diagonal of the matrix.

$$\widetilde{\boldsymbol{A}} = \boldsymbol{A} + s \cdot \boldsymbol{e}_s \boldsymbol{e}_s^T \tag{3.33}$$

According to the general bordering algorithm, the sensitivity of mode shapes can be expressed exactly using the formulation of

$$\partial \boldsymbol{\phi}_j / \partial \gamma = \boldsymbol{g}^{\phi} - \boldsymbol{g}^{\lambda} (\partial \lambda_j / \partial \gamma) + \alpha \boldsymbol{g}^{e} \tag{3.34}$$

where

$$\widetilde{\boldsymbol{A}} \boldsymbol{g}^{\lambda} = \boldsymbol{b}; \quad \widetilde{\boldsymbol{A}} \boldsymbol{g}^{\phi} = \boldsymbol{c}; \quad \widetilde{\boldsymbol{A}} \boldsymbol{g}^{e} = s \boldsymbol{e}_j \tag{3.35}$$

and

$$\alpha = \left(\frac{\boldsymbol{b}^T \boldsymbol{g}^{\lambda}}{\boldsymbol{b}^T \boldsymbol{g}^{e}} \right) (\partial \lambda_j / \partial \gamma) - \frac{\boldsymbol{b}^T \boldsymbol{g}^{\phi}}{\boldsymbol{b}^T \boldsymbol{g}^{e}} \tag{3.36}$$

The calculation of the vectors $\boldsymbol{g}^{\lambda}$,$\boldsymbol{g}^{\phi}$ and $\boldsymbol{g}^{e}$ is done by solving the system of linear equations in Eq. (3.35). Note that the factorization of the matrix $\widetilde{\boldsymbol{A}}$ and the calculation of $\boldsymbol{b}$, $\boldsymbol{g}^{\lambda}$, $\boldsymbol{g}^{e}$, $\boldsymbol{b}^T\boldsymbol{g}^{e}$ and $(\boldsymbol{b}^T\boldsymbol{g}^{\lambda})/(\boldsymbol{b}^T\boldsymbol{g}^{e})$ is done only once for a considered mode shape. This must be considered for structures that have a large number of design variables. In case of bladed disks with 72 blades, the number of design variables describing the anisotropy axis orientation of the monocrystalline blade is $72 \cdot 3 = 216$. The calculation of $\boldsymbol{c}$, $\boldsymbol{g}^{\phi}$ and λ' is done for every design variable of the system.

The advantage of the proposed method is that only the eigenpair and the sensitivity of the eigenvalue for which the eigenvector sensitivities are calculated are necessary for the calculation for obtaining the sensitivity of the eigenvector. In modal analysis of large systems, normally the lowest first m eigenvalues are calculated and using the proposed method there is no need for the calculation of additional eigenvalues and eigenvectors to obtain the derivative of the mode shape $\boldsymbol{\phi}_m$ with respect to the design variables. The proposed method also allows for an exact solution can be calculated without removing rows and columns from matrix $\boldsymbol{A}$. Additionally, this algebraic method is simple to program.

3.4 Forced response and its sensitivity for bladed disks

In this work, two major types of bladed disks are analyzed: (i) mistuned bladed disks (ii) tuned bladed disks.

For tuned bladed disks, cyclic symmetric conditions can be applied, but for mistuned systems a whole bladed disk is modeled, where each single crystal blade has a varying crystal orientation. For the nonlinear forced response calculations the code ContaDyn developed by E.P. Petrov is used, which is based on the multiharmonic balance and fully analytical formulation for nonlinear contact interactions (see Refs. [69, 76, 78, 85]).

3.4.1 Forced response and its sensitivity for linear mistuned bladed disks

For linear mistuned bladed disks, the equation of motion can be written in the form:

$$\boldsymbol{K}\boldsymbol{x}(t) + \boldsymbol{C}\dot{\boldsymbol{x}}(t) + \boldsymbol{M}\ddot{\boldsymbol{x}}(t) = \boldsymbol{p}(t) \tag{3.37}$$

Where, $\boldsymbol{K}, \boldsymbol{C}$ and $\boldsymbol{M}$ are structural stiffness, damping and mass matrices; $\boldsymbol{x}(t)$ is the time varying forced response for all degrees of freedom in the mistuned bladed disk; $\boldsymbol{p}(t)$ is harmonic excitation applied on the mistuned bladed disk. The periodic excitation of the bladed disk is a traveling wave type, and it takes the form:

$$\boldsymbol{p}(t) = \{\boldsymbol{p}_1(t), \boldsymbol{p}_1(t-\alpha), ..., \boldsymbol{p}_1(t-(N-1)\alpha)\}^T \tag{3.38}$$

Where, $\boldsymbol{p}_1(t)$ is the harmonic load applied on first sector of the bladed disk model. The dynamic load can be applied to a single node or distributed over several nodes of the FE mesh. The value $\alpha = T/N$ is the phase shift in the applied forces from one sector to next one; the period is $T = 2\pi/\omega$, where ω is the principal excitation frequency that is $\omega = \omega_m \cdot EO$, the machine rotation speed multiplied by engine order number (EO). For the harmonic excitation in the from $\boldsymbol{p}(t) = \boldsymbol{P}e^{i\omega t}$, the solution of the vibration is sought in the form of $\boldsymbol{x}(t) = \boldsymbol{X}e^{i\omega t}$.

The equation of motion takes in frequency domain the form:

$$\left[\boldsymbol{K} + i\omega\boldsymbol{C} - \omega^2\boldsymbol{M}\right]\boldsymbol{X} = \boldsymbol{P} \tag{3.39}$$

For linear systems, the forced response displacements can be calculated with the modal superposition method. With the natural frequencies and mode shapes already calculated for the mistuned bladed disk, the forced response amplitudes can be written in the form:

$$\boldsymbol{X} = \sum_{j=1}^{N_m} \frac{\boldsymbol{\phi}_j^T \boldsymbol{P}}{(1+i\eta_j)\omega_j^2 - \omega^2}\boldsymbol{\phi}_j = \sum_{j=1}^{N_m} c_j\boldsymbol{\phi}_j \tag{3.40}$$

Where, ω_j, $\boldsymbol{\phi}_j$ and η_j are natural frequency, mode shape and modal damping factor for j-th mode; in the modal expansion N_m number of modes are included; and the unit imaginary number is $i = \sqrt{-1}$. The high-fidelity finite element models of mistuned bladed disks include millions of DOFs. The advantage of the modal superposition method is that only the degrees of freedom of the nodes where harmonic excitation is applied and the nodes of interest need to be included in the calculations, which reduces the computation time significantly.

Sensitivity of linear forced response for mistuned bladed disks

For linear systems the sensitivity of forced response can be calculated by taking the derivative Eq. (3.40) with respect to the anisotropy design parameter γ:

$$\frac{\partial \boldsymbol{X}}{\partial \gamma} = \sum_{j=1}^{N_m} \frac{\partial c_j}{\partial \gamma} \boldsymbol{\phi}_j + c_j \frac{\partial \boldsymbol{\phi}_j}{\partial \gamma} \tag{3.41}$$

Where, the sensitivity of the mode shapes is already available and the sensitivity of the modal expansion coefficients can be calculated as:

$$\frac{\partial c_j}{\partial \gamma} = \frac{\boldsymbol{P}^T(\partial \boldsymbol{\phi}_j/\partial \gamma)}{(1+i\eta_j)\omega_j^2 - \omega^2} - \frac{\boldsymbol{P}^T \boldsymbol{\phi}_j \left[(1 + i\left((\partial \eta_j/\partial \gamma) \right) \omega_j^2 + 2\left(1 + i\eta_j\right) \omega_j \left(\partial \omega_j/\partial \gamma\right) \right]}{\left[\left(1 + i\eta_j\right) \omega_j^2 - \omega^2 \right]^2} \tag{3.42}$$

3.4.2 Nonlinear forced response and its sensitivity for mistuned bladed disks with friction joints

For nonlinear mistuned bladed disks with friction contact interfaces, the equation of motion is extended with the term $\boldsymbol{f}(\boldsymbol{x}(t))$ describing the nonlinear friction forces as:

$$\boldsymbol{K}\boldsymbol{x}(t) + \boldsymbol{C}\dot{\boldsymbol{x}}(t) + \boldsymbol{M}\ddot{\boldsymbol{x}}(t) + \boldsymbol{f}(\boldsymbol{x}(t)) = \boldsymbol{p}(t) \tag{3.43}$$

The turbine bladed disk assemblies used in practical applications many frictional contact surfaces. The nonlinear forces occur on blade-root disk interfaces, on the surfaces of under-platform dampers, blade retainers and on the shroud interfaces of the adjacent blades. Moreover, high-energy rubs can occur between the blade tip and honeycomb sealing material of the casing. The main sources of nonlinearities on the contact interfaces are the friction forces, unilateral interaction of the paired interfaces, gap closure and opening etc. The analytically formulated nonlinear contact forces have been derived in Refs. [76, 74]. The 3D nonlinear contact elements used in this work allow for the interactions of relative motion along the two surface tangential and normal directions.

For the calculation of the periodic forced response vibrations, the multiharmonic balance method is applied. The dynamic system is excited by a harmonic excitation, and therefore the solution of Eq. (3.43) is sought for in the form of a restricted Fourier series.

$$\boldsymbol{x}(t) = \boldsymbol{X}_0 + \sum_{j=1}^{N_h} \boldsymbol{X}_j^{(c)} \cos(k_j\omega t) + \boldsymbol{X}_j^{(s)} \sin(k_j\omega t) \tag{3.44}$$

where, $\widetilde{\boldsymbol{X}} = \{\boldsymbol{X}_0, \boldsymbol{X}_1^c, ..., \boldsymbol{X}_n^s\}$ can be defined as the vector of harmonic coefficients describing the vibration for all degrees-of-freedom; the harmonic coefficients are k_j and the number of harmonics included in the Fourier series are N_h, and ω is the principal excitation frequency. Similarly, the nonlinear forces $\boldsymbol{f}(\boldsymbol{x}(t))$ and the excitation forces $\boldsymbol{p}(t)$ can be written in the multiharmonic expression as

$$\boldsymbol{f}(t) = \boldsymbol{F}_0 + \sum_{j=1}^{N_h} \boldsymbol{F}_j^{(c)} \cos(k_j\omega t) + \boldsymbol{F}_j^{(s)} \sin(k_j\omega t) \tag{3.45}$$

$$\boldsymbol{p}(t) = \boldsymbol{P}_0 + \sum_{j=1}^{N_h} \boldsymbol{P}_j^{(c)} \cos(k_j\omega t) + \boldsymbol{P}_j^{(s)} \sin(k_j\omega t) \tag{3.46}$$

where similarly, the $\boldsymbol{F} = \{\boldsymbol{F}_0, \boldsymbol{F}_1^c, ..., \boldsymbol{F}_n^s\}$ and $\boldsymbol{P} = \{\boldsymbol{P}_0, \boldsymbol{P}_1^c, ..., \boldsymbol{P}_n^s\}$ can be defined as the vectors of harmonic coefficients for the nonlinear forced and excitation forces.

After applying the harmonic balance method, the nonlinear equation for harmonic number j for vector $\widetilde{\boldsymbol{X}}_j$ is written as:

$$\left[\boldsymbol{K} + i\omega_j \boldsymbol{C} - \omega_j^2 \boldsymbol{M}\right] \widetilde{\boldsymbol{X}}_j + \boldsymbol{F}_j(\widetilde{\boldsymbol{X}}_j) = \boldsymbol{P}_j \tag{3.47}$$

In general the large-scale finite element models of bladed disks consist of millions of degrees of freedom. Solving equation (3.47) directly for such systems would be computationally prohibited. In order to reduced the computational effort, the reduction of model is necessary. For this the high-accuracy model reduction method, which has been presented in Ref. [85], is used. The reduction method allows for significant reduction in the number of degrees of freedom, because only the DOFs of the nonlinear contact interaction need to be kept in the reduced order model. At the same time, the reduction method offers exceptionally high accuracy for the reduced model. Using this approach, the equation of motion in frequency domain can be reformulated as:

$$\boldsymbol{R}(\boldsymbol{X}) = \boldsymbol{X} - \boldsymbol{X}_{lin} + \boldsymbol{A}(\omega)\boldsymbol{F}(\boldsymbol{X}) \tag{3.48}$$

Where, on the left-hand side of the equation $\boldsymbol{R}$ is the residual vector for all nonlinear degrees of freedom; the vector $\boldsymbol{X}$ is the nonlinear multiharmonic amplitudes determined for all DOF on the nonlinear contact interfaces; $\boldsymbol{F}(\boldsymbol{X})$ is the multiharmonic nonlinear contact forces and $\boldsymbol{X}_{lin}$ is the vector of harmonic coefficients without the application of nonlinear contact forces. The multiharmonic forced response function (FRF) matrix $\boldsymbol{A}(\omega)$ is expressed through the FRF matrices of the individual harmonics:

$$\boldsymbol{A}(\omega) = diag\left(\boldsymbol{A}_0, \begin{bmatrix} \boldsymbol{A}_{k_1}^{\mathrm{Re}} & \boldsymbol{A}_{k_1}^{\mathrm{Im}} \\ -\boldsymbol{A}_{k_1}^{\mathrm{Im}} & \boldsymbol{A}_{k_1}^{\mathrm{Re}} \end{bmatrix}, \ldots, \begin{bmatrix} \boldsymbol{A}_{k_n}^{\mathrm{Re}} & \boldsymbol{A}_{k_n}^{\mathrm{Im}} \\ -\boldsymbol{A}_{k_n}^{\mathrm{Im}} & \boldsymbol{A}_{k_n}^{\mathrm{Re}} \end{bmatrix}\right) \tag{3.49}$$

The FRF matrix calculation for dynamic problems with friction forces can be done with high accuracy using the reduction method developed in Ref. [85]. The method allows to calculate the relative displacement of the contact pairs by using of the local flexibility information of for the degree of freedom on the contact interfaces. The FRF matrix is written in the form:

$$\boldsymbol{A}_{k_j} = \boldsymbol{A}^0 + \boldsymbol{A}^d(k_j\omega) \tag{3.50}$$

Where, $\boldsymbol{A}^0$ is the flexibility matrix calculated exactly for the contact nodes at a reference frequency ω_0 as

$$\left[\boldsymbol{K} - \omega_0^2\boldsymbol{M}\right]\boldsymbol{A}^0 = \boldsymbol{I} \tag{3.51}$$

On the right-hand side of the equation $\boldsymbol{I}$ is the unit matrix. The value of the reference frequency ω_0 for most practical applications can be chosen as 0. For structures with rigid body motions, the reference frequency needs to be chosen as non-zero, but far from every natural frequency. For $\omega = 0$ the equation system for the flexibility matrix calculation simplifies to:

$$\boldsymbol{K}\boldsymbol{A}^0 = \boldsymbol{I} \tag{3.52}$$

The flexibility matrix is only calculated once, before the nonlinear solution of the forced response. For solving Eq. (3.51), the CalculiX FE solver is used.

The second, dynamic term, in Eq. (3.59), is expressed as:

$$\boldsymbol{A}^d(\omega) = \sum_{j=1}^{N_m} \frac{\left(\omega^2 - \omega_0^2 - i\eta_j\omega_j^2\right)\boldsymbol{\phi}_j\boldsymbol{\phi}_j^T}{\left(\omega_j^2 - \omega_0^2\right)\left((1+i\eta_j)\omega_j^2 - \omega^2\right)} \tag{3.53}$$

Where, N_m is the number of mode shapes included in the reduced order model; ω_j, $\boldsymbol{\phi}_j$ and η_j are the j-th natural frequency, mode shape and damping.

The solution of the equation of motion in Eq. (3.48) is obtained with the Newton-Raphson method. The initial solution is iteratively calculated using the following expression:

$$\boldsymbol{J}\left(\boldsymbol{X}^{(k)}\right)\left(\boldsymbol{X}^{(k+1)} - \boldsymbol{X}^{(k)}\right) = \boldsymbol{R}\left(\boldsymbol{X}^{(k)}\right) \tag{3.54}$$

where the Jacobian matrix of the nonlinear equation $\boldsymbol{J} = \partial\boldsymbol{R}/\partial\boldsymbol{X}$ is calculated analytically (see Refs. [76] and **??**). The solution along the frequency range of interest is efficiently obtained using solution continuation techniques.

Sensitivity of nonlinear forced response for mistuned bladed disks

The sensitivity of the nonlinear forced response amplitudes for a converged solution $\boldsymbol{X}^*$ can be calculated by taking the derivative of the residual equation, Eq. 3.48. With the help of the already calculated Jacobian matrix it can be written:

$$\frac{\partial \boldsymbol{R}(\boldsymbol{X}^*)}{\partial \gamma} = \boldsymbol{J}(\boldsymbol{X}^*)\frac{\partial \boldsymbol{X}^*}{\partial \gamma} = \left[\frac{\partial \boldsymbol{A}^0}{\partial \gamma} + \frac{\partial \boldsymbol{A}^d}{\partial \gamma}\right](\boldsymbol{F}(\boldsymbol{X}^*) - \boldsymbol{P}) \tag{3.55}$$

The sensitivity of the static term of the FRF matrix, the flexibility matrix, is calculated only once using CalculiX as:

$$\left[\boldsymbol{K}(\boldsymbol{r}) - \omega_0^2 \boldsymbol{M}\right]\frac{\partial \boldsymbol{A}^0}{\partial \gamma} = \frac{\partial \boldsymbol{K}(\boldsymbol{r})}{\partial \gamma}\boldsymbol{A}^0 \tag{3.56}$$

The derivative of the dynamic term with respect to the anisotropy parameter is

$$\frac{\partial \boldsymbol{A}^d(\omega, \boldsymbol{r})}{\partial r_k} = \sum_{j=1}^{N_m} \frac{\partial c_j}{\partial r_k}\boldsymbol{\phi}_j\boldsymbol{\phi}_j^T + c_j\left(\frac{\partial \boldsymbol{\phi}_j}{\partial r_k}\boldsymbol{\phi}_j^T + \boldsymbol{\phi}_j\frac{\partial \boldsymbol{\phi}_j^T}{\partial r_k}\right) \tag{3.57}$$

where $c_j = \left(\omega^2 - \omega_0^2 - i\eta_j\omega_j^2\right) / \left[\left(\omega_j^2 - \omega_0^2\right)\left((1 + i\eta_j)\omega_j^2 - \omega^2\right)\right]$; ω_j, η_j and $\boldsymbol{\phi}_j$ are natural frequency, modal damping and mode shape; the derivative $\partial c_j / \partial \gamma$ is calculated taking into account the dependency of the modal properties of the bladed disk on the anisotropy angles and obtaining the modal sensitivity properties as it is described in the previous section; N_m is the total number of modes used for the calculation of the dynamic FRF matrix component, $\boldsymbol{A}^d$.

3.4.3 Nonlinear forced response of tuned bladed disks

The cyclic symmetry condition can be applied for the analysis of forced response of tuned bladed disks as it has been proven in Ref. [70].

The equation of motion for a cyclic symmetric sector can be written in the form:

$$\begin{aligned} &\boldsymbol{K}_S\boldsymbol{x}(t) + \boldsymbol{C}_S\dot{\boldsymbol{x}}(t) + \boldsymbol{M}_S\ddot{\boldsymbol{x}}(t) + \\ &+\boldsymbol{f}_S(\boldsymbol{x}(t)) + \boldsymbol{f}_l(\boldsymbol{x}(t - T/N), \boldsymbol{x}(t)) + \boldsymbol{f}_r(\boldsymbol{x}(t), \boldsymbol{x}(t + T/N)) = \boldsymbol{p}_1(t) \end{aligned} \tag{3.58}$$

where $\boldsymbol{K}_S$, $\boldsymbol{C}_S$ and $\boldsymbol{M}_S$ are stiffness, damping and mass matrices for the substructure sector; $\boldsymbol{x}(t)$ is vector of displacements for the sector ; $\boldsymbol{f}_S(\boldsymbol{x}(t))$ is the vector of nonlinear forces applied to nodes belonging to the sector; $\boldsymbol{f}_l(\boldsymbol{x}(t - T/N), \boldsymbol{x}(t))$, $\boldsymbol{f}_r(\boldsymbol{x}(t), \boldsymbol{x}(t + T/N))$ are nonlinear forces obtained in the results of interaction with neighboring sectors at the left and at the right sector boundaries. The vibration of any j-th sector of tuned bladed disk can be expressed through $\boldsymbol{x}(t)$ in the form: $\boldsymbol{x}_j = \boldsymbol{x}(t - \alpha(j - 1))$.

For the tuned bladed disks, the same high-accuracy model reduction method can be applied, and one arrives to Eq. (3.48).

The FRF matrix, for tuned bladed disks is expressed as

$$\boldsymbol{A}_{k_j} = \boldsymbol{A}_{ND}^{0} + \boldsymbol{A}_{ND}^{d}(k_j\omega) \tag{3.59}$$

Where, $\boldsymbol{A}_{ND}^{0}$ is the flexibility matrix calculated exactly for the contact nodes. For tuned bladed disks, modeled with sector model, the flexibility matrix and the mode shapes have sinusoidal spatial distribution along the circumference of the bladed disk, they are described by the number of nodal diameters, ND. For the calculation of the FRF matrix not all ND modes and flexibility matrices are required. The ND of the spatial harmonic used is dependent on the harmonic describing the time variation, given by the equation:

$$ND\left(k_j\right) = \begin{cases} \mathrm{mod}(k_j, N) \text{for mod } (k_j, N) \leq N/2 \\ -\left(N - \mathrm{mod}(k_j, N)\right) \text{for mod } (k_j, N) > N/2 \end{cases} \tag{3.60}$$

The flexibility matrix, the first term in Eq. (3.59) is calculated at a reference frequency ω_0 as

$$\left[\boldsymbol{K}_S^{ND} - \omega_0^2 \boldsymbol{M}_S^{ND}\right] \boldsymbol{A}_{ND}^{0} = \boldsymbol{I} \tag{3.61}$$

The matrices $\boldsymbol{K}_S^{ND}$ and $\boldsymbol{M}_S^{ND}$ are the stiffness and mass matrices of the sector model for the given nodal diameter. On the right-hand side of the equation $\boldsymbol{I}$ is the unit matrix. The value of the reference frequency ω_0 for most practical applications can be chosen as 0. For structures with rigid body motions, the reference frequency needs to be chosen as non-zero, but far from every natural frequency. For $\omega = 0$ the equation system for the flexibility matrix calculation simplifies to a linear static problem:

$$\boldsymbol{K}_S^{ND} \boldsymbol{A}_{ND}^{0} = \boldsymbol{I} \tag{3.62}$$

Equation (3.61) is solved only once, before the nonlinear solution of the forced response. For this purpose, the CalculiX FE solver is used.

The second frequency dependent dynamic term, in Eq. (3.59), is expressed as:

$$\boldsymbol{A}_{ND}^{d}\left(\omega\right) = \sum_{j=1}^{N_m} \frac{\left(\omega^2 - \omega_0^2 - i\eta_{NDj}\omega_{NDj}^2\right) \boldsymbol{\phi}_{NDj}\boldsymbol{\phi}_{NDj}^T}{\left(\omega_{NDj}^2 - \omega_0^2\right)\left((1 + i\eta_{NDj})\omega_{NDj}^2 - \omega^2\right)} \tag{3.63}$$

Where, N_m is the number of mode shapes included in the reduced order model; ω_{NDj}, $\boldsymbol{\phi}_{NDj}$ and η_{NDj} are the j-th natural frequency, mode shape and damping for the selected ND.

The Newton-Raphson method for obtaining the solution of the equation of motion can be applied in the same manner as for mistuned bladed disks.

3.4.4 Modeling of additional parts of the bladed disk assembly for non-linear forced response

Bladed disks, as its name suggests, consist of a disk where the individual blades are inserted. While they are never integral parts for turbine stages, for the forced response analysis they are always considered together. In certain bladed disk assemblies additional parts, such as under-platform dampers (UPD) and retainers are included. Generally friction forces are negligible on the retainers, but if under-platform dampers are included in the bladed disk design the appearing friction forces contribute to the damping of the forced vibrations.

A method has been developed for including additional parts such as under-platform dampers into the bladed disk assembly. The input of the modal properties and flexibility matrix is handled separately from the rest of the bladed disk structure. Which means, the finite element model of the UPD model is created. The damper is placed in the global coordinate system of the 1$^{\mathrm{st}}$ blade and its coordinates are defined by its place under the blade platform. In agreement with the method of high-accuracy model reduction, which requires free contact interfaces, the damper does not have any boundary conditions. Therefore, modal properties calculated for the UPD include the rigid-body modes.

The modal properties and the flexibility matrix of stand-alone UPD is read by Conta-Dyn and it is included in the reduced order model of the bladed disk.

For asymmetric mistuned bladed disks the mode shapes and the flexibility matrix of UPDs are rotated to the position between the respective blades. The mode shape j for the i^{th} UPD is obtained by the rotation

$$\boldsymbol{\phi}_j^i = \boldsymbol{R}_B^i \boldsymbol{\phi}_j \tag{3.64}$$

where, $\boldsymbol{\Phi}_j$ is mode shape j of the stand-alone UPD and $\boldsymbol{R}_B^i$ is the rotation matrix for bladed disk sector i.

The rotation of the flexibility matrix for blade sector i is done by

$$\boldsymbol{X}^i = \boldsymbol{R}_B^i \boldsymbol{A}_0 {\boldsymbol{R}_B^i}^T \tag{3.65}$$

where, $\boldsymbol{A}_0$ is the flexibility matrix for the stand-alone UPD.

3.4.5 Calculation of the sensitivities with respect to material anisotropy angles described in the local coordinate system of the blades

For the application of single crystal bladed disks, the commonly used description of the single crystal material orientation are the anisotropy angles. However, in the open-source

FE software CalculiX a more general set of parameters are used for the description of anisotropy orientation. This set of parameters are the rotation vector components that are used for the sensitivity calculations [46]. The advantage of the rotation vectors is that they are defined in the global CS. By choosing the rotation vectors as design variables CalculiX can be used for the calculation of the sensitivities of any other structure with anisotropic material.

The material CS describing the crystal orientation of each blade in the global CS is defined by the rotation vector:

$$\boldsymbol{v} = \begin{bmatrix} v_x \\ v_y \\ v_z \end{bmatrix} \tag{3.66}$$

The rotation matrix can be then expressed as:

$$\boldsymbol{R}(\boldsymbol{v}) = \boldsymbol{I} + \frac{\sin(\|\boldsymbol{v}\|)}{\|\boldsymbol{v}\|}\widetilde{\boldsymbol{\omega}}_{\boldsymbol{v}} + \frac{1-\cos(\|\boldsymbol{v}\|)}{\|\boldsymbol{v}\|^2}\widetilde{\boldsymbol{\omega}}_{\boldsymbol{v}}\widetilde{\boldsymbol{\omega}}_{\boldsymbol{v}} \tag{3.67}$$

Where, $\widetilde{\boldsymbol{\omega}}_{\boldsymbol{v}}$ is the skew-symmetric matrix defined in the global coordinate system by the rotation vector components as:

$$\widetilde{\boldsymbol{\omega}}_{\boldsymbol{v}} = \begin{bmatrix} 0 & -v_z & v_y \\ v_z & 0 & -v_x \\ -v_y & v_x & 0 \end{bmatrix} \tag{3.68}$$

and $\boldsymbol{I}$ is the identity matrix.

The sensitivities of the finite element calculations are obtained with respect to the rotation vector components, defined in the global CS, but for assessment of the anisotropy effect the sensitivity with respect to measured experimental angles are needed. In order to calculate the sensitivities with respect to the anisotropy angles, the sensitivities to the rotation vectors must be transformed into the blade coordinate system. The transformation can be carried out using the chain rule:

$$\frac{\partial a}{\partial \boldsymbol{\Gamma}} = \begin{bmatrix} \partial v_x/\partial\alpha & \partial v_y/\partial\alpha & \partial v_z/\partial\alpha \\ \partial v_x/\partial\beta & \partial v_y/\partial\beta & \partial v_z/\partial\beta \\ \partial v_x/\partial\zeta & \partial v_y/\partial\zeta & \partial v_z/\partial\zeta \end{bmatrix} \frac{\partial a}{\partial \boldsymbol{v}} = \frac{\partial \boldsymbol{v}}{\partial \boldsymbol{\Gamma}} \cdot \frac{\partial a}{\partial \boldsymbol{v}} \tag{3.69}$$

where a is any parameter of interest, and in this case this is natural frequency, modal displacement or forced response displacement. The derivation of the Jacobian matrix, $\boldsymbol{J} = \partial \boldsymbol{v}/\partial \boldsymbol{\Gamma}$, is derived here in analytical form.

3.5 Calculation of the transformation matrix between global and blade coordinate systems

For the expression derived for the Jacobian in Eq. (3.69) it can be stated, that the infinitesimal rotations expressed through rotation matrices of both coordinate systems: global CS and blade CS, are identical. The infinitesimal rotation $\delta\boldsymbol{\omega} = \{\delta\omega_x, \delta\omega_y, \delta\omega_z\}$ can be expressed through the rotation matrix in the form, see Ref. [12]:

$$\delta\widetilde{\boldsymbol{\omega}} = \delta\boldsymbol{R}\boldsymbol{R}^T \tag{3.70}$$

Substituting Eq. (3.6) in Eq. (3.70) the expression for infinitesimal rotations is obtained in through manufacturer material anisotropy angles in the form:

$$\begin{gathered}\delta\widetilde{\boldsymbol{\omega}} = \delta\boldsymbol{R}_G\boldsymbol{R}_G^T = \left(\boldsymbol{R}_B\frac{\partial\boldsymbol{R}_M}{\partial\alpha}\boldsymbol{R}_M^T\boldsymbol{R}_B^T\right)d\alpha + \\ \left(\boldsymbol{R}_B\frac{\partial\boldsymbol{R}_M}{\partial\beta}\boldsymbol{R}_M^T\boldsymbol{R}_B^T\right)d\beta + \left(\boldsymbol{R}_B\frac{\partial\boldsymbol{R}_M}{\partial\zeta}\boldsymbol{R}_M^T\boldsymbol{R}_B^T\right)d\zeta\end{gathered} \tag{3.71}$$

Taking into account that the matrix $\delta\widetilde{\boldsymbol{\omega}}$ obtained from Eq. (3.71) is a spin matrix (see Eq. (3.68)) and that each summand in Eq. (3.71) is a spin matrix, this equation can be rewritten in a vector form:

$$\delta\boldsymbol{\omega} = \boldsymbol{\omega}_\alpha\delta\alpha + \boldsymbol{\omega}_\beta\delta\beta + \boldsymbol{\omega}_\zeta\delta\zeta \tag{3.72}$$

On another side, the vector of infinitesimal rotations can be expressed through the rotation vector, $\boldsymbol{v}$, describing the material anisotropy in global CS. Using an available expression (see Refs. [12] and [68]), we have:

$$\delta\boldsymbol{\omega} = \boldsymbol{T}^T\delta\boldsymbol{v} \tag{3.73}$$

where the tangent operator matrix, $\boldsymbol{T}$, is expressed as:

$$\boldsymbol{T}(\boldsymbol{r}) = \boldsymbol{I} + \frac{\cos(\|\boldsymbol{v}\|) - 1}{\|\boldsymbol{v}\|^2}\widetilde{\boldsymbol{\omega}}_{\boldsymbol{v}} + \frac{\|\boldsymbol{v}\| - \sin(\|\boldsymbol{v}\|)}{\|\boldsymbol{v}\|^3}\widetilde{\boldsymbol{\omega}}_{\boldsymbol{v}}\widetilde{\boldsymbol{\omega}}_{\boldsymbol{v}} \tag{3.74}$$

Equalizing the terms upon independent variations of the rotation matrix parameters in Eqs. (3.72) and (3.73), we obtain the equations for the determination of the rows of the Jacobian matrix, $\boldsymbol{J}$, used for the transformation between the two coordinate systems: the global CS and blade CS:

$$\boldsymbol{T}^T\frac{\partial\boldsymbol{v}}{\partial\alpha} = \boldsymbol{\omega}_\alpha \ , \ \boldsymbol{T}^T\frac{\partial\boldsymbol{v}}{\partial\beta} = \boldsymbol{\omega}_\beta \ , \ \boldsymbol{T}^T\frac{\partial\boldsymbol{v}}{\partial\zeta} = \boldsymbol{\omega}_\zeta \tag{3.75}$$

3.6 Visualization of forced response in time domain

The forced response amplitudes are only calculated directly for the nodes that are included in the reduced order model. For bladed disks, these nodes are the nodes on the nonlinear contact patches, the nodes where the harmonic excitation is applied and some nodes of interest (e.g. blade tip or mid-span). In many cases, these nodes are sufficient for the evaluation of the forced response.

In some cases, it is necessary to obtain the forced response amplitudes for the whole FE mesh. The visualization of the operational deflection shape for all FE nodes gives additional information compared the linear mode shapes and the nonlinear forced response amplitudes of the nodes of interest. The screening for the nodes of interest is done on the linear mode shapes. For some nonlinear systems with friction forces the node of maximum displacement can change along the airfoil and to identify such change the visualization of the forced response for the full model is an ideal tool. Moreover, due to the mistuning the location of the maximum forced response can vary between blades.

3.6.1 Recovery of forced response in time domain for asymmetric systems

The equations for the calculation of the forced response displacement in time domain are written in the form of modal expansion, for asymmetric dynamic systems as

$$\boldsymbol{x}(\tau) = \sum_{k=1}^{nHarms} \sum_{j=1}^{nModes} \boldsymbol{\phi}_j Re\left(e^{i \cdot kHarm(k) \cdot \tau} \overline{c}_{k,j}\right) \tag{3.76}$$

where $\boldsymbol{\phi}_j$ is the j-th mode shape, $\overline{c}_{k,j}$ is the complex conjugate of the modal coefficient for k-th harmonic number and j-th mode, $nModes$ is the number of modes and $nHarms$ is the number of harmonics used for the forced response calculation. The τ discrete pseudo time is defined on $\tau \in [0, 2\pi]$ and $kHarm$ is a vector of the harmonics used for the forced response calculation.

3.6.2 Recovery of forced response in time domain for symmetric systems

The recovery of the displacements for cyclic symmetric systems takes the form

$$\boldsymbol{x}(\tau) = \sum_{k=1}^{nHarms} Re\left(\sum_{j=1}^{nModes} \boldsymbol{\phi}^j_{ND(k)} e^{i \cdot kHarm(k) \cdot \tau} \overline{c}_{k,j}\right) \tag{3.77}$$

where $\boldsymbol{\phi}^j_{ND(k)}$ is j-th mode shape of $ND(k)$ nodal diameter that corresponds to k-th harmonic number. The discrete pseudo time for cyclic symmetric systems is defined on

$\tau \in [0, 2\pi/EO]$, where EO is the engine order of the principal excitation. The relationship between time harmonics and the spatial harmonic (ND) of the mode shapes is described in Eq. 3.60. For the mode shapes with negative ND values (negative harmonic index), the following relationship is applied: $\boldsymbol{\phi}_{ND} = \overline{\boldsymbol{\phi}}_{-ND}$.

3.6.3 Recovery of sensitivity of forced response in time domain for asymmetric systems

For mistuned bladed disks, the sensitivity of the mode shapes can be visualized for all FE nodes, by taking the derivative of Eq. 3.76 with respect to the respective material anisotropy angles:

$$\frac{\partial \boldsymbol{x}(\tau)}{\partial \gamma} = \sum_{k=1}^{nHarms} \sum_{j=1}^{nModes} \frac{\partial \boldsymbol{\phi}_j}{\partial \gamma} Re\left(e^{i \cdot kHarm(k) \cdot \tau} \overline{c}_{k,j}\right) + \boldsymbol{\phi}_j Re\left(e^{i \cdot kHarm(k) \cdot \tau} \frac{\partial \overline{c}_{k,j}}{\partial \gamma}\right) \quad (3.78)$$

where γ can be any design variable describing crystal orientation of single crystal blades.

The implementation of the previous equations has been carried out in the framework of the current project. The InterDyn code reads the mode shapes and the modal coefficients that are stored in CalculiX result file (.frd) and in ContaDyn result file formats respectively. After evaluating the summations, the nodal values for each time step are written in the results format of CalculiX. This allows for the visualization of the time domain results with the already available capabilities of CalculiX GraphiX.

It is worth noting, that the above formulations calculate the forced response as a modal expansion, neglecting the local flexibilities on the contact interfaces. The method gives sufficient accuracy for the visualization of the forced response on the airfoil. However, it is not suitable for detailed investigation of the contact behavior of the nonlinear friction elements in time domain.

During the multiharmonic nonlinear forced response calculation, the harmonic coefficients of the contact forces and relative displacements are calculated. By evaluating the Fourier expansion formula for the relative displacements and for the contact forces, the time domain solution can be obtained. Using InterDyn the nodal values of the contact forces and relative displacements are written in CalculiX result format and can be visualized on the FE mesh in CacluliX GraphiX. The relative displacements and contact forces can be used for the identification of the contact separation in time domain.

3.7 Development of integrator-interface code InterDyn and its use for the analysis of nonlinear forced response and sensitivities

For the calculation of the nonlinear forced response and its sensitivities an automated workflow has been developed, see Fig. 3.2. During the PhD project it has been of particular importance of developing a user interface that allows the efficient pre- and post-processing for the forced response analyses.

The implementation is based on three main modules, namely CalculiX, ContaDyn and InterDyn. The FE calculations are done using CalculiX. The nonlinear forced response solver code is called ContaDyn. InterDyn is used as a pre-processing tool for the selection of pair of nonlinear contact nodes, provides an interface for the input data for ContaDyn from CalculiX. Additionally, it provides an interface from ContaDyn to CalculiX for the visualization of the forced response results.

The workflow of the nonlinear forced response analysis of the bladed disks starts with a sector model of the bladed disk. The user is requested to select the nodes where the harmonic loads will be applied and where the output of the forced response amplitudes and sensitivities will be requested. For nonlinear studies with friction interfaces, the user is also requested to select FE nodes on the contact interfaces. At these FE nodes nonlinear friction contact elements will be applied for the forced response analysis. For coarse FE meshes or for fine FE meshes of tuned bladed disks, nonlinear contact elements can be applied to all FE nodes on the contact interfaces. However, for fine meshes or for full mistuned bladed disks, using all nodes on the contact patches for nonlinear forced response calculations would be computationally very expensive. In order to reduce computational effort by a coarser discretization in the ROM, the user is allowed to select a subset of nodes on the contact patch. The selection of the nonlinear contact nodes needs to be done only for one of the contact patches in the contact interaction.

In the next step, the InterDyn script will find select the nearest FE node on the matching contact interface for each nonlinear contact nodes that has previously been selected. The nonlinear contact elements are applied for the contact pairs selected this way.

In case of the mistuned bladed disk study, the full model of the bladed disk is created with the *ccx_complex* code developed in [46]. When the full FE model of bladed disk is created, all set of nodes previously selected for the sector model will be expanded for the other blade sectors of the bladed disk. Additionally, all boundary conditions such as

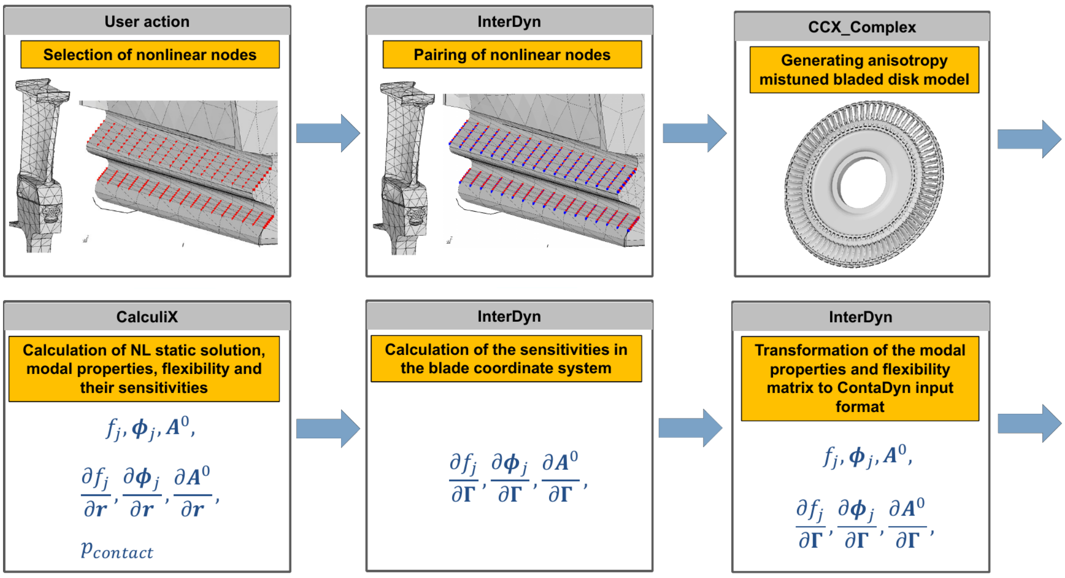

(a) Part 1

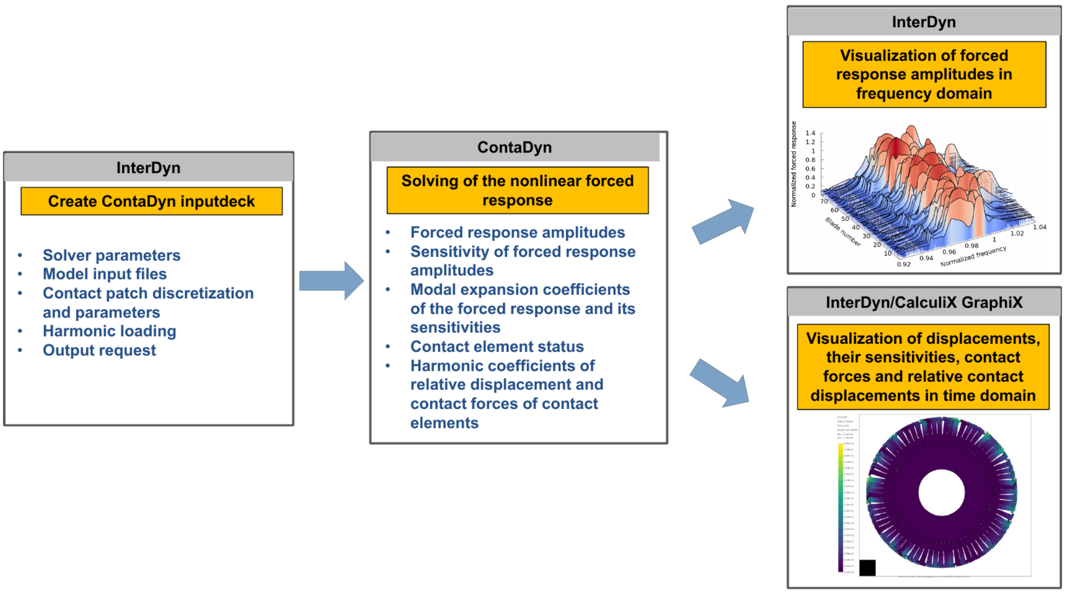

(b) Part 2

Figure 3.2: Workflow of the nonlinear forced response calculations

single-point constraints (SPC), multi-point constraints (MPC) or friction contact elements are expanded for all bladed disk sectors. The script allows the definition of user-defined or random anisotropy mistuning pattern.

In the next step, the static displacement field due to centrifugal loading and gas load is calculated including nonlinearities from friction contact interfaces and large deflections. For the solving the static problem, the FE solver of CalculiX is used: CalculiX CrunchiX. Static normal pressure values obtained on the nonlinear friction contact interfaces and stored for the subsequent forced response analysis. For each contact element, the static contact pressure is assigned individually.

For the subsequent modal calculation, the nonlinear contact interfaces are freed. The nonlinear friction contact elements are removed and the free modes are obtained. The stiffness matrix used in the modal calculation is the tangent stiffness matrix of the last converged step from the nonlinear static solution.

The flexibility matrix is obtained around the same converged static solution as the modal properties. The nonlinear contact elements are removed for the flexibility calculation. The flexibility matrix is obtained for all degrees of freedom that are included in the reduced order model of the nonlinear forced response calculation. The equation 3.51 is solved for every DOF separately, by applying unit force for the specific DOF.

For anisotropy mistuned bladed disks, the sensitivity of the nonlinear forced response with respect to the anisotropy angles can be obtained. In order to do that, the forced response solver requires the sensitivities of the modal properties and the flexibility matrix. These sensitivities can be obtained with CalculiX after the modes and the flexibility matrix is obtained. In CalculiX, the sensitivities are calculated with respect to the rotation vector components defined in the global coordinate system.

The crystal orientation of the single crystal blades are measured for each blade individually. The measured anisotropy angles are defined in the coordinate system of the blades. Because the interest is in the sensitivity with respect to the anisotropy angles that are defined in the local coordinate system of each blade, the sensitivities need to be transformed into the coordinate system of the blades. This calculation can be done with the code in InterDyn.

As the next step, the efficient interface implemented in InterDyn is used for taking the results (modes, flexibility matrix and their sensitivities) and convert them in the input format of ContaDyn.

The ContaDyn simulations can be started with the help of an inputdeck text file.

This inputdeck can get very lengthy for nonlinear forced response simulations of tuned and mistuned bladed disks. Therefore, InterDyn provides capabilities for fast creation of ContaDyn inputdecks.

In the ContaDyn inputdeck the following data are provided

- Simulation title
- Solver parameters
- Name of the modal and flexibility input files
- Name of the sensitivity files
- Local coordinate system of the contact interfaces
- Contact pairs
- Surface area values for each contact pair
- Normal contact pressure values for each contact pair
- Contact stiffness values of the contact interfaces
- Harmonic excitation
- Output requests

ContaDyn calculates the forced response amplitudes directly for nodes included in the reduced order model. If a sensitivity study is carried out, the output for the sensitivity of the forced response amplitudes can be requested for the nodes in the reduced order model. The amplitudes are obtained over the calculated frequency range. The amplitudes can be nodal maximum or maximum in the spatial directions.

ContaDyn allows the output of the modal expansion coefficients for the forced response displacements and their sensitivities. If the mode shapes are available for all nodes in the FE model, the forced response amplitudes can be recovered for all nodes in the model. Similarly, if mode shape sensitivities for all nodes are available, forced response sensitivities can be recovered. The recovery of the forced response and their sensitivities are done for selected excitation frequency in time domain. User is allowed to select the temporal discretization for the displacement recovery over a period of vibration. The recovered displacements and their sensitivities are written in the .frd result format that can be read by the pre- and post-processing module of CalculiX: CalculiX GraphiX.

For a detailed analysis of the contact situation at the interacting surfaces, the data regarding the contact elements are written. For each frequency and for each contact element the contact status, the multiharmonic components of the relative displacement of the contact node pairs and the multiharmonic components of the contact forces are written in the local coordinate system of the contact interface. With the help of the InterDyn code, the contact forces and the relative displacements can be calculated in time domain and visualized for the contact nodes in CalculiX GraphiX.

3.8 Conclusions

In this chapter, the methods used for the analyses about the effect of blade anisotropy orientation variation on the dynamic characteristics have been presented. Important aspect is how the anisotropy orientation is modeled in the finite element models. For the finite element modeling whole bladed disk models are used and the anisotropy orientation for each blade is defined by a rotation matrix. The anisotropy angles, $\mathbf{\Gamma} = \{\alpha, \beta, \zeta\}$, measured for every blade are defined in the blade local coordinate system. The well-known expressions for the calculation of modal properties have been presented. The key differences between the modal properties for symmetric and asymmetric systems have been shown. The methods for calculation of the linear and nonlinear forced response have been presented. The forced response calculation for tuned bladed disks with cyclic symmetric conditions have been presented because such systems allow fast calculations and therefore parametric studies can be quickly done. For bladed disks with under-platform dampers, the modal parameters of damper are not calculated together with the rest of the bladed disk assembly, but as individual parts and the models are assembled in the forced response analysis.

In this research, the major development is with respect to the sensitivity analysis of the dynamic characteristics. For which the first step is to obtain the sensitivities with respect to the anisotropy angles. New methods, based on [82] and [83], have been presented for the calculation of eigenvectors. The two methods for the calculation of mode shape sensitivities, modal and algebraic methods, include computational parameters for which, the ideal value needs to be studied. When the sensitivity of the modal parameters are available, the sensitivity of the linear and nonlinear forced response can be obtained by the method presented above. Because the anisotropy angles are defined the local coordinate system of the blades, and the FE tool CalculiX calculates the sensitivities with respect to the rotation vector parameters defined in the global coordinate system, the sensitivities need to be transformed to the for each blade individually. The method for this calculation s based on equivalence of the infinitesimal rotations in both reference frames.

In the InterDyn toolbox, which serves as the interface and integrator tool, the major capabilities for the post-processing of the forced response results have been implemented. Namely, the recovery of the forced response displacements and their sensitivities in time domain, which can after post-processing be visualized in the CalculiX GraphiX.

Last, but not least a general overview of the implemented (or already available) methods that are used in this research was presented.

Chapter 4

Validation of the methods for the calculation of the sensitivity of forced response

The verification for the implemented methods presented in the chapter before is shown in this chapter. The validation for the calculation of modal properties is not required, as CalculiX is constantly validated with every new release. The calculation of linear forced response using ContaDyn can be verified against other readily available tools, e.g. CalculiX. The validation of the nonlinear forced response amplitudes is presented in chapter 7, together with the modeling strategies for the nonlinear forced response calculation. The emphasis in this chapter is on the validation of the calculated sensitivities for modal properties and forced response.

For the verification studies, three models are used: (i) cantilever beam (ii) simplified bladed disk (iii) realistic bladed disk, see Fig. 4.1.

4.1 Validation of the calculation of linear forced response

The linear forced response amplitudes calculated with ContaDyn are compared with forced response amplitudes obtained with CalculiX. CalculiX also uses the modal superposition method for the calculation of the steady state dynamic response and the method implemented in CalculiX already has been validated. Moreover, another advantage is that both CalculiX and ContaDyn use the same mode shapes for the calculation process.

For the validation, the simplified mistuned bladed disk model, shown in Fig. 4.1b is used. The bladed disk has 72 blades, and every blade has a random anisotropy axis orient-

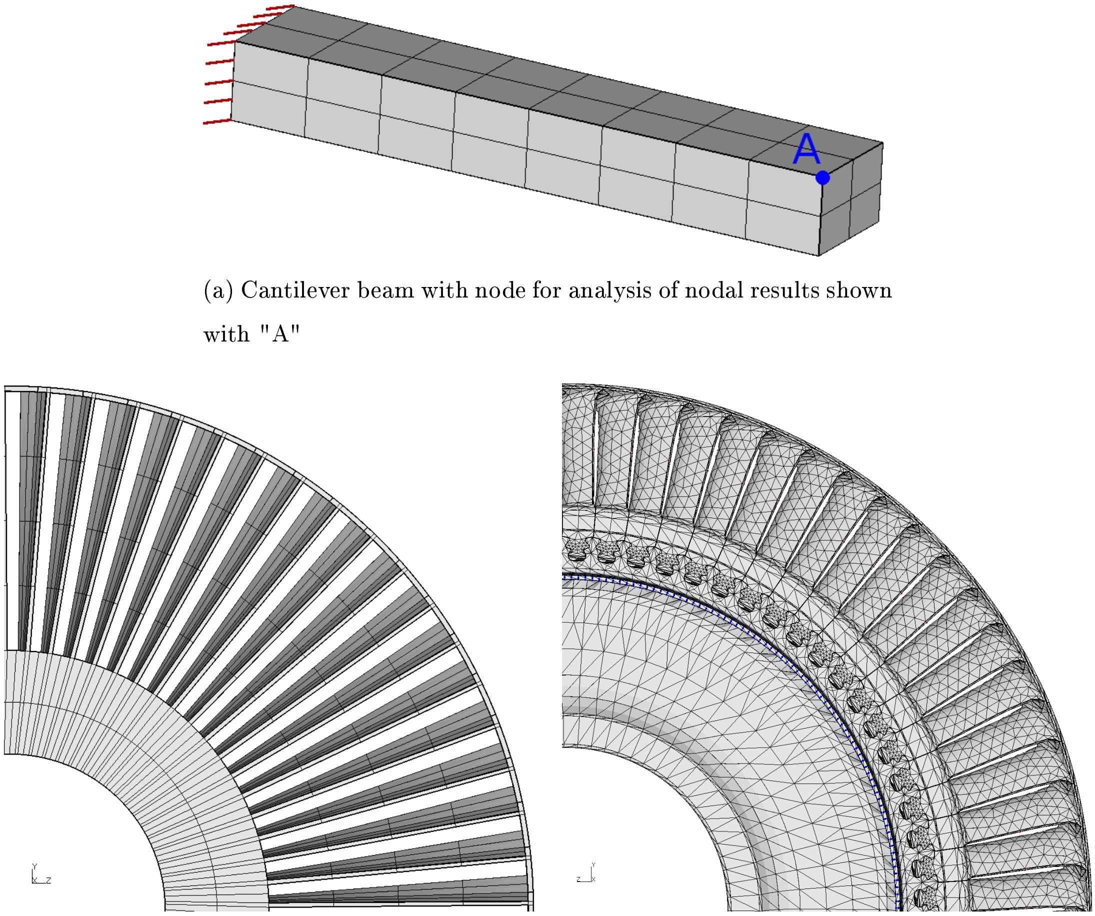

(a) Cantilever beam with node for analysis of nodal results shown with "A"

(b) Quarter of simplified bladed disk

(c) Quarter of realistic bladed disk

Figure 4.1: Models used for numerical analyses in the verification of the

ation. The modal properties are obtained considering a perturbed state due to centrifugal loading.

For the first validation example only a single concentrated harmonic force is applied on the mid-span of blade No. 1. The forced response amplitude calculated using CalculiX and ContaDyn for blade 1 shown in Fig. 4.2. The forced response amplitudes are in good agreement for the whole frequency range.

For the second validation example, the bladed disk is excited on all blades with engine order 8 excitation. For each blade, the harmonic force is applied on the same node in axial direction. The phase of the excitation force for blade j is $\alpha_j = j \cdot EO \cdot 2\pi/N$, where N is the number of blades in the bladed disk. It is worth noting that in order to obtain the same forced response the harmonic excitation need to be applied as backward traveling wave. This means, the phase shift $\alpha_j^{(CCX)} = -\alpha_j$ is applied with negative sign in CalculiX.

The linear forced response calculated at blade 1, for the engine order 8 excitation is shown in Fig. 4.3. The results calculated with ContaDyn and CalculiX are in good

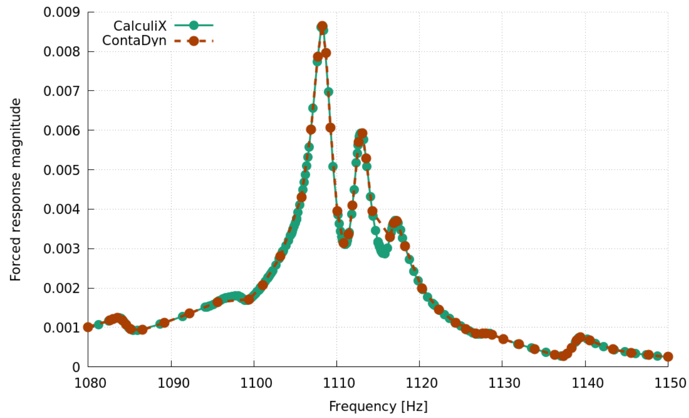

Figure 4.2: Comparison of forced response amplitudes of blade #1 calculated to excitation of one concentrated harmonic force on blade #1 using CalculiX and ContaDyn

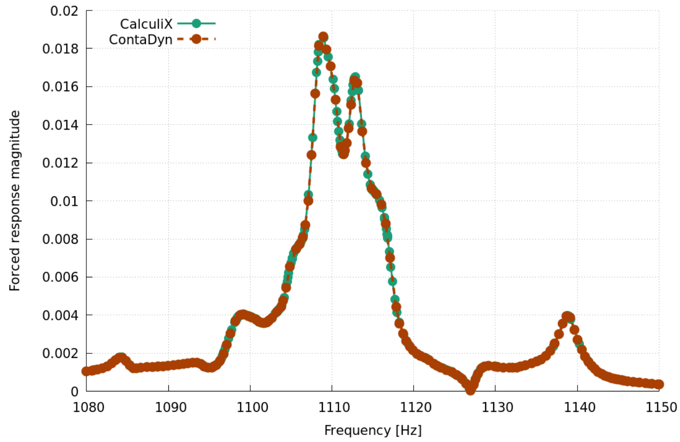

Figure 4.3: Comparison of forced response amplitudes of blade #1 calculated for EO8 excitation using CalculiX and ContaDyn

agreement for all excitation frequencies.

With the comparison of the forced response amplitudes, it can be stated the in-house code ContaDyn is validated against CalculiX. Moreover, the validated linear forced response calculation also means, that InterDyn, the interface that transfers the mode shapes between CalculiX and ContaDyn, works as expected.

4.2 Optimal finite difference step size for the calculation of the derivative of the stiffness matrix

In order to calculate the sensitivity of the eigenpairs, the derivative of the stiffness matrix with respect to the design variable need to be calculated, as derived in Eqs. (3.12) and

(3.23). As discussed earlier, in this work the finite difference evaluation of the sensitivity of the stiffness matrix is used.

For the finite difference evaluation, see Eq. (3.17), it is critical to choose an optimal finite difference step value. If finite difference step is large, it will cause large round-off errors. If the finite difference step is set too small, it will result in large truncation error. An optimal value of the finite difference step can be found, when the total error is minimum [86].

For linear problems, when $\boldsymbol{K}$ is not dependent on the displacements, the derivative of the stiffness matrix with respect to the material anisotropy angles can be expressed analytically, see Ref. [46]. Hence, the exact analytical solution for the sensitivity of natural frequencies can be used as a reference in this study.

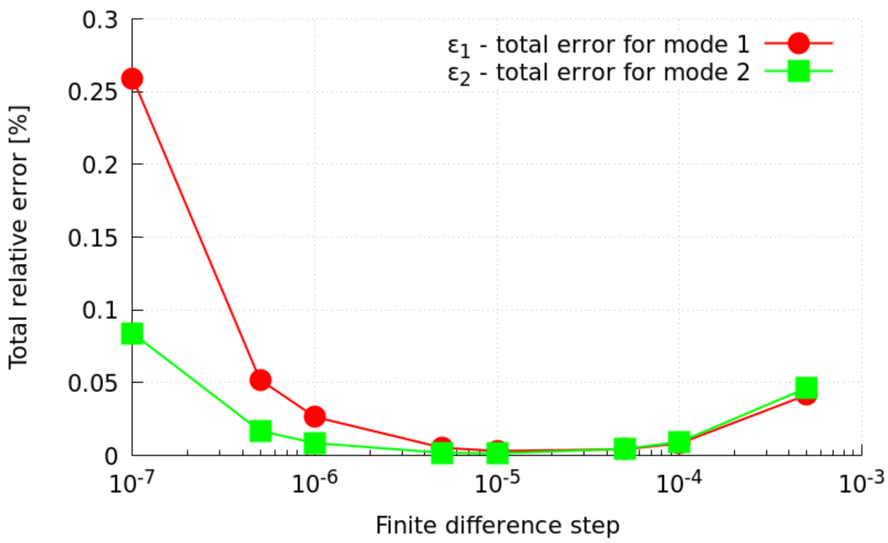

Figure 4.4: Error of the sensitivities for the 1st and 2nd natural frequencies with varying finite difference steps

The sensitivity of natural frequencies are calculated for a series of different crystal orientations. The crystal orientations were defined by the rotation vector component, which were varied between -0.5 and 0.5 in 0.1 for all three spatial directions. The crystal orientations were assigned for all possible combinations, which is $N = 1331$ individual crystal orientations. For each crystal orientation, the sensitivity of natural frequencies using the analytically derived stiffness matrix derivative and the one calculated using the finite difference method. The sensitivity has been calculated for the following finite difference steps: $\Delta h = \{10^{-7}, 5\cdot 10^{-7}, 10^{-6}, 5\cdot 10^{-6}, 10^{-5}, 5\cdot 10^{-5}, 10^{-4}, 5\cdot 10^{-4}\}$. For each finite difference step, the total error of the sensitivities has been calculated with the following equation:

$$\epsilon_j = \frac{1}{3}\sum_{i=3}^{3}\left\{\frac{1}{N}\sum_{k=1}^{N}\frac{\left|\left(\frac{\partial f_j^k}{\partial r_i}\right)_A - \left(\frac{\partial f_j^k}{\partial r_i}\right)_{FD}\right|}{max\left(\frac{\partial f_j^k}{\partial r_i}\right)_A}\right\}\cdot 100\% \tag{4.1}$$

The total error calculated for the 1st and 2nd natural frequencies, see Fig. 4.4, show that the error in the sensitivity calculation is lowest if finite difference step 10^{-5} is used. Therefore, this is the finite difference step used in the current implementation in CalculiX. For both modes, the error of sensitivities increases when smaller or larger finite steps are used.

4.3 Validation of the sensitivity of natural frequencies

The sensitivities of the natural frequencies calculated with the semi-analytic method, described in section 3.3, are compared with the sensitivity values obtained by the finite difference method. The calculation of the approximation of the derivatives by the finite difference method is performed as:

$$\frac{\partial f_j\left(\gamma\right)}{\partial \gamma} \approx \frac{f_j(\gamma+\Delta\gamma)-f_j(\gamma)}{\Delta\gamma} \tag{4.2}$$

where $\Delta\gamma = 0.001rad$ and $f_j(\gamma)$ is the j-th natural frequency.

It should be noted that the finite difference approximation allows the validation the implementation of the new method, however its accuracy is generally lower in comparison with the newly implemented semi-analytical method. The sensitivities calculated with the value of $\Delta\gamma = 0.001rad$ has been found to result in the most accurate results. The reason for the loss of accuracy in the sensitivities calculated using the finite difference method is the limited precision of the natural frequency, used in Eq. (4.2).

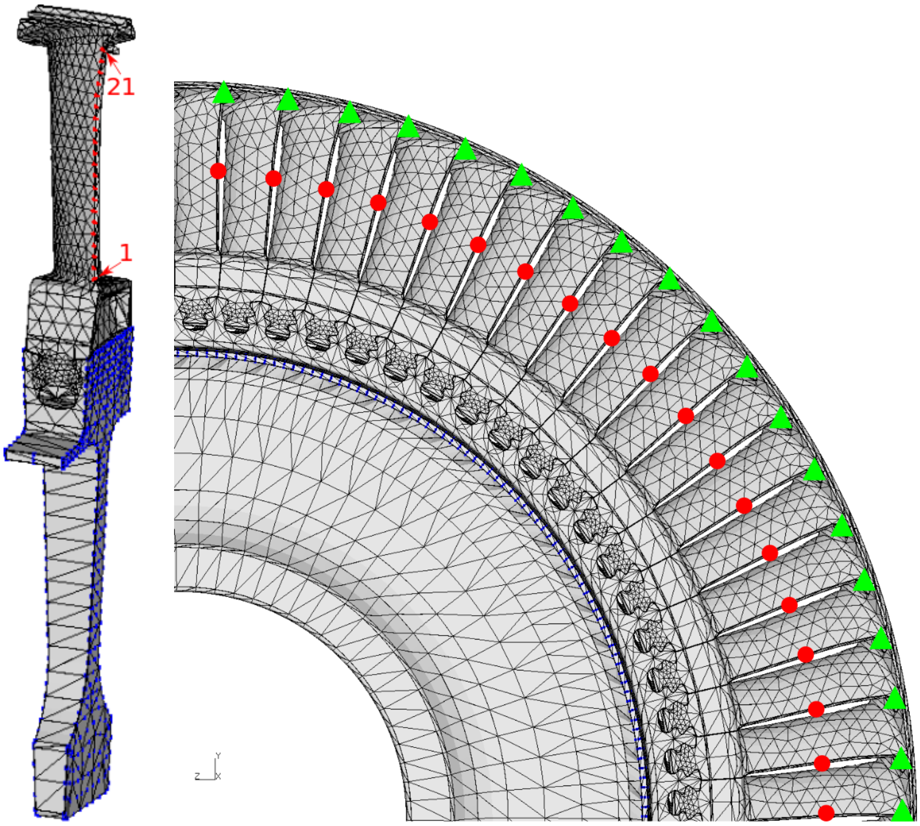

(a) Single blade

(b) Quarter of the bladed disk

Figure 4.5: Finite element models used for the validation of the sensitivity calculations

The validation of the sensitivity calculations for natural frequencies has been done for realistic bladed disk models. First, the sensitivities of the first ten natural frequencies of a single blade were calculated. The finite element model consists of quadratic tetrahedral elements with approximately 19,000 nodes. The material of the disk segment is isotropic, and the blade material is orthotropic. Fixed boundary conditions have been applied on the two sides of the disk segment (blue nodes in Fig. 4.5a), the contact interfaces on the blade-root joints are fully stuck and the shrouds are free. Centrifugal load has been applied and the static calculation has been carried out with nonlinear geometric effects included. The modal properties were calculated around the converged static solution.

The sensitivities were obtained with respect to all three anisotropy angles, $\Gamma = \{\alpha, \beta, \zeta\}$. The validation for the calculation of the natural frequency sensitivities using the new method was first done for a single blade. The sensitivities calculated using the new method are shown with filled symbols and the results obtained from the finite difference formulation is plotted with empty symbols in Fig. 4.6. The normalized natural frequency values calculated with the two methods, that are overlapping in the plot, reveal a good correspondence.

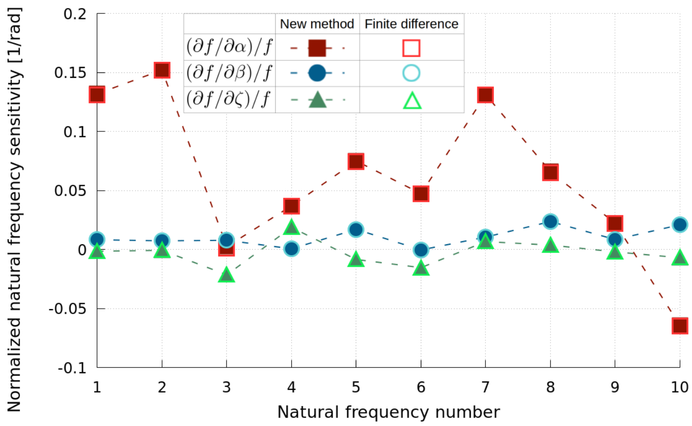

Figure 4.6: Normalized natural frequency sensitivities with respect to anisotropy angles for single blade calculated using the new method and finite differences

For the analysis of a mistuned bladed disk a full model of a bladed disk with 75 blades has been created. The random mistuning pattern was generated using realistic statistical distribution provided by the blade manufacturer for all the anisotropy angles. The finite element model consists of approximately 0.5 million nodes. The nodes shown in blue in Fig. 4.5b have fixed boundary conditions applied in axial and tangential directions. At the contact interfaces on the fir-tree and on the shrouds are fully stuck. The static analysis with centrifugal loading is performed with nonlinear geometric effects included and the static stress distribution are used as a perturbation for the subsequent modal analysis step.

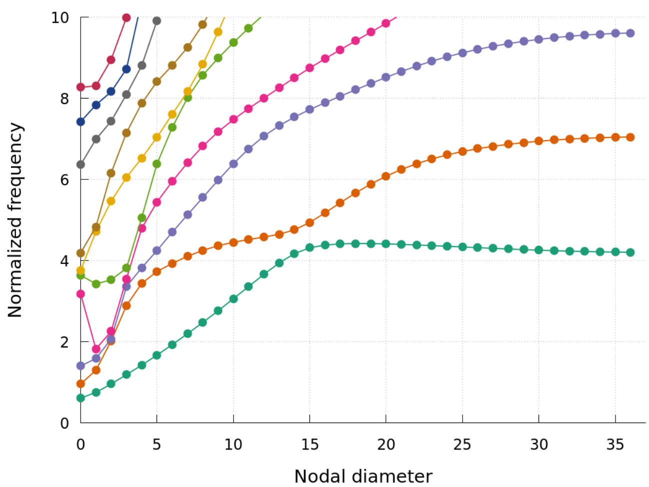

Figure 4.7: Natural frequency-nodal diameter diagram of the cyclic symmetric bladed disk model with full contact on the shrouds

The calculation of sensitivities of the natural frequencies have been validated for mistuned bladed disks by the comparison with the finite difference method. Each natural frequency sensitivity has been normalized by the perspective natural frequency.

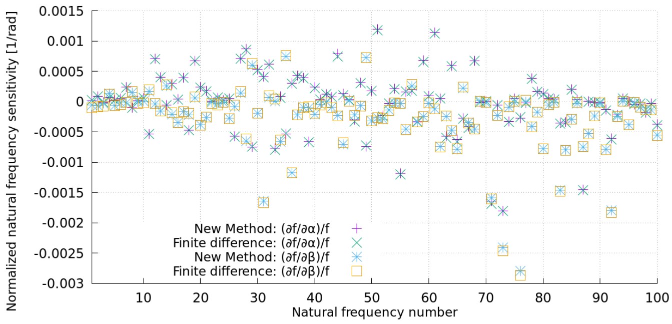

(a) Comparison of the natural frequency sensitivities for the first 100 modes obtained with two methods

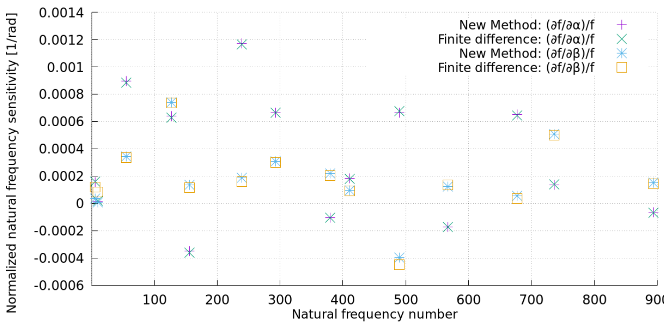

(b) Comparison of the natural frequency sensitivities for selected modes from the first 12 mode families obtained with two methods

Figure 4.8: Validation of sensitivity of natural frequencies with respect to the anisotropy angles of blade 5 for mistuned bladed disk

The results of the validation for the first 100 modes in Fig. 4.8a and for selected higher natural frequency sensitivities in Fig. 4.8b, show a good correspondence with the finite difference reference approximation values. The sensitivities are shown here with respect to anisotropy angles α, β and ζ of blade 5.

The validation of the natural frequency sensitivity calculation has been done for systems with nonlinear friction contact interfaces. For the finite difference approximation of the sensitivities, see Eq. (4.2), the natural frequencies were calculated for the perturbed and the unperturbed crystal orientations. For both calculations, the static pre-stress state is obtained for unperturbed anisotropy crystal orientations. Which means, the natural frequencies in the subsequent step are calculated for the same system matrices. For the calculation with the perturbed crystal orientation, change in the anisotropy orientation is introduced for the modal calculation step.

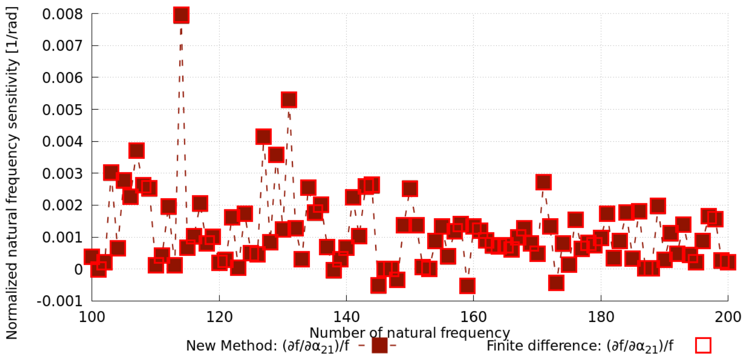

Figure 4.9: Validation of the sensitivity of natural frequencies for mistuned blade disks with (i) stuck interfaces (modes 100 to 200)

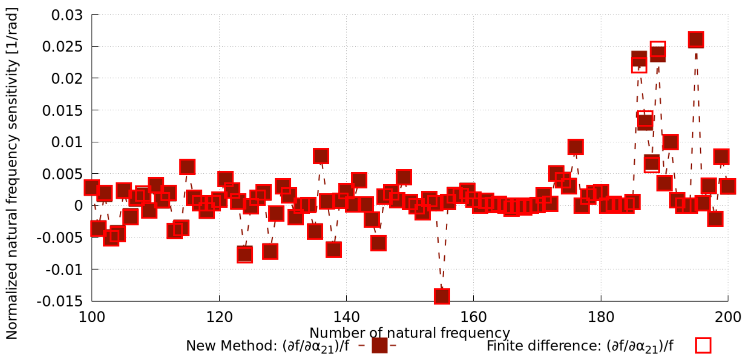

Figure 4.10: Validation of the sensitivity of natural frequencies for mistuned blade disks with (ii) sliding interfaces (modes 100 to 200)

The static calculation preceding the modal analysis is done with nonlinear friction elements included on the contact. In order to linearize the dynamic system for the modal analysis two options were studied (i) increasing the friction coefficient to a very high value resulting in a fully stuck contact (ii) decreasing the friction coefficient to 0 resulting in a perfect sliding contact.

For this validation a mistuned bladed disk with a random anisotropy mistuning pattern is used. For this bladed disk surface to surface nonlinear friction contact elements are applied on the root and shroud interfaces for every blade. The validation of the sensitivities has been done for the first 200 natural frequencies (approximately 3 mode families) with respect to the primary anisotropy angle (α) of blade number 21. The choice for blade 21 has been arbitrary. The sensitivity of natural frequencies, shown in Figs. 4.9, and 4.10, show good agreement for the new semi-analytical method and the finite difference method.

For some modes negligible differences can be observed, which is considered to be due to limited accuracy of the finite difference method.

4.4 Validation and optimal parameters for the calculation of the sensitivity of mode shapes

In section 3.3, two methods have been proposed for the calculation of the sensitivity of mode shapes of mistuned bladed disks. In this section, a numerical study is carried out for the above presented methods on the accuracy and the computational effort. The study focuses on the application for large scale finite element models with high spectral density, such as the anisotropy mistuned bladed disks.

For the enhanced modal method of the mode shape sensitivity calculation, the optimal selection for the value of parameter λ_0 is studied. For the algebraic method, the effect of the placement of the regularization coefficient is studied.

4.4.1 Optimal value of parameter for the enhanced modal method

For the first analyses, a cantilever beam is used for which the first 20 mode shapes and their sensitivities are calculated. The model consists of 720 degrees of freedom. The material of the beam is anisotropic, and the anisotropy orientation is described by the rotation vector components defined in the global coordinate system. The sensitivities are calculated with respect to the three rotation vector components.

The sensitivity of the mode shapes are calculated using the modal and the algebraic methods. For each calculation of the mode shape sensitivity with the enhanced modal method the λ_0 value has been gradually changed. Its value is varied stepwise, such that between each eigenvalue 100 λ_0 value has been selected for the mode shape sensitivity calculation.

The sensitivity of the mode shapes are analyzed for the nodal values at node A, see Fig. 4.1a, for all three spatial directions. These sensitivities are normalized with the reference values calculated with finite differences. In order to apply the finite difference formulation, the mode shapes are calculated twice, once with an initial anisotropy orientation and once with one of the rotation vector components describing the anisotropy orientation changed by a small value: $\Delta r_i = 10^{-5}$.

$$\frac{\partial \boldsymbol{\phi}(r_i)}{\partial r_i} \approx \frac{\boldsymbol{\phi}(r_i + \Delta r_i) - \boldsymbol{\phi}(r_i)}{\Delta r_i} \tag{4.3}$$

The sensitivities of the eigenvectors calculated with the enhanced modal method using continuously increasing λ_0 values are shown with continues lines. The sensitivities obtained using $\lambda_0 = (\lambda_j + \lambda_{j-1})/2$, where j is the number of mode shape under consideration, is shown with filled circle symbols. The sensitivities calculated with the algebraic method are shown with empty circle symbols. For this study the mode shapes 3, 6, 14 and 20 are picked.

The sensitivity of mode shape #3, see Fig. 4.11a, show little dependency on the value of λ_0 for most sensitivities. The negligible effect of λ_0 is due to the having 20 modes included in the modal expansion. For modes, for which the mode shape sensitivity is calculated for, has significantly lower eigenvalue that the eigenvalue of the highest mode included in the modal expansion, the value of λ_0 can be chose 0, as it is shown in [98].

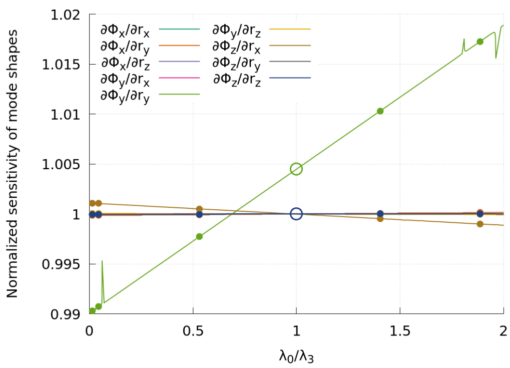

(a) Sensitivity of mode shape 3

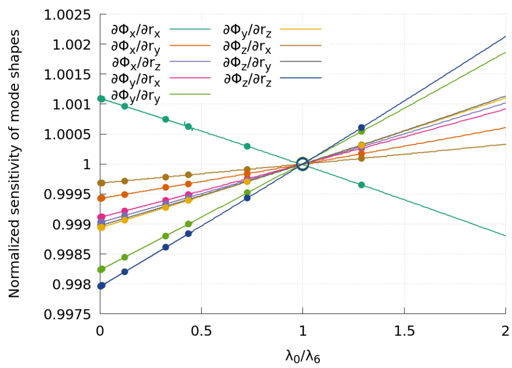

(b) Sensitivity of mode shape 6

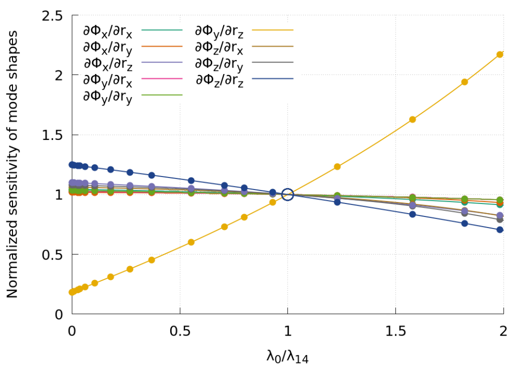

(c) Sensitivity of mode shape 14

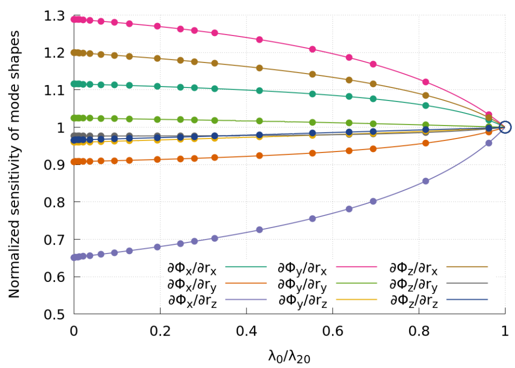

(d) Sensitivity of mode shape 20

Figure 4.11: Sensitivity of mode shapes calculated with the modal method for beam model at node A with increasing value of λ_0

The value of the sensitivity $\partial\phi_y/\partial r_y$ is changing as the parameter λ_0 is varied. This sensitivity has orders of magnitude smaller numerical value compared to the other sensitivity values. For $\partial\phi_y/\partial r_y$ when $\lambda_0 = (\lambda_j + \lambda_{j-1})/2$, the finite difference method did not provide the exact same value, however the 0.5% deviation is considered to be acceptable.

The sensitivities of mode shape 6 and 14, in Fig. 4.11b and 4.11c, show a more noticeable dependency on the λ_0 value. The closer this parameter value is chosen to λ_j, the eigenvalue of the mode under consideration, the better the residual term accounts for the truncated modes. As λ_0 cannot be chosen to be equal to λ_j in order to avoid singularity in Eq. (3.27), a good compromise is to choose the method parameter as $\lambda_0 = (\lambda_j + \lambda_{j-1})/2$. This introduces negligible error in the sensitivity calculation for the eigenvectors, but ensures that singularity does not occur. The sensitivity of mode shapes calculated with the algebraic method provides accurate value, shown with empty circles.

The highest mode calculated for this beam model is mode 20. The sensitivities with respect to the design variable $\boldsymbol{r}$, shown in Fig. (4.11d) calculated with the enhanced modal method using $\lambda_0 = 0$ show errors up to 30%. This can be reduced to maximum 5% if $\lambda_0 = (\lambda_j + \lambda_{j-1})/2$ and further reduced by coming closer to the value of λ_{20}. The proposed algebraic method provides accurate results for the sensitivities of the highest calculated mode shape.

It is worth noting that for the sensitivity of higher modes, the value of the method parameter λ_0 more drastically influences the numerical value of the sensitivity of eigenvectors. For example if the $\lambda_0 = 0$ is used as the value of the method parameter, for modes 3 and 6, the error introduced is less than 1%, but for higher modes, such as 14 or 20, the relative error is 10-60%.

For practical dynamic systems with large degrees of freedom only a subset of modes are calculated. If for these systems the sensitivities need to be obtained for all calculated modes using the modal method, then accounting for the mode shapes that have not been calculated are necessary. The optimal selection of the method parameter λ_0 is essential for obtaining correct numerical values for the sensitivity of mode shapes. A good approximation can be obtained for the sensitivity of lower modes of the MDOF system, by using the traditional method [98] when $\lambda_0 = 0$. For the higher calculated mode shapes, the λ_0 value needs to be very close to λ_j, but cannot be equal to that as it would lead to a singular system of equations in Eq. (3.27). A good compromise is to set $\lambda_0 = (\lambda_j + \lambda_{j-1})/2$ for every mode shape j. This way, accurate enough results can be obtained for the sensitivity of mode shapes, and the method can also cope with models with high frequency density.

4.4.2 Studies for the ideal placement of the regularization coefficient

In order to use the algebraic method for the calculation of the sensitivity of eigenvectors in practice, the regularization coefficient needs to be added to an optimal member in the system matrix $\boldsymbol{A}$, see Eq. 3.33. When the regularization coefficient is inserted into matrix $\boldsymbol{A}$, the matrix $\widetilde{\boldsymbol{A}}$ becomes regular so the system of linear equations can be solved with sufficient accuracy. Several of the investigated strategies for the location of the regularization coefficient have been studied with the aim of finding a strategy that consistently avoids singular matrices with low condition numbers.

Here, two approaches have been studied for the ideal placement of the regularization term adding it to the element on the diagonal of the matrix $\boldsymbol{A}$ (i) that has the smallest absolute value and (ii) that corresponds to the degree of freedom with the largest modal displacement for the mode, which the sensitivity is calculated for. In order to quantify how these approaches perform in regularizing the singular system, the condition number of matrix $\widetilde{\boldsymbol{A}}$ has been calculated. Here it is worth noting that the matrix $\boldsymbol{A}$ is different for each mode shape, see Eqs. (3.30) and (3.31).

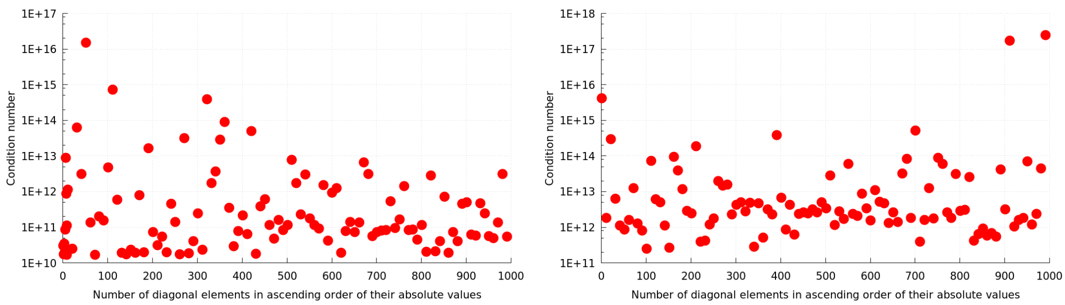

(a) Condition numbers for mode 5 (b) Condition numbers for mode 15

Figure 4.12: Condition numbers for $\widetilde{\boldsymbol{A}}$ depending on the placement of the regularization coefficient when ordered in ascending absolute main diagonal value

For the study of method (i) the diagonal members have been ordered in increasing absolute numerical values and the regularization coefficient s has been added to every 10^{th}. This has been done 100 times and the calculated condition numbers have been calculated for each of the 100 $\widetilde{\boldsymbol{A}}$. The stiffness and mass matrices, moreover the first 100 eigenvalues are calculated for a simplified bladed disks, shown in Fig. 4.1b. The finite element model consists of approximately 110,000 degrees of freedom. This bladed disk is anisotropy mistuned. As examples, the condition numbers are shown in Fig. 4.12 for Modes 5 and 15. The figures show that there is a significant scatter between the condition

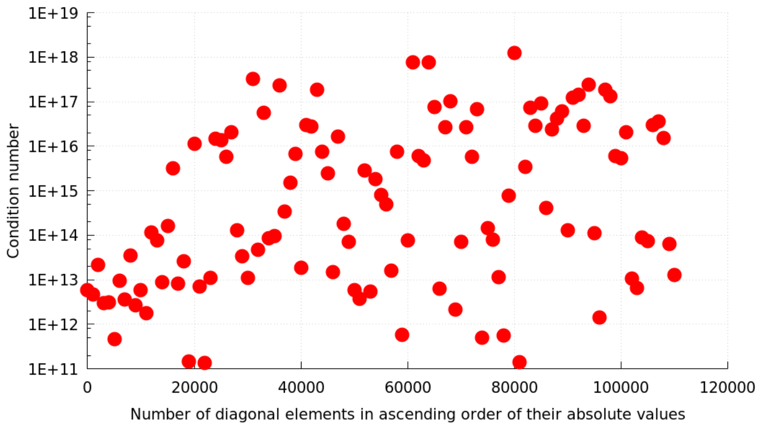

Figure 4.13: Condition number for mode 60 depending on the placement of the regularization coefficient when ordered in ascending absolute main diagonal value

numbers, depending on which member of matrix they are added to. Moreover, there is no clear correlation visible between the numerical value of the diagonal member and the calculated condition number. Adding the regularization term to the lowest absolute value of main diagonal provides acceptable condition numbers for some modes, e.g. mode 5, but for others e.g. mode 15 the condition number of $\widetilde{\boldsymbol{A}}$ is large.

In order to analyze the general behavior, the condition number has been calculated for the matrix when the regularization constant has been added to every 1000$^{\text{th}}$ member of the main diagonal of the matrix in increasing absolute value order. The condition values in Fig. 4.13 show a great variation of the condition number for matrix $\widetilde{\boldsymbol{A}}$, the condition number does not increase as the absolute numerical value of the diagonal member increases.

The studies using approach (ii) for adding the regularization term has been done for several mode shapes. As an example, here a localized mode shapes from the first family of modes is chosen. The mode shape of mode no. 60 is shown in Fig. 4.14. The condition number has been calculated after adding s to three different entries of the diagonal of the matrix: (a) to the DOF with the largest modal displacement (b) to one of the DOF on the disk (c) and to the DOF corresponding to the lowest absolute value of the diagonal of the matrix. The nodes for the corresponding DOFs are shown in Fig. 4.14. When the condition numbers are evaluated, they result as (a) $1.4 \cdot 10^{11}$, (b) $6.0 \cdot 10^{12}$ and (c) $3.3 \cdot 10^{14}$. This shows, that if the regularization term is added to the diagonal member that corresponds to the DOF with the largest modal displacement, then the regularization is the most effective.

In order to study the correlation between the condition number of matrix $\widetilde{\boldsymbol{A}}$ and the

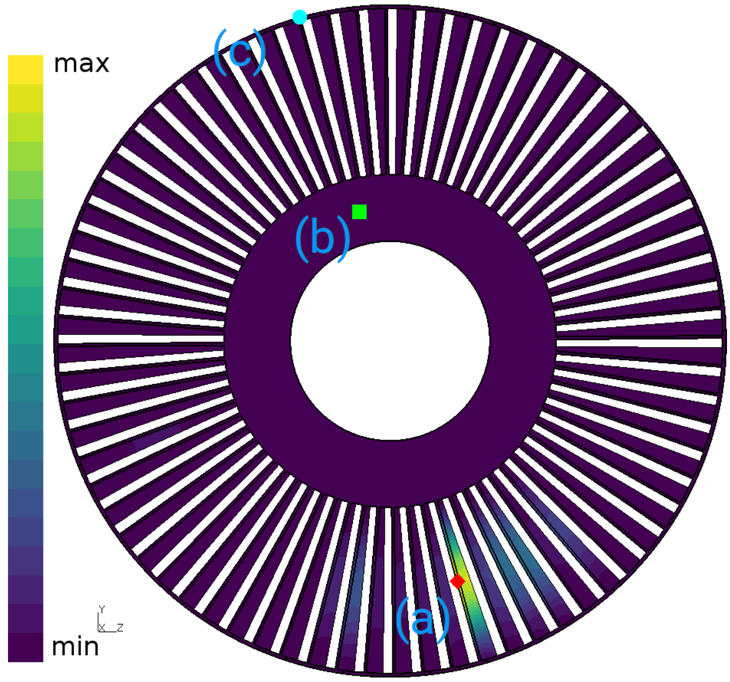

Figure 4.14: Mode shape 60 for the simplified mistuned bladed disk with regularization coefficient degrees of freedom shown

location on the main diagonal depending on the absolute value of the modal displacement for the corresponding DOF, the following study was done: The DOF absolute values of the mode shape 60 have been sorted in descending order, and the regularization term has been added for every 1000$^{\text{th}}$ diagonal, and for each regularized matrix $\widetilde{\boldsymbol{A}}$, the condition number has been calculated. The results shown in Fig. 4.15 show a clear correlation, namely if s is added to diagonal term corresponding to a degree of freedom with large modal displacement, the resulting condition number is the smallest. The condition number increases as it is added to diagonal terms corresponding to DOF with smaller modal displacements.

The two regularization strategies are compared in Fig. 4.16 for the first 100 modes of the blade disk system. It shows that adding s to the diagonal member of the DOF with the largest modal displacement provides lower condition number than adding it to the lowest absolute value of the diagonal member. This corresponds to the findings of Nelson in [64], where the rows and columns corresponding to the maximum eigenvector value are deleted.

This study shows that by selecting the highest degree-of-freedom of the mode shape under analysis and adding the regularization coefficient to the corresponding term on the main diagonal of $\boldsymbol{A}$ consistently provides low regularization coefficients. Therefore, this has been selected as the strategy for the regularization in the algebraic method for calculation of sensitivity of mode shapes.

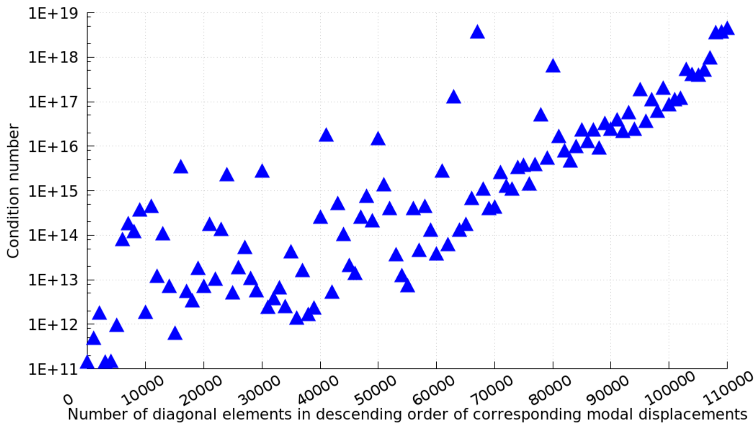

Figure 4.15: Condition number depending on the placing of the regularization coefficient for mode 60

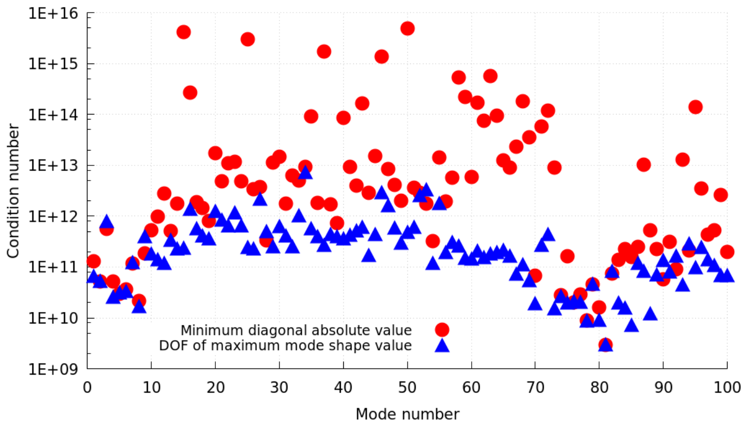

Figure 4.16: Condition number calculated for the matrices obtained with the two regularization strategies for the first 100 modes

4.4.3 Comparison of the two methods presented for the calculation of the mode shape sensitivities

The study of the accuracy of the two previously presented methods, the modal method and the analytic method, is done using the earlier presented simplified anisotropy mistuned bladed disk, shown in Fig. 4.1b. The bladed disk has 72 blades, which results in 216 design variables specifying the anisotropy orientation of all blades. The dynamic characteristics of the bladed disks can be studied using the natural frequency-nodal diameter diagram. Using this plot, shown in Fig. 4.17, the mode families of the bladed disk can be identified. It is shown that the disk stiff and frequency against nodal-diameter curve becomes flat very quickly. This results in high modal density in certain frequency ranges, therefore

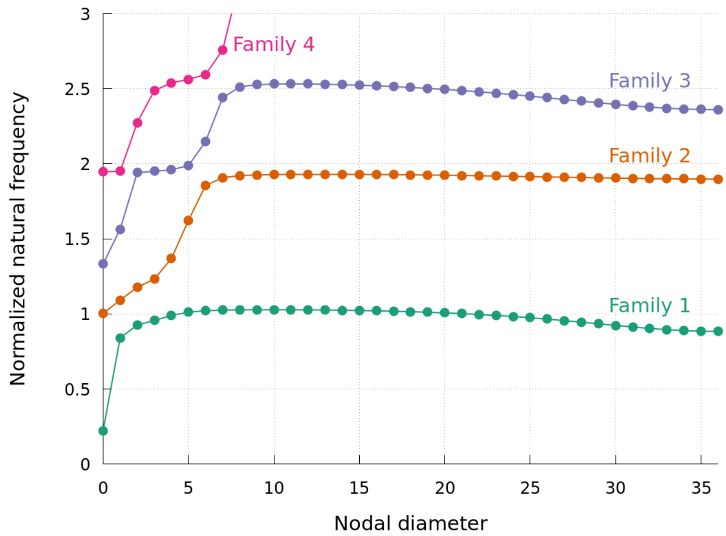

Figure 4.17: Normalized natural frequency values plotted against the nodal diameter number for the simplified bladed disk shown in Fig. 4.1b that is used for the comparison of the algebraic and modal method for calculation of mode shape sensitivities

this bladed disk model is ideal for testing the capabilities of the proposed methods for the calculation of the eigenvector sensitivities.

It has previously been shown, using the beam model, that both methods provide accurate numerical results for the sensitivity of the mode shapes. According to what has been concluded in the earlier sections, for the enhanced the $\lambda_0 = (\lambda_j + \lambda_{j+1})/2$ is used, which is updated for every mode. This means that the equation system in Eq. (3.27) needs to be factorized for every mode once. For this bladed disk, Eq. (3.27) needs to be solved as many times as the number of design variables, 216. Therefore, for such systems with many design variables, the relative effort of the LU decomposition of the system of linear equations becomes less significant. In the modal expansion basis, see Eq. (3.19), all calculated modes are included.

For the algebraic method, the regularization coefficient s is added to the main diagonal member of matrix $\boldsymbol{A}$, that corresponds to the DOF with the largest modal displacement.

The sensitivity of the mode shapes are analyzed at one particular node: in the mid-span of blade 20. The sensitivities are calculated with respect to all three rotation vector components of blade 20 $\boldsymbol{r} = \{r_{x20}, r_{y20}, r_{z20}\}$ and for all 3 spatial directions $\boldsymbol{\phi}_j = \{\phi_{j,x}, \phi_{j,y}, \phi_{j,z}\}$. The sensitivity of the first 100 eigenvectors of the mistuned bladed disk are calculated using the modal method (MM) and the algebraic method (AM). In order to be able to compare the numerical values obtained using the two methods, relative errors

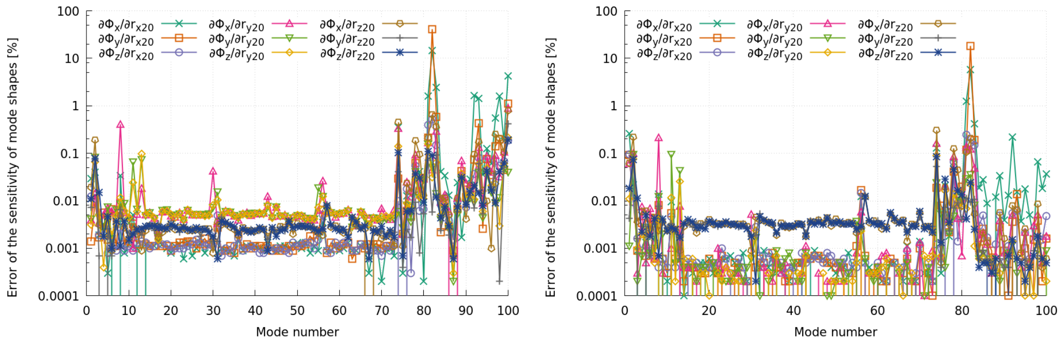

(a) 100 modes in the modal expansion for MM (b) 200 modes in the modal expansion for MM

Figure 4.18: Error of the sensitivity of mode shapes calculated with algebraic method (AM) and with the modal method (MM) using Eq. 4.4

are calculated for all mode shape sensitivities under investigation:

$$\epsilon_j = \frac{(\partial \boldsymbol{\phi}_j / \partial \boldsymbol{r})_{AM} - (\partial \boldsymbol{\phi}_j / \partial \boldsymbol{r})_{MM}}{(\partial \boldsymbol{\phi}_j / \partial \boldsymbol{r})_{AM}} \tag{4.4}$$

The calculated errors of the sensitivities of the first 80 mode shapes, shown in Fig. 4.18a, with 100 modes in the expansion basis for the MM, are negligible. This is because in the expansion basis all the modes from the first mode family are included, therefore their sensitivities are calculated accurately.

The error between sensitivities calculated using the two methods is larger than 10% for mode number 82 for $\boldsymbol{\phi}_{82,x}/r_x$ and $\boldsymbol{\phi}_{82,y}/r_x$. The numerical value of the sensitivities is very small, therefore this large relative error is acceptable.

The error calculated for the last modes in the 100 modes range has an increasing tendency. This is expected for the results calculated with the MM, because the sensitivities of modes shapes are obtained with 100 modes in the expansion formulation. The accuracy of the sensitivities calculated can be increased by using more mode shapes for the eigenvector sensitivity calculations. As an example, Fig. 4.18b shows the relative errors with 200 modes retained in the series expansion basis.

The studies done for the modal and algebraic method for the calculation of the sensitivity of mode shapes done for the simple bladed disk model has proved, that both methods can be applied for structures with high frequency density. The comparison of the sensitivities calculated for both methods, showed that the modal method that accounts for the mode shapes not included in the series expansion basis provides accurate results except for the highest modes included.

4.4.4 Study of the convergence characteristics of the modal method for high-fidelity bladed disk models

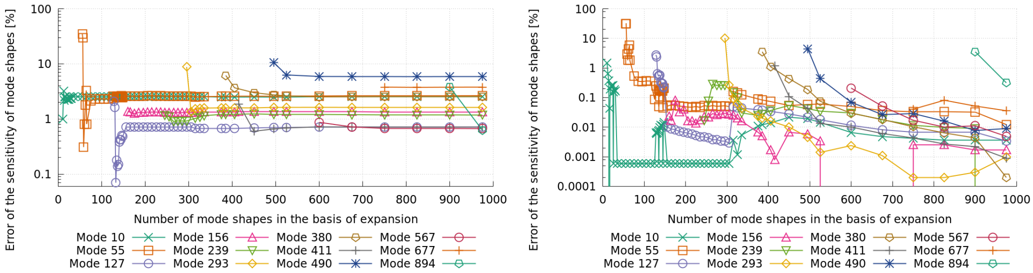

(a) As reference the sensitivities calculated with finite difference method is chosen (see Eq. 4.5)

(b) As reference the sensitivities calculated with algebraic method is chosen (see Eq. 4.6)

Figure 4.19: Relative error of the sensitivities calculated with modal method for different number of modes in the modal expansion basis

The convergence characteristics of the sensitivity of the mode shapes, calculated using the modal method, have been studied for higher family of mode shapes using a high-fidelity bladed disk model. This realistic bladed disk model, shown in Fig. 4.1c, has 0.5 million nodes, about 1.5 million degrees-of-freedom. For the convergence study, from the first 1000 modes, 12 has been arbitrarily selected from different families of modes. The sensitivity of these modes have been calculated with different number of mode shapes included in the expansion basis. In Fig. 4.19a, the relative error of the sensitivity of mode shapes have been calculated for modal displacement in x direction with respect to x component of rotation vector of the material anisotropy orientation of blade 42 $v_{42,x}$. The relative error is calculated with respect to the approximation of the sensitivities using finite difference (FD) method such as

$$\epsilon_{FD} = \frac{(\partial\phi/\partial r_{42,x})_{MM} - (\partial\phi/\partial r_{42,x})_{FD}}{(\partial\phi/\partial r_{42,x})_{FD}} \tag{4.5}$$

It needs to be mentioned here, that for bladed disk structures the sensitivities calculated using the FD method is generally less accurate. Nevertheless, it can be used to validate the sensitivity calculations with the proposed methods. The results shown in Fig. 4.19a show a fast convergence of the mode shape sensitivities over the mode shapes. The error reduces to less than 2% for all modes except for mode 490 which has a small value of mode shape sensitivities; therefore these results are acceptable.

The relative error of the sensitivities of the modes analyzed earlier can be calculated

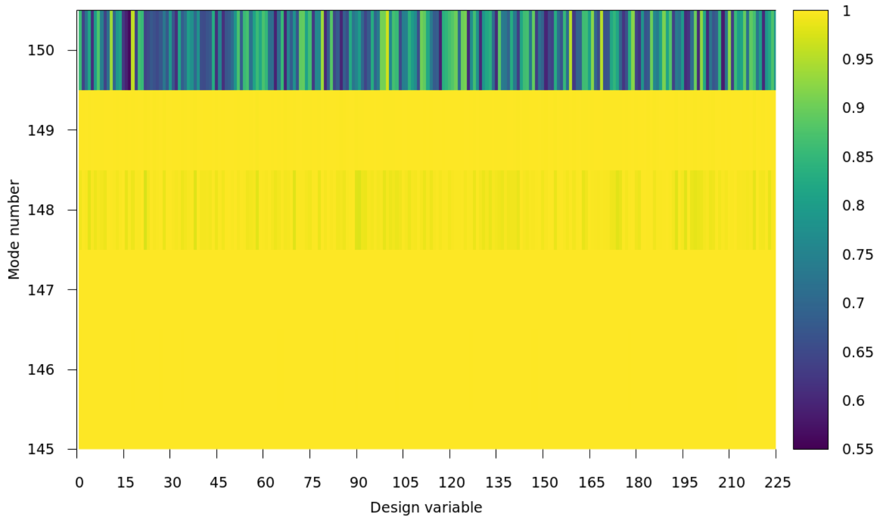

Figure 4.20: MAC numbers calculated for sensitivity of mode shapes calculated using the modal and algebraic method, as Eq. 4.7

by taking the exact solution obtained with the algebraic method.

$$\epsilon_{AM} = \frac{(\partial \phi / \partial r_{42,x})_{MM} - (\partial \phi / \partial r_{42,x})_{AM}}{(\partial \phi / \partial r_{42,x})_{AM}} \tag{4.6}$$

The relative error values shown in Fig 4.19b show significantly lower values compared to the ones shown in Fig. 4.19a. The convergence characteristics of the modal method can clearly be seen in this graph, as the error of the mode shape sensitivities are 1%-10% when the sensitivities are calculated for the highest mode shapes that is included in the series expansion formulation. When an additional 10-20 modes are included in the expansion, the error becomes negligible. As an example, the relative error for sensitivity of mode shape 293 is 10.3% when 295 mode shapes are used for the calculation of the mode shapes. If 305 modes are used for the series expansion, the error becomes 0.27%.

The vector of sensitivity of mode shapes calculated for using AM and MM can be compared with the help of MAC values, using the formulation

$$MAC\left(\left(\frac{\partial \boldsymbol{\phi_j}}{\partial \boldsymbol{r}}\right)_{MM}, \left(\frac{\partial \boldsymbol{\phi_j}}{\partial \boldsymbol{r}}\right)_{AM}\right) = \frac{\left|\left(\frac{\partial \boldsymbol{\phi_j}}{\partial \boldsymbol{r}}\right)_{MM}^T \cdot \left(\frac{\partial \boldsymbol{\phi_j}}{\partial \boldsymbol{r}}\right)_{AM}^T\right|^2}{\left(\frac{\partial \boldsymbol{\phi_j}}{\partial \boldsymbol{r}}\right)_{MM}^T \cdot \left(\frac{\partial \boldsymbol{\phi_j}}{\partial \boldsymbol{r}}\right)_{MM} \cdot \left(\frac{\partial \boldsymbol{\phi_j}}{\partial \boldsymbol{r}}\right)_{AM}^T \cdot \left(\frac{\partial \boldsymbol{\phi_j}}{\partial \boldsymbol{r}}\right)_{AM}} \tag{4.7}$$

where $(\partial \boldsymbol{\phi_j} / \partial \boldsymbol{r})_{MM}$ and $(\partial \boldsymbol{\phi_j} / \partial \boldsymbol{r})_{AM}$ are the mode shape sensitivities of the j-th mode calculated using the modal and algebraic method respectively.

The MAC values have been calculated for the mode shape sensitivities for the first

150 modes with respect to all 225 design variables. For the bladed disk 150 modes were calculated, therefore MAC values for the sensitivity of mode shape calculated using the modal method and the algebraic method decreases for the mode no. 150 and 148, see Fig. 4.20.

4.4.5 Comparison of the computational efforts

For the methods proposed in this work it is essential to assess the computational effort associated to each method, especially the calculation time. For this study, the already presented simplified bladed disk modal, see Fig. 4.1b, and a bladed disk model with 0.5 million nodes are used. This more detailed model, shown in Fig. 4.1c, can represent the calculation efforts that are currently typical for industrial applications.

The calculation times of the derivative of the eigenpairs have been calculated for 100 and 400 modes, using the simplified bladed disk model. For these calculations, there cannot be a significant difference observed in the calculation times. When the same analysis was done for 100 and 600 modes of the realistic bladed disk model, the difference is more notable.

Table 4.1: Calculation times for the modal and algebraic methods for calculation of the sensitivity of mode shapes

Finite element model	Number of modes	Calculation time [hours]	
		Modal method	Algebraic method
Simplified bladed disk	100	1.4	1.2
Simplified bladed disk	400	5.1	2
Realistic bladed disk	100	10.2	5.7
Realistic bladed disk	600	195.7	33.7

It is worth, noting that the calculation time of the enhanced modal method increases significantly as the number of modes for which the sensitivity of eigenpairs increase. This is mainly due to the fact, that the number of coefficients used in the series expansion increase, see Eq. 3.29, and with that the calculation time as well. A way to improve the calculation time could be to restrict the number of modes used in the expansion basis for the sensitivity calculation of the lower modes.

4.5 Validation of the sensitivity calculation of forced response

The sensitivity of natural frequencies and mode shapes serve as input for the calculations of the sensitivity of forced response amplitudes. In this section, the validation of the sensitivity calculation for forced response of linear and nonlinear anisotropy mistuned bladed disks is done.

4.5.1 Validation for the calculation of sensitivity for linear forced response

First, the sensitivity of the linear forced response has been verified. All contact interfaces of the bladed disk are considered to be welded together. For the bladed disk, the natural frequency-nodal diameter plot is shown in Fig. 4.7. For the bladed disk a traveling wave type excitation is applied with engine order 11 that excites the 2^{nd} mode family. The harmonic excitation is applied on one node for each blade at the forced response amplitudes are obtained for these nodes. The amplitudes for all 75 blades are on shown in Fig. 4.21. the frequency range of the 2^{nd} mode are shown. The forced response amplitudes are normalized with respect to the amplitudes calculated for a tuned bladed disk where all blades have anisotropy angles $\alpha = \beta = \zeta = 0$ and the excitation is the same engine order and same frequency range. The excitation frequency is normalized with the natural frequency of the stand-alone blade with open shrouds.

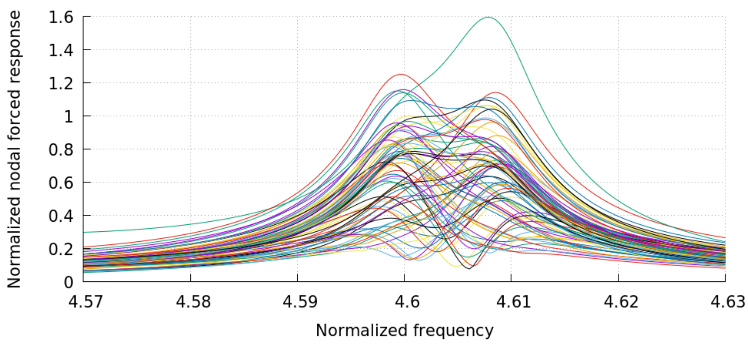

Figure 4.21: Normalized forced response of all 75 blades at EO11 for mode family 2

In Fig. 4.21, it can be identified that one of the blades (blade 10) has higher vibration

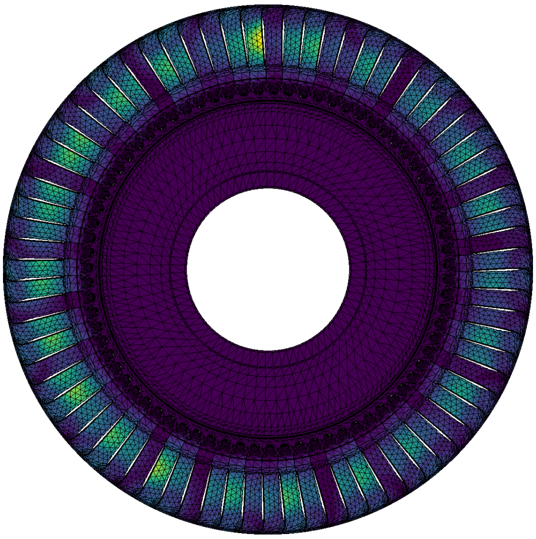

Figure 4.22: Recovered forced response in time domain of all 75 blades at EO11 for mode family 2 at $f = 4.608$ for the time instant where the maximum forced response displacement occurs

amplitudes at normalized frequency $f = 4.608$. Using the capabilities of the forced response recovery for all the FE nodes, the forced response can be visualized for the time instant where blade 10 has maximum vibration amplitudes, see Fig. 4.22.

For the validation of the sensitivity calculation, the sensitivity with respect to blade 10 is analyzed for the forced response displacements of all blades. The sensitivity calculated with the new methodology is compared with sensitivities calculated using the finite difference method. The sensitivities obtained with both methods are in good agreement for all blades, as shown in Fig. 4.23. The small differences are due to limited accuracy of the finite difference method.

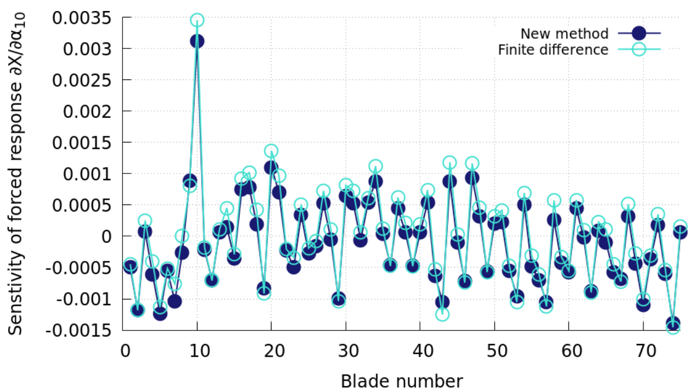

Figure 4.23: Validation of sensitivities of the forced response (calculated with the new method and with finite differences) with respect to α angle of blade 10 at $f = 4.608$

4.5.2 Validation for the calculation of sensitivity for nonlinear forced response

The sensitivity of the nonlinear forced response has been validated for a two-blade model with nonlinear friction contact interfaces. The two-blade model, shown in Fig. 4.24, is fixed on lower and on the higher side of the disk sector. On the shroud interfaces on the two ends of the sector model, sliding boundary conditions are applied. These sliding boundary conditions restrict all motions on the normal direction of the contact surfaces, while allowing tangential movement. Nonlinear contact elements are defined on the root interfaces of both blades and on the shroud interfaces between the two blades.

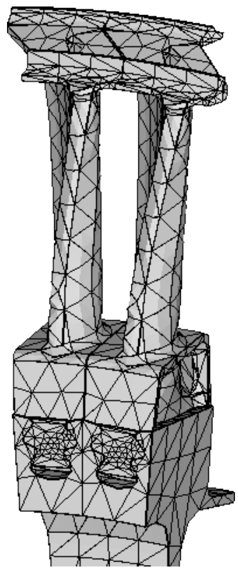

Figure 4.24: Two-blade model

On each of the 4 root interfaces 12 nonlinear contact elements are applied. On the two contact interfaces on the shroud contact patches, 3 and 3 contact elements are applied. The harmonic excitation is applied at the mid-span of the trailing edge. The harmonic excitation has 38.4° phase shift between the two blades, that would be equivalent to EO8 excitation for a full blade model.

The sensitivities with respect to anisotropy angles of the left blade has been calculated with the new method and with finite difference method. The calculated sensitivities and the nonlinear forced response are shown in Fig. 4.25. The sensitivities calculated with the two methods are in good agreement, therefore it can be concluded that sensitivity calculation of the nonlinear forced response with respect to the anisotropy angles of single crystal bladed disks are validated.

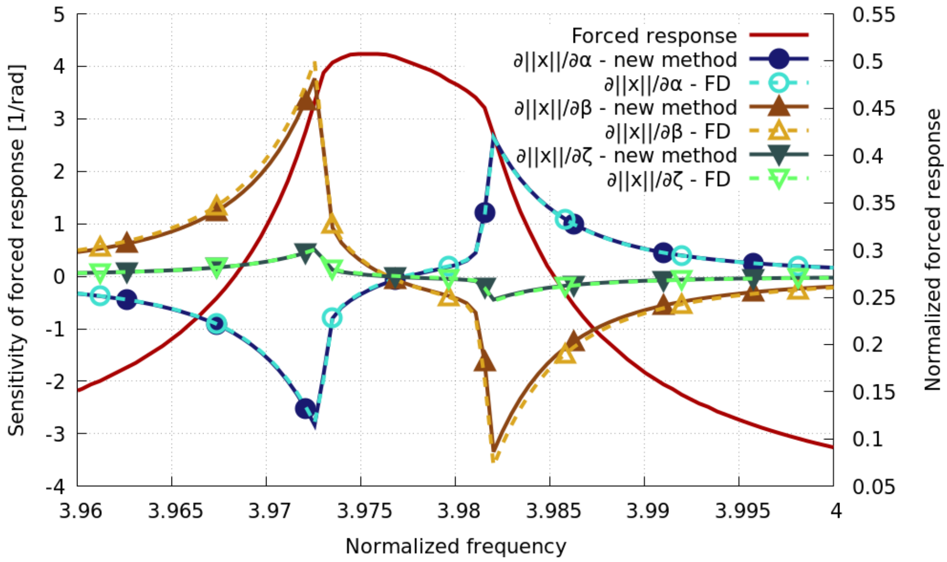

Figure 4.25: The forced response amplitudes and their sensitivities with respect to anisotropy angles α, β and ζ calculated with the new method and with finite differences around the resonance

4.6 Validation of the calculation of the forced response displacement recovery in time domain

The forced response amplitudes are calculated by ContaDyn only for the degrees of freedom included in the reduced order model. For any selected frequency, the forced response amplitudes in time domain can be obtained by Eqs. 3.76 and 3.77 for all DOF the finite element model. The method and the implementation for the recovery of the forced response amplitudes and their sensitivities, described in in section 3.6, has been validated for asymmetric and symmetric bladed disk structures.

4.6.1 Asymmetric bladed disk structure

The two-blade structure shown in Fig. 4.26 is used for the validation for the calculations of an asymmetric bladed disk structure. The two blades are fixed at the root and in normal direction on the shrouds. Between the two blades there are two nonlinear contact interfaces and they are discretized by one contact element for each patch. The two blades are harmonically excited on the leading edge of the blades. The two blades are single crystal blades with different crystal orientation, which results in distinct natural frequencies. For the forced response calculation and for the displacement recovery, 50 modes are included. Moreover, in the forced response function calculation the harmonics 1 and 3 are included.

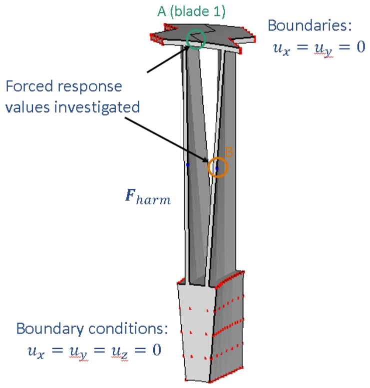

Figure 4.26: Two-blade structure used for the validation of the recovered forced response and their sensitivities

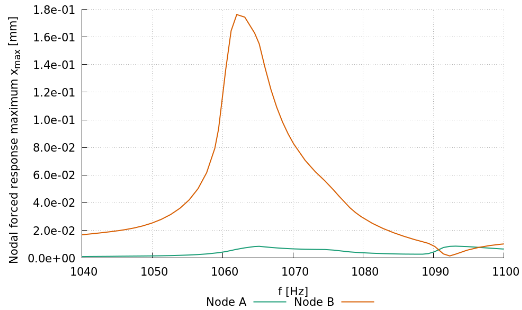

Figure 4.27: Forced response of nodes A and B of the two-blade structure

The forced response is plotted for node A, where the contact element is applied on the left blade (blade 1), and for blade B around the resonance in Fig. 4.27. The recovered displacements are calculated at 1065 Hz for 31 time steps over the vibration period. The recovered displacements can be animated over the period using CalculiX GraphiX, in Fig. 4.28 the displacements for the time instants when the 2$^{\text{nd}}$ blade has extreme deflections are shown.

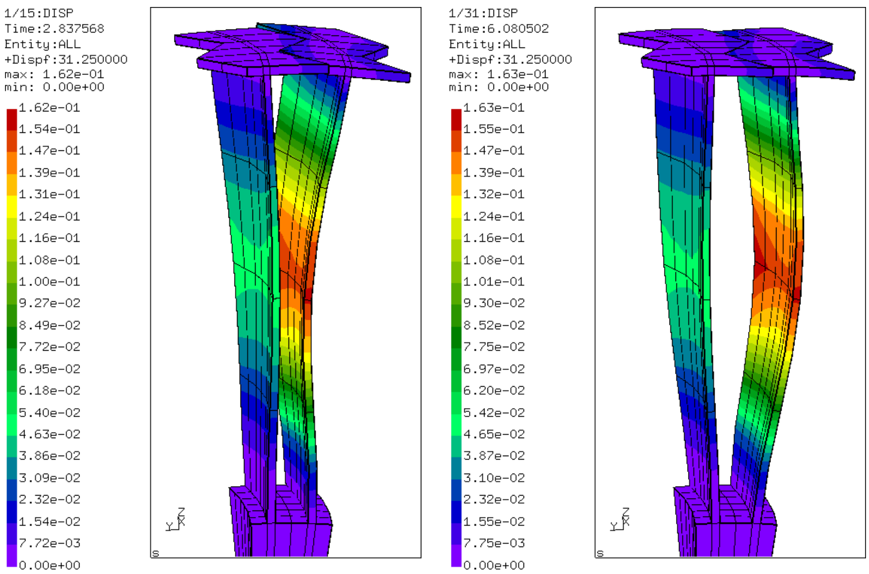

(a) Time instant of maximum deflection of blade 1 in positive y direction

(b) Time instant of maximum deflection of blade 2 in negative y direction

Figure 4.28: Recovered displacements at two time instants for $f = 1065Hz$

The deflections in Fig. 4.28 show the first bending mode for the shrouded blade. In order to validate the forced response amplitudes, the recovered displacements are compared

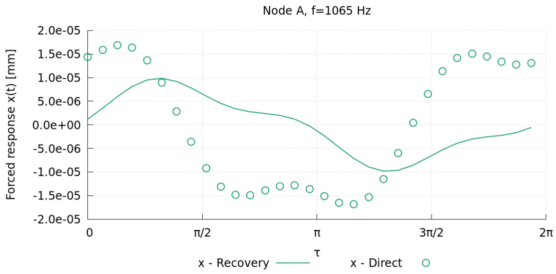

(a) Node A, x direction

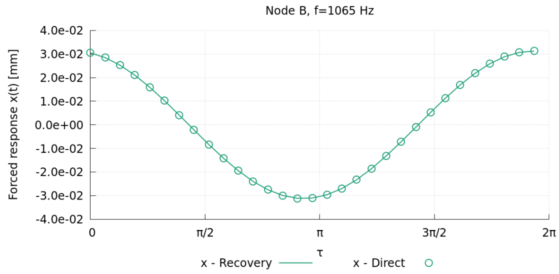

(b) Node B, x direction

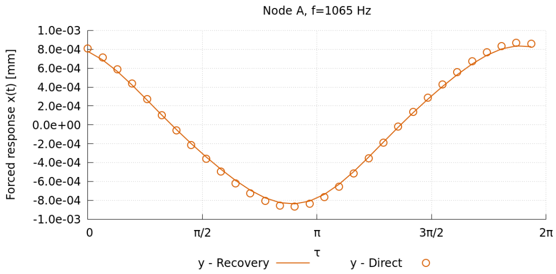

(c) Node A, y direction

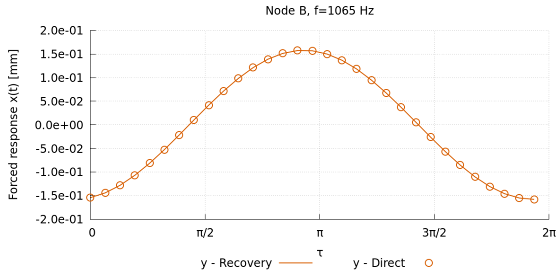

(d) Node B, y direction

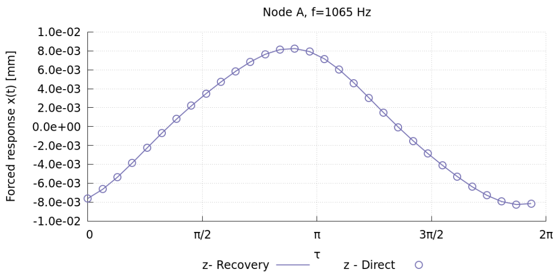

(e) Node A, z direction

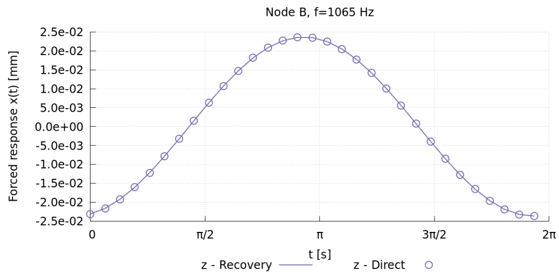

(f) Node B, z direction

Figure 4.29: Validation of recovered forced response displacements for two-blade system, where the displacements are recovered using the mode shapes or the displacements are calculated from the harmonic coefficients

with the harmonic coefficients of the forced response amplitudes placed in the time domain equation of the forced response in Eq. 3.44. This is called here as the direct calculation. The comparison can be done for the nodes included in the reduced order model, therefore for the analysis A and B nodes are selected. The forced response amplitudes calculated with the two methods, shown in Fig 4.29, are in good agreement with each other. The forced response of node A in x direction is several magnitudes lower than the other forced response amplitudes, which explains the deviation between the forced response in time domain. With this, the validation of the nonlinear forced response recovery for asymmetric (i.e. mistuned) systems has been successfully done.

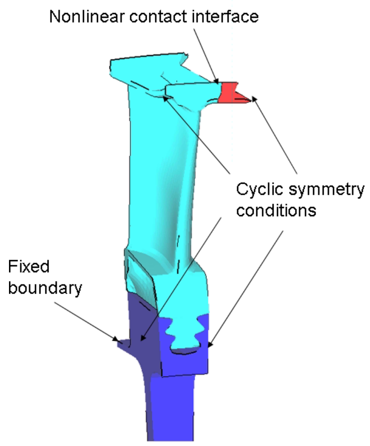

Figure 4.30: Bladed disk used for the validation of the recovered tuned forced response

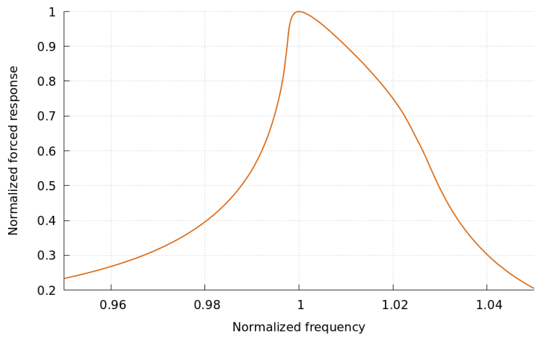

Figure 4.31: Forced response of tuned bladed disks to EO20 excitation of mode 2

4.6.2 Symmetric bladed disk structure

The recovery of the cyclic symmetric forced response displacements is validated in a similar manner, using the cyclic symmetric bladed disk shown in Fig. 4.30. The bladed disk is fixed on the rotor in axial and tangential direction. The nonlinear contact is considered on the leading edge side of the shroud interface. Some FE elements have been removed from the left side and moved to the right side, shown with red color. Cyclic symmetric condition has been applied on the surfaces that have been cut due to the moving of the above mentioned FE elements. Nonlinear friction contact has been modeled with 35 friction contact elements on the shroud interface. The root contact between the blade and the disk is considered to be fully stuck.

The bladed disk is excited on the airfoil with EO20 excitation, that excites the 2^{nd} mode of the bladed disk. The nonlinear forced response is calculated using time harmonics 0, 20, 40, 60 and 80. The forced response obtained for an airfoil node is plotted around the resonance in Fig. 4.31. The forced response shows, that the system response is strongly nonlinear due to the friction forced that appear on the shrouds. For such systems, the flexibility matrix included in the FRF calculation is essential to calculate the FRF matrix accurately.

The comparison of the forced response recovery is done at resonance frequency for 2 nodes that are included in the reduced order model: one node on the airfoil trailing edge and one on the shroud contact patch. The normalized forced responses at the resonance frequency are plotted for all three degrees of freedom for the two nodes under investigation.

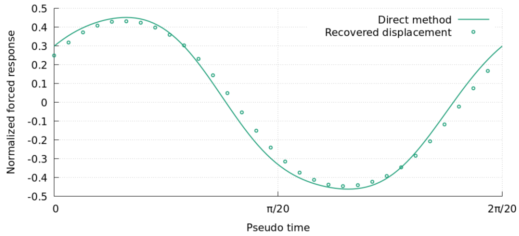

(a) Trailing edge, x direction

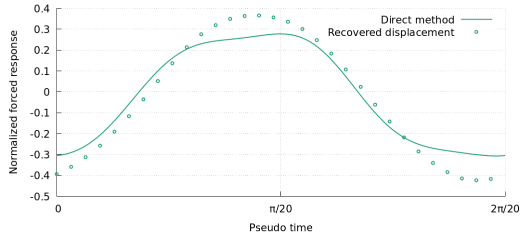

(b) Shroud contact interface, x direction

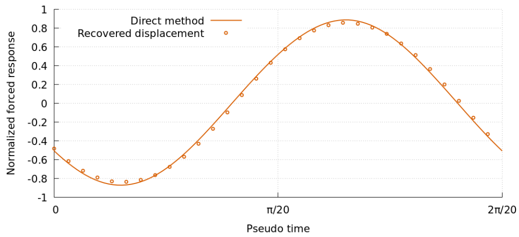

(c) Trailing edge, y direction

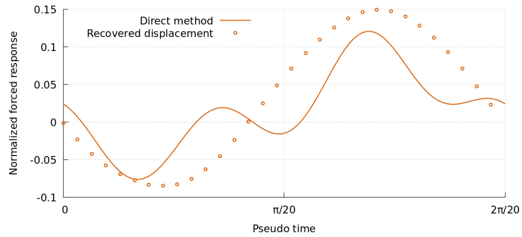

(d) Shroud contact interface, y direction

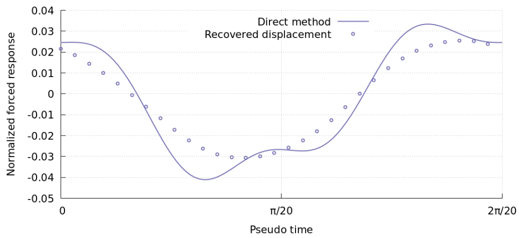

(e) Trailing edge, z direction

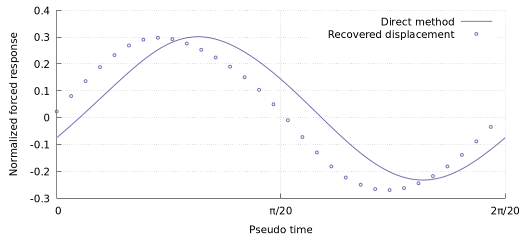

(f) Shroud contact interface, z direction

Figure 4.32: Validation of the recovered forced response displacements of the cyclic symmetric bladed disk

The displacements have been normalized with the maximum vibration amplitude of the node on the trailing edge.

The recovered forced response displacements show good agreement for the node on the trailing edge for x and y directions, see Fig. 4.32. The amplitude of the displacements in z direction is smaller, resulting in some discrepancy over the period.

The forced response compared on the shroud interfaces obtained with the two different method shows more noticeable discrepancy between the results. Similarly to the node on the trailing edge, the results with larger vibration amplitudes are in better agreement.

The difference between the time-domain solutions is contributed to the lack of flexibility information, which is particularly important for the friction contact interfaces where the nonlinear friction forces are acting. Far from the nonlinearities, e.g. on the airfoil, the importance of the flexibility information reduces and the recovered displacements allow for an accurate representation of the operational deflection shape.

4.7 Conclusions

In this chapter the verification of the methods used in research has been presented. The validation of the implemented methods for the sensitivity needed to be done before the extensive analyses for mistuned bladed disks had been started.

The validation was first completed for the linear forced response. The forced response amplitudes calculated using ContaDyn, the forced response tool in this work, has been compared with CalculiX, for which the linear forced response calculations have been validated. As both tools use the modal basis with the same mode shapes, complete coincidence in the amplitudes have been obtained.

The sensitivity calculation of the element stiffness matrices in CalculiX are done by finite differences. In order to find an optimal finite difference step size, the sensitivity of natural frequencies were calculated with different step sizes and compared with the sensitivity of natural frequency obtained using the analytically calculated derivative of the element stiffness matrix. Because the analytical formulation for the elements stiffness matrix derivative cannot be used, the optimal value for the finite difference is used for the sensitivity calculations: 10^{-5}.

The calculation of sensitivity of natural frequencies have been validated for single blades and for mistuned bladed disks. The sensitivities obtained directly from CalculiX using the new method has been compared with sensitivities obtained the finite differences of two separate modal calculations. The sensitivity values showed a very good agreement.

The derivative of the eigenvectors cannot directly be expressed, therefore two different methods have been proposed ([82] and [83]) for the calculation of the mode shape sensitivities. The modal and algebraic methods have been implemented in CalculiX. Both methods require a parameter to be chosen, which has been investigated in detail. For the modal method, a reference frequency needs to be set, for which the optimal value is the mean of the eigenvalue of the mode for which the sensitivity is calculated for and the eigenvalue of the mode one lower. For the algebraic method, the regularization coefficient needs to be added to one of the members on the main diagonal of the system matrix. For this the optimal strategy is to add this value to the main diagonal member that corresponds to the largest modal displacement of the mode for which the sensitivity is calculated for.

For the modal method of the mode shape sensitivity, the convergence characteristics have been studied. In general, it can be stated, that in order to obtain accurate results for the derivative of the mode shapes, at least one more mode family needs to be included than the mode for which the sensitivity is calculated for.

The sensitivity of linear and nonlinear forced response has been presented in this chapter. The sensitivities calculated using the new method and the finite differences are in good agreement and the negligible differences are considered to be due to the limited accuracy of the derivative approximated by the finite difference method.

InterDyn allows to calculate the forced response and their sensitivities in time domain for all FE nodes of the original model at a selected frequency. The recovered displacements then can be visualized in the pre- and post-processing tool CalculiX GraphiX. The validation for the degrees of freedom included in the reduced order model could be done by the comparison of the displacements obtained through the direct harmonic expression.

Chapter 5

Sensitivity analysis of the modal characteristics of the anisotropy mistuned bladed disks

The modal properties of mistuned bladed disks are an important indicator about the dynamic characteristics of the structure. The linear modal properties are also the basis for calculation of the linear and nonlinear forced response function, as shown in chapter 3. Similarly, the sensitivity of natural frequencies and mode shapes also carry important information about the sensitivity of the dynamic behavior of the mistuned bladed disk.

In this chapter, the influence of varying crystal orientation angles for single blade and varying anisotropy mistuning patterns on the modal characteristics are studied. Furthermore, the sensitivity of the eigenpairs of mistuned bladed disks are analyzed for selected modes of a mistuned bladed disk.

5.1 Effect of anisotropy orientation axis scatter on the single blade natural frequencies

The effect of the anisotropy angle variation of the single crystal blades on the natural frequencies is shown for a single stand-alone sector of bladed disk model.

The finite element model, shown in Fig. 5.1a consists of 19,000 nodes. The material of the blade is anisotropic and the material of the disk is isotropic. The two areas on the side of the segment on the disk have been fixed. On the blade a centrifugal loading has been applied and the modal properties have been calculated around the converged static solution. The contact interfaces between the disk and the blade are modeled to be fully

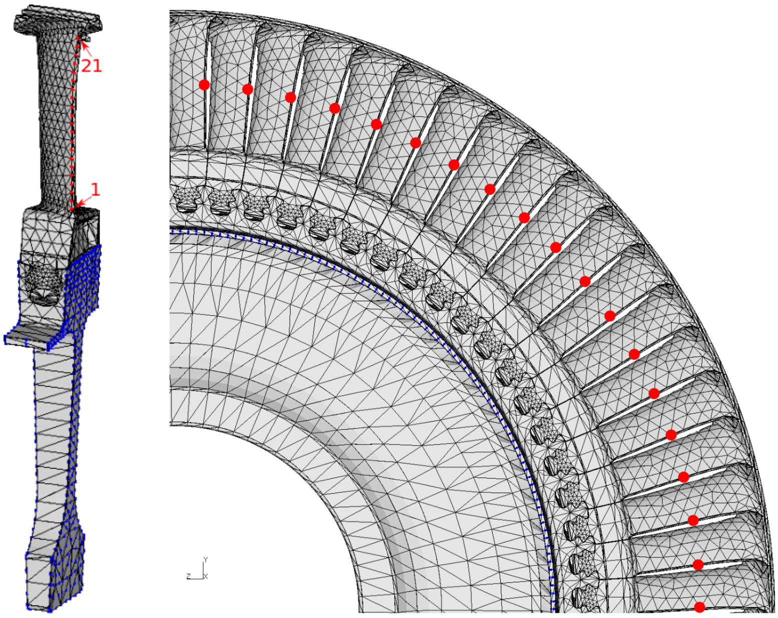

(a) Single blade (b) Quarter of the bladed disk

Figure 5.1: Finite element models used for the study of anisotropy orientation variation on the modal properties and their sensitivities

stuck.

For the description of the crystal orientation of the blade material, anisotropy angles have been randomly generated. The random values of α, β and ζ have been sampled from the corresponding statistical distribution described by the manufacturer of the blades. There have been 10,000 different crystal orientations obtained and for this 10,000 blade sector model, the first six natural frequencies have been calculated. Additionally, the natural frequencies for 2 models with special anisotropy angles have been calculated, (i) one with anisotropy orientation coinciding with the blade stacking axis and (ii) on with anisotropy angles equal to the mean value of the statistical distribution of the respective angle.

The range of the normalized natural frequencies are shown in Fig. 5.2. The values in this plot have been normalized with respect to the natural frequencies calculated for the blade with anisotropy axis coinciding with the stacking axis. These values of natural frequencies are shown with symbols of green triangles. The empty red circles in the figure show the natural frequencies calculated for the bladed disk sector with mean anisotropy angles. The filled blue circles are showing the result of the mean value of the 10,000 natural frequencies obtained for the first six natural frequencies.

The range of variation show, that for the first (1^{st} flap, 1F), the second (1^{st} edgewise,

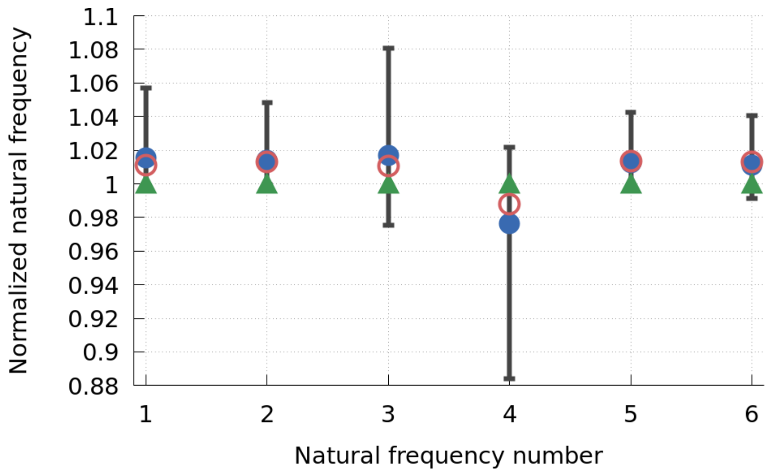

Figure 5.2: Normalized natural frequency of single blade with varied crystal orientation

1E), the fifth (2^{nd} edgewise - 2E) and the sixth (3^{rd} edgewise, 3E) natural frequencies the crystal orientation variation mainly results in increase in the value of natural frequencies, compared to the natural frequencies calculated for the blade with crystal orientation coinciding with the stacking axis. Similarly, For the values of the natural frequencies three (2^{nd} flap, 2F) and four (1^{st} torsional, 1T) both increase and decrease can be observed.

The largest variation of the natural frequency, 13.8% can be observed for mode 4. The smallest variation has been obtained for mode 5, 4.7%.

It is worth noting, that for modes 2,5 and 6 the mean value of natural frequencies calculated for the 10,000 crystal orientations are almost the same as the natural frequencies calculated for the blade with mean angles, but for modes 1,3 and 4 a deviation can be observed in these values.

It is also important to note, that while the range of variation can be quite significant, the mean values of the calculated natural frequencies do not lie very far from the value of the natural frequency calculated for the blade with crystal orientation coinciding with the stacking axis. The histogram of the first six modes also confirms this, as for the first five modes the bin with maximum count is within 1% range of the natural frequency of the blade with anisotropy axis coinciding with the stacking axis.

The histograms for the large number of seeded anisotropy orientations are shown in Fig. 5.3. These figures also show that the distribution of the resulting blade alone natural frequencies are asymmetric and they change from one mode to another. The modes belonging to the same mode families e.g. bending or edge-wise modes also show distinct distributions therefore, the effect of anisotropy orientation mistuning needs to be individually assessed for every mode.

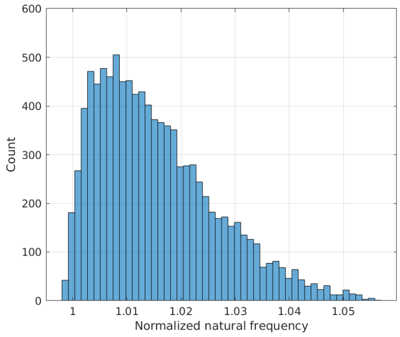

(a) Normalized natural frequency 1 (1F)

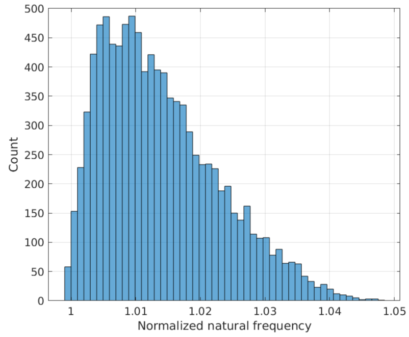

(b) Normalized natural frequency 2 (1E)

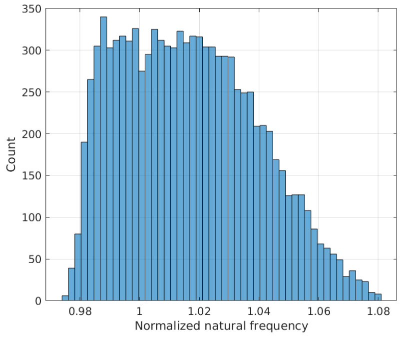

(c) Normalized natural frequency 3 (2F)

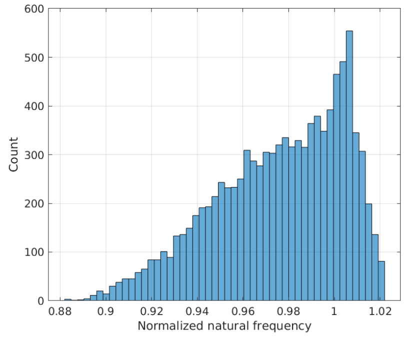

(d) Normalized natural frequency 4 (1T)

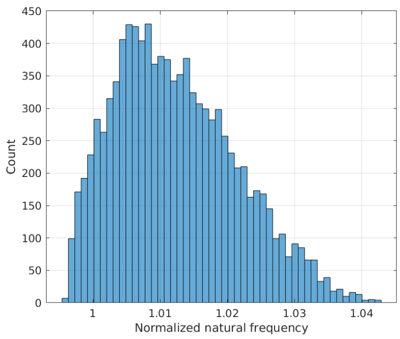

(e) Normalized natural frequency 5 (3F)

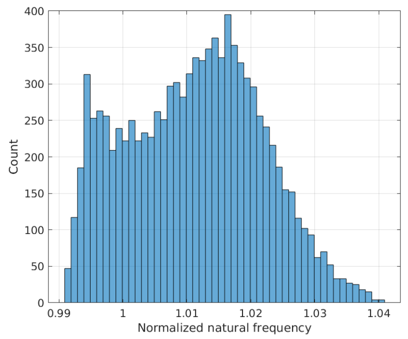

(f) Normalized natural frequency 6 (2E)

Figure 5.3: Histogram for the first six normalized natural frequencies due to random crystal orientation variation

In order to visualize the effect of the crystal orientation variation on the value of natural frequencies, two of the anisotropy angles, α and β have been gradually changed and the natural frequencies calculated. The third anisotropy angle, ζ has been kept constant at value 0. The normalized natural frequencies are shown in Fig. 5.4 for the first 6 modes.

For modes 1,3 and 5, that are all bending modes, the natural frequencies change in a very similar manner. The values of the natural frequencies increase monotonously with

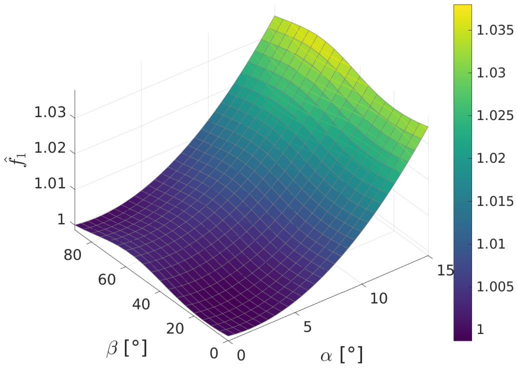

(a) Normalized natural frequency 1 (1F)

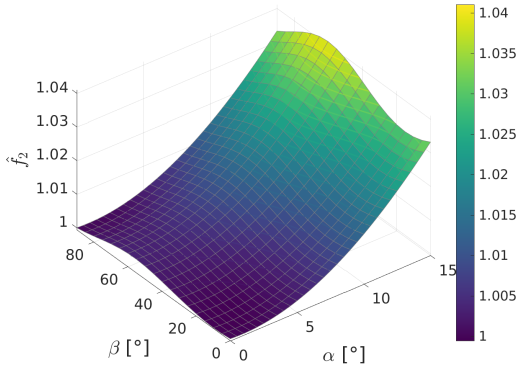

(b) Normalized natural frequency 2 (2F)

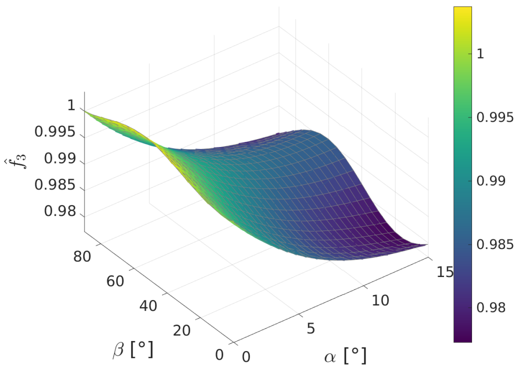

(c) Normalized natural frequency 3 (1E)

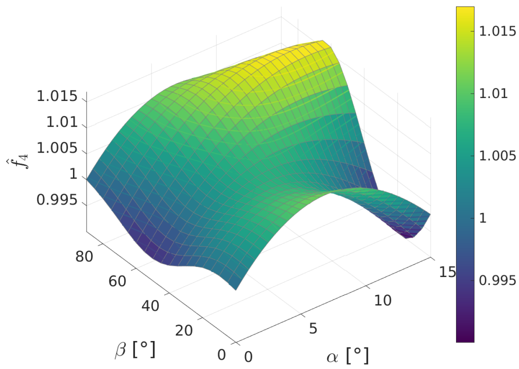

(d) Normalized natural frequency 4 (1T)

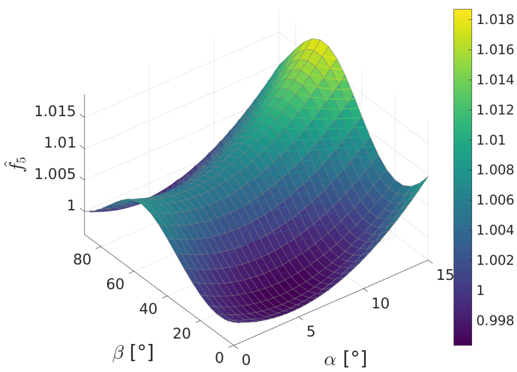

(e) Normalized natural frequency 5 (3F)

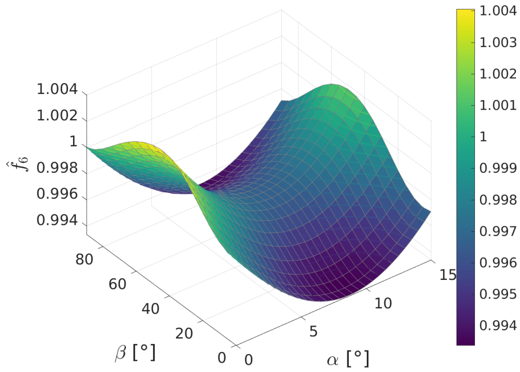

(f) Normalized natural frequency 6 (2E)

Figure 5.4: Normalized natural frequency of six modes with varying crystal orientation

the change increasing α value, that represent a deviation of [001] material axis from the stacking axis of the blade. The rate of change of natural frequencies increases as the value of α increases: the gradient is larger on $\alpha \in [10°, 15°]$ than on the range of $\alpha \in [0°, 5°]$. For these modes, the natural frequencies are more sensitive to the change in the value of α anisotropy angle, compared to β. It is worth noting that for large value of α, the sensitivity with respect to β increases.

For the edgewise modes (modes 3 and 6) a softening effect can be noticed for $\alpha \in [0°, 7°]$. This softening continues for the first edgewise mode, but for the second edgewise mode again a stiffening occurs on $\alpha \in [10°, 15°]$.

For mode 4 (1T), as expected the secondary angle also has a significant influence on the value of the natural frequency, which effect increases as α increases.

The variation of natural frequencies due to anisotropy axis orientation can be significant. The results show that for some of the modes, the natural frequencies can change within the range of up to 5-6%. For some higher modes, the change in crystal orientation can both stiffen or soften the blade. For the study carried out with 10,000 random crystal orientations, the mean value of the natural frequencies of the sample population is close in value to the natural frequency calculated for the blade with anisotropy orientation axis coinciding with the stacking axis. The studies show, that the primary anisotropy angle α has the most significant influence on the natural frequencies of the fundamental bending and edgewise modes, but for the first torsional mode both α and β are influential parameters.

5.2 Effect of anisotropy orientation axis scatter on the mistuned bladed disk mode shapes

In the previous section it has been shown, how the anisotropy orientation of the single crystal blade influences the natural frequencies for the stand-alone turbine blades. In the following, the effect of anisotropy orientation scatter on the mode shapes are discussed for mistuned turbine bladed disks.

For the studies the finite element model of a bladed disk with 75 blades is used, shown in Fig. 5.1b. The finite element mesh consists of 500,000 nodes. The model is constrained in axial direction at the blue nodes on the shoulder of the disk shown in Fig. 5.1b. For this bladed disk there are contact interfaces on the disk-blades joints and between the blades on the shrouds. For this study all these contact interfaces are considered to be stuck, which is modeled by linear multi-point-constraints (MPC).

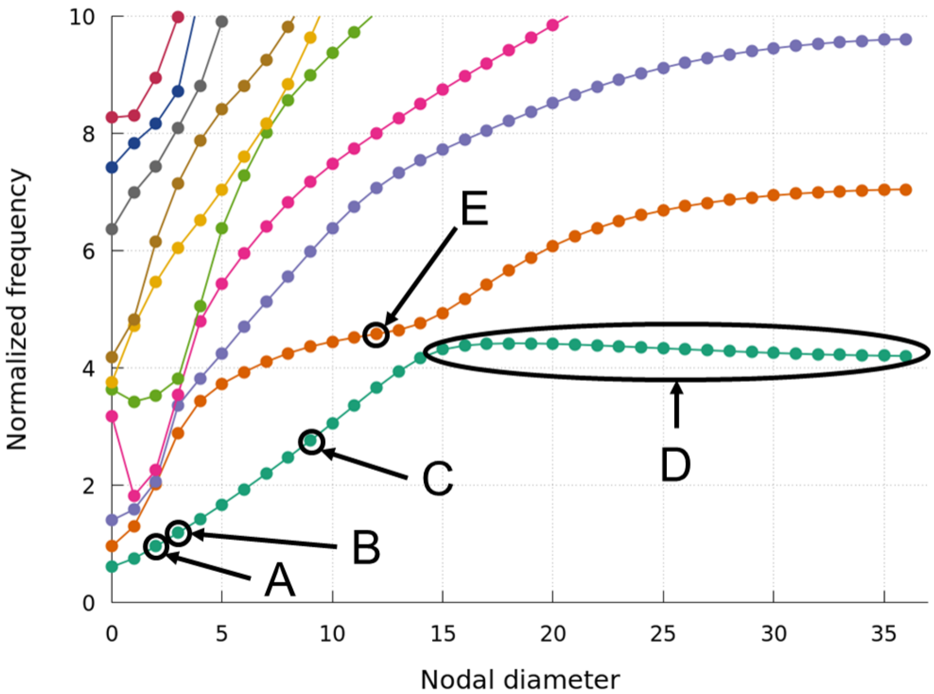

Figure 5.5: Natural frequency-nodal diameter diagram of the cyclic symmetric bladed disk model with full contact on the shrouds used in the subsequent analyses. Where the modes of interest are denoted by circles and Latin letters

The natural frequency - nodal diameter diagram has been calculated using the cyclic symmetric sector model of the bladed disk, see Fig. 5.5. In this figure, three different type of modes have been identified for the upcoming studies: (i) low nodal diameter (ii) high nodal diameter and (iii) transition modes. For the low nodal diameter modes the slope of the curves in Fig. 5.5 is nonzero. Due to the low nodal diameter pattern the disk is relatively flexible in comparison to the blades, therefore these modes are dominated by the disk modes. For the high nodal diameter modes the slope of the frequency-ND curves is 0 or close to 0. Because of the high nodal diameter pattern of the mode, the disks become stiff, and the mode of the bladed disk is dominated by the individual blade modes. Finally, the transition modes are defined where the slope of the frequency-ND curves level off and it includes characteristics of both disk and blade dominated modes. In Fig. 5.5 A and B are examples for disk dominated modes, C and E are examples for transition modes, and the modes in range D are blade dominated. Here, the transition modes are defined in the veering regions where mode shapes show the characteristics of blade dominated and disk dominated modes.

For the study of showing the influence of the crystal orientation variation on the mode

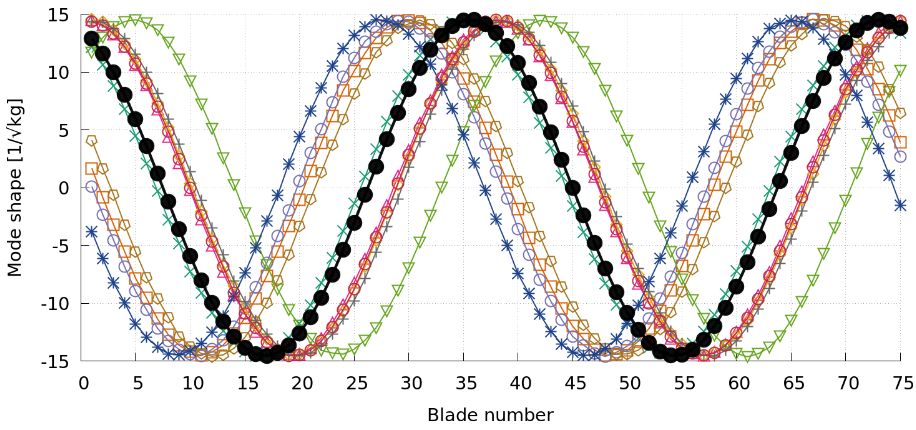

(a) Mode shape A, a disk dominated mode with $ND = 2$

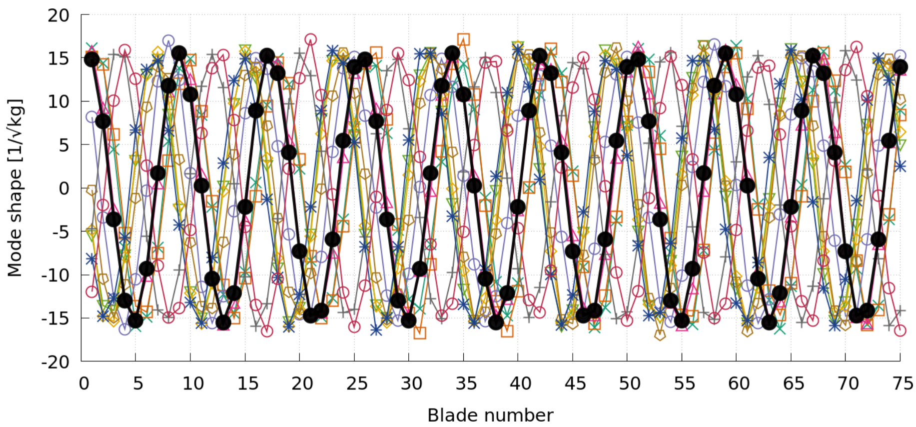

(b) Mode shape C, a transition mode between disk and blade dominated modes with $ND = 9$

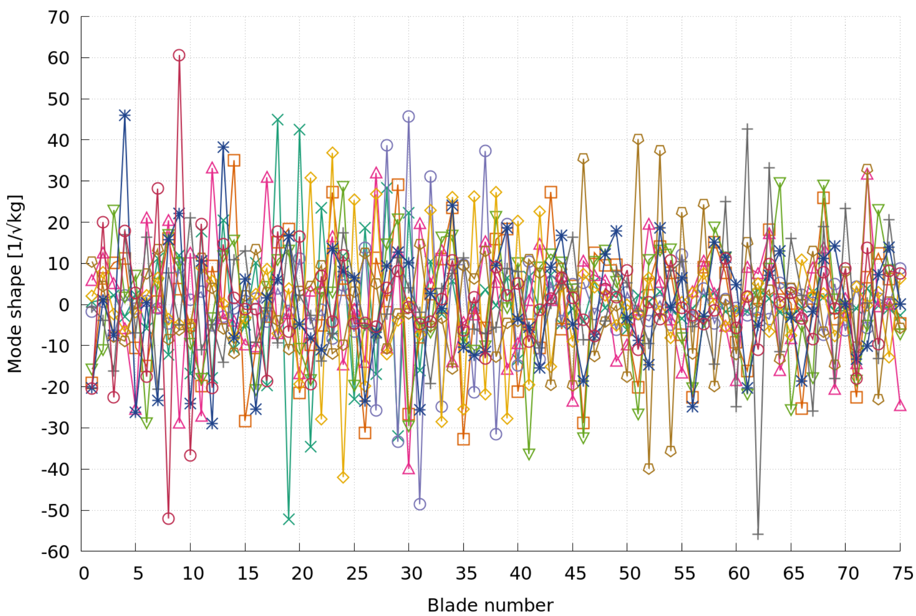

(c) Mode shape D, a strongly disk dominated mode without recognizable ND pattern

Figure 5.6: Mode shape along the bladed disk circumference showing the mode shape for tuned bladed disks (black line) and the variation for mistuned bladed disks with 10 different anisotropy mistuning patterns (colored lines)

shapes, modes A,C and range D are selected. In the study, the mode shapes for 50 mistuned bladed disks with random mistuning patterns have been calculated. Each crystal orientation for all the blades have been randomly evaluated based on the statistical distribution provided by the blade manufacturer.

The nodal value of the axial component of the mode shapes are plotted along the circumference of the bladed disk at one node for each blade. This node is at the midspan of the leading edge, shown with red circles in Fig. 5.1b. In order to be able to see the individual mode shapes, in Fig. 5.6 only the mode shapes of 10 different anisotropy mistuning pattern are plotted. Additional to the mistuned mode shapes, the tuned mode shapes for the full bladed disk has been plotted with thick black lines for modes A and C in Figs. 5.6a and 5.6b. Because the mistuned mode shapes in mode range D are highly localized, it was not possible to find a tuned equivalent.

For the disk dominated mode A, shown in Fig. 5.6a with 2 nodal diameter, other than phase shift between the modes shapes of the individual mistuning patterns, no other significant change can be seen.

For the transition mode C, shown in Fig. 5.6b, with 9 nodal diameters, a phase shift can be observed between the mode shapes of different mistuned bladed disks. However, for this higher nodal diameter mode shape, there is a small variation in the maximum value of the mode shape from mistuning pattern to mistuning pattern.

For the blade dominated mode, from range D, for each mistuning pattern the mode shape 76 has been selected, shown in Fig. 5.6c. It is clearly visible, that the nodal diameter pattern is very distorted and localization of the mode shape occurs. Depending on the mistuning pattern the extreme value of the mode shape and its location around the circumference of the bladed disk varies significantly.

5.3 Investigation of the sensitivity of modal characteristics for disk

The new capabilities for the calculation of the modal characteristics of bladed disks allow for the visualization of the sensitivity of the mode shapes using the already existing facilities of CalculiX GraphiX.

As an example the contour plot of the mode shape amplitudes are shown for mode 70, one of the blade dominated modes from range D, in Fig. 5.7a. This mode shape has a localization at blade 25 and in its neighboring blades. For this mode shape, the sensitivities

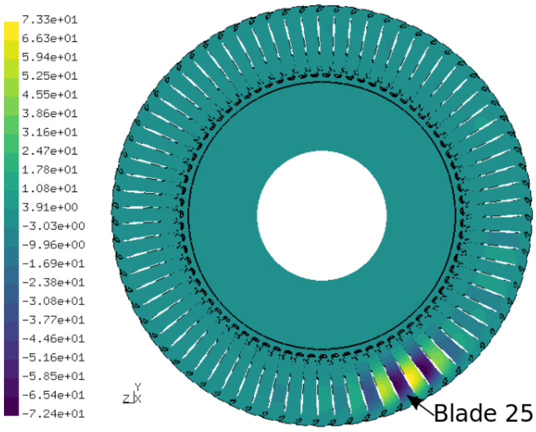

(a) Mode shape

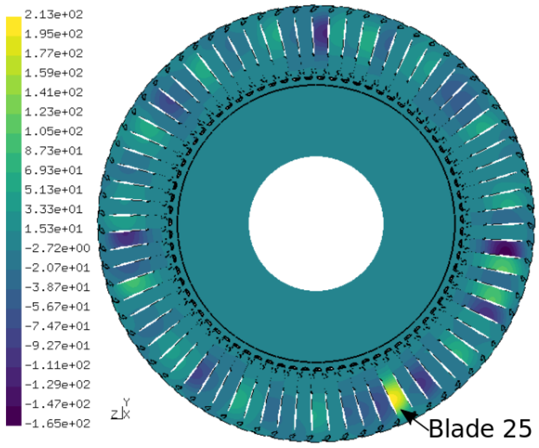

(b) Mode shape sensitivity

Figure 5.7: Mode shape D (70) and its sensitivity with respect to anisotropy angle α of blade 25

can be calculated with respect to all three anisotropy angles of the 75 blades. In Fig. 5.7b, the sensitivity of the mode shape amplitudes with respect to the primary angle α of blade 25 is shown for all FE nodes of the bladed disk. It is worth noting, that despite the mode shape being highly localized, the sensitivity with respect to the anisotropy angle has a global effect. The sensitivity maximum is for blade 25, but significant sensitivity values can also be observed around the circumference of the bladed disk. It is worth noting, that the mode has maximum amplitudes at the midspan of the blade, typical for 1F mode of shrouded blades, and the sensitivity of the mode shape has maximum values at the midspan of the blades.

The study of the sensitivities is divided into three groups: (i) disk dominated modes (ii) blade dominated modes and (iii) transition modes. In order to gain a comprehensive insight into the sensitivity of the modal characteristics, for each mode under investigation, the mode shape, the sensitivity of natural frequencies and the sensitivity of mode shapes are discussed together. There has been many anisotropy mistuning patterns studies, however here an example the results for one mistuning pattern are discussed in detail.

5.3.1 Disk dominated modes

As disk dominated mode, the mode B from Fig. 5.5 is analyzed. The mode shape of this mode, shown is Fig. 5.8a has 3 nodal diameter and it has the largest modal displacement in axial direction. The sinusoidal shape of the nodal diameter mode shape does not visibly get distorted.

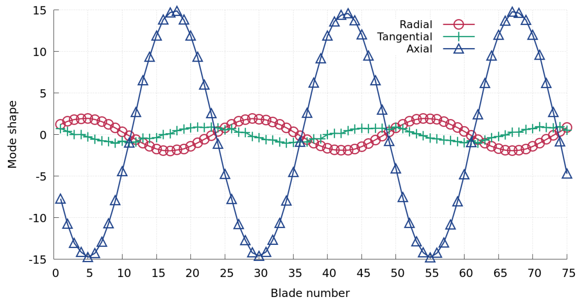

(a) Modal displacements in three spatial direction along the bladed disk circumference

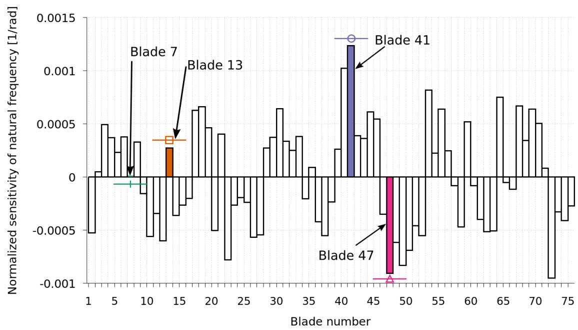

(b) Sensitivity of natural frequency to α angles of all blades

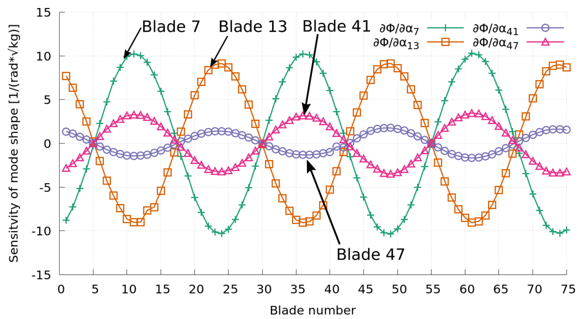

(c) Sensitivity of axial modal displacements of the mode shape to α angles of selected blades along the bladed disk circumference

Figure 5.8: Mode B: Mode shape and sensitivity of modal characteristics for a disk dominated mode

The normalized value of the sensitivities of the natural frequency with respect to the all the 75 primary angles of the bladed disk are shown in Fig. 5.8b. The values of the sensitivities of the natural frequency are small.

The sensitivity of the disk dominated mode shape with respect selected primary anisotropy angles have been plotted in Fig. 5.8c. The anisotropy angles shown in the figure have been selected such: (i) two are the primary angles with respect to the maximum and minimum natural frequency Sensitivities have been obtained (blades 41 and 47), and (ii) two blades for which the maximum and minimum value of the mode shape sensitivity is obtained along the circumference of the bladed disk (blades 7 and 13). The α anisotropy angles of blades 41 and 47 has the largest effect on the natural frequency of the bladed disk however, the sensitivity of the mode shape with respect to these anisotropy angles are small. On the other hand, the blades that influence the mode shape the most have small sensitivity of the natural frequencies.

It is also worth noting that sensitivities of the modes shapes are shifted to the mode shapes by 90° along the circumference of the bladed disk. The sensitivity of mode shape has extreme value where the mode shapes are null and has null value where the mode shapes have extreme value. This confirms the earlier made conclusions that the variation of the anisotropy mistuning patterns do not change the maximum value of the modal displacements, however the phase along the circumference of the bladed disk can vary from one mistuning pattern to another.

5.3.2 Blade dominated modes

From range D, shown in Fig. 5.5, mode number 70 has been selected for the study of a blade dominated mode. This mode is from the first family of modes, and the mode shape is localized for approximately seven blades, shown in Fig. 5.9a. For this mode shape, the tangential and axial modal displacements are the largest.

The sensitivity of the natural frequencies with respect to all the primary angles α in the bladed disk are shown in Fig. 5.9b. The figure shows that the largest sensitivity of natural frequencies are with respect to the blades that have large modal displacements, blades 22-28. The sensitivities with respect to the anisotropy angles of the blades with small modal displacements are negligible. For this mode, the normalized natural frequency sensitivities are larger than for mode B.

The sensitivities of the mode shape with respect to selected α anisotropy angles are shown in Fig. 5.9c. Here, the sensitivities are shown with respect to selected anisotropy angles. Anisotropy angles to which high natural frequency sensitivity is calculated and one primary angle α to which the sensitivity of natural frequency is negligible (blade 50). The sensitivities of the mode shape with respect to the anisotropy angles of blades 25, 26 and 28 are large around the whole circumference of the bladed disk. The extreme value of the mode shape sensitivities are for the blades 25 and 28 and with respect to their respective primary anisotropy angles. It is worth noting, that the sensitivities of the mode shapes are not localized, meaning that changing the anisotropy angle of a blade with large

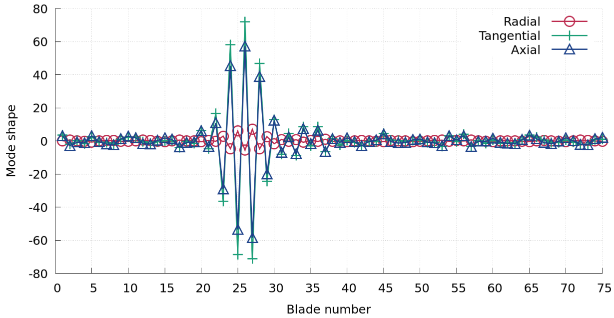

(a) Modal displacements in all three spatial direction for mode 70 (D) along the bladed disk circumference

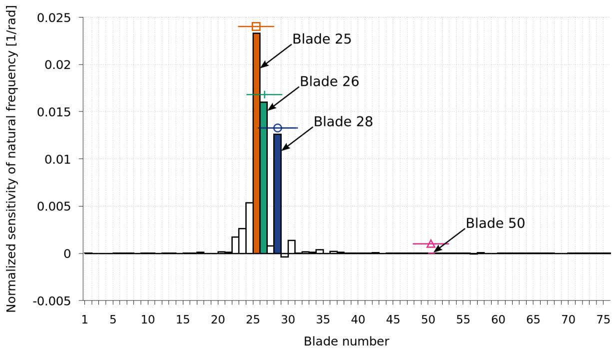

(b) Sensitivity of natural frequency to α angles of all blades

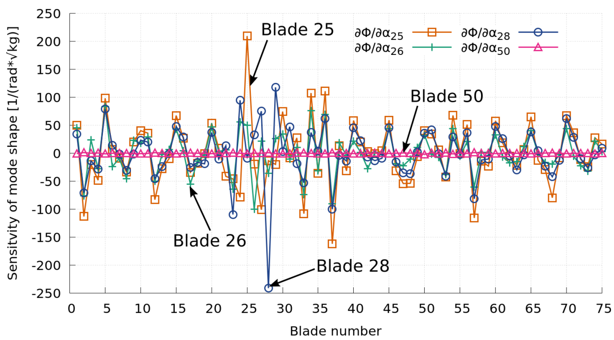

(c) Sensitivity of tangential modal displacements of the mode shape to α angles of selected blades along the bladed disk circumference

Figure 5.9: Mode 70 (D): mode shape and sensitivity of modal characteristics for a blade dominated mode

modal displacement can influence many blades in the bladed disk stage. The value of the sensitivities of the mode shapes for disk dominated modes are at least one magnitude larger than for disk dominated modes.

5.3.3 Transition modes

The mode shape of transition mode E in Fig. 5.5 is shown in Fig. 5.10a. The mode shape has a distorted nodal diameter pattern with 12 nodal diameters.

The sensitivities of the natural frequency with respect to all the α angles of the blades are shown in Fig. 5.10b. Because there is no localization in the mode shape, the sensitivities of the natural frequency are also not only significant for a restricted number of blades. With only a few exceptions all primary anisotropy angles increase this natural frequency of the bladed disk.

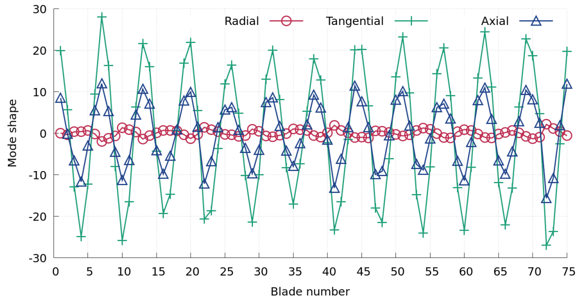

(a) Modal displacements in all three spatial direction for mode E along the bladed disk circumference

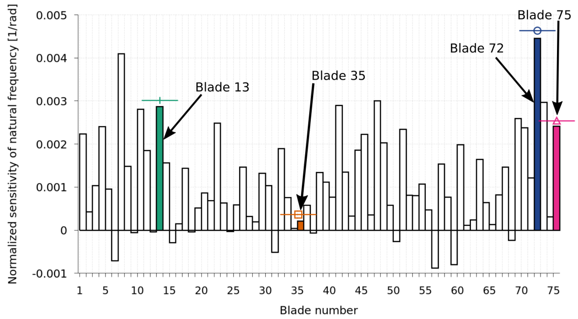

(b) Sensitivity of natural frequency of mode E to α angles of all blades

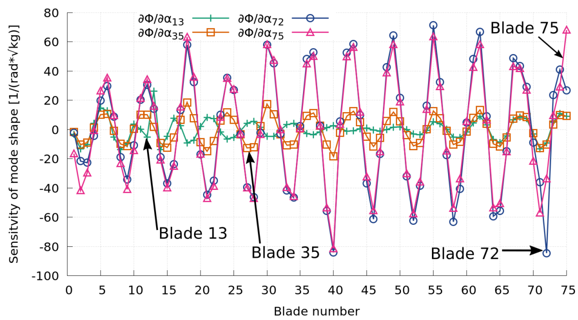

(c) Sensitivity of modal tangential displacements of mode shape E to α angles of selected blades

Figure 5.10: Mode E: sensitivity of modal characteristics for a transition mode of a mistuned bladed disk

The sensitivity of the mode shapes, shown in Fig. 5.10, with respect to selected blades. Blade 72 and 75 has large influence on the natural frequency and on the mode shape, with sensitivities with respect to blade 72 having extreme value for both sensitivities. The crystal orientation of blade 35 has little influence on the natural frequencies, however the sensitivity of the mode shape with respect to this blade cannot be neglected. On the other hand, the sensitivity of the natural frequency with respect to the α anisotropy angle of blade 13 is relatively large, the sensitivity of mode shape is not more significant than the sensitivity with respect to blade 35 anisotropy angle.

Therefore, it can be concluded that the transition nodes have the characteristics for disk and blade dominated modes. The sensitivity of natural frequencies and mode shapes with respect to some blades are coupled, meaning they are both relatively large. But for some blades are not coupled, meaning that they have high influence on the natural frequency but small influence on the mode shape or the other way around.

It is worth noting, that for transition modes, the value of the normalized sensitivities are larger than for disk dominated modes, but smaller than for blade dominated modes.

5.4 Maximum value of sensitivity of natural frequencies for the first family of modes with analysis for the effect of shroud boundary conditions on the sensitivity of natural frequencies

The examples presented in the section above, showed the characteristics of the sensitivity of modal properties for disk and blade dominated and for transition modes for anisotropy mistuned bladed disk. In this section the sensitivity of natural frequencies are studied further for all the modes of the first mode family. For the first 80 modes, the maximum and minimum value of the sensitivity of natural frequency is calculated with respect to anisotropy angles α, β and ζ. This calculation is carried out for three kind of contact conditions between the shrouds of the blades: (i) stuck shroud, the same as it has been used in the previous examples (ii) perfectly sliding shroud interfaces (iii) no contact between the shroud interfaces.

The extreme values with respect to the anisotropy angles are shown in Fig. 5.11 for stuck shrouds. For the first 10 modes, the value of the sensitivities are negligible, these modes are disk dominated modes with nodal diameter mode shape pattern. The transition modes ranging from mode 25 to 69 show increasing values for the sensitivities of the natural frequencies. These modes are the transition modes. The modes ranging from 70 to 80 are blade dominated modes with localized mode shapes, which results in high values of natural frequency sensitivities. It is worth noting that the largest positive values of the sensitivities are with respect to the primary anisotropy angles α, but the largest negative sensitivities are with respect to the β anisotropy angles for this mistuning pattern. The sensitivities of the natural frequencies with respect to ζ anisotropy angles are negligible for all 80 modes.

For the bladed disk with perfectly sliding shroud contact conditions, the extreme value plot of the natural frequencies change, see Fig. 5.12. The sensitivities with respect to

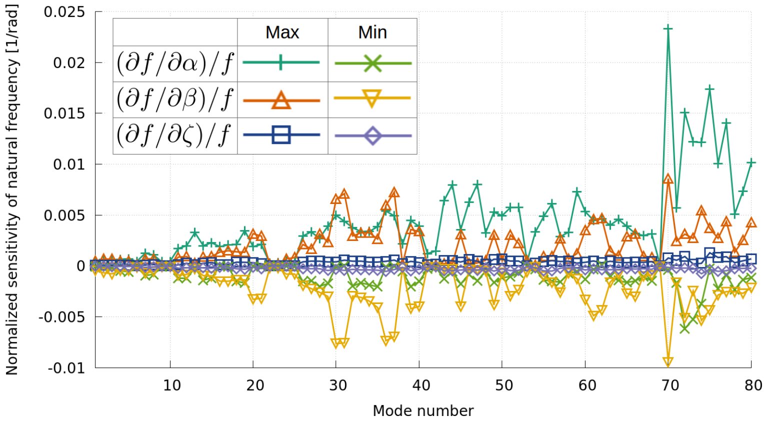

Figure 5.11: Highest value of the normalized natural frequency sensitivity with respect to all anisotropy angles for a mistuned bladed disk with stick contact on the shrouds

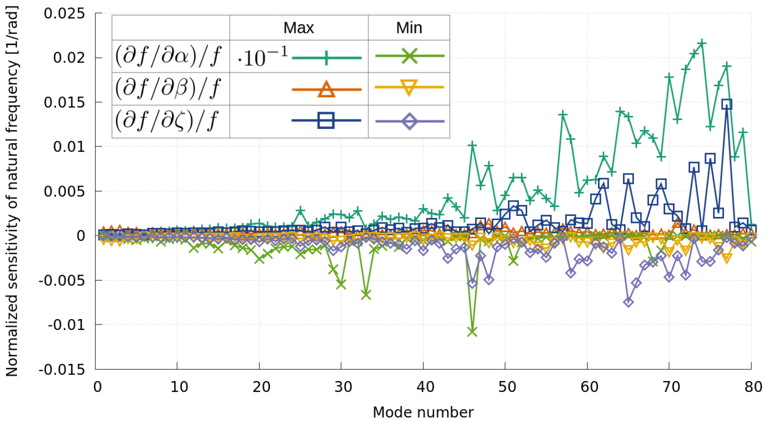

Figure 5.12: Highest value of the normalized natural frequency sensitivity with respect to all anisotropy angles for a mistuned bladed disk with sliding contact on the shrouds

the primary angle α increase significantly. This is due to the earlier localization of the blade dominated modes as the coupling between the blades are reduced as the contact condition is changed to sliding. With the increase of the sensitivity of the primary angles, the sensitivities with respect to ζ also increase. This is due to the coupling between the two anisotropy angles, because ζ is defining the position of the [001] material axis on a polar coordinate basis. This results in sensitivities that are larger with respect to ζ than to α or β for most localized modes.

The coupling between the blades further reduced when the contact definition between the blade shrouds are removed. The sensitivities with respect to α increase compared to the results calculated for the bladed disk with sliding contact. The sensitivities with respect to β and ζ are similar to what has been obtained for the bladed disk with sliding contact.

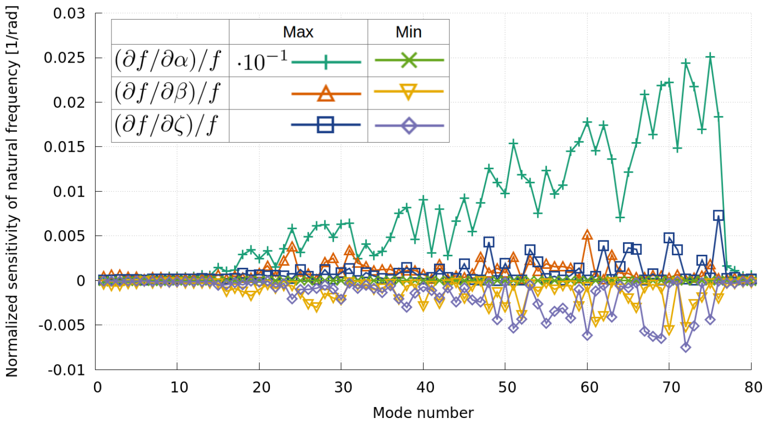

Figure 5.13: Highest value of the normalized natural frequency sensitivity with respect to all anisotropy angles for a mistuned bladed disk without contact on the shrouds

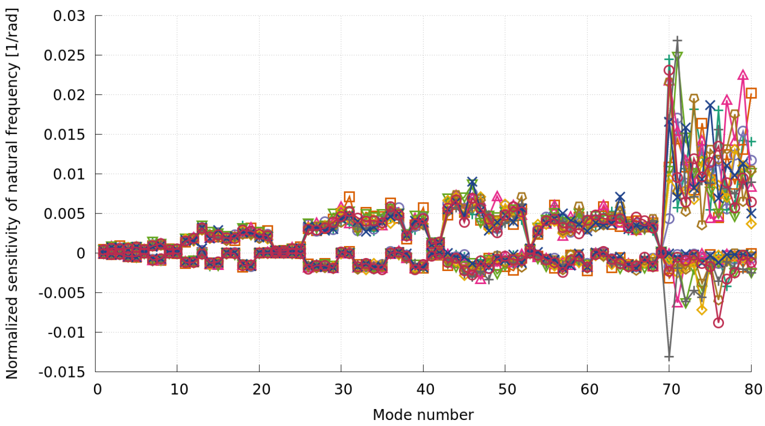

Figure 5.14: Highest value of the normalized natural frequency sensitivities to α for ten different mistuning pattern and with stuck contact on the blades shrouds

In order to see the validity of the results for more mistuning patterns, the sensitivity of the natural frequencies have been calculated for 10 different mistuning patterns. In Fig. 5.14 the maximum and minimum values of the sensitivity of the first 80 natural frequencies are shown with respect to the primary anisotropy angle α. The numerical value of the extreme values of the sensitivities are very close for the 10 different mistuning patterns in case of the lower modes. The modes higher than 70, that are blade dominated modes, the values significantly increase and vary for the different mistuning patterns.

5.5 Conclusions

In this chapter the effect of the anisotropy mistuning has been studied for modal properties and their sensitivities of single blades and bladed disks. The effect of natural frequency for stand-alone blades have been studied by a series of random sampling. The results show that the crystal orientation can increase and decrease the natural frequencies and the distribution of natural frequencies are asymmetric.

The anisotropy axis scatter for bladed disks have been studied for disk dominated, blade dominated and transition modes. The modes with low nodal diameter patterns do not significantly change due to mistuning. The effect of the mistuning for blade dominated modes resulted in strong localization, where the modal displacements are significantly larger for a few blades when compared with the rest of the blades.

The analysis of the sensitivity of the natural frequencies and mode shapes showed that the localized mode shapes of the mistuned bladed disks are most sensitive to the change in the crystal orientation. In case of the localized mode shapes the sensitivities with respect to the anisotropy angles of the blades where localization occurs highly influence the modal properties.

The study of the effect of the different boundary conditions of the shrouded blade disks on the natural frequency sensitivities has been performed. The analyses showed that the sensitivity with respect to anisotropy angles increases as the coupling with the neighboring blades reduces.

Chapter 6

Linear forced response and its sensitivity for the anisotropy mistuned bladed disks

The study of many linear systems is relevant for many bladed disks. For example the modern compressor stages are integrated bladed rotors and therefore inherently linear dynamic systems. For turbine bladed disks with friction joints, it can be advantageous to linearize the models. Linear models can be used to obtain forced response amplitudes of bladed disks faster and there is no need to calculate forced response with a computationally expensive nonlinear solver. The linearization of bladed disks can be done if measurement data is available for the turbine stage [31]. And applying an equivalent linear damping coefficient by a half-power method in the measurement data. Calculating equivalent linear damping is particularly successful if individual resonance peaks can be isolated and there are no strong nonlinearities in the system, e.g. partial opening of shroud interfaces, that can cause the forced response function to have overhanging branches.

In the current study a realistic mistuned bladed disk with 75 blades with approximately 0.5 million FE nodes, see Fig. 5.1b.

6.1 Comparison of the modeling methods of frequency mistuning and anisotropy mistuning for linear forced response of monocrystalline mistuned bladed disks

Traditionally mistuned bladed disks are modeled with frequency mistuning that is introduced by adding lumped masses or by changing the Young's and/or the shear modulus to change the natural frequency of the individual blades. In this section, the traditional method of modeling mistuning is compared with the direct anisotropy modeling, used in this work.

First, a random anisotropy mistuning pattern is created for all blades in the bladed disk. The five first natural frequencies are calculated for all stand-alone blades with random crystal orientations and the nominal elasticity and shear modulus. The stand-alone blades are calculated together with the disk sector, that is fixed on the sector edges. The natural frequencies are calculated for non-rotating blades i.e. without any pre-stress applied.

Second, the mean value of the anisotropy angles is calculated and the corresponding crystal orientation is set for all stand-alone blades. At the same time, the Young's modulus and shear modulus is scaled such that the same stand-alone first natural frequencies are obtained. The scaling factor is calculated for i-th blade using equation

$$c_i = \left(\frac{\omega^i_{anisotropy}}{\omega_{mean}} \right)^2 \tag{6.1}$$

where $\omega^j_{anisotropy}$ is the first natural frequency of the anisotropy mistuned stand-alone blade and ω_{mean} is the first natural frequency of the stand-alone blade with mean crystal orientations and nominal stiffness properties.

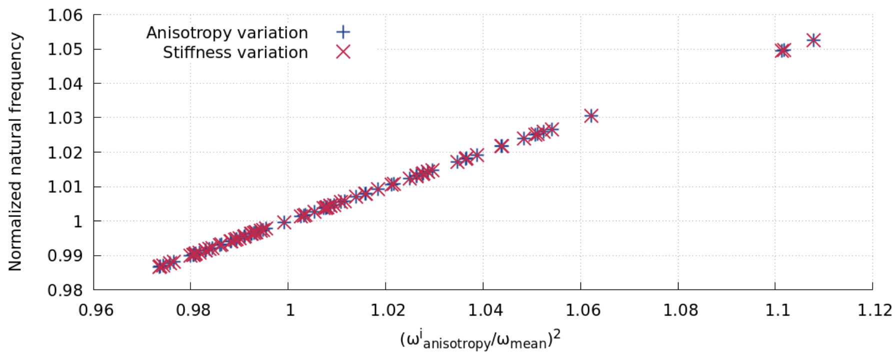

Figure 6.1: First natural frequencies calculated for anisotropy and stiffness detuned stand-alone blade against scaling factor value

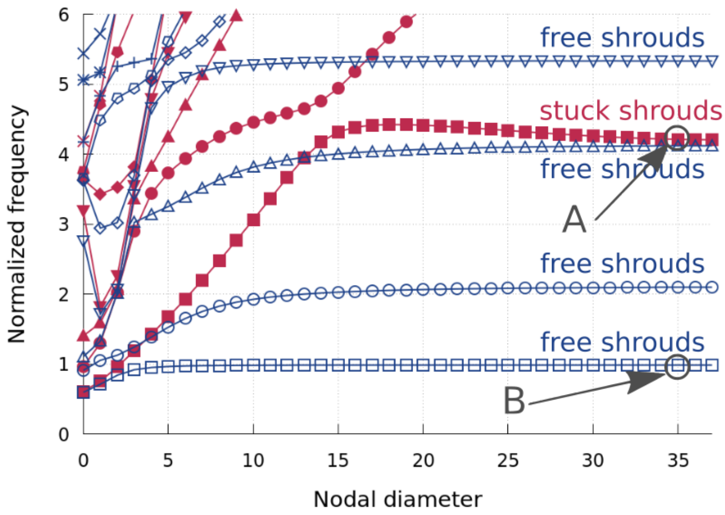

Figure 6.3: Natural frequency-nodal diameter diagram of the cyclic symmetric model with stuck and free shroud interfaces

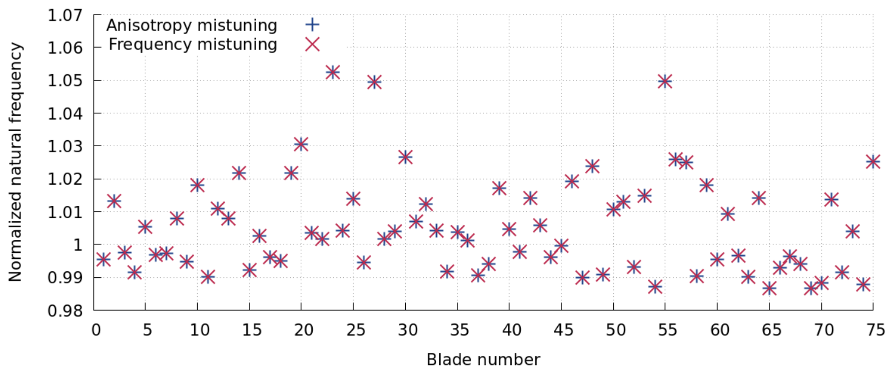

Figure 6.2: First natural frequencies calculated for anisotropy and stiffness detuned stand-alone blade against blade number

In the next step, the natural frequencies and mode shapes have been calculated for the frequency mistuned and for the anisotropy orientation mistuned bladed disk. The first natural frequencies are equal when calculated with both detuning methods, see Figs. 6.1 and 6.2.

The full model of mistuned bladed disk is assembled using the stand-alone blades with frequency detuning. The first 150 modes of the mistuned bladed disks have been calculated. The contact interfaces of the bladed disks are modeled linearly using MPCs. Two different modeling has been considered on the shroud interfaces of the mistuned bladed disk: (i) fully stuck contact and (ii) no contact.

For shroud contact conditions (i) and (ii), the forced response has been calculated to

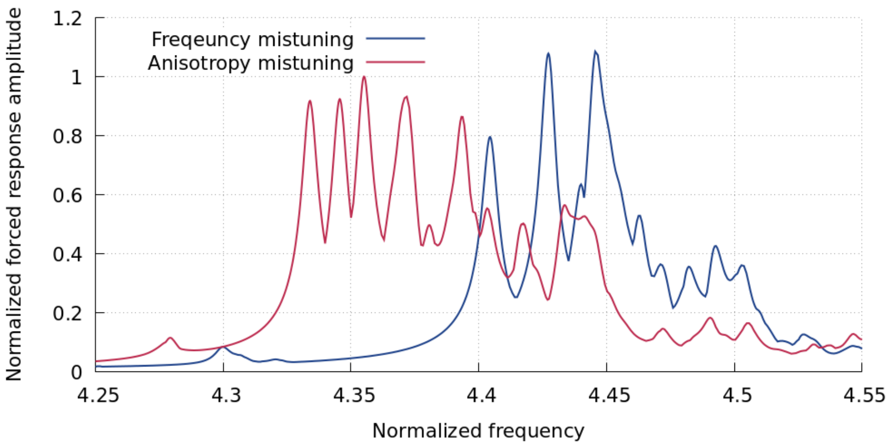

Figure 6.4: Envelope of the linear forced response calculated with anisotropy and frequency mistuning for EO35 excitation of mode 1 with stuck shrouds

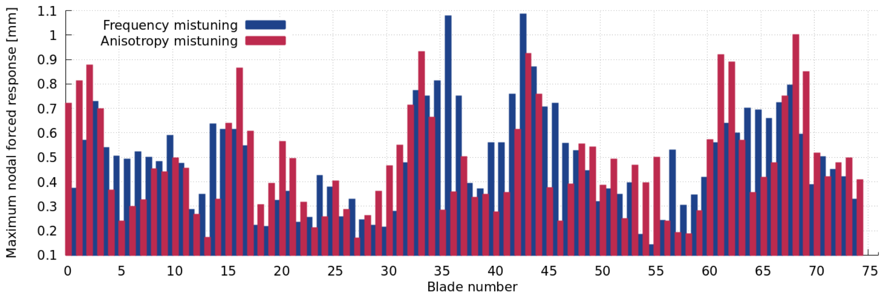

Figure 6.5: Maximum forced response amplitude of each blade over the analyzed frequency range for anisotropy and frequency mistuned bladed disk to EO35 excitation to mode 1 with stuck shrouds

EO35 excitation for the first mode family, marked by A and B in Fig. 6.3. The forced responses have been obtained for bladed disks with anisotropy and frequency mistuning.

The envelope of the forced response for bladed disk with stuck shrouds (i) when mode A is excited is shown in Fig. 6.4. The resonance frequency of the forced response of the mistuned bladed disk modeled with frequency mistuning shows 2% increase compared to full modeling of anisotropy mistuning. The envelope of the response shows difference in the maximum forced response amplitudes, 9% increase compared to when frequency mistuning is applied. The distribution of the maximum forced response amplitudes along the circumference of the mistuned bladed disk shows significant differences when compared for the two modeling methods, as seen in Fig. 6.5. The results obtained show, that for the analysis of the turbine bladed disks with shroud contact, the method of frequency mistuning based on the natural frequencies of stand-alone blades does not provide sufficient accuracy.

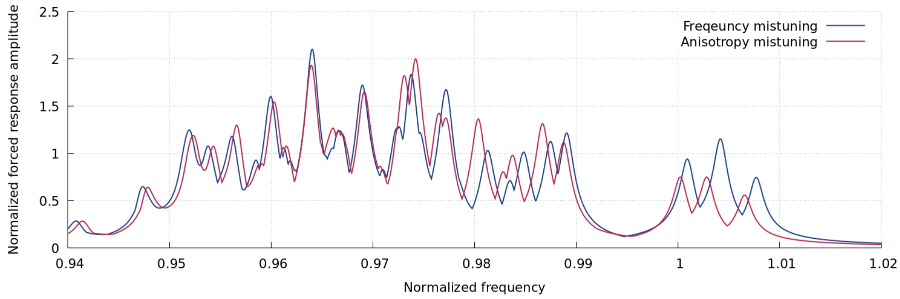

Figure 6.6: Envelope of the linear forced response calculated with anisotropy and frequency mistuning for EO35 excitation of mode 1 with free shrouds

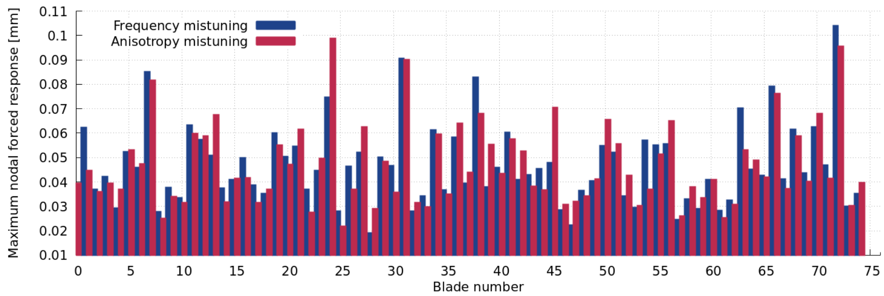

Figure 6.7: Maximum forced response amplitude of each blade over the analyzed frequency range for anisotropy and frequency mistuned bladed disk to EO35 excitation to mode 1 with free shrouds

Additionally, the forced response of the mode 1 for bladed disks with (ii) open shrouds were analyzed using the two methods for the modeling of mistuning. Because the first mode family of the bladed disk without shroud contact is very similar to the first mode of the stand-alone blade, the envelope and the distribution of the forced response amplitudes are very similar when calculated using the two mistuning modeling methods. The resonance frequency of the forced response function, as shown in the Fig. 6.6, is from a practical view identical for both mistuning modeling methods. The study of the distribution of the maximum forced response, shown in Fig. 6.7, show that the maximum amplitude on the calculated frequency range varies when they are calculated with anisotropy mistuning or frequency mistuning modeling. Nevertheless, the observed differences in case of open shrouds are smaller than for the bladed disk with closed shrouds.

For the 2$^{\text{nd}}$ mode of the same bladed disk with (ii) open shrouds the comparison of the two modeling methods for the mistuning modeling was done. The modeling of the frequency mistuning uses the same coefficients as previous studies, using Eq. (6.1) for mode 1 of the stand-alone blades. The envelope of the two mistuned forced responses

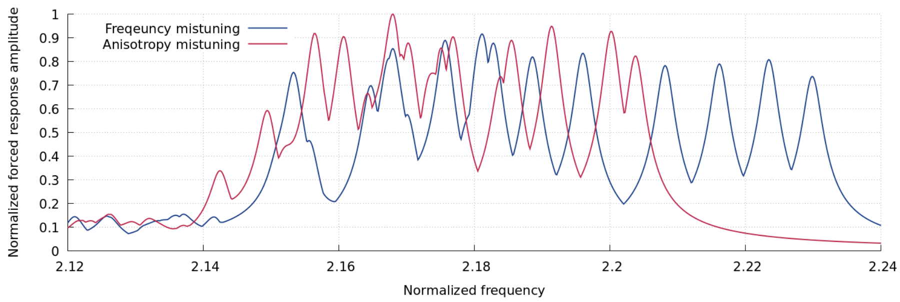

Figure 6.8: Envelope of the linear forced response calculated with anisotropy and frequency mistuning for EO35 excitation of mode 2 with free shrouds

in Fig. 6.8 show larger deviation between the forced response curves calculated with the two mistuning modeling methods. In order to be able to obtain acceptable results, the frequency mistuning coefficients need to be calculated for the 2^{nd} mode of the stand-alone blade.

The above presented studies show that it is essential to use high-accuracy modelling of the anisotropy mistuned bladed disk. The studies above investigated the forced response of the bladed disk modes to high engine order excitations. Due to the high stiffness of the disk the high nodal diameter modes are blade dominated, which also means that the bladed disk modes are very similar to the restricted stand-alone blade modes. The deviation between the forced response functions obtained with frequency mistuning and high-accuracy anisotropy mistuning are expected to be larger.

For the analysis of the nonlinear forced response, it is essential to use the high-accuracy anisotropy mistuning modeling, because in the nonlinear forced response calculation all modes are involved.

6.2 Effect of anisotropy orientation scatter on the forced response of mistuned bladed disks

The study of anisotropy orientation variation of the single crystal turbine bladed disks on the linear forced response was studied by generating 10 random mistuning patterns. The 10 random anisotropy mistuning patterns were created by random sampling from the statistical distributions described for the anisotropy angles. The effect of anisotropy mistuning has been analyzed for resonances of the modes shown in Fig. 6.9. For the selection of the modes several criteria has been considered: (i) both lower fundamental modes and higher modes were analyzed (ii) low nodal diameter (disk dominated), high nodal diameter

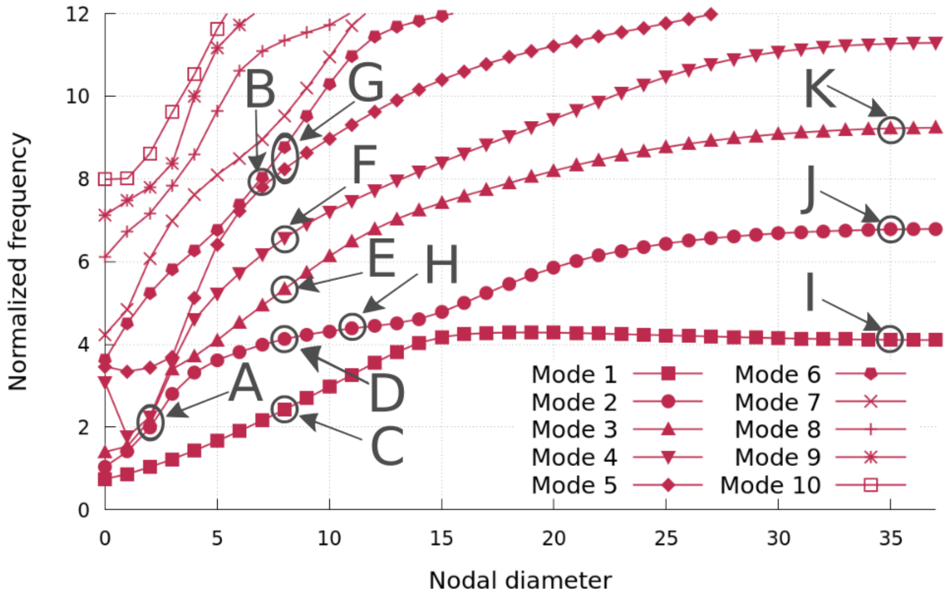

Figure 6.9: Natural frequency-nodal diameter diagram of tuned bladed disk with stuck root and shroud interfaces

(blade dominated) and modes with nodal diameter values in between (transition modes) have been studied (iii) veering regions where two or more modes can interact.

For each mode the amplification factor has been calculated, such that maximum forced response amplitude of the mistuned bladed disk has been divided by the maximum forced response of the tuned bladed disk on the analyzed frequency range. The tuned bladed disks have all blade crystal orientation aligned with the stacking axis ($\alpha = \beta = \zeta = 0$). The forced response is calculated for 15 nodes on the airfoil directly from the reduced order model. The nodes are shown in Fig. 6.10, where each node is referred to by its radial (A to E) and by its axial (1 to 3) location. For each mode of the tuned bladed disk a screening is done to decide which node has the largest displacement and the amplitude of this node will be used to calculate the amplification factor of the mistuned bladed disks.

In Figure 6.11 the mean value of the amplification factors for the 10 random mistuning patterns are plotted. The largest amplification factors are observed for the veering region B when EO7 excitation is applied, the maximum mistuned forced response is more than 2.6 higher than for the tuned bladed disk. The large amplification factor is due to the interaction between other modes in this frequency range.

For modes in range G, the frequency gap between modes 5 and 6 increases due to the anisotropy mistuning. Therefore, the interaction between the two modes is not significant. This results in a lower average amplification factor: 1.61. The amplification factors for the

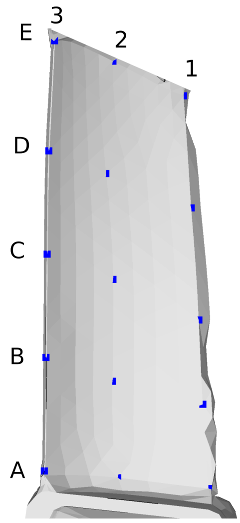

Figure 6.10: Nodes of output on the pressure side of the airfoil

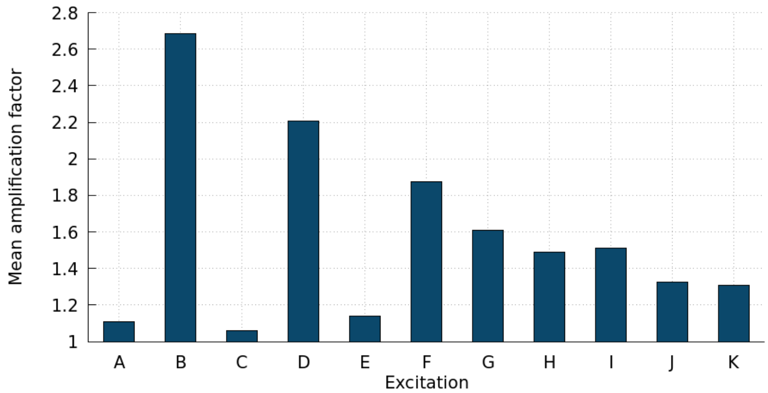

Figure 6.11: Average amplification factors calculated for linear forced response of several modes for 10 different anisotropy mistuned bladed disks

disk dominated modes e.g. modes A, C and E are the lowest, under 1.2.

In Fig. 6.12, the envelope of forced response for 10 different mistuning patterns and the forced response for two tuned bladed disks are shown. The tuned bladed disks are either set-up such that the anisotropy axis is aligned with the stacking axis for all blades (tuned: 0) or all anisotropy angles are set to the mean value of their respective statistical distributions (tuned:mean). The forced response envelopes for these disk dominated modes show little sensitivity to the anisotropy orientation of the single crystal blades, only the splitting of the resonance frequencies can be observed. Further learning is that the resonance frequencies of the mistuned bladed disks are in between the resonance frequency of the two tuned forced responses. It is also worth noting, that all mistuning patterns have amplification factors higher than 1, which is in agreement with the expectations.

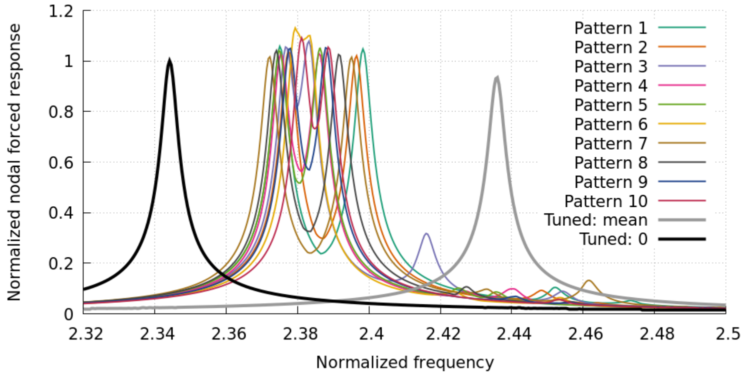

Figure 6.12: Envelopes of the forced response calculated for 10 different anisotropy mistuning patterns at 8EO for mode family 1 (C)

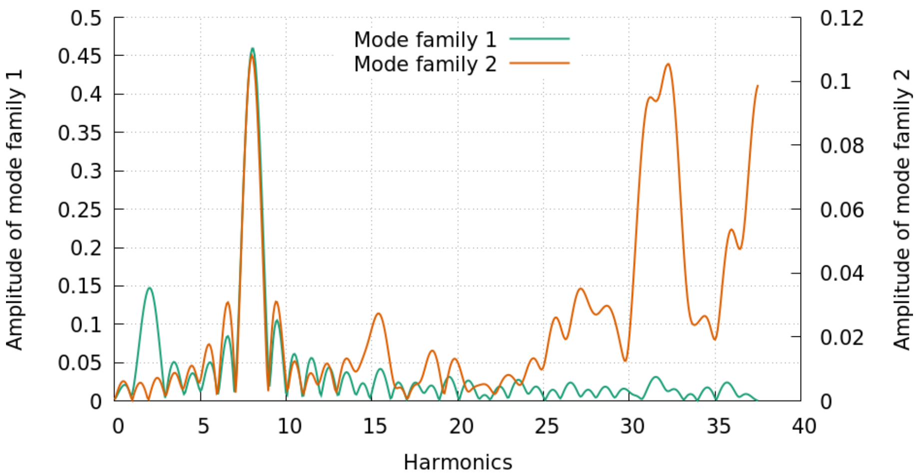

Figure 6.13: Harmonic spectrum of the response for 8EO excitation of mode family 1 (B) and 2 (D)

For the modes of D and F, the low engine order 8 excitation is applied. Because the bladed disk is mistuned, in the modes in the same frequency range but with high nodal diameter are also excited. To study which modes of the mistuned system are excited, the Fourier transformation of the tangential displacements along the circumference of the bladed disk has been calculated for modes B and D, see Fig. 6.13. The analysis of the harmonic coefficients shows that for the first mode (mode B) the 8^{th} nodal diameter mode is dominant. When mode D is excited then nodal diameter 8 and also the higher nodal diameter modes of mode family 1 is excited, which results in the larger values of amplification factor.

The forced response envelopes of the 10 random mistuned bladed disks are shown in Fig. 6.14 for mode D. The resonance frequencies of the mistuned systems are, similarly

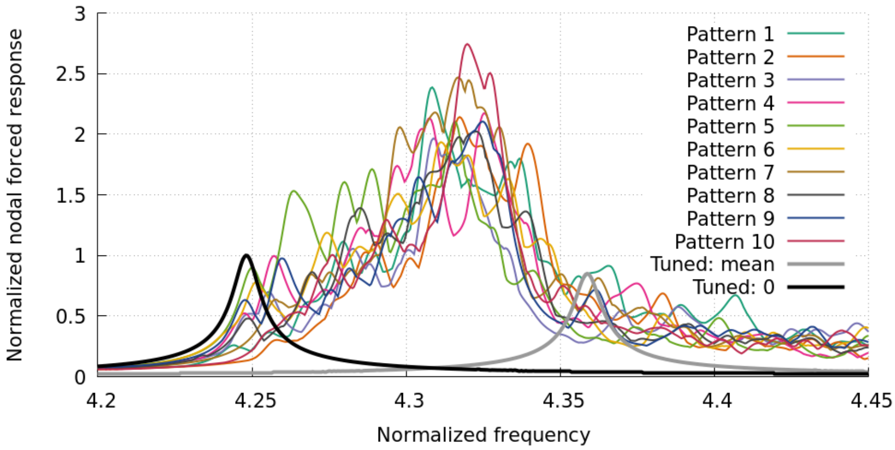

Figure 6.14: Envelopes of the forced response calculated for 10 different anisotropy mistuning patterns at 8EO for mode family 2

as for mode C, between the resonance frequencies of the two tuned forced responses. The shape of the forced response envelopes indicate that the response is dominated by localized modes.

The modes I,J and K that are excited by EO35 excitation. The high engine order excitation stiffens the disk, and therefore the individual blade modes become more dominant, therefore an average amplification of 1.31-1.51 is obtained that is larger than what has been calculated for the purely disk dominated modes of A,C and E. The large engine order excitation cannot excite the modes with lower nodal diameter, which results in a lower amplification factor that is observed for modes D and F.

6.3 Sensitivity analysis of the forced response of the anisotropy mistuned bladed disk

For the sensitivity analysis of the anisotropy mistuned bladed disk the modes have been selected: (i) a disk dominated, mode C (ii) disk dominated mode that is coupled with higher nodal diameter blade dominated mode, mode D and (iii) blade dominated mode of the first family, mode I. For all modes the mistuning pattern 1 is selected for the further sensitivity analyses.

6.3.1 Disk dominated modes

The forced response of the mistuned bladed disk to EO8 excitation in the frequency range of the first mode family (mode C) is shown in Fig. 6.15a. The forced response function

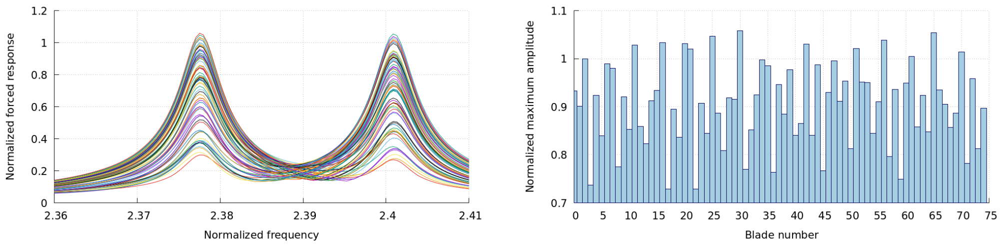

(a) Forced response function of all blades

(b) Maximum forced response for each blade over

Figure 6.15: Forced response function and maximum forced response amplitudes of all blades for 8EO excitation of mode family 1

shows doubling of the resonance frequency. The forced response for all blades is shown considering the screening for the maximum forced response over the nodes on airfoil, as shown in Fig. 6.10. The maximum forced response amplitudes are located at the tip or the airfoil, between nodes E1,E2 and E3, for all 75 blades.

The maximum forced response of every blade over the given frequency range is depicted in Fig. 6.15b, which shows that no blade has significantly larger, localized large amplitude. Moreover, it is worth noting that the maximum forced response amplitude along the circumference of the bladed disk shows an imperfect periodicity with 8 nodal diameter pattern.

The location on the airfoil for the mistuned system has been identified for all blades on the frequency range of mode family 1. All blades have the maximum vibration amplitudes at the tip of the airfoil, row E in Fig. 6.10, which is expected for a coupled-disk "umbrella" mode. The Fig. 6.16 shows that almost all blades have the largest vibration amplitudes at the trailing edge (node E3), but a small portion of blades have the location of maximum forced response at nodes E1 and E2. This change of the maximum forced response amplitudes is another example for the effect of anisotropy mistuning on the forced response functions, here namely the change of the operational deflection shape of the mistuned system compared to the tuned bladed disk.

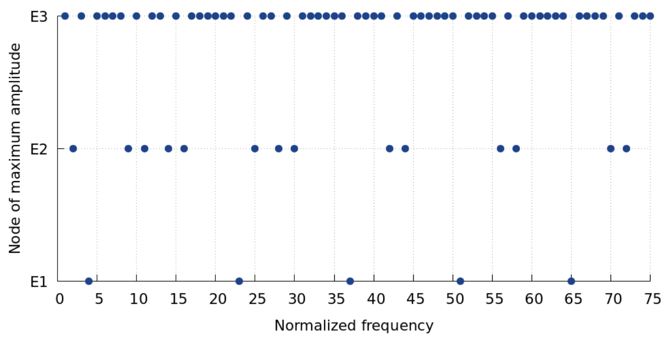

Figure 6.16: Location of maximum forced response for each blade on the airfoil for 8EO excitation of mode family 1 over $f \in [2.36, 2.41]$

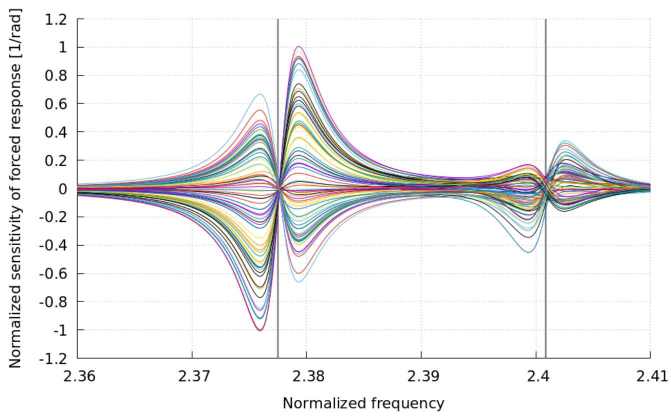

Figure 6.17: Sensitivity of normalized forced response amplitude of blade 31 with respect to the α angle of all the blades for 8EO excitation of mode family 1

For the subsequent sensitivity analysis, first the blade with the largest forced response amplitude, its location on the airfoil and its resonance frequency is selected: location E3 on blade 31 at normalized frequency $f = 2.374$. The sensitivities of the normalized maximum nodal displacement of blade 31 is shown with respect to the α angles of all the blades in Fig. 6.17. The vertical lines in the plot show the two resonance frequencies of the mistuned bladed disk. The sensitivities with respect to primary angles of all blades show a similar behavior: the sensitivities are changing sign around both resonance frequencies. The change of signs around the resonance indicates that the change in the anisotropy angles shifts the resonance peaks. The zero value of sensitivity at resonance $f = 2.374$ and the small value of sensitivity at $f = 2.398$ indicate that the maximum forced response amplitudes have small sensitivity to the crystal orientations. This learning is in agreement with the low amplification factors observed for 10 mistuned bladed disks at mode C, see

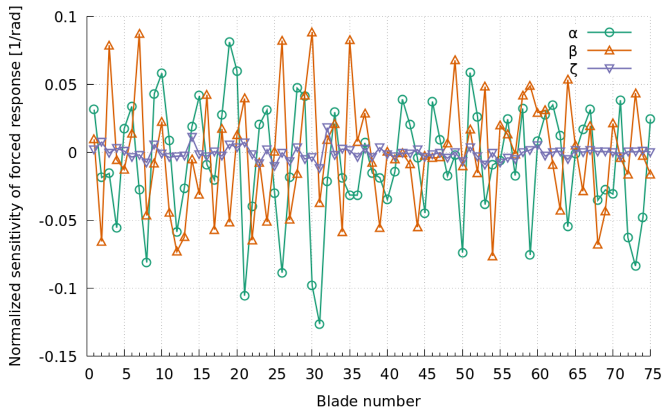

Figure 6.18: Sensitivity of the amplification factor at blade 31 with respect to all anisotropy angles of all the blades for 8EO excitation at $f = 2.377$ of mode family 1

Fig 6.12.

The values of the sensitivities with respect to α anisotropy angle of all blades at $f = 2.377$, where the maximum value of sensitivity is observed is show in Fig. 6.18. The maximum forced response sensitivity is largest with respect to the α primary angle of the blade 31, nevertheless it is not significantly larger than the sensitivities with respect to anisotropy angles of the other blades. It is worth noting, for the modes that are not significantly distorted by the anisotropy mistuning pattern, sensitivities are small and have an imperfect periodic pattern.

6.3.2 Disk dominated mode coupling with blade dominated mode

The forced response and its sensitivities have been studied for mistuned bladed disk for the frequency range D, excited by engine order 8. The normalized forced response is shown for all blades with forced response amplification factor 1.5 and above in Fig. 6.19a. From the 75 blades 10 blades have such large amplification factor, which is typical for blade dominated modes of mistuned bladed disks. The maximum forced response amplitudes along the circumference of the mistuned bladed disk also show that the operational deflection shape is localized only for certain blades , see Fig. 6.19b. A significant influence of the anisotropy angles on the mode shapes have been identified by investigating the location of the maximum forced amplitudes for each blade, see Fig. 6.20. Most of the blades have the maximum forced response on the mid-span of the trailing edge, which is expected for the first bending mode of the shrouded blades with thin trailing edges. Nevertheless, for a significant number of blades, the node with the maximum forced response changes to another node along the trailing edge of the blade.

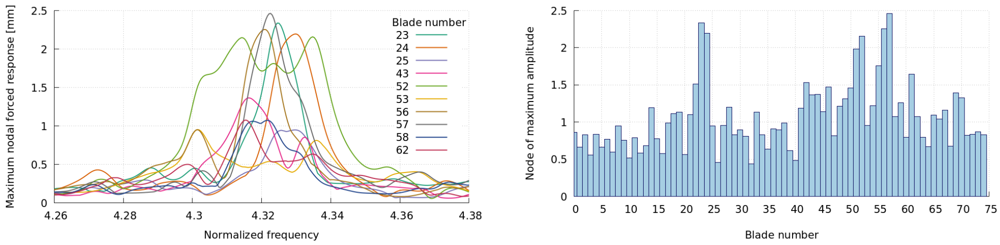

(a) Forced response function of selected blades (b) Maximum forced response for each blade

Figure 6.19: Forced response function and maximum forced response amplitudes for 8EO excitation of mode family 2

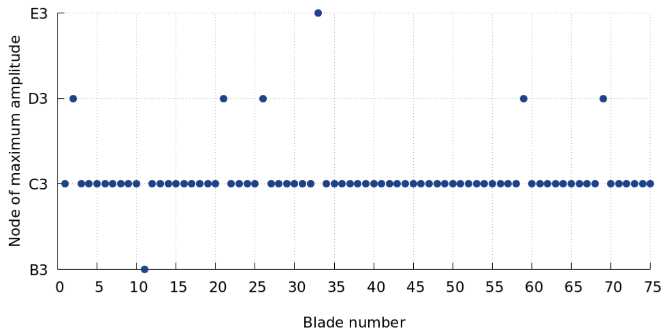

Figure 6.20: Location of maximum forced response for each blade on the airfoil for 8EO excitation of mode family 2 over $f \in [4.26, 4.38]$

For the study of the sensitivity analysis, the maximum forced response has been identified for blade 57 at the midspan location (C3) for excitation frequency $f = 4.321$. The sensitivities of the forced response amplitudes are expected to be the largest for this mode with respect to the primary anisotropy angles. This is shown in Fig. 6.21 where the value of the sensitivity of forced response amplitude with respect to all anisotropy angles in the bladed disk are shown at the excitation frequency $f = 4.321$. As a general trend, it can be observed that the forced response at the resonance frequency is the most sensitive to the blades that have high vibration amplitudes or are located in the vicinity of a blade that has high displacements, see also Fig. 6.19b. The neighboring blades can have a high influence on the forced response, as the coupling is high between the blades, because of the stuck shrouds.

Because the forced response sensitivities are the largest with respect to the primary anisotropy angles, the sensitivities with respect to α angles of selected blades are plotted along the frequency range of interest, see Fig. 6.22. The sensitivities are plotted with respect to those blades that have a large influence on the forced response amplitudes and

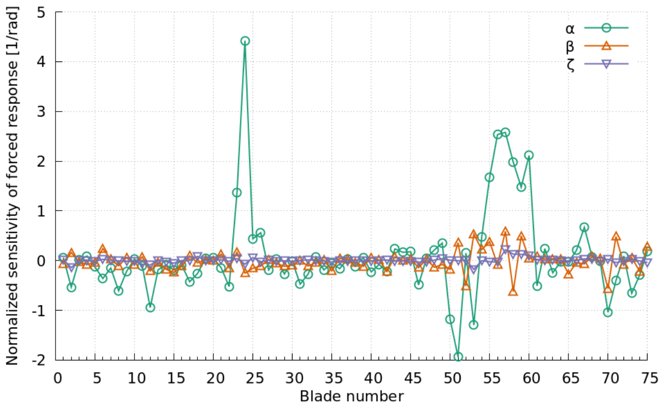

Figure 6.21: Sensitivity of the amplification factor at blade 57 with respect to all anisotropy angles of all the blades for 8EO excitation at $f = 4.321$ of mode family 2

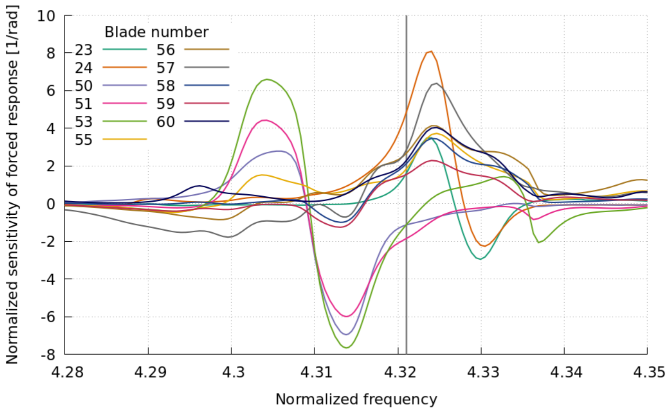

Figure 6.22: Sensitivity of forced response amplitude of blade 57 with respect to the α anisotropy angle of selected blades for 8EO excitation of mode family 2

the excitation frequency where blade 57 has the maximum forced response amplitude is shown with a vertical line at $f = 4.321$. For this mode, the sensitivities are non-zero at $f = 4.321$, which means that the change of anisotropy orientation parameter can result in a change of forced response amplitudes of blade 57 which can change the amplification factor of the whole mistuned bladed disk. The minimum and maximum of the sensitivities are at slightly higher and lower frequency than the excitation frequency of $f = 4.321$, which means that the change of anisotropy angles can also result in shift in individual blade resonance frequencies. The above-mentioned indications of the sensitivities are also visible in the forced response functions of the 10 mistuned bladed disk samples, see Fig. 6.14. The excitation frequency of the blade with maximum forced response amplitude and the amplitude of that blade have a significant variation between the 10 samples.

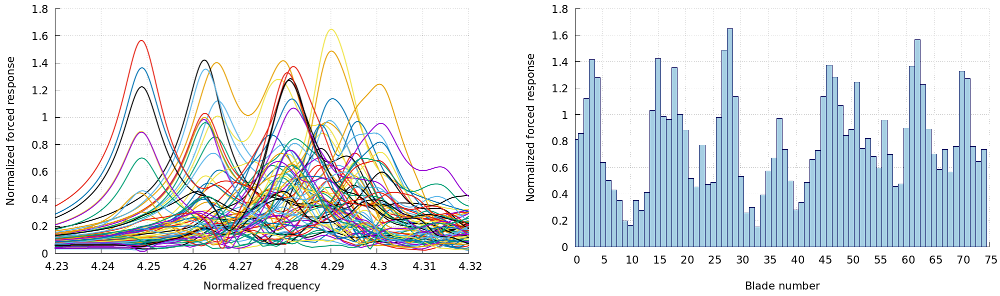

(a) Forced response function of all blades (b) Maximum forced response for each blade

Figure 6.23: Forced response function and maximum forced response amplitudes for 35EO excitation of mode family 1

6.3.3 Blade dominated mode

The sensitivity of the response for 35EO excitation has been analyzed for the 1st family of modes (I), with the same anisotropy mistuning pattern as for mode D. The fist mode family has been chosen, because it provided the highest amplification factor of 1.85 from all purely blade dominated modes excited by EO35.

The forced response amplitudes of all blades over the analyzed frequency range, in Fig. 6.23a, show that the maximum amplitudes and the frequency of maximum forced response amplitudes greatly vary from blade to blade. Such behavior is expected for blade dominated modes. The maximum forced response amplitude distribution shows that only a portion of blades have larger than 1 amplification factors and they are clustered together due to the coupling between the blades via the shrouds. It is worth noting, that although the maximum amplification factor the this mode is lower than for more (D), there are more blades that are within the 20% range of the maximum forced response amplitude. It is also important to mention, that although the mistuning pattern of the bladed disk is the same as for mode D, the distribution of the maximum forced response amplitude is different for this mode. This is contributed to the fact that when the engine order 35 excitation is applied, the lower nodal diameter modes, such as ND8 of mode 2 is excited to lesser extent. The forced response amplitudes of the mistuned bladed disk are the largest for node C3. While a difference in the operational deflection shape is expected from one blade to another, the resolution of the output nodes in the reduced model could not resolve them.

For the sensitivity analysis, the blade number with the maximum vibratory amplitudes and its excitation frequency is identified: blade 29 at $f = 4.290$. The sensitivities with respect to all anisotropy angles are shown in Fig. 6.24 at the resonance frequency of

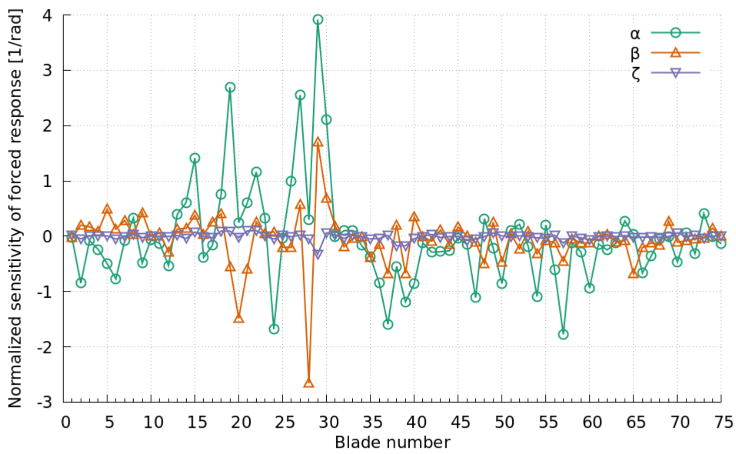

Figure 6.24: Sensitivity of the amplitude of blade 29 with respect to all anisotropy angles of all the blades for 35EO excitation at $f = 4.290$ of mode family 1

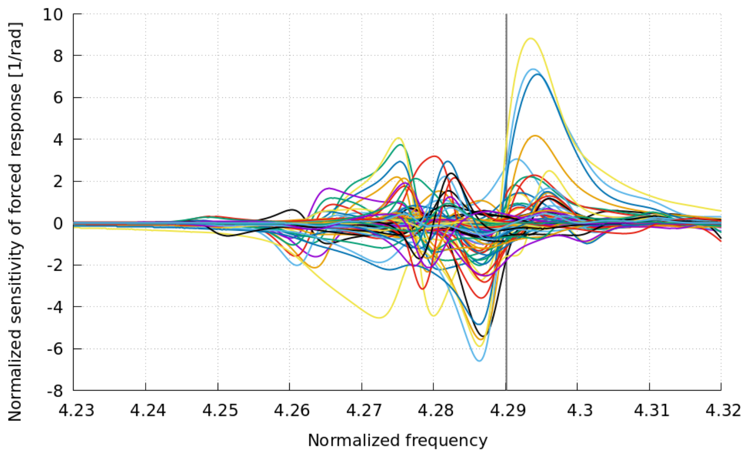

Figure 6.25: Sensitivity of forced response amplitudes of blade 29 with respect to the α anisotropy angle of all blades for 35EO excitation of mode family 1

blade 29. The sensitivities at this frequency are largest with respect to primary angles α followed by second angles β, while ζ sensitivities are the smallest. In agreement with the conclusions drawn for mode D, here also the sensitivities with respect to blade 29 and to its neighboring blades are the largest and the value of maximum normalized forced response sensitivities are in the same order of magnitude. The sensitivities with respect to all α angle over the frequency range of interest show non-zero sensitivities with respect to most anisotropy angles.

6.3.4 Conclusions

In this chapter the effect of anisotropy orientation has been studied for linear bladed disks. The linear forced response has been calculated for several excitations and with different mistuning patterns. The average amplification factors for the bladed disks with several different realistic mistuning pattern can reach values up to 2.6 for some modes. Generally, blade dominated modes have higher amplification factors.

The effect of anisotropy mistuning on the forced response for disk dominated modes is mainly the splitting of the resonance peaks. For blade dominated modes, the operational deflection shape shows localization to a few blades. For these modes, variation in forced amplitudes and resonance frequencies are significant from one mistuning pattern to another. For both type of modes, some variation of the location of maximum forced response amplitude on the airfoil surface occurs over the blades in the bladed disk assembly. This is particularly interesting, as due to anisotropy orientation variation, the HCF limiting location on the airfoil may change.

The above studies showed that the local sensitivities are significant when blade dominated modes are excited. The sensitivities indicate that the calculated forced response amplitudes of the blade with the maximum vibratory response can change due variation of the crystal orientation its own anisotropy angles. Large sensitivities were also observed with respect to the neighboring blades because of the strong coupling through the disk and shrouds. The disk dominated modes with low nodal diameter operational deflection shape pattern show that the sensitivities of the forced response function indicate the shift of resonance frequency by change of sign for the sensitivities around the resonance frequency.

Chapter 7

Validation and modeling of the nonlinear forced response calculation

Before the calculation of the forced response there are several modeling decisions need to be made. The way of modeling and the parameters of the forced response calculations can greatly influence the calculated forced response functions. In order to be able to calculate meaningful results of the sensitivity of forced response amplitudes, it needs to be made sure that the calculated forced response is sufficiently robust and have a good basis for the influence of the input numerical and mechanical parameters.

Moreover, for the calculation of the nonlinear forced response for bladed disks with friction contact interfaces, it is essential to have the method for calculation of the vibration amplitudes validated.

In this chapter the modeling issues are discussed together with the measurement data, if available. The combined discussion gives an insight to how the modeling parameters change the forced response amplitudes and resonance frequencies in relation to their measured data.

The validation of the calculation forced response is generally done against other, already validated, software or against measured vibration amplitudes that are obtained with vibration experiments.

According to the knowledge of the authors, currently there is no commercially available FE program that can calculate nonlinear forced response in frequency domain of dynamic systems with friction contact elements. The calculation of the steady state solution of the forced response with time domain solvers is prohibitive for large scale bladed disk models. During the implementation phase of the PhD studies, a validation campaign has been done at MTU Aero Engines, during which the forced response amplitudes have been

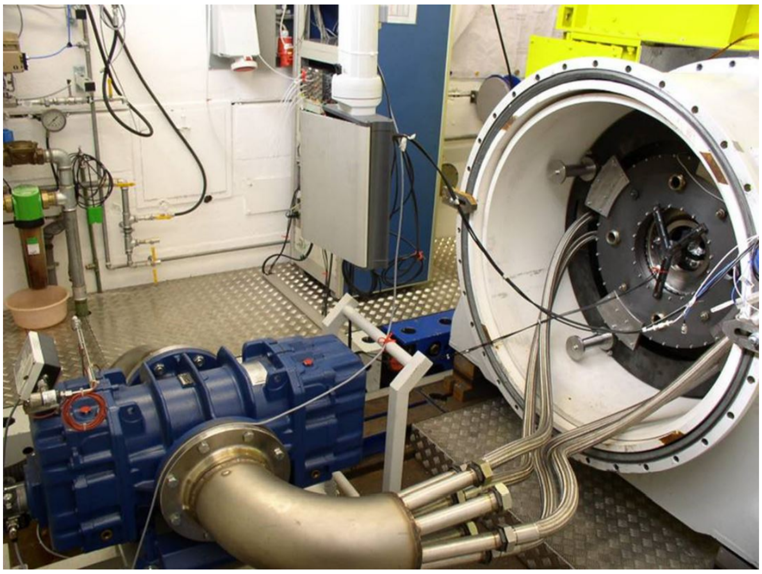

Figure 7.1: Rotating excitation rig [34], which was used to obtain measured forced response amplitudes and resonance frequencies used for the validation

validated against the measurement data obtained from the rotating excitation rig [31]. The excitation rig is capable of easily controlling the resulting force level of the air jets that are ejected for a pre-defined engine order excitation [34].

The validation campaign was done for the bladed disks, "stage A" and "stage B" for which a validation campaign was done earlier, see [32], and the experimental data is available at MTU. An overview of the analyzed configurations can be seen in Table 7.

Configuration	Stage	Engine order	Mode	Root damping	Shroud damping	UPD	Tuned	Mistuned
1	A	low	1/1F	X	-	-	X	-
2	A	high	1/1F	X	X	-	X	-
3	B	low	1/1CD	X	X	-	X	-
4	B	high	2/1F	X	X	-	X	X
5	B	low	1/1CD	X	X	X	X	X
6	B	high	2/1F	X	X	X	X	X

For stage A, the forced response of tuned bladed disks were calculated with (1) root damping and open shrouds and (2) with root and shroud damping (closed shrouds). For stage B, tuned and mistuned bladed disks were calculated for (3) to low engine order excitation with root and shroud damping and (4) to high engine order excitation with root and shroud damping. For stage B, under-platform dampers (UPD) were added to the already existing models of (3) and (4) which resulted in the most complex models of (5) and (6).

The vibratory displacements were measured using MTU in-house non-contact vibration measurement system for shrouded turbine blades. The measurement system is can capture the maximum amplitude for all blades for each experimental run. Because after several measurement runs a large amount of data is collected, the measurement data for each configuration is distilled into minimum, maximum and mean values and standard deviation for the forced response amplitudes and for the resonance frequencies. It is worth noting, especially when measured data is compared with forced response results for tuned bladed disks, that the bladed disk measured in the tests is inherently mistuned.

7.1 Modeling strategies for tuned bladed disks

The modeling strategies were first studied on tuned bladed disks. By taking advantage of the cyclic symmetric conditions, a higher discretization can be used for the finite element and contact interface modeling and the nonlinear forced response analyses are calculated faster. Moreover, the validity of the learning from the studies of the forced response of the tuned bladed disks are relevant in industrial applications and are a good basis for further studies for mistuned bladed disks.

7.1.1 Effect of number and distribution of contact elements

The number of nonlinear contact elements used for the nonlinear forced response simulation has, together with the included harmonics, the largest influence on the computational effort. The following studies are on the effect of the number and distribution of the blade root joints nonlinear contact elements on the nonlinear forced response. For the analyses the considered schemes of the contact element distributions are shown in Fig. 7.2. Here one of four contact patches at the blade fir-tree root is shown. The nodes of the FE mesh at this patch where the contact elements are applied are marked by green squares.

The nonlinear forced response has been calculated for all schemes shown in Fig. 7.2 and for low and high harmonic excitation levels, see Fig. 7.3.

Contact node schemes with 56 and 63 nodes per contact patch are obtained by selecting every second row of the FE mesh. From Fig. 7.3 we can see that 56 friction contact scheme provide higher the maximum amplitude and resonance frequency than 63 contact element scheme.

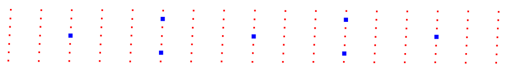

(a) 7 nodes

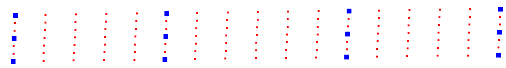

(b) 12 nodes

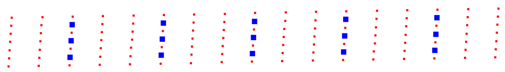

(c) 15 nodes, variant A

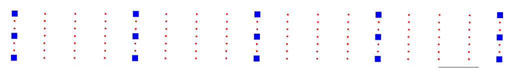

(d) 15 nodes, variant B

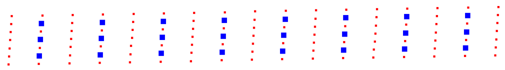

(e) 24 nodes

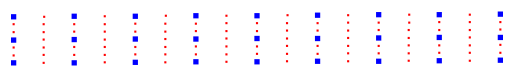

(f) 27 nodes

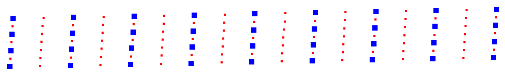

(g) 36 nodes

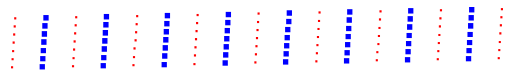

(h) 56 nodes

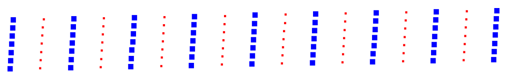

(i) 63 nodes

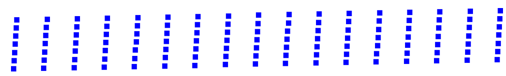

(j) 119 nodes, all FE nodes

Figure 7.2: Location of nonlinear contact nodes on one blade contact patch (total number of patches: 4)

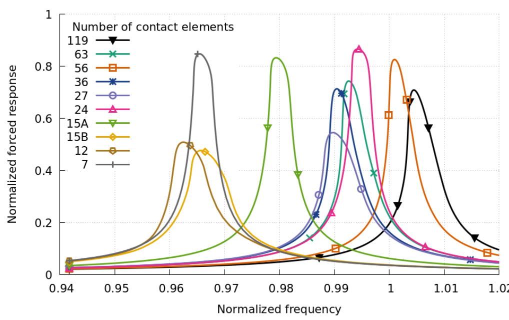

(a) Forced response for the lower excitation level: excitation level 1

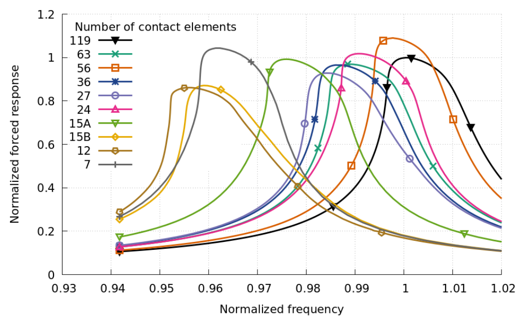

(b) Forced response for the higher excitation level: excitation level 5

Figure 7.3: Nonlinear forced response of cyclic symmetric bladed disk with different number of contact elements on the root contact interfaces

The forced response amplitudes calculated with 36 contact elements on each contact patch are very close to the amplitudes calculated with 119 contact elements, for low and high excitation levels. The scheme 36 would be recommended for the study of tuned bladed disks if faster calculation time is required. Such analyses can be parametric or studies to acquire statistical properties.

The evenly distributed nodes for the scheme with 36 contact elements are capable of capturing the slip occurring locally when excitation level 1 is applied.

If less contact elements are used, the amplitudes are either overestimated or underestimated for the low excitation level. The forced response is underestimated when 12, 15 variant B or 27 nodes are applied. For these schemes, many of the nodes are located at the edge of the contact interface. This is where contact pressure concentrations occur however, if the nodes on the contact interface are not coinciding, the calculated contact pressures are low. At these nodes, especially at the top of the interface where slipping starts as vibration amplitudes increase.

The schemes with 7 and 15 nodes variant A, all nodes are located within the edge of the contact interface. The forced response calculated for these schemes overestimate the forced response as it cannot capture the localized micro-slip on the contact surface.

Forced response calculated for high excitation level, shown in Fig. 7.3b, show less difference between the nonlinear contact distribution schemes in respect of the maximum amplitudes. This is due to the fact, that when high levels of harmonic excitation is applied, most of the upper fir-tree contact patch slips. This behavior can be captured accurately even with 7 to 15 nonlinear contact elements per surface.

The resonance frequency for both excitation levels decrease in the same manner as the number of nonlinear contact elements are reduced. With 36 nodes on each of the contact surfaces, the resonance frequency decreases about 1% compared to the reference solution calculated with 119 contact elements. This is negligible for most practical applications.

With 12 elements per each contact interface, the maximum decrease in resonance frequency is 4.5%. This deviation is more significant and needs to be considered for practical applications.

From this study it can be concluded that there is noticeable dependency of the nonlinear forced response on the number and location of the nonlinear contact elements. As a general tendency, by using less contact elements than what is available in the FE model, the resonance frequency decreases, for the current model this decrease was 1-4%. This is due to the decrease of the stiffness of the dynamic system.

The second reason for the change of maximum forced response is the significant variation of the contact pressure values over the contact interface surfaces. The choice of different number of nodes over the contact interfaces changes the location of the contact nodes. The energy dissipated by friction is generally higher, for the considered operating conditions, if contact elements are located where the contact pressure is relatively low. If the contact elements are located at the parts of the contact surfaces where pressure levels is high enough to suppress the slip then these elements do not contribute to the friction damping.

This effect is particularly important when the level of harmonic excitation is low, see Fig. 7.3a. In order to obtain representative forced response amplitudes it recommended to use a well-structured scheme, such as the one shown in Fig. 7.2g with 36 nodes.

7.1.2 Number of mode shapes considered

The operation deflection shape of the nonlinear bladed disks with friction joints is calculated as the combination of the linear mode shapes. Generally, one mode is dominant in the vibration response, but due to the nonlinearities energy is transferred to higher modes, and they are also excited. Therefore, to accurately calculate the forced response function many structural modes need to be included in the modal basis. It is worth noting here, that the mode shapes included in the FRF calculation are obtained for bladed disks with open contact surfaces. Which means, in general more modes of the structure with free contact interfaces are required to capture the structure in contact.

The study for the effect of the number of mode shapes on the nonlinear forced response has been done for MTU production bladed disks and calculated forced responses were compared with the measurement data obtained from the excitation rig. For this study the bladed disks forced response for configurations #2, #3 and #4 were calculated, see Table 7.

In general, it can be stated that for all analyzed tuned bladed disks, a converged solution can be reached and the convergence over the number of modes included in the FRF calculation is fast.

The analyses have shown that the number of modes included do not affect the calculation time of the nonlinear forced response. Nevertheless, it is worth remembering that the number of linear modes calculated in the modal analysis can take significant computational effort for large systems when many modes are calculated.

Configuration #2, stage A excited with high EO with root and shroud damping

The bladed disk geometry and the FE model of bladed disk is the production version of the bladed disk used in the majority of this work, see for example Fig. 5.1. The bladed disk four contact interfaces on the blade-root interfaces and two contact patches on the blade outer shrouds. The reduced order model includes 440 nonlinear contact elements, which results in a fine contact discretization on all contact interfaces. The contact parameters,

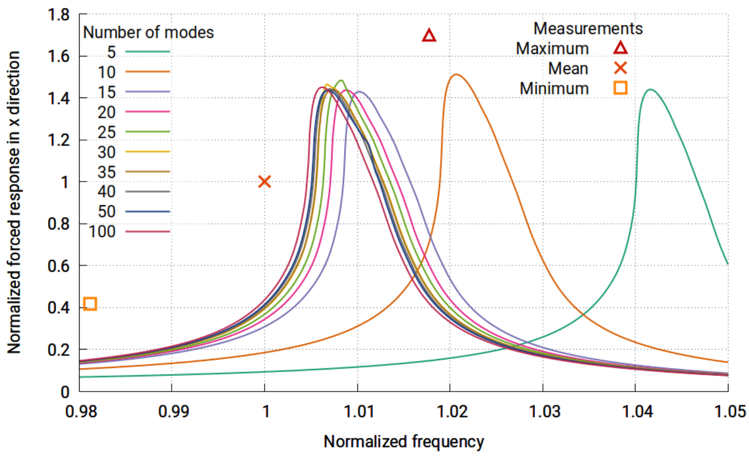

Figure 7.4: Nonlinear forced response of tuned bladed disks with varying number of modes included, compared with minimum, mean and maximum over all measured data for configuration #2

contact stiffness and friction coefficients, have an initial value $k_n = k_t = k_0$, $\mu_{shroud} = \mu_0^s$ and $\mu_{root} = \mu_0^r$. How the value of contact parameters affect the nonlinear forced response is discussed in subsection 7.1.4.

The high engine order excitation is applied on the airfoil mid-span suction side. The excitation frequency range is selected such that the first bending mode (1F) is excited. The node of output is located on the trailing edge in the mid-span of the airfoil.

Th calculation here is done with harmonics 0,1,2 and 3 included. The forced response of the tuned bladed disk calculated with 5 to 100 modes included, is shown in Fig. 7.4. The forced response amplitudes can be captured well even for 5 modes, but with respect to the resonance frequency, at least 30 modes are required to achieve converged solution.

The forced response amplitudes and resonance frequency is normalized in Fig. 7.4 with respect to the mean forced response amplitudes and resonance frequencies. In this figure, the minimum, maximum and the mean value over all blades and for several measurement runs are plotted, together with the calculated forced response curves. The calculated forced response amplitude and the resonance frequency is within the mean and maximum measured data, which is expected for the forced response amplitude calculated for tuned bladed disks. The maximum forced response amplitude is larger than the mean measured value, which is expected: the mean value of the forced response amplitude for mistuned bladed disks is less than the amplitudes for tuned bladed disks.

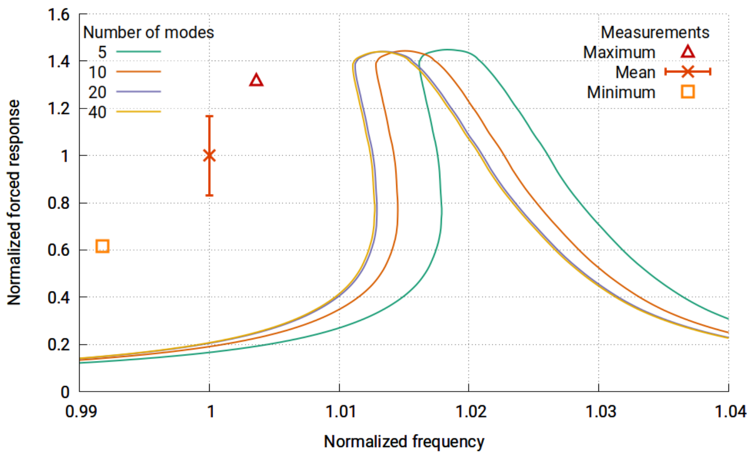

Figure 7.5: Nonlinear forced response of tuned bladed disks with varying number of modes included, compared with minimum, mean, maximum and standard deviation over all measured data #3

Configuration #3, stage B excited with low EO with root and shroud damping

The bladed disk of stage B has 4 contact interfaces on the blade roots and 1 contact interface between the shrouds. The contact interfaces are discretized with 410 contact elements in the reduced order model of the bladed disk. The contact parameters, contact stiffness and friction coefficients, have an initial value $k_n = k_t = k_0$, $\mu_{shroud} = \mu_s^0$ and $\mu_{root} = \mu_r^0$. How the value of contact parameters affect the nonlinear forced response is discussed in subsection 7.1.4. The low engine order excitation, applied on the suction side of the airfoil near the blade tip and the trailing edge, excites the first coupled blade-disk mode (1CD).

The calculation here is done with harmonics 0,1,2, and 3 included. The forced response of the tuned bladed disk calculated with 5 to 40 modes included, is shown in Fig. 7.5. The forced response amplitudes can be captured well even for 5 modes, but with respect to the resonance frequency, at least 20 modes are required to achieve converged solution.

The forced response amplitudes and resonance frequency is normalized in Fig 7.5 with respect to the mean forced response amplitudes and resonance frequencies. The calculated forced response amplitude and the resonance frequency is outside of the range of minimum and maximum measured data. The measured frequency range for the resonances is very narrow, therefore in order to accurately capture the resonance frequency a very fine FE mesh needed for the modal analysis. Here, the deviation from the mean measured resonance frequency is within 2%.

The minimum, maximum and the mean value over all measured forced response amplitude are also shown in Fig. 7.5. In this figure the standard deviation of the forced response amplitudes are also plotted around the mean value. The two ends of the line represent the standard deviation added and extracted from the mean value.

The calculated forced response amplitude is 5% higher for this mode than the measured amplitude. The deviation for the vibration amplitudes is assumed to be caused by the following factors: (i) the evaluation of the measurement data was done using linear modes (ii) the uncertainty in the contact parameters, see subsection 7.1.4 (iii) static calculation of the pres-stress state was done with nonlinear contact on the shroud which resulted in contact only in a small portion of the contact interface leading to a softer system when compared with a bladed disk with cyclic symmetric conditions on the shroud contact interface (iv) forced response calculations generally show higher amplitudes than mean values of mistuned bladed disks.

Configuration #4, stage B excited with high EO with root and shroud damping

In this study the 2$^{\text{nd}}$ mode (1F) of stage B is excited by a high engine order excitation. The excitation is applied on the suction side at the midspan of the airfoil. The contact parameters, contact stiffness and friction coefficients, have an initial value $k_n = k_t = k_0$, $\mu_{shroud} = \mu_s^0$ and $\mu_{root} = \mu_r^0$. How the value of contact parameters affect the nonlinear forced response is discussed in subsection 7.1.4.

The calculation here is done with harmonics 0, 1, 2, and 3 included. The forced response amplitudes and resonance frequency is normalized in Fig 7.6 with respect to the mean forced response amplitudes and resonance frequencies.

To reach converged solution, here more modes are needed than in the earlier studies: the excited structural mode is from the second mode family. With 30 modes, convergence can be reached. For any practical reason, with 10-15 modes the forced response is calculated sufficiently accurate.

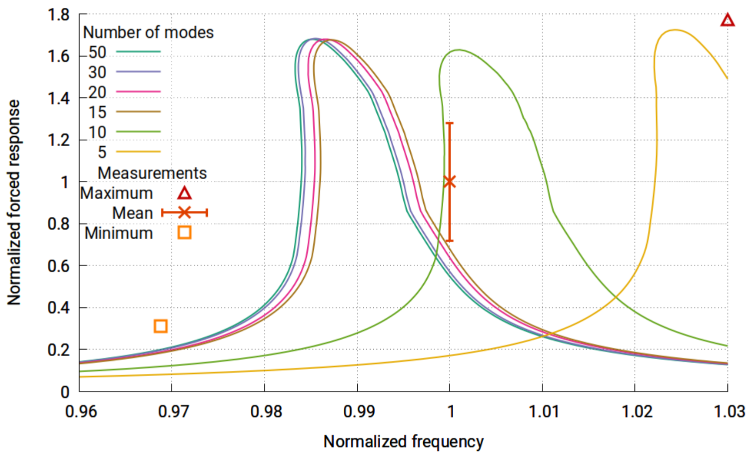

Figure 7.6: Nonlinear forced response of tuned bladed disks with varying number of modes included, compared with minimum, mean, maximum and standard deviation over all measured data for configuration #4

The maximum forced response amplitude and the resonance frequency is within the range of the measured values. The calculated amplitudes are within the measured mean and maximum values resulting in successful validation.

7.1.3 Number of harmonic coefficients

The number of harmonic coefficients included in the FRF evaluation is one of the most important parameters during the nonlinear forced response analyses. In order to be able to capture the energy transfers to the higher harmonics, the higher harmonic coefficients need to be included. The change of the static equilibrium can be captured by including the 0^{th} harmonic number in the FRF calculation.

On the other hand, the size of the equation system of the nonlinear forced response increases proportional to the number of harmonics included, which has a significant influence on the numerical efforts. Moreover, the by considering the change of the static equilibrium in normal and tangential directions, the number of bifurcation points along the solution paths can increase leading to challenging path-following problems.

Configuration #1, stage A excited with low EO with root damping

The bladed disk studied in configuration #1 has contact on the blade roots, the shrouds contacts are open and do not come into contact. The results of the study of nonlinear forced response with different number of harmonic coefficients is shown in Fig. 7.7. The nonlinear forced response function converges fast over the number of harmonics included.

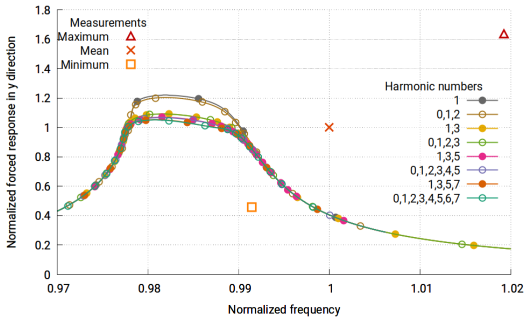

(a) Forced response curves with measurement data

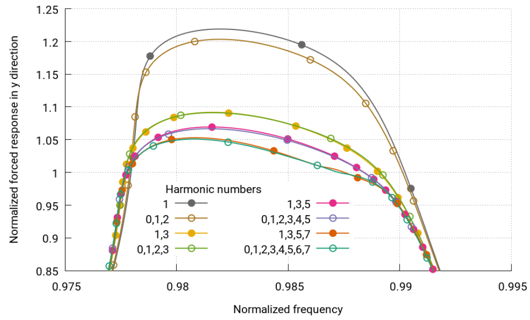

(b) Forced response curves zoomed for resonance peak

Figure 7.7: Nonlinear forced response of cyclic symmetric bladed disk with different number of harmonic coefficients included, compared with minimum, mean and maximum over all measured data for configuration #1

With harmonics 1 and 3 an accurate calculation can be calculated which is very near the forced response function calculated with harmonics 0, 1,2,3,4,5,6 and 7. It is worth noting, that the when the even harmonics and the 0^{th} harmonic coefficients are included in the FRF calculations, the solution does not change. The reason for that is that the contact interfaces on the blade roots do not separate over the vibration period.

For bladed disks with root contact, it is sufficient to include only odd harmonic numbers and with harmonics 1 and 3 sufficiently accurate forced response amplitudes when compared with the measurement data. The calculated forced response amplitude is within 5% of the measured mean forced response amplitude. The resonance frequency is 2% lower than the mean measured resonance frequency, the deviation has been attributed to the lower natural frequency of FE model of the bladed disk.

Configuration #2, stage A excited with high EO with root and shroud damping

The bladed disk of configuration #2 has nonlinear contact interfaces on the blade roots and on two contact patches of blade outer shrouds. The nonlinear forced response shown in Fig. 7.8 shows a very fast convergence over number of harmonics included in the FRF. With harmonics 0,1,2,3,4 converged results are obtained. For this bladed disk, the 0^{th} harmonic coefficient is noticeable but not very significant because the contact separation for this bladed disk with two contact patches on the shrouds does not happen.

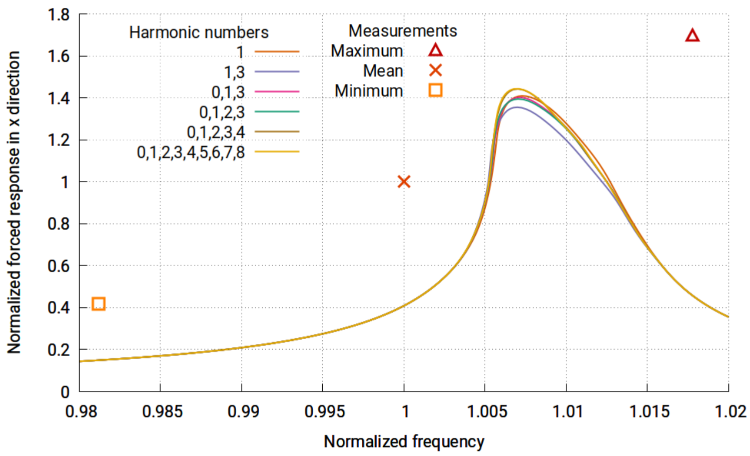

Figure 7.8: Nonlinear forced response of tuned bladed disks with varying number of harmonic coefficients included, compared with measurements for configuration #2

Configuration #3, stage B excited with low EO with root and shroud damping

The effect of the number of harmonics on the nonlinear forced response was studied for tuned bladed disk that is excited by low EO excitation, see configuration #3 in Table 7. The results in Fig. 7.9a show that without including the 0^{th} harmonic number, the forced response amplitude and the resonance frequency is overestimated. The 0^{th} harmonic coefficients are required to capture the contact separation on the shroud contact interfaces. Moreover, not including the even harmonics leads to underestimated forced response amplitudes.

The forced response functions plotted in figure 7.9b show that convergence is very fast once 0^{th}, the first two odd and the first even harmonics are included. By including the first 10 harmonic numbers, the change in forced response amplitudes is within a few %.

For the mode under investigation, the nonlinear forced response is calculated accurately when the 0^{th} harmonic numbers are included in the forced response function calculation. The need for the 0^{th} harmonic number is attributed to the partial separation of the shroud contact interfaces. To investigate to what extent the contact interfaces separate, the relative normal displacement of the contact pairs are investigated at resonance frequency in time domain. The relative displacements in time domain are obtained by evaluating the Fourier expansion formula as

$$\boldsymbol{x}_r(t) = \boldsymbol{X}_{r,0} + \sum_{j=1}^{N_h} \boldsymbol{X}_{r,j}^{(c)} \cos(k_j \omega t) + \boldsymbol{X}_{r,j}^{(s)} \sin(k_j \omega t) \tag{7.1}$$

where the $\boldsymbol{x}_r(t)$ is the relative displacement of the contact nodes in time domain and $\boldsymbol{X}_{r,0}$

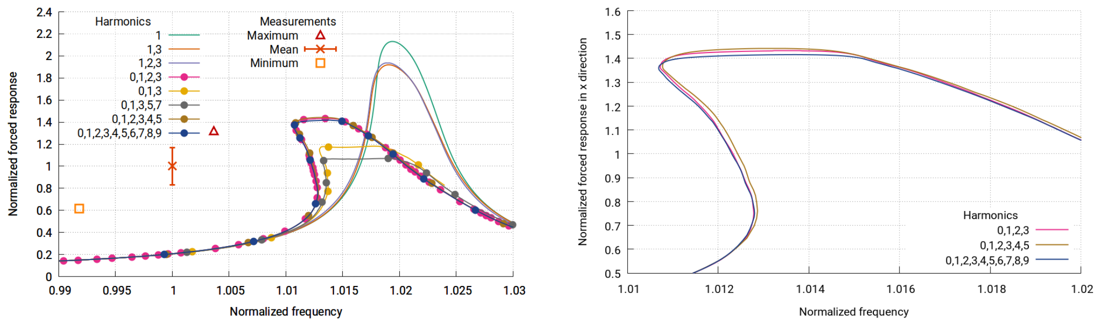

(a) Forced response curves with measurement data

(b) Forced response at resonance calculated with 0, odd and even harmonics

Figure 7.9: Nonlinear forced response of cyclic symmetric bladed disk with different number of harmonic coefficients included, compared with minimum, mean, maximum and standard deviation over all measured data for configuration #3

are the 0^{th} harmonic coefficients and $\boldsymbol{X}_{r,j}^{(c)}$ $\boldsymbol{X}_{r,j}^{(s)}$ are the j-th harmonic coefficients.

The contact interface on the outer shroud near the leading edge, is discretized by 38 nonlinear contact elements. The forced response is calculated with 0^{th} and the first 7 harmonic numbers included, which allows for an accurate harmonic discretization, making the identification of contact-separation possible. The relative forced response displacements can be recovered for arbitrary number of time points over the period, here 31 time points are used.

For the contact elements the same static pre-stress level has been set. The over-closure is expressed as $u = p_{contact}/k_n - u_0$, where u_0 is the over-closure to pre-stress and k_n is the contact stiffness in normal direction. Depending on the static pre-stress level and the normal contact stiffness, the contact separation happens at a certain relative displacement, which can be express by $u = -u_0$. The relative displacements in Fig. 7.10 have been normalized by the value of the static over-closure u_0. The relative displacement where contact separation occurs is indicated with a horizontal line at normalized relative displacement -1.

For confidentiality reasons, the blade shrouds cannot be shown. In order to illustrate the kinematics of the blade shroud contact interface, the relative displacements of the contact elements are shown. The contact patch is making a rocking motion, over one half of the period one side is separating and the other is in full contact. The contact elements on the two sides of the contact patch, see Figs. 7.10a and 7.10c, separate with large maximum relative displacements with approximately 90° degree phase shift. The Fig. 7.10b shows that 15 contact elements in the middle of the contact surface separate twice

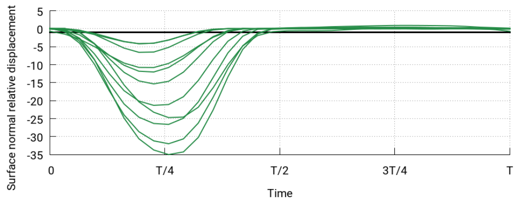

(a) Contact elements closer to leading edge

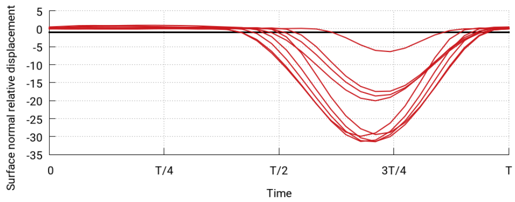

(b) Contact elements closer to trailing edge

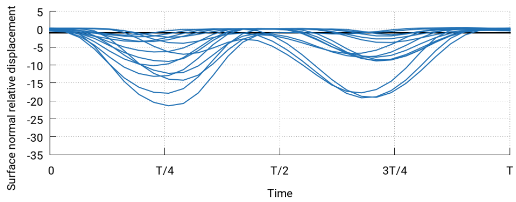

(c) Contact elements around the middle of the contact patch

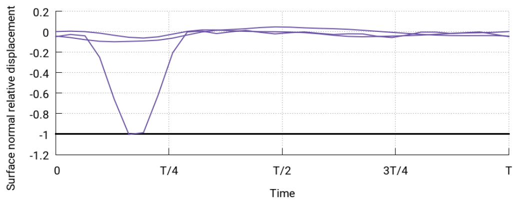

(d) Contact elements in the middle of the contact patch

Figure 7.10: Surface normal relative displacements for all nodes on the shroud contact interface for configuration #3

over the period. There are only 3 contact elements that do not separate over the period, see Fig. 7.10d. There is no time instant when all contact elements are separating which would lead to hammering of the contact interfaces.

This study showed significant separation occurs on the shroud contact patches, and in order to accurately determine the contact-separation the 0^{th} harmonic coefficients are required.

Configuration #4, stage B excited with high EO with root and shroud damping

The effect of the number of harmonics on the nonlinear forced response was studied for tuned bladed disk that is excited by high EO excitation, see configuration #4 in Table 7. The results in Fig. 7.11 show that without including the 0^{th} harmonic number, the forced response amplitude and the resonance frequency is overestimated. The 0^{th} harmonic coefficients are required to capture the contact separation on the shroud contact interfaces. Moreover, not including the even harmonics leads to underestimated forced response amplitudes. In Fig. 7.11b, the forced response calculated for 0^{th}, odd and even harmonics show a very fast convergence.

In order to confirm the assumption that the 0^{th} harmonic coefficient is required for the dynamic systems where contact-separation occurs, the contact status over the period at resonance frequency is studied for this mode of the bladed disk. Compared to the results shown for the mode 1 excited with low EO excitation, shown in Fig. 7.10, for this mode

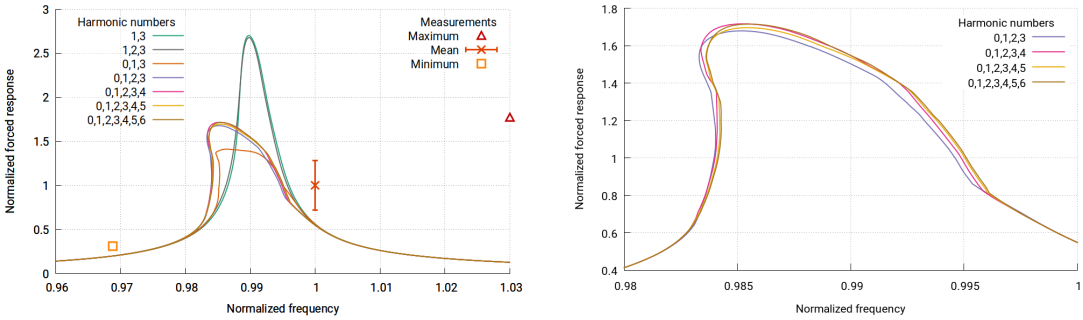

(a) Forced response with measurement data

(b) Forced response zoomed to resonance calculated with 0, odd and even harmonics

Figure 7.11: Nonlinear forced response of tuned bladed disks with varying number of harmonic coefficients included, compared with minimum, mean, maximum and standard deviation over all measured data for configuration #4

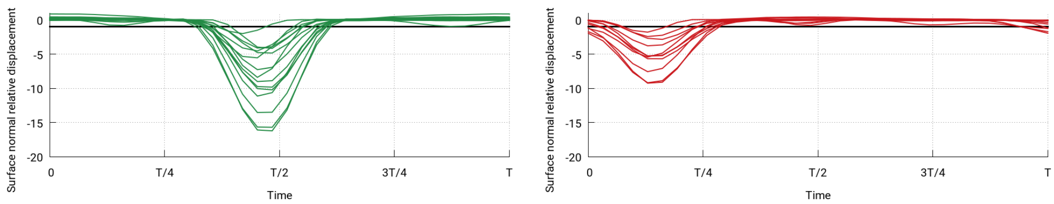

(a) Contact elements closer to leading edge

(b) Contact elements closer to trailing edge

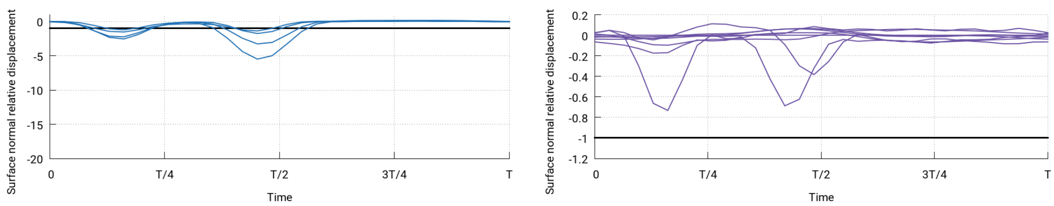

(c) Contact elements around the middle of contact patch

(d) Contact elements in the middle of contact patch

Figure 7.12: Surface normal relative displacements for all nodes on the shroud contact interface for configuration #4

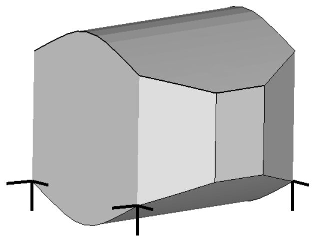

Figure 7.13: Under-platform damper with springs for stage B

the more nonlinear contact elements are in contact over the whole period of vibration. The relative normal displacements in Fig. 7.12 show that time intervals of separation are reduced and the number of contact pairs in contact over the entire period increase to 8. It is worth noting that the from the 38 nodes on the contact interfaces, 30 contact node pairs separate at least at one time instant during the period.

The forced response calculation for this mode, despite that less separation occurs on the blade shrouds compared to the bladed disk in configuration #3, requires the 0^{th} harmonic for the accurate calculation.

Configuration #6, stage B excited by high EO with root, shroud and UPD damping

The effect of the number of harmonics is studied for the bladed disk in configuration #6. The bladed disk is excited with the same harmonic forces on the same frequency range as for configuration #4, but here an under-platform damper is included in the assembly see Fig. 7.13. In the study for the harmonics included in the forced response calculation for the bladed disk mode for configuration #4, it has been shown that the 0^{th} harmonics are need to be included in the FRF calculation due to the separation on the blade outer shrouds. With the introduction of the under-platform damper, the forced response amplitudes are expected to decrease and through that the separation on the outer shrouds are also expected to reduce. Which would mean that the error in the calculated forced response amplitudes by not including the 0^{th} harmonic coefficients are is expected to reduce. The relative displacements in surface normal direction, shown in Fig. 7.14 shows that the number of contact elements in separation decreases. The focus of this study has been the modeling of bladed disks with under-platform dampers including the 0^{th} harmonic coefficients in the FRF calculation.

The mode shapes and the flexibility matrix of the under-platform damper is calculated separately from the rest of the bladed disk structure. In order not to detune the natural

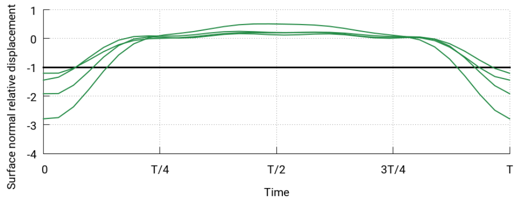

(a) Contact elements closer to leading edge

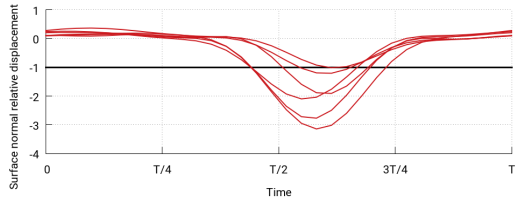

(b) Contact elements closer to trailing edge

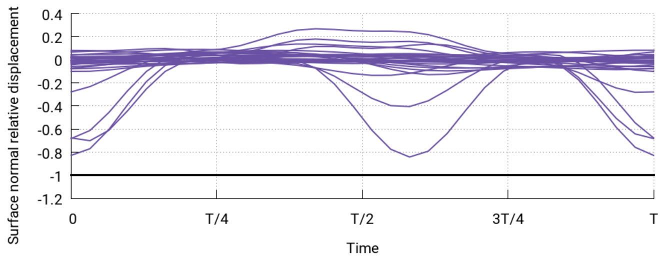

(c) Contact elements around the center of the contact patch

Figure 7.14: Surface normal relative displacements for all nodes on the shroud contact interface for configuration #6

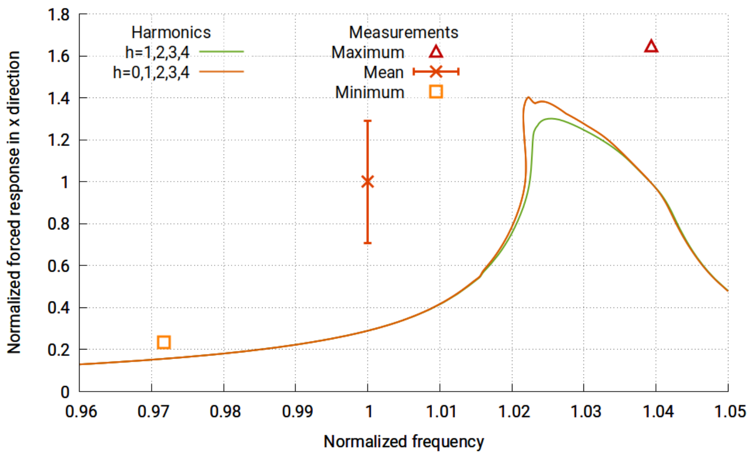

Figure 7.15: Nonlinear forced response of tuned bladed disks with varying number of harmonic coefficients included, compared with measurements for configuration #6

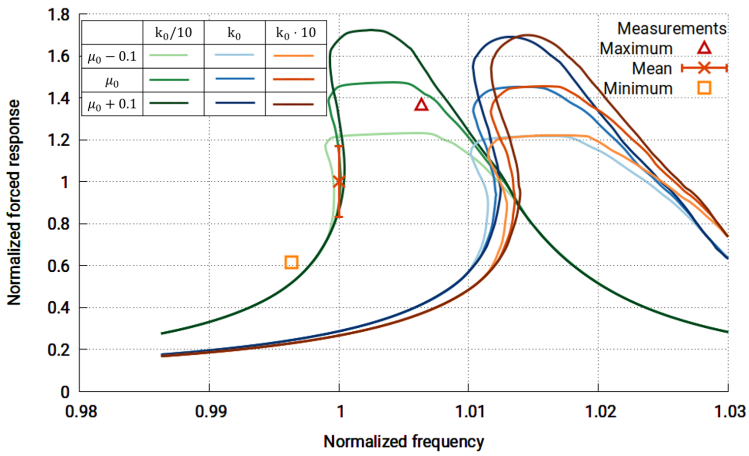

Figure 7.16: Sensitivity study of the nonlinear forced response of tuned bladed disks with varying contact stiffness and friction coefficient, compared with measurements for configuration #3

frequencies of the damper, its boundary conditions are modeled as close to free-free boundaries as possible. If free-free boundary conditions are applied, the first six modes of the damper are rigid body modes. If the 0^{th} harmonic coefficients are included in the FRF calculation for a dynamic system with rigid body modes, the forced response amplitudes become infinite. In order to achieve sensible results the following work-around is proposed: the underplatform damper is placed on soft spring, as shown in Fig. 7.13.

7.1.4 Effect of variation of contact stiffness and friction coefficients

During the lifetime of the turbine blades, the contact surfaces are prone to fretting wear and in certain cases to hammering on shroud contact interfaces. This leads to changing contact parameters as the jet engine accumulates cycles, such as contact stiffness and friction coefficients. Another reason for the study of the effect of the contact parameters on the nonlinear forced response is the difficulty when measuring the stiffness of the micro-asperity layer of the rough contact surfaces.

The sensitivity studies for the friction coefficients and for the contact stiffness are presented for the bladed disks and for the modes described in configurations #3 and #4. The bladed disks have contact interfaces on the blade shrouds and blade roots, for which an initial value of contact stiffness and friction coefficient are assigned: $k_{normal} = k_{tangential} = k_0$, $\mu_{shroud} = \mu_s^0$ and $\mu_{root} = \mu_r^0$. In this sensitivity study, the value of the contact parameters are increased and decreased to account for the uncertainties.

The forced response functions for the varying contact parameters are shown in Figs.

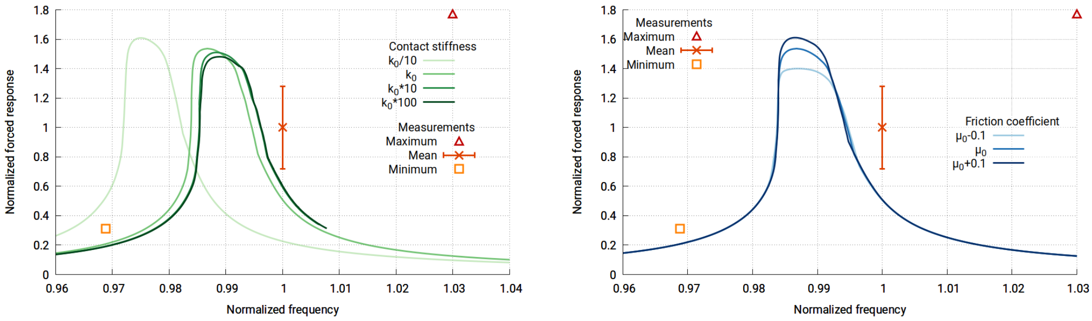

(a) Varying contact stiffness (b) Varying friction coefficient

Figure 7.17: Sensitivity study of the nonlinear forced response of tuned bladed disks with varying contact stiffness and friction coefficient, compared with measurements for configuration #4

7.16 and 7.17. The friction coefficients for the blade root and for the blade shrouds are varied together in 0.1 steps. As for the contact stiffness, by decreasing the stiffness value the system becomes softer resulting in lower resonance frequency and higher amplitudes. For k_0 and above forced response function converges and increasing the contact stiffness has negligible effect on the forced response. It is worth mentioning here, that setting the contact stiffness to a large value may lead to difficulty to converge and to longer calculation times.

The effect of the change of friction coefficients on the nonlinear forced response is similar for both modes. By increasing the friction coefficient the split limit μF_n is increased, therefore reducing the damping effect of the contact interfaces. It is also worth noting that for configuration #3 (Fig. 7.16) the reduction of the friction coefficient values leads to a more sharp-edged forced response function.

7.1.5 Effect of multi-point-constraints between blade and disk

The mode shapes used for the FRF matrix calculation need to be mode shapes of the bladed disk structure with free boundary conditions for the degrees of freedom where the nonlinear contact elements are to be applied. Therefore, the contact elements of the nonlinear friction joints are removed in the modal analysis. For some bladed disk assemblies the removal of the the contact elements lead to rigid body modes. Moreover, because modes are calculated in the rotating reference frame, the rigid body modes have complex natural frequencies attributed to them. For these reasons, it is beneficial to include additional multi-point-constraints (MPC) in the modeling, in order to remove the rigid body modes. The MPCs

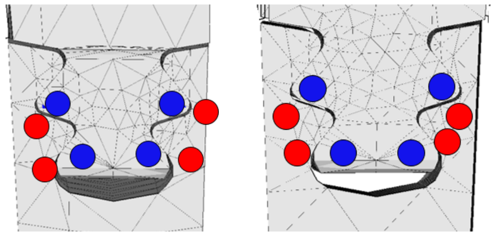

(a) Leading edge view (b) Trailing edge view

Figure 7.18: Multi-point-constraint setup 1

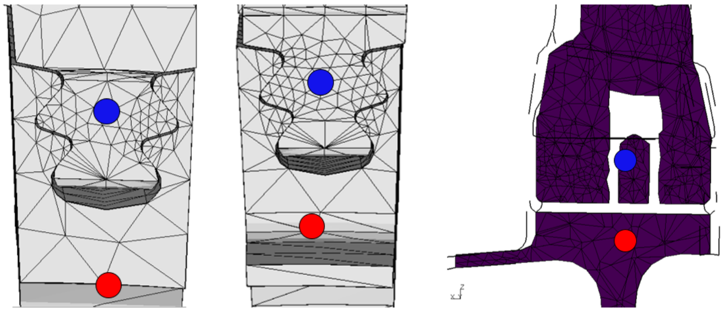

(a) Leading edge view (b) Trailing edge view (c) Cross-section view

Figure 7.19: Multi-point-constraint setup 2

are applied to a very small number of FE nodes so it does not change dynamic behavior. Here, the effect of the choice of nodes used for the application of MPCs was performed.

Two different setups for the MPCs are used: see Figs. 7.18 and 7.19. The node pairs shown in red and blue are coupled for all 3 degrees of freedom at each pair of nodes. Setup 1 has 8 pairs of nodes coupled by MPCs, which is stiffer. This setup restricts motion near the edge of the contact interfaces. On the other hand, MPC setup 2 has only 3 pairs of nodes coupled, which results in mode shapes that are closer to the mode shapes with fully free contact interfaces.

The nonlinear forced response has been calculated for two difference excitation levels (low and high) and with varying number of contact elements used for the root damping discretization, see Fig. 7.20 The forced responses calculated for the two different MPC setups show little difference when detailed contact description is applied using large number of nonlinear contact elements. When small number of friction contact nodes (e.g. 7 and 15) is applied, then the additional stiffness introduced in MPC setup 1 has a noticeably effect on the forced response: maximum amplitudes are higher (about 10%) and resonance

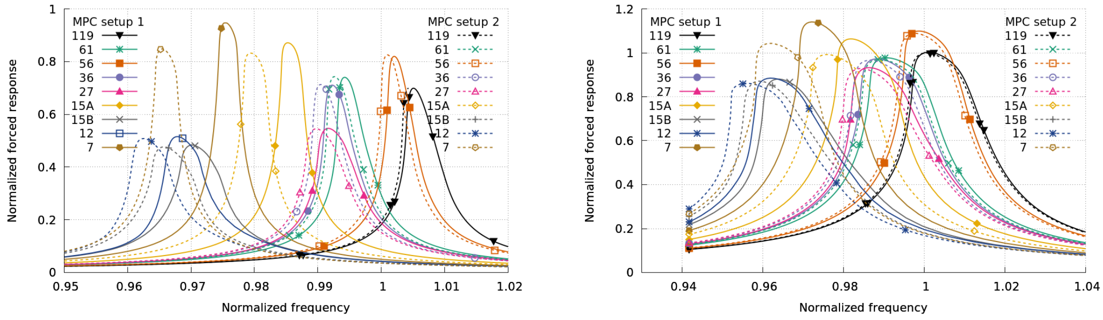

(a) Excitation level 1

(b) Excitation level 5

Figure 7.20: Nonlinear forced response of tuned bladed disk with different number of nodes on the contact interfaces and MPC setups

frequency is slightly higher (about 1%).

7.2 Modeling strategies for mistuned bladed disks

The nonlinear forced response calculations require more computational efforts than of the simulations for their tuned counterparts. Therefore it is important to have an assessment on the influence of the parameters that also affect the computational efforts. The effect of the number of contact elements, number of mode shapes and number of harmonic coefficients are considered on the nonlinear forced response of mistuned bladed disks. For some bladed disks measurement data is available according to Table 7.

7.2.1 Effect of contact pressure variation on shroud contact interfaces

The dynamic change of contact status is, among other factors, dependent on the static prestress state of the contact interfaces. For mistuned bladed disks with contact interfaces, the static contact pressures vary from one sector to another. In order to accurately capture the change in the normal pressure values of the contact joints, a sufficiently detailed FE discretization needs to be used. The desired accuracy can easily be achieved on the blade root contact patches. The contact stresses on the fir-tree interfaces are generally evenly distributed and their value is large. On the other hand, the contact interfaces on the outer shroud transfer the contact forces on a small surface area and the contact forces are an order of magnitude lower than the normal contact forces on the blade root contact surfaces. The relatively low value of the contact pressures on the shroud contact surfaces function as an effective damping device, but the accurate calculation of the contact pressures with the FE models of mistuned bladed disks is challenging.

In order to illustrate the effect of the shroud contact pressure variation on the nonlinear forced response a tuned and a mistuned bladed disk with 75 blades are used. The damping on the root is not considered for the analyses, the blade root - disk contact is modeled with linear multi-point-constraints. There are two contact patches between each blade on the shrouds, one near the leading edge and another one near the trailing edge. First, the nonlinear contact interfaces are discretized by 5 contact elements per contact patch, which results in 10 contact elements per blade and in 450 nonlinear contact elements in the mistuned bladed disk. The calculations are done for one mistuned bladed with random anisotropy orientation distribution. For the nonlinear static calculation, surface-to-surface contact elements are applied on the two shroud contact interfaces for every blade. For the static pre-stress state of the nonlinear contact elements of the forced response analysis, the nodal normal pressure values of the converged nonlinear static solution is used. Due to the variation of the anisotropy parameters from one blade to another, the contact pressures, and potential contact gaps, are changing from one blade to another. The natural frequencies and modal shapes calculated for the anisotropy mistuned blade disks are included in the reduced order model.

In the model for the nonlinear forced response calculation there are two kinds of mistuning included: modal mistuning through the mistuned modal basis and static mistuning through the mistuned pre-stress field of the contact elements. On the bladed disk EO28 harmonic force is applied that excites the first mode (1F). The excitation amplitude is kept contact for all analyses. For the calculation of the FRF harmonic numbers 1 and 3 are included.

The envelope of the nonlinear forced response for tuned and mistuned bladed disks are shown in Fig. 7.21. The normal stresses on the contact patches for the tuned and for the modal mistuned bladed disks are the same. The envelope of the forced response shows that the modal mistuned bladed disk has an amplification factor higher than 1. On the other hand, the maximum forced response of the bladed disk with both static and modal mistuning, is lower than the maximum forced response of the tuned bladed disk. For mistuned bladed disks, amplification factor of smaller than 1 is against the expectations. According to general observations vibration amplitude reduction of the mistuned bladed disks are only obtained if aeroelastic effects are included in the analysis [73]. The variation of the static contact condition on the shroud interfaces causes an increase in the damping and results in reduction of forced response amplitudes for all blades. Such behavior, while is worth studying in further detail, due to the relatively coarse FE mesh on the contact

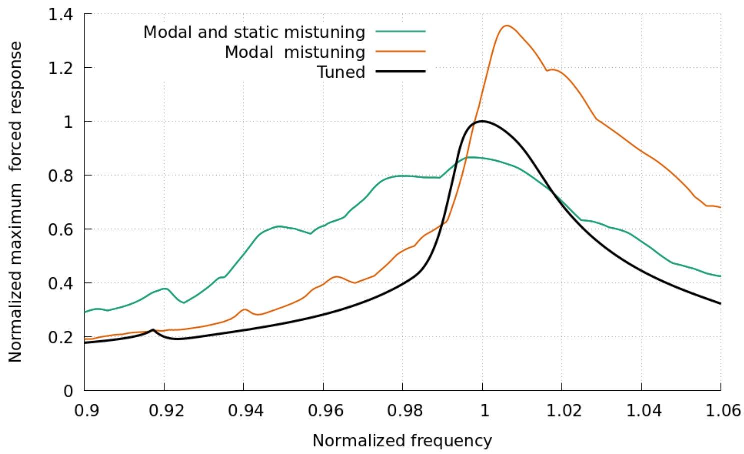

Figure 7.21: Nonlinear forced response of mistuned bladed disks with modal mistuning and with combined modal and static mistuning

interfaces, the accurate evaluation of the contact pressure values on the shroud contact interfaces are not possible.

Therefore, the effect of the contact pressure values on the nonlinear forced response of the mistuned bladed disk are studied for tuned static pre-stress states on the shrouds. The same value of the contact pressure is applied for every nonlinear contact element and the value of contact pressure is changed in gradual steps. For the tuned bladed disk the normal pressure value of 18 MPa is chosen. The contact pressure of the mistuned bladed disks is varied between 2 and 20 MPa. The contact pressures applied for the shroud contact interfaces are in the range that is realistic for turbine bladed disks.

The envelope of the nonlinear forced response of the mistuned bladed disks and the forced response amplitudes of the tuned bladed disk is shown in Fig. 7.22. The results show that small differences in the contact pressure values on the shroud interfaces have significant influence on the forced response amplitudes on the midspan of the bladed disk. The amplitudes of the mistuned bladed disk for contact pressure values of 16 MPa or more are higher than the amplitudes of the tuned bladed disk with 18 MPa contact pressures applied. For lower contact pressure values, the stick-slip transition occurs for lower amplitudes and results in increased damping. This study shows that for the assessment of the amplification factors of mistuned bladed disks with friction joints on shroud interfaces, the accurate assessment of the static contact status including contact pressure values is essential.

It is important to note here, that the contact pressure values not only influence maximum forced response amplitudes, but also the distribution and the variance of the maximum forced response along the circumference of the bladed disk. The results of the studies

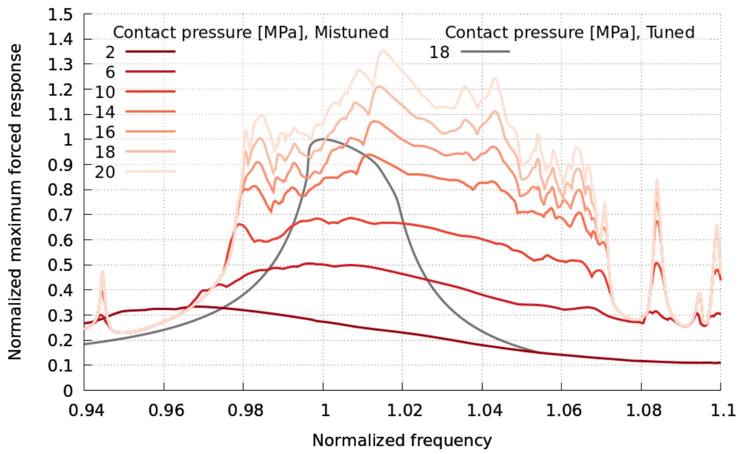

Figure 7.22: Nonlinear forced response of mistuned bladed disks with varying tuned contact pressures

are summarized in chapter 8.

7.2.2 Effect of contact pressure variation on root contact interfaces

The effect of the static contact pressure variation due to anisotropy mistuning is studied for a bladed disk with 75 blades, root damping and free shrouds. The contact pressure values are obtained from the nonlinear static calculation. The static calculation is obtained under centrifugal loading at the rotation speed of the EO14/1F crossing, see excitation B in Fig. 6.3. The structural mesh on the root contact interfaces and the relatively high contact pressure values allow for a reliable contact calculation using surface to surface contact elements. Similarly to the analysis for the shrouds, the effect of the separate modal mistuning and the combined effect of the modal and static mistuning on the nonlinear forced response is studied. Under the modal mistuning here the mistuning of natural frequencies, mode shapes and flexibility matrix are considered.

The reduced order model of the nonlinear forced response analysis is discretized by 6 nonlinear contact elements on the 4 contact patches of each blade root. The total number of nonlinear contact elements in the bladed disk is 1800.

In order to quantify the effect of the static mistuning on the nonlinear forced response two types of simulations were done: (i) mistuned modal properties and flexibilities but applying the contact pressure values calculated for the tuned bladed disk model on the nonlinear contact elements (ii) mistuned modal properties, flexibilities and contact pressure values on the blade root interfaces.

In Fig. 7.23 the envelope of the forced response is shown for two mistuning patterns

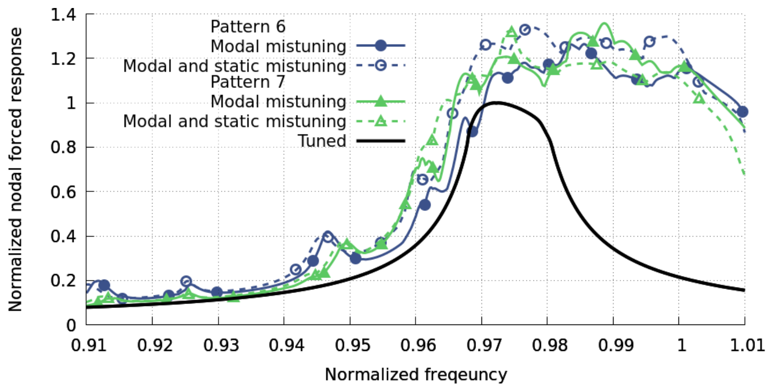

Figure 7.23: Maximum nonlinear forced response with separate and combined mistuning effects for excitation frequency B

using both simulation input parameters. Both calculations resolve the resonance on the same frequency range of 0.97 to 1. Nevertheless, it is worth noting that the frequency of the highest response is different for the two forced response functions. For mistuning pattern 6 the maximum amplitude of the fully mistuned bladed disk is higher by 6.5%, but for mistuning pattern 7 the maximum amplification factor of the fully mistuned bladed disk resulted in 3% lower value compared to the model where only modal mistuning was introduced.

As described earlier, the envelope for the static and combined static and model mistuning is similar. To see the differences between the forced responses amplitudes calculated with the two modeling methods, the maximum forced response distribution for all the blades is shown in Fig. 7.24 for pattern 7. In this figure the maximum amplitude of the blades significantly differ if the mistuning is only introduced in the modal characteristics or in the static pressure values as well.

The study showed, accounting for the mistuning of the static pressure values is essential for the accurate calculation of the forced response. If only the modal mistuning is considered, there is an error in the maximum forced response amplitude and resonance frequency. On the contrary to the analyses with shroud contact only, the contact pressure on the root friction interfaces can be reliably obtained with FE simulations using surface to surface contact elements. Accounting for the combined effect of modal and static mistuning is essential for obtaining correct distribution of the maximum forced response amplitude distribution along the blades.

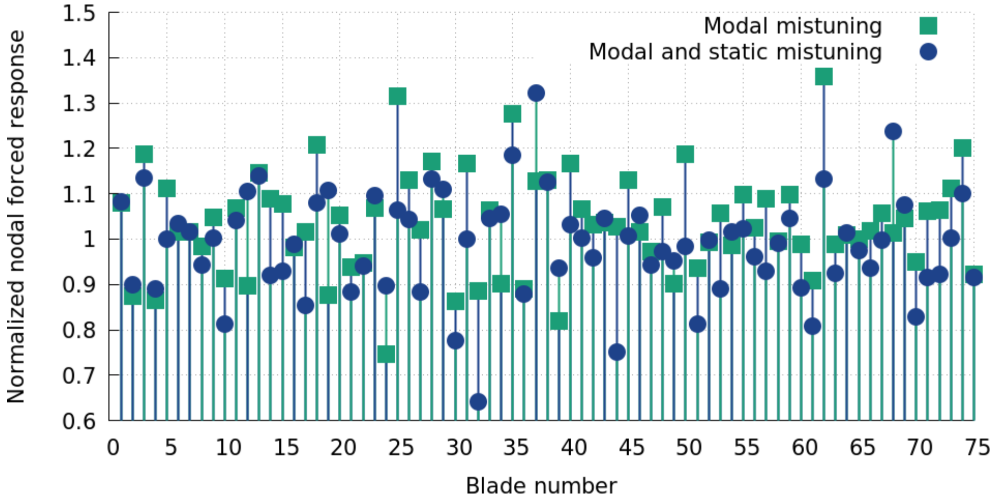

Figure 7.24: Blade maximum forced response distribution with separate and combine mistuning effects for excitation frequency B and pattern 7

7.2.3 Number of contact elements

The computational effort associated with the calculation of the nonlinear forced response for mistuned bladed disks is highly dependent on the number of nonlinear contact elements used for the discretization of the friction contact interfaces. The effect of the number of contact elements was studied by varying the number of contact elements on the outer shrouds. Where on the one contact interface between neighboring shrouds of the 84 blades are discretized by 4, 9 and 12 contact elements for each blade. The studies were done for the modes in configuration #4, #5 and #6, see Table 7. The envelope of the forced response for the modes under analysis are shown in Figs. 7.25-7.27.

For forced response of the mistuned bladed disk with UPD shown in Fig. 7.26 and 7.27, the studies with varying contact elements show an expected behavior. By increasing the number of contact elements, the stiffness of the dynamic system increases. The increased stiffness shifts the resonance frequencies higher and decreases the vibratory amplitudes. For the bladed disk with UPD and excited with low EO excitation (configuration #5), the difference in the maximum amplitudes between the calculations with 9 and 12 contact elements is approximately 10 %. For the bladed disk excited with high EO, the difference in amplitudes between discretizing the contact interfaces with 9 or 12 elements is negligible.

For the tuned bladed disk without UPD and for high engine order excitation of the 1F mode, it has been shown that at resonance majority of the contact elements separate at least at one time point during the period, see Fig. 7.12. Therefore, to achieve accurate forced response calculations that can capture strong nonlinearities, the high spatial

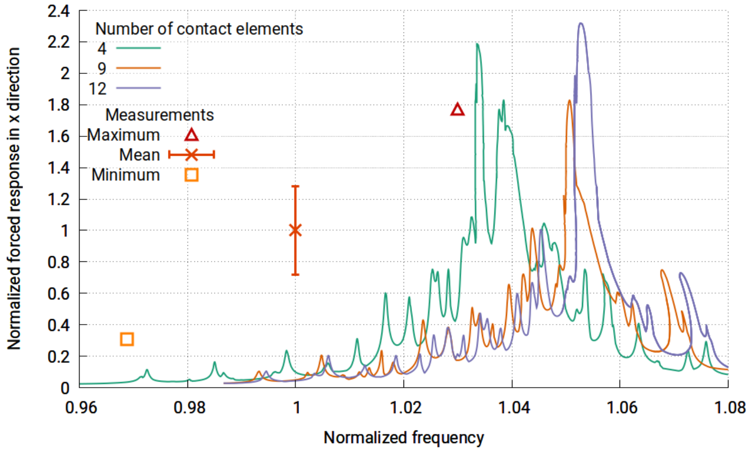

Figure 7.25: Envelope of nonlinear forced response of mistuned bladed disks (configuration #4) for varying number of contact nodes for each blade sector

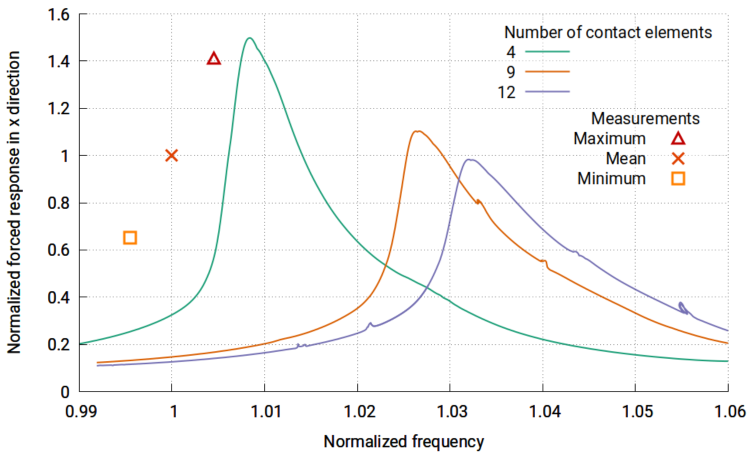

Figure 7.26: Envelope of nonlinear forced response of mistuned bladed disks (configuration #5) for varying number of contact nodes for each blade sector

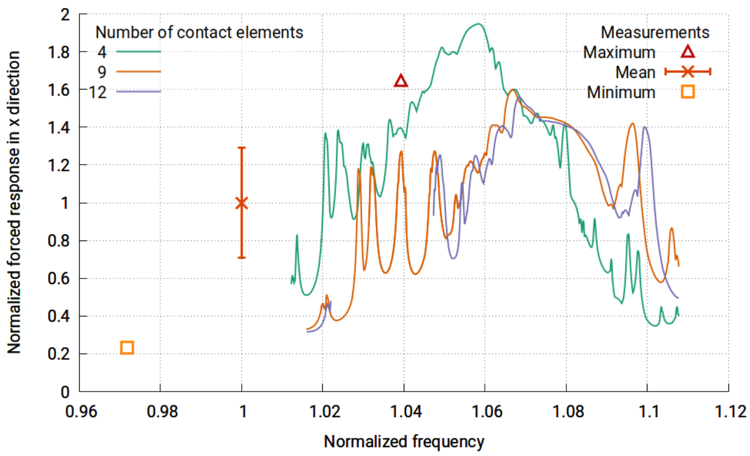

Figure 7.27: Envelope of nonlinear forced response of mistuned bladed disks (configuration #6) for varying number of contact nodes for each blade sector

discretization is required. For this mode, the maximum forced response amplitudes show significant variation depending on the number of contact elements applied. The maximum amplitudes along the bladed disk circumference are dominated by mode localization that leads to separation in the current analyses. To prove the validity of such behavior more finely modeled calculation would be required.

7.2.4 Number of mode shapes considered

While the number of mode shapes included in the modal basis for the nonlinear forced response calculations does not noticeably influence the calculation effort, in the FE programs the modal analysis is a very computationally intensive procedure. Therefore, it is recommended to only include as many modes in the basis as required for the forced response calculations. The studies have been done with different bladed disk structures.

Mistuned bladed disks with shroud damping

The study of the number of mode shapes included in the FRF calculation is done for the bladed disk with 75 blades. The analyses are for mistuned bladed disks (i) with stuck root contact and 3 contact elements on each of the two shroud contact interfaces for each blade and (ii) with nonlinear root contact discretized by 28 contact elements on the fir-tree and free shroud. The bladed disk with closed shroud is excited EO28 excitation, the bladed disk with open shroud with EO14 excitation. The bladed disk with root damping has mistuned static contact pressure, for the bladed disk with closed shrouds 8 MPa surface normal pressure is applied.

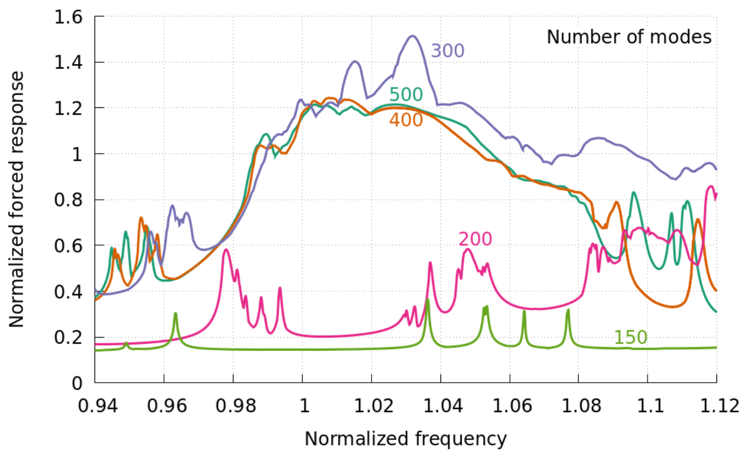

Figure 7.28: Nonlinear forced response of mistuned bladed disks with shroud damping for varying number of modes included

The effect of the number of modes included in the forced response function calculation was studied first for the mistuned bladed disk with shroud damping. The number of modes included were varied on the range of 150 to 500 modes, which is equivalent to approximately 1.5 to 5 mode families. The envelope of the nonlinear forced response in Fig. 7.28, show that with less than 200 modes included, the resonance cannot be captured. Using 300 modes, the resonance can be captured, but due inaccuracies the maximum forced response amplitude is not yet converged. For a practically converged solution, 400 modes, about 4 mode families are required.

Mistuned bladed disks with under-platform damper

The effect of the number of mode shapes on the forced response of mistuned bladed disks with under-platform dampers have also been studied. To this end, the first bending mode of a mistuned bladed disk with open shrouds under EO14 excitation was studied, see A in Fig. 8.1. The blade root contact interfaces are considered to be fully stuck, and the under-platform damper has a cottage roof design. On two upper surfaces of the UPD, where the friction forces appear, three nonlinear contact elements are applied. For the forced response function calculation harmonics 1,2,3 and 4 were included. In 3.4.4 it has been described that the input of the model description of the nonlinear forced response calculation for bladed disks assemblies with UPD are provided separately for the bladed disk structure and for the damper structure. This means that the effect of the change in the number of mode shapes can be studied independently in regard of the bladed disk and the under-platform damper modes.

The nonlinear forced response calculations were done for the number of bladed disk structure modes, on the range 40-500. Because the system does not include any friction damping elements in the bladed disk structure, the convergence can be achieved faster than for the bladed disks with root or shroud damping. This is due to the fact, that the linear mode shapes of the bladed disk assembly are calculated for the FE model, where multi-point constraints are applied between the blade roots and the disk. This results in a very fast convergence over the mode shapes: with 80 mistuned bladed disk modes the converged forced response function can be obtained, see the forced response envelope in Fig. 7.29. Here, 20 UPD modes were included.

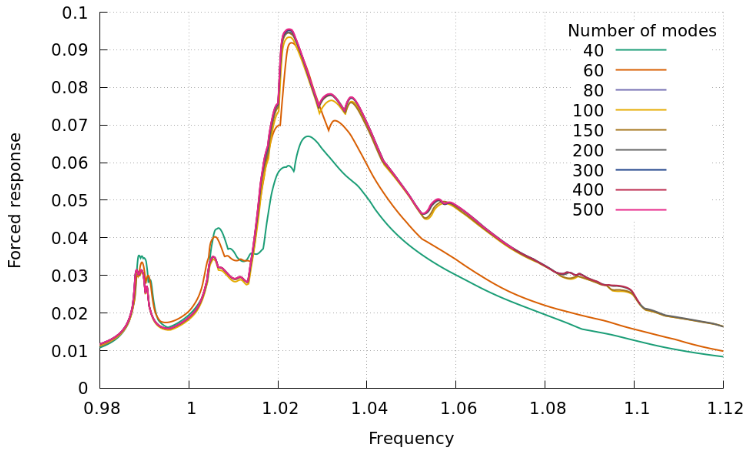

Figure 7.29: Nonlinear forced response of mistuned bladed disks with under-platform damper for varying number of bladed disk modes included

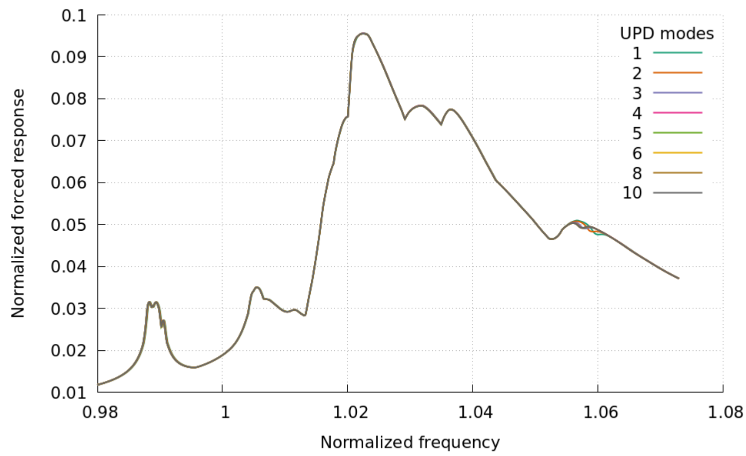

Figure 7.30: Nonlinear forced response of mistuned bladed disks with under-platform damper for varying number of UPD modes included

In the subsequent analyses, the forced response with varying number of under-platform damper modes were done, using 500 bladed disk modes. The damper model does not include any boundary condition, which results in the first six modes of rigid body modes. The forced response envelope curves in Fig. 7.30, show that there is no change in the forced response of the bladed disk when the number of UPD modes are varied. The forced response analysis does not include the 0 harmonic component, which means that no energy is transferred to the rigid body modes of the dampers. The higher damper modes, with non-zero eigenvalues, have at least 20 times higher natural frequency than the bladed disk mode excited.

Mistuned bladed disk with shroud damping and UPD

For the mistuned bladed disk calculated with the parameters of configuration #5, the effect of the number of modes included in the forced response calculation was studied. The envelope of the forced response, shown in 7.31, shows that with 500 modes (approximately 5 mode families) convergence is reached. The excited mode is from the first mode family, therefore 200 modes (more than 2 mode families) are sufficient for capturing the resonance. By including 300 modes in the forced response calculation, the resonance frequency is showing a converging tendency and the maximum amplitude fluctuates around the converged amplitude. It is also worth noting that for the calculation with 400 modes, some overhanging branches are calculated at $f = 1.035$ and at $f = 1.048$. The phenomena is assumed to be due to energy transferred into higher modes. It is assumed that for 400 modes the mode family where the energy is transferred to is only partially included. Therefore, the energy transfer takes place but there are not all modes included to accurately capture it. For the calculation with 500 modes, the forced response function smoothens out on these frequency ranges, showing that including more modes can stabilize the forced response calculation.

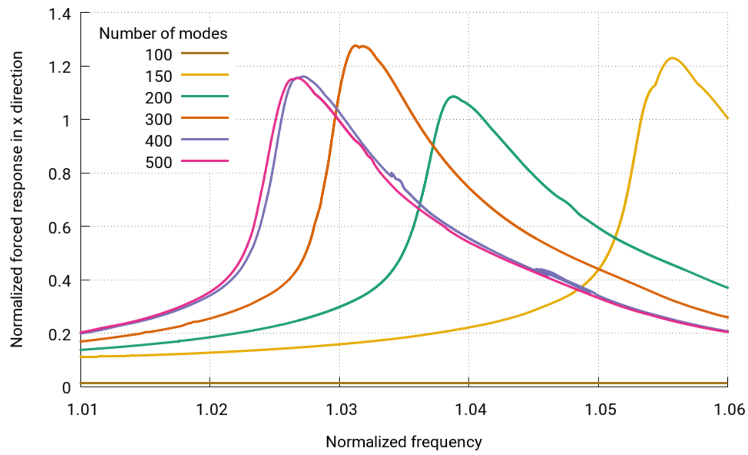

Figure 7.31: Nonlinear forced response of mistuned bladed disks (configuration #5) with shroud damping and under-platform damper for varying number of bladed disk modes included

Mistuned bladed disks with root damping

Similarly, for the blade disk with free shrouds and root damping, the effect of number of modes included on the nonlinear forced response amplitudes was studied. The envelope of the forced response for mistuned bladed disk to EO14 excitation of mode 1, see A in Fig. 8.1 is shown in Fig. 7.32 for modes ranging 100 to 400. With low number of modes, 100-150, the resonance cannot accurately be captured. By including at least two mode families, the resonance is accurately calculated.

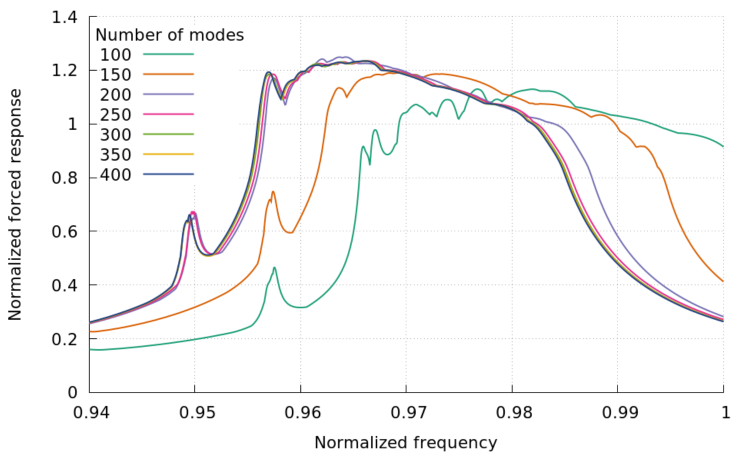

Figure 7.32: Nonlinear forced response of mistuned bladed disks with root damping for varying number of modes included

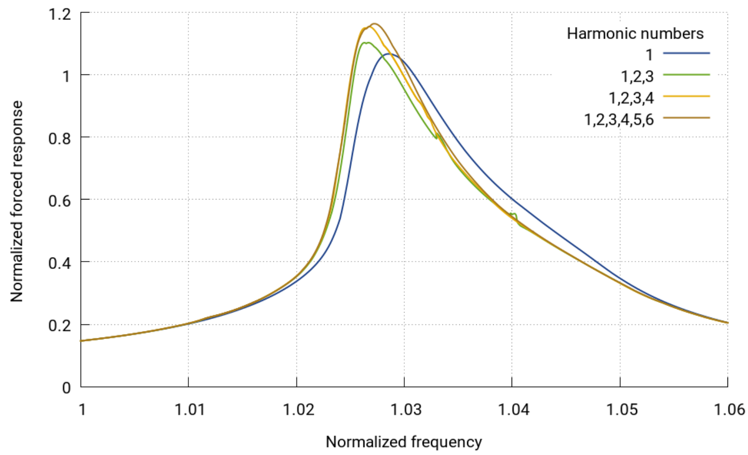

Figure 7.33: Nonlinear forced response of mistuned bladed disks (configuration #5) with shroud damping and under-platform damper for varying harmonic numbers included

7.2.5 Number of harmonic coefficients

The computation effort of the nonlinear forced response, apart from the number of nonlinear contact elements, is greatly dependent on the number of harmonic coefficients included. In order to find a balance between the computation effort and the accuracy of the nonlinear forced response it is worth looking at the harmonic numbers included.

For this study, the production models of turbine bladed disks with UPD are used. In the earlier section, it has already been shown that by including the underplatform damper, the separation on the outer shrouds are significantly reduced. This allows for not including the 0^{th} harmonic numbers for the calculations.

For the coupled-disk mode excited by low EO excitation, see Fig. 7.33, the already monoharmonic calculation gives a relatively good approximation. Converged solution can be reached by including the first 6 harmonics. The noticeable difference between calculations with harmonics 1, 2, 3 and 1, 2, 3, 4 indicates that both even and odd harmonics need to be included. The difference in forced response amplitudes between including the first four and first six harmonics is negligible, therefore, to save on the computation efforts, including the first four harmonic numbers are sufficient.

For the 1F mode excited by high EO excitation, see Fig. 7.34, the monoharmonic calculation gives an inaccurate approximation for the forced response amplitudes. The difference in the maximum forced response for the calculation with the first four and first six harmonics is noticeable. On the contrary for the previous analysis, here by including more harmonic numbers as the forced response calculation converges, maximum amplitudes decrease. It is worth noting that the calculations show that including the even harmonics

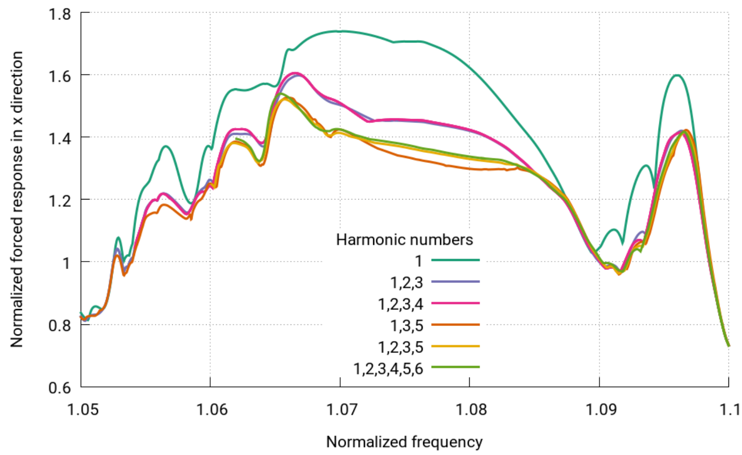

Figure 7.34: Nonlinear forced response of mistuned bladed disks (configuration #6) with shroud damping and under-platform damper for varying harmonic numbers included

only has limited influence on the forced response amplitudes.

7.3 Validation of the forced response amplitudes for mistuned bladed disks

For the validation of the nonlinear forced response for mistuned bladed disks the configurations 4 and 6 for stage B have been chosen. The modal basis for the FRF calculation includes 800 modes, about 9 mode families, and the harmonics 0, 1, 2 and 3 were included. The blade root interfaces are considered to be completely stuck, and the major source of energy dissipation through friction forces is on the shrouds, which is discretized by 12 nonlinear contact elements on each blade. Based on the learnings from the analyses for the tuned bladed disks, the number of modes and harmonics will be sufficient for accurate calculation. The modal properties, flexibility, stiffness and mass matrices were calculated using the anisotropy mistuned whole bladed disk FE model.

Comparison of calculated and measured forced response amplitudes for configuration 4

For configuration 4, the nonlinear forced response has been calculated two different configurations for the shroud contact pressures. First, tuned contact pressure is applied, i.e. for all blade shroud contact interfaces the contact force in normal direction is the same. The mistuned contact pressure distribution of the normal forces has been calculated based on the mistuned bladed disk FE model and are shown in Fig. 7.35.

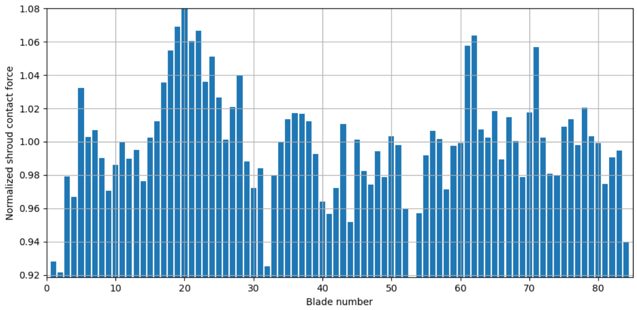

Figure 7.35: Normal shroud contact force variation along bladed disk circumference

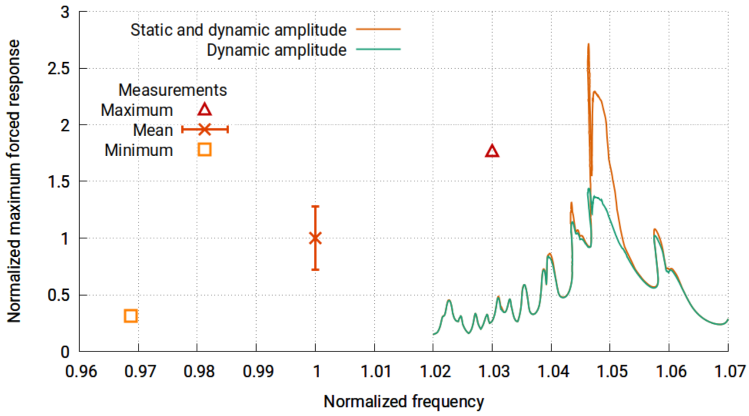

Figure 7.36: Envelope of the mistuned forced response for configuration 4

The nonlinear forced response for the mistuned bladed disk and using the tuned contact pressures has been directly obtained from the reduced order model for one node along the trailing edge of each blade. The maximum forced response along over all blades for every excitation frequency, i.e. the envelope of the forced response, is shown in Fig. 7.36. For the calculation of the nonlinear forced response, the 0^{th} harmonics were included in for all three spatial directions for all nonlinear degrees of freedom. When the maximum forced response amplitudes over the period are evaluated, the 0^{th} harmonics are considered, see Eq. 3.44. In general, if the acceleration rate is slow enough, the contactless measurement techniques do not measure the static components of the vibration, which is generally due to change of equilibrium on the nonlinear contact interfaces.

Therefore, it is worth visualizing the maximum forced response amplitudes over the period (i) with accounting for static components (i.e. 0^{th} harmonic components) and (ii) with considering only the dynamic components. The two envelopes in Fig. 7.36, show that when only the dynamic displacements are included in the calculation of maximum forced

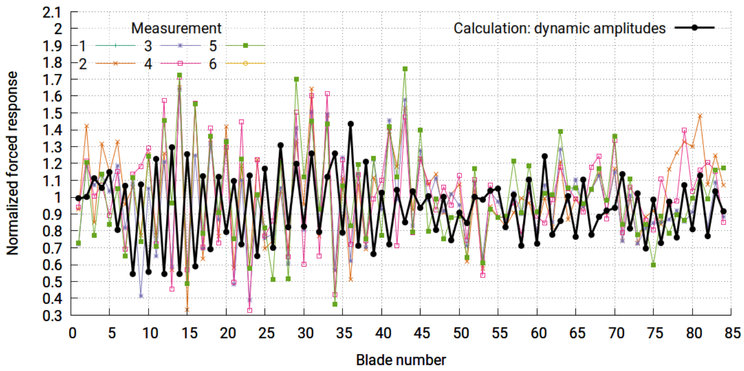

Figure 7.37: Measured and calculated dynamic forced response amplitude distributions for anisotropy mistuned bladed disk of configuration 4 using tuned contact pressures

response amplitudes, the maximum forced response is higher than the measured mean and lower than the measured maximum value. The envelope for the maximum amplitude considering the static component of the vibration, is significantly larger than the maximum measured forced response amplitude for the main resonance at $\omega = 1.046$.

The forces response has also been calculated for mistuned contact pressure conditions. A direct comparison of the maximum blade (i) combined static and dynamic and (ii) only dynamic amplitudes is shown in Fig. 7.38. For all practical reason, there is no difference in dynamic amplitudes for the two calculations. A limited effect of the mistuned contact pressures can be seen in Fig. 7.38a, where the forced response amplitude considering both static and dynamic response is plotted. By the introduction of the contact mistuning, the maximum forced response amplitude slightly increases. The results show that the effect of anisotropy orientation on the blade stiffness has a greater influence on the nonlinear forced response than the contact pressure distribution introduced through the anisotropy orientation scatter.

The BSSM-T measurement technique allows to capture the maximum dynamic forced response amplitudes around the resonance measured. This offers the opportunity to do a blade-to-blade comparison between the measured and calculated forced response amplitudes. In Fig. 7.37 the individual blade maximum forced response amplitudes are plotted for six different vibration survey runs and for the dynamic displacements calculated with ContaDyn. In these figures it can be seen that the characteristics of the distribution for the vibration amplitudes along the bladed disk circumference are captured. The mean value over the amplitudes is in good agreement with the measured data and the high nodal diameter pattern with local amplitude increases is also reproduced. The agreement between

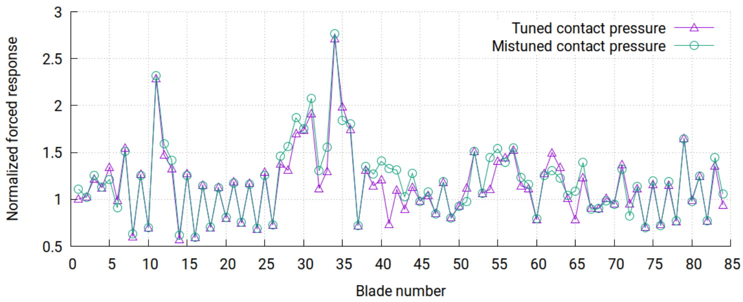

(a) Comparison of amplitudes for combined static and dynamic response

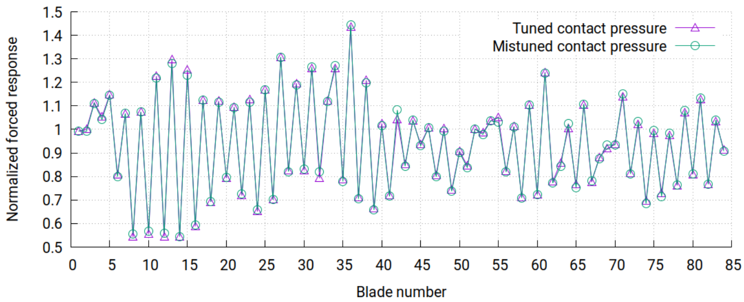

(b) Comparison of amplitudes for dynamic response

Figure 7.38: Dynamic only and combined static and dynamic forced response distribution for configuration 4 calculated with tuned and mistuned normal contact forces

the measured and calculated forced response is especially noteworthy considering that the only source of mistuned included in the calculations were the crystal orientation variation of the single crystal blades. The range of variation of the maximum forced response amplitudes is not fully captured, see Table 7.1, where the variation for the calculated forced response is 30% lower compared to the measurements. This discrepancy is considered to be due other sources of mistuning that are not modeled here e.g. variation of contact parameters, airfoil geometry variation, etc.

In Fig. 7.38a, it can clearly be seen that some blades have significantly larger vibratory amplitudes than others due to static component of the nonlinear vibration. The static components describe the change of equilibrium state on the contact interfaces due to the nonlinear vibration. It is worth investigating the contact status of the nonlinear contact elements for the individual blade shrouds, see Fig. 7.39.

The contact status "fully stuck contact with positive/negative shift" is to be understood that the 0^{th} harmonic coefficient is non-zero and depending on the definition of surface normal it defines either a positive or negative shift of the static equilibrium. The "slip-stick

Table 7.1: Statistical parameters for maximum forced response amplitudes along the bladed disk circumference for configurations 4 and 6

Configuration	Mean		Standard deviation	
	Calculation	Measurement	Calculation	Measurement
4	0.94	1.0	0.2	0.28
6	1.18	1.0	0.13	0.29

Figure 7.39: Contact status distribution for shroud contact interfaces along the bladed disk circumference at resonance frequency $\omega = 1.046$

transition with full contact" means that there is at least one time instant in the vibration period when contact pairs of the element is slipping, nevertheless there is no separation at any time instant. Similarly, the "contact-separation with friction" means that during the period there is at least one time instant when the contact pairs are separating.

In Fig. 7.39, it can be seen that for the blades that have a high static component in the vibration of the airfoil, also have a large proportion of the nonlinear contact elements on the shroud separating. As an example blade numbers 11, 30, 34 and 51 can be mentioned. Therefore, the separation of the contact elements on blade shrouds results in shift of equilibrium point of the vibration. Due to the mistuning in the bladed disk, such effects occur locally, only for a few blades.

Comparison of calculated and measured forced response amplitudes for configuration 6

The mistuned bladed disk in configuration 4 is extended with under-platform dampers, see Fig. 7.13 where the red nodes denote the location nonlinear contact elements applied in forced response analysis.

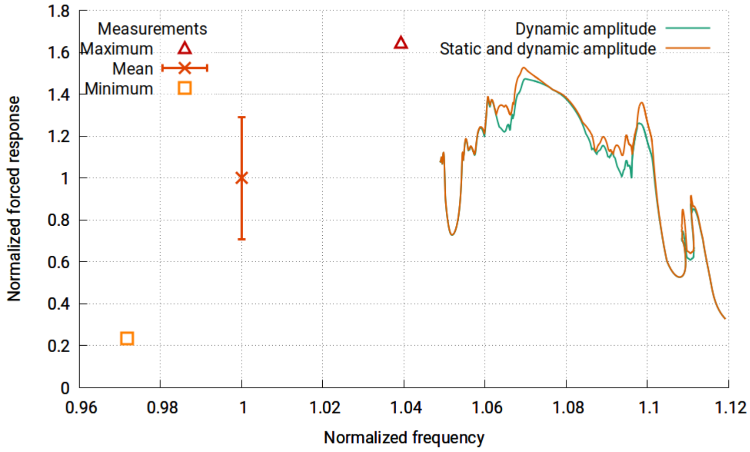

Figure 7.40: Envelope of the mistuned forced response for configuration 6

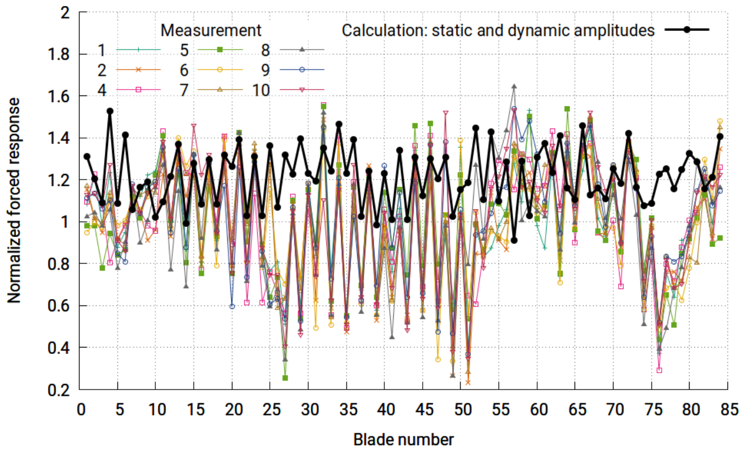

Figure 7.41: Measured and calculated forced response amplitude distributions for mistuned bladed disk of configuration 6

The envelope of the forced response shown in Fig. 7.41 show that the maximum forced response amplitudes are in good agreement with the measured amplitudes. On the contrary to the anisotropy mistuned bladed disk in configuration 4., here the static component of the nonlinear forced response is significantly lower: the difference between the envelopes for dynamic only and dynamic and static amplitudes are small. The contact status along the individual blades in the bladed disk assembly, see Fig. 7.41, also give a confirmation that there is no blade shroud contact interface where significantly high portion of contact elements are in separation.

The distribution of the forced response amplitudes along bladed disk circumference is shown in Fig. 7.41. The calculated forced response amplitudes are conservatively estimated compared to the measured amplitudes: the calculated mean is 20% higher than the

Figure 7.42: Contact status distribution for shroud contact interfaces along the bladed disk circumference at resonance frequency $\omega = 1.069$

measured one. For this configuration, the characteristics of amplitude distribution is well reproduced, i.e. the EO pattern is visible and the trend of higher and lower amplitudes for some blades are in agreement.

The full range of variation compared to the maximum measured forced response amplitudes are not captured, see Table 7.1 where the normalized standard deviation of the maximum amplitudes from the measurement is 0.29 and for the calculation 0.13. The reason for calculating low standard deviation for the simulation results clearly lies within the lack of capturing the low vibratory amplitudes. For this configuration it may be possible that the UPD works significantly better for some blades as to others. Together with the learnings that for configuration 4 the amplitude variation was only 30% higher than for the calculated results, a possible reason for not capturing the variation lies in the UPD mistuning.

7.4 Conclusions

In this chapter, the modeling methods for the calculation of the nonlinear forced response and its validation against measurement data has been done.

The numerical and physical parameters for the nonlinear forced response calculation of structures with friction joints were done. During this validation, the effects of modeling and friction interface parameters on the accuracy of forced response predictions are assessed including: (i) the number of mode shapes included in the bladed disk FRF matrices, (ii) the number of harmonics included in multiharmonic periodic forced response representation, (iii) the values of contact parameters: friction coefficients and contact stiffness and (iv) number of nonlinear contact elements used for the discretization of friction joints. By changing the mentioned numerical parameters the accuracy of the forced response and the computational efforts are changing. Because the forced response analyses for the whole model of mistuned bladed disks require significant computational efforts, the appropriate selections of theses parameters are required. Depending on the expected behavior of the structure, recommendations have been formulated regarding the number of modes, harmonic and contact elements required for the analyses.

The studies regarding the contact pressure variation on the shroud contact interfaces have been done, highlighting the effect on the nonlinear forced response amplitudes.

The calculated nonlinear forced responses are compared with the experimental values obtained for different bladed disk configurations for tuned and mistuned bladed disks including cases of: (i) blade root damping only; (ii) blade root and shroud damping and (iii) blade root, shroud and under-platform damper damping. The cases of lower and higher order excitations of bladed disk vibrations by traveling wave excitations are considered. The comparison shows sufficient accuracy of the predicted results. The calculated forced response amplitudes are within the scatter of blade amplitudes observed in the experiments: slightly higher than the measured mean amplitudes and lower than the maximum measured values.

The new facility of ContaDyn and InterDyn for the calculation of nonlinear forced response for anisotropy-mistuned bladed disks, where the differences in the crystal orientation of the single- crystal blades are considered, have been validated for two configurations. The comparison of the calculated and measured maximum amplitudes obtained for all blades in the anisotropy-mistuned show a general agreement for the configuration with shroud friction contacts. This indicates that when the nonlinear forced response for anisotropy-mistuned bladed disks is considered, the mean amplitude over all blades is accurately obtained and part of blade-to-blade variation is captured. Moreover, to some extent the characteristics of the blade-to-blade variation along the circumference, e.g. localizations are captured. For the mistuned bladed disk with under-platform dampers, the mean response level is conservatively calculated but the variation of amplitudes is underestimated.

Chapter 8

Nonlinear forced response and its sensitivity for the anisotropy mistuned bladed disks

Until now, the tools for the calculation of the nonlinear forced response and its sensitivities have been validated. This chapter is on the nonlinear forced response of the mistuned bladed disks and their sensitivities with respect to the anisotropy orientation of the single crystal turbine blades.

The studies are first are focused on the nonlinear forced response of the nonlinear forced response. The variance of the maximum forced response amplitude distribution along the circumference of the mistuned bladed disk has been analyzed. The studies have considered varying input parameters, such as the level of harmonic excitation, multiharmonic excitation, engine order and mistuning pattern.

The sensitivity of the nonlinear forced response is studied for a pair of blades and realistic bladed disks with and without under-platform damper.

8.1 Nonlinear forced response of mistuned bladed disks

Parametric studies were done for mistuned bladed disks regarding the harmonic excitation levels and the value of contact pressure on the friction contact interfaces. For tuned and mistuned bladed disk the damping efficiency of an UPD design was studied for varying engine order excitation.

8.1.1 Effect of harmonic excitation level on the nonlinear forced response of mistuned bladed disks

The level of harmonic excitation can vary within a certain range during the engine operation. A robust friction damper design is effective on a wide range of excitation levels. The effect of the harmonic excitation level was studied for a mistuned bladed disk with root damping and for a mistuned bladed disk with shroud damping and under-platform damper.

Mistuned bladed disk with root damping

First, the forced response of the bladed disk is analyzed for a model where the nonlinear contact interfaces are only on the root and the shrouds are considered to be free. Using this model the effect of the root damping can be assessed for the anisotropy mistuned bladed disks. For each blade root 24 contact elements are applied, resulting in 1800 nonlinear contact elements for the whole bladed disk. The static pre-stress of the contact elements, in the form of contact pressure are obtained from a nonlinear static calculation with surface-to-surface penalty contact. For the static calculation the actual anisotropy-mistuning pattern is used, meaning that the contact pressure values on the blade root are inherently mistuned.

For the FRF calculation the harmonic numbers 1,3 and 5 are included, as there are not separations expected on the blade roots which would require the use of 0^{th} and even harmonics.

The harmonic excitation forces are applied on the pressure side of each blade and excitation force is equally distributed over 8 nodes. The forced response amplitudes are studied for each blade on the same node on the trailing edge. For the radial location of the node of interest, the blade tip is chosen where the maximum forced response of the bladed disk is. To investigate the nonlinear forced response for different excitation levels, the normalized harmonic loading is changed between the values of 0.2, 0.6 and 1. The studied harmonic excitation engine order is the 8^{th} and 35^{th} and it excites the first family of modes, denoted with A and B in Fig. 8.1. The two engine order excitations are assumed to be at the same rotation speed, meaning that the rotation speed dependency of the modal properties and the static contact pressures is not included.

The 500 modes, equivalent to approximately 6 mode families, included in the forced response function calculation are sufficient for accurately capturing the nonlinear forced response of the 1^{st} mode.

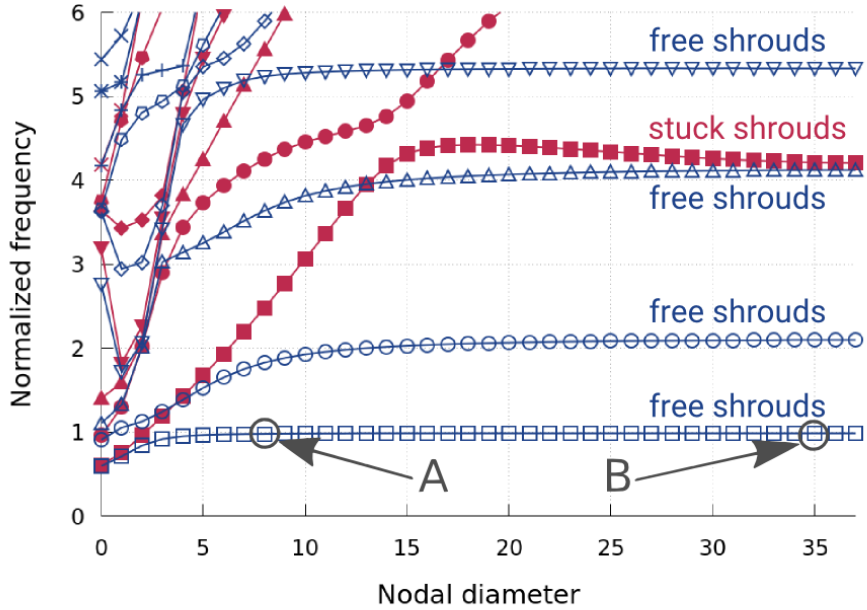

Figure 8.1: Natural frequency-nodal diameter diagram of the cyclic symmetric model with stuck and free shroud interfaces

For the studies, five different anisotropy mistuning patterns are generated using random sampling from the realistic statistical distributions defined for each of the anisotropy angles (α,β and ζ) of the single crystal turbine blades. To be able to assess the amplification factors due to mistuning, the forced response of the tuned bladed disk is calculated. For the tuned bladed disk, the material axis [001] of all blades is coinciding with the stacking axis of the blade, meaning that $\alpha = 0$.

The forced response for all blades at the same node of the blade tip is shown for mistuning pattern 1 in Fig. 8.2. This figure shown different maximum forced response amplitude and the frequency of the maximum forced response amplitude also varies for each blade. Here, the largest $||\boldsymbol{p}|| = 1$ excitation amplitude is applied, which initiate high vibratory response on the airfoil and also on the blade roots which results in high frictional damping. The high frictional damping results in wider and reduced resonance peaks.

For the mistuned bladed disks, the maximum forced response over all blades is higher than the maximum forced response of the tuned blade disk. This means, that the amplification factor larger than 1 amplification factor can be observed in Figs. 8.3 an8.4, where the envelope of the forced response is shown for bladed disks with 5 mistuned patterns.

The amplification factor is different for harmonic excitation level. Nevertheless, for all mistuning patterns it follows the same tendency, namely that for higher excitation levels, the amplification factor decreases.

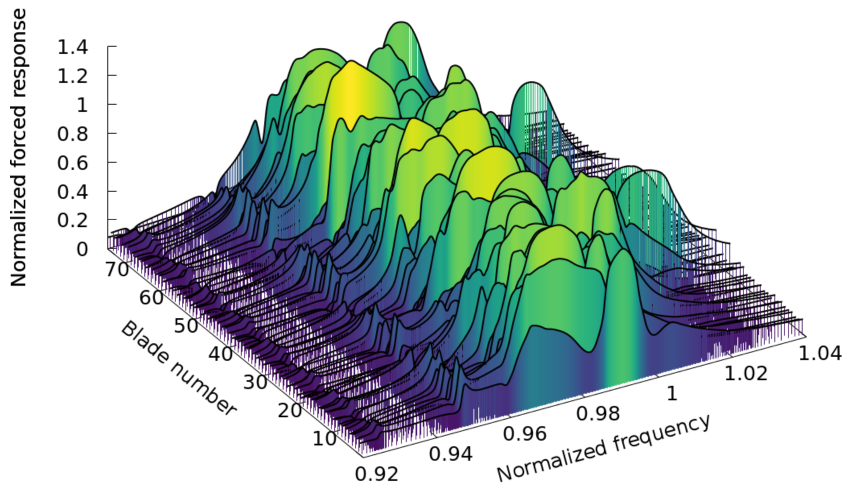

Figure 8.2: Forced response of all blades of the mistuned bladed disk with root damping for pattern 1 using excitation level $||\boldsymbol{p}|| = 1$ at excitation frequency A (EO8)

The Figs. 8.3 and 8.4, apart from the forced response envelopes also include the mean value of maximum forced response amplitudes and their frequency averaged over all blades in the five different mistuned bladed disks.

In case of EO8 the mean value of the forced response for each bladed disk is lower than the maximum forced response of the tuned bladed disk: it is between 91% and 99% of the tuned forced response. This value for EO35 is larger than calculated for the tuned forced response: between 107% and 117% compared to the tuned forced response to EO35. It is worth noting that the mean value of the forced response is lower, as the damping increases through the increased excitation level.

The bladed disk only includes damping of the blade root interfaces and the shrouds are free. Therefore, the coupling between the blades is small and only happens via the disk. This results in a noticeable variation of the frequency of maximum forced response amplitude for each blade in the mistuned bladed disk. This variation is noticeable in the three-dimensional plot of Fig. 8.2 and also in the wide resonance peaks in the forced response envelopes, see Figs. 8.3 and 8.4.

The effect of the excitation level on the amplification factor of the mistuned bladed disks averaged over the bladed disks with the five different mistuning patterns is shown in Fig. 8.5. In this Figure, the mean value of the amplification factors to both EO8 and EO35 excitation of the first bending mode is shown for varying excitation levels. The results show that for both engine orders the amplification factor monotonously decreases as the excitation amplitude increases.

Furthermore, the maximum forced response distribution along the blades has been

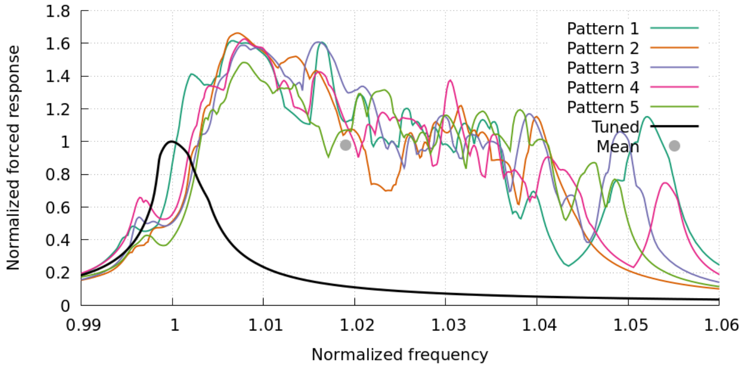

(a) Forced response to low excitation level: $||\boldsymbol{p}|| = 0.2$

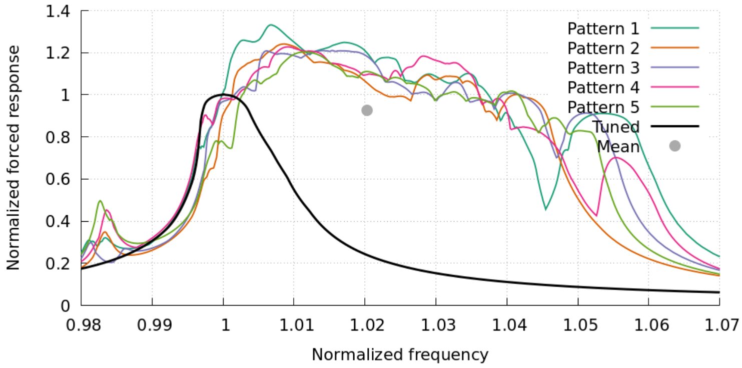

(b) Forced response to medium excitation level: $||\boldsymbol{p}|| = 0.6$

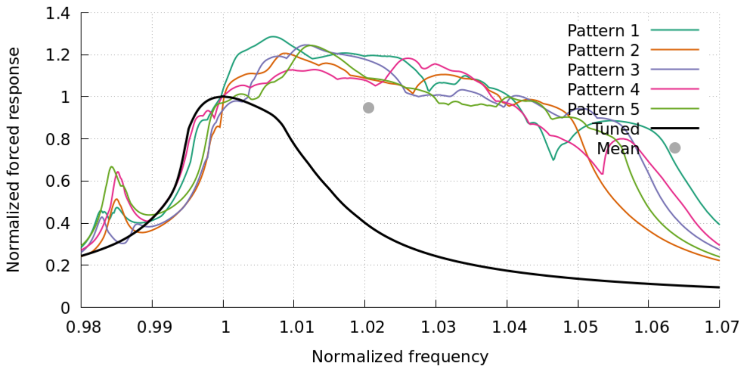

(c) Forced response to high excitation level: $||\boldsymbol{p}|| = 1$

Figure 8.3: Forced response envelope of anisotropy-mistuning bladed disks with root damping for 5 different mistuning patterns to excitation frequency A

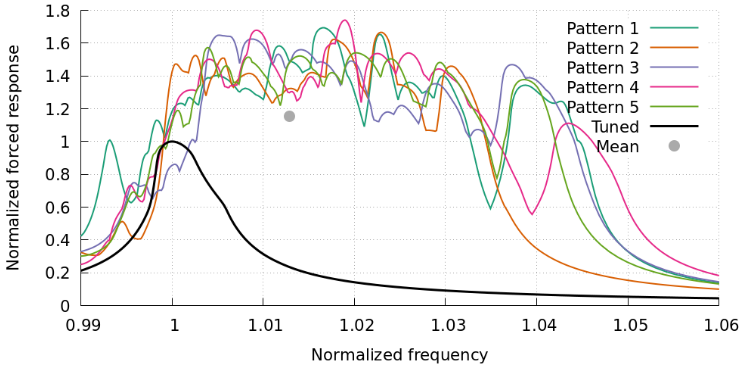

(a) Forced response to low excitation level:$||\boldsymbol{p}|| = 0.2$

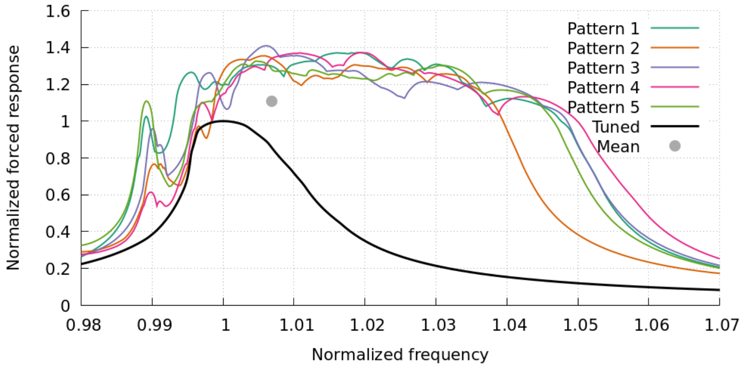

(b) Forced response to medium excitation level:$||\boldsymbol{p}|| = 0.6$

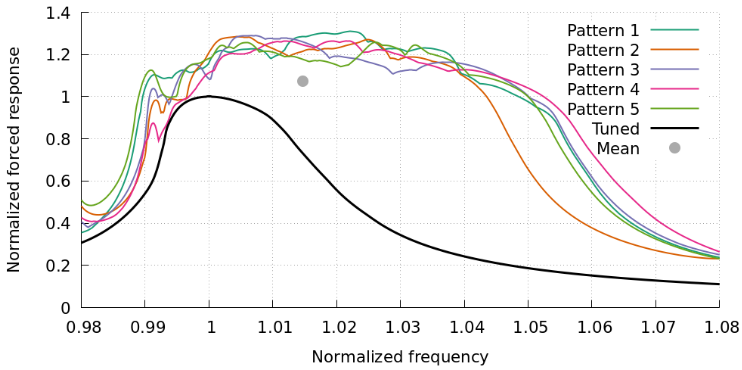

(c) Forced response to high excitation level:$||\boldsymbol{p}|| = 1$

Figure 8.4: Forced response envelope of anisotropy-mistuning bladed disk with root damping for 5 different mistuning patterns to excitation frequency B (EO35)

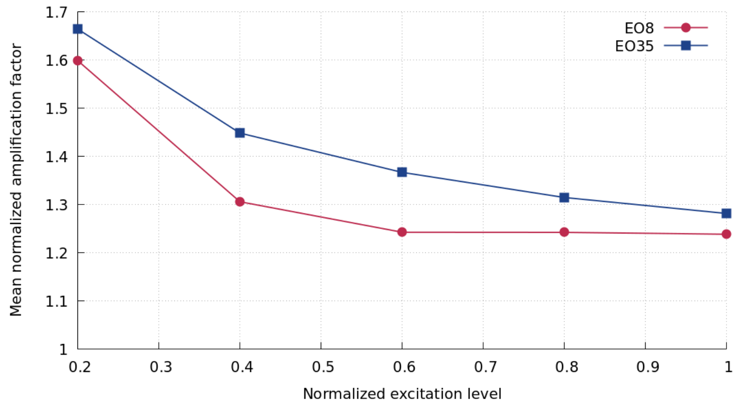

Figure 8.5: Mean of amplification factor for varying excitation level for excitation frequency A (EO8) and B (EO35) in the case of mistuned bladed disks with root damping

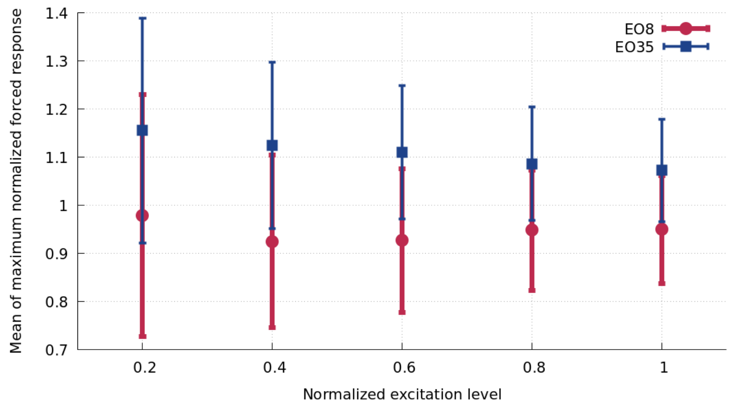

Figure 8.6: Averaged mean and standard deviation of maximum forced response for all blades along the circumference of the mistuned bladed disk with root damping for varying excitation level for excitation frequency A (EO8) and B (EO35)

studied for the five excitation levels. As an overview, the mean value and the standard deviation of the maximum forced response amplitudes along the circumference of the bladed disk is shown in Fig. 8.6, for EO8 and EO35 considering varying levels of excitation amplitude. Similarly to the averaged amplification factors, the averaged standard deviation of the maximum blade amplitudes for the mistuned bladed disks monotonously decrease as the excitation amplitude increases.

The maximum forced response distribution along the blades has been visualized in Fig. 8.7 for the frequency range 0.9-1.04 of interest. The plots show the forced response amplitudes for the anisotropy mistuning pattern 1 and for three excitation amplitudes, $||\boldsymbol{p}|| = 0.2$, $||\boldsymbol{p}|| = 0.6$ and $||\boldsymbol{p}|| = 1$. The similarity between the maximum forced response

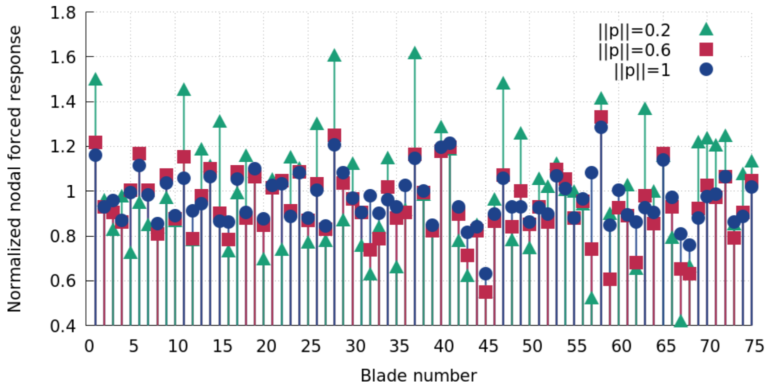

Figure 8.7: Blade maximum forced response distribution for different excitation levels for mistuned bladed disk with root damping

values for all the blades can be seen for $||\boldsymbol{p}|| = 1$ and $||\boldsymbol{p}|| = 0.6$. For these excitation levels the nonlinear friction forces appear on the blade roots. The maximum amplitude distribution of the blades is significantly different for excitation level $||\boldsymbol{p}|| = 0.2$. It can be seen that the excitation level influences the maximum blade response distribution and as shown earlier, the variation of the maximum forced response over the blades.

Mistuned bladed disk with shroud and under-platform damping

The effect of the change in excitation amplitude on the nonlinear forced response of mistuned bladed disks was studied for an anisotropy-mistuned bladed disk with nonlinear contact interfaces on one shroud surface and on two blade to under-platform damper contact interfaces for each blade. The contact interfaces between the blade-root and disk is considered to be fully stuck, therefore it is modeled by linear multi-point-constraints. This also means that the modal properties can be calculated with fully stuck blade-root contact interfaces, requiring to calculate less bladed disk modes. For the FRF calculations 400 bladed disk and 20 UPD modes are included. The calculation uses all harmonic numbers from 0 to 5. Because the FRF calculation includes the 0^{th} harmonic number, the UPD needs to be constrained to avoid the rigid body modes. The under-platform damper is placed on soft springs in the four lower corners of the UPD body, see Fig. 8.8. In all four positions there are three springs in the three spatial directions. One end of the spring has fixed BCs and the other end is connected to the damper. In order, not to detune the higher modes and not to include noticeable additional stiffness, the spring stiffness is set low: $k_s = 10^{-3} N/mm$. The natural frequency of the first six modes of the UPD is between 5 and 13 Hz, which is sufficiently far from the rigid body modes and from the excitation

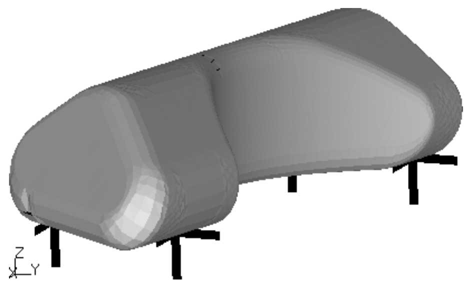

Figure 8.8: Under-platform damper placed on soft springs

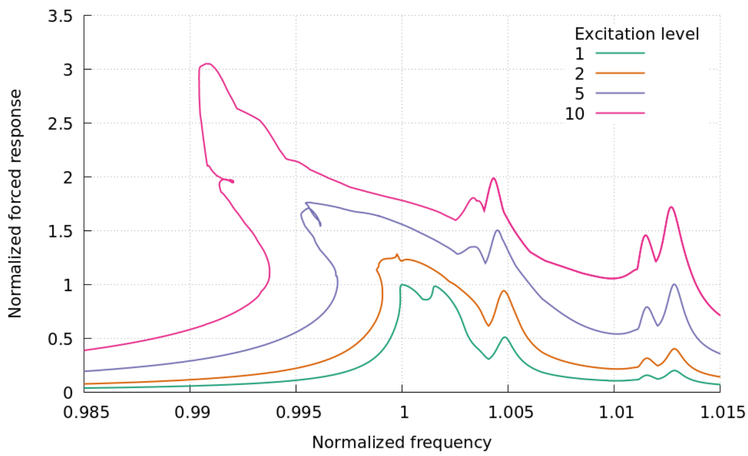

Figure 8.9: Envelope of forced response for different excitation levels for mistuned bladed disk with shroud and UPD damping

frequency.

For the contact interfaces on the shrouds a fine discretization is used, with 14 nonlinear contact elements for every sector. There are 3-3 contact elements on both sides of the cottage-roof style under-platform damper. In the whole bladed disk there are 15,000 nonlinear contact elements included. There is no static mistuning introduced: for the contact elements the same contact pressure is used for every sector. Moreover, the contact pressure for all contact elements on the shrouds are the equal. Similarly, the contact pressure for all UPD contact elements are the same.

The bladed disk is anisotropy-mistuned, where the blades have random anisotropy angles sampled from their realistic statistical distribution. The harmonic excitation is applied on the trailing edge of each blade with the phase shift of EO20. The effect of the amplitude of the harmonic excitation on the nonlinear forced response amplitudes is studied on the normalized range of 1 to 10.

The envelope of the nonlinear forced response is shown for the varying excitation amp-

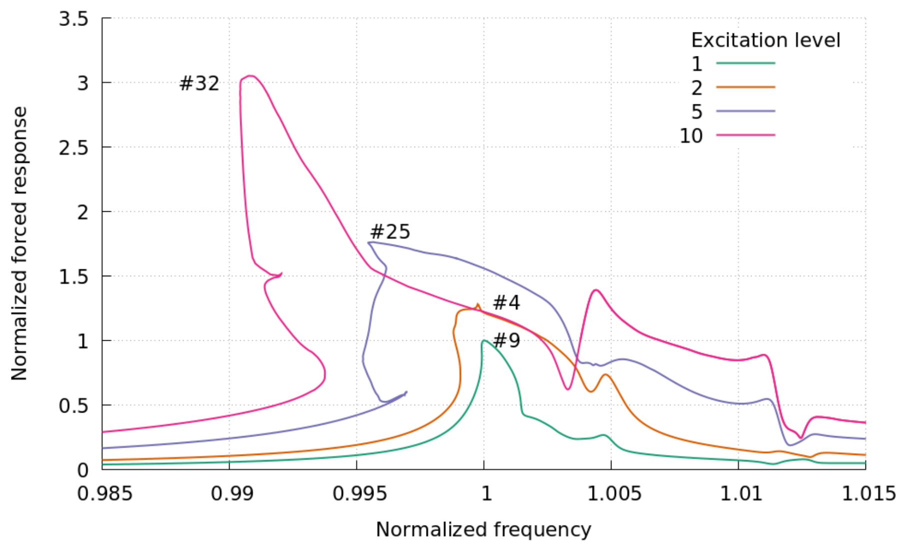

Figure 8.10: Forced response of the blade with maximum amplitude on the frequency range for different excitation levels for mistuned bladed disks with shroud and UPD damping

litudes in Fig. 8.9. In order to illustrate the change of the forced response amplitudes over the excitation frequency, the forced response of the blade with the maximum displacements are shown in Fig. 8.10. The figures show that forced response function for excitation level 1 is asymmetric around the resonance and there are two distinct resonance peaks. For excitation level 1 the forced response does not have any overhanging branches. By increasing the level of excitation the relative displacements between the contact interfaces of the neighboring blades increase, resulting in partial contact separation. Due to the change in the bladed disk stiffness results in multi-valued forced response functions for the excitation levels 2 and above. In Fig. 8.10 the blade number of the maximum forced response is also shown for every excitation level. The blade number for the maximum forced response amplitude is different for every excitation amplitude. This shows that for mistuned bladed disks with strong nonlinearities, the distribution of the maximum forced response amplitudes along the bladed disk circumference are significantly influenced by the excitation amplitude.

8.1.2 Effect of contact pressure level on the nonlinear forced response of mistuned bladed disks with shroud contact interfaces

The analysis of the effect of contact pressure level at the outer shroud contact patches on the nonlinear forced response was studied for the mistuned bladed disk studied in subsection 7.2.1. The input parameters of mistuning pattern, harmonic excitation etc. are

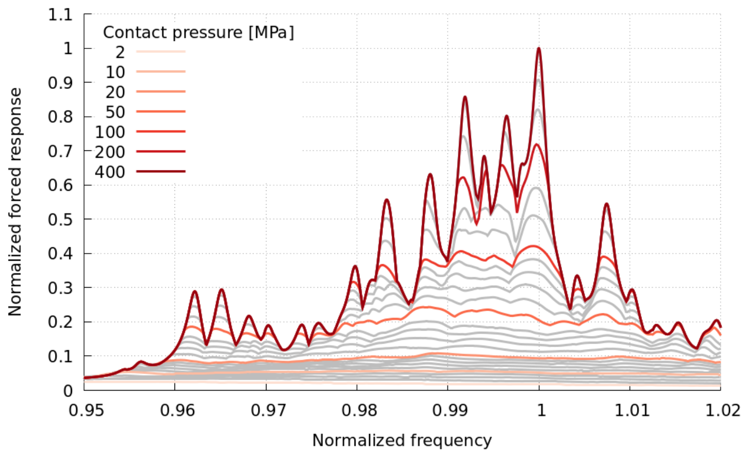

Figure 8.11: Nonlinear forced response of mistuned bladed disks with varying tuned contact pressures

kept the same as before.

For this study, the maximum forced response distribution was analyzed for different contact pressure values in two comparisons: (i) for contact pressure values 16, 18 and 20 MPa (ii) for contact pressure values 6,12 and 30 MPa. In order to be able to compare the forced response amplitudes, the maximum forced response of each blade on the frequency range has been normalized by the mean forced response amplitude of the bladed disk. The forced response amplitudes were normalized for different contact pressure values separately.

For contact pressure values 16 to 20 MPa, the maximum forced response amplitude is for blade number 15. In relation to the maximum forced response in the bladed disk, there is a small change in the amplitude distribution, see Fig. 8.12. For some blades, the difference is negligible, e.g. blade number 26. For some other blades, such as blades number 12 and 15, the relation to the mean forced response amplitude differs. For these blades the deviation from mean is larger in the bladed disks where higher contact pressure was applied.

When the analysis is extended for a larger contact pressure range, i.e. 6, 12 and 30 MPa in Fig 8.13, one can see that the distribution of the maximum amplitudes along the bladed disk circumference significantly changes. As an example: for blade 62 the forced response amplitude obtained with 6 MPa is smaller than the mean amplitude, while for contact pressures 12 and 30 it is larger. The results demonstrate that for the same mistuning pattern, the response of the individual blades and the distribution of the forced response amplitudes significantly impacted by the coupling between the blades. The static contact pressure influences the contact status and the nonlinear friction forces, which in turn affect

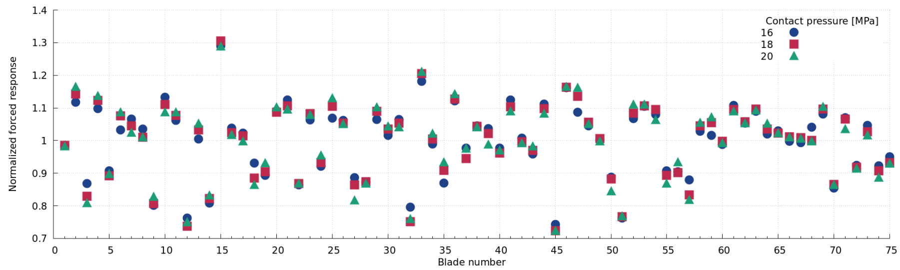

Figure 8.12: Nonlinear forced response amplitude distribution for mistuned bladed disks with contact pressures values varied between 16 and 20 MPa

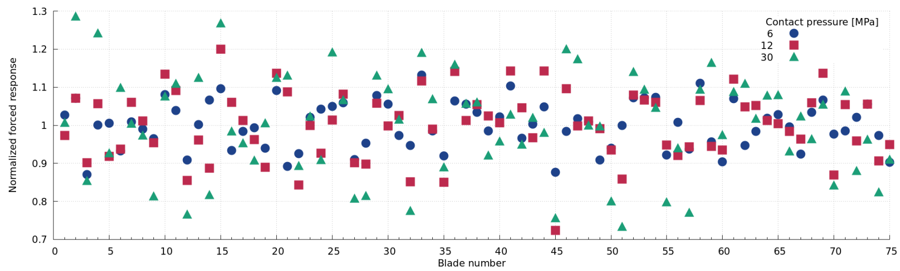

Figure 8.13: Nonlinear forced response amplitude distribution for mistuned bladed disks with contact pressures values varied between 6 and 30 MPa

the coupling between the neighboring blades.

The change in the contact pressure on the outer shroud contact interfaces, results in a change of the distribution of the maximum forced response amplitude of the mistuned bladed disk. The change in the amplitude distribution also results in change of the blade for which maximum forced response amplitudes are observed. This is shown, in Fig. 8.14, where it can be seen that for contact pressures above 70 MPa, the maximum forced response amplitude is for blade 36. For low contact pressure values, the amplitude distribution is sensitive to the contact pressure variation: the blade of maximum forced response amplitudes changes as the contact pressure is increased. For contact pressure values between 12 and 25 MPa, blade #15 and for contact pressure between 30 and 60 MPa, blade #2 has maximum forced response amplitude.

To further investigate the phenomena of the dependence of variation of the forced response amplitudes of mistuned bladed disk on the shroud contact pressure, the minimum and maximum forced response amplitudes along the circumference have been observed for the same mistuned bladed disk as the contact pressure on the shroud interfaces were varied on the range of 4 to 400 MPa. The minimum and maximum amplitudes for all calculations have been divided by the mean amplitude along the circumference of the bladed disk for the

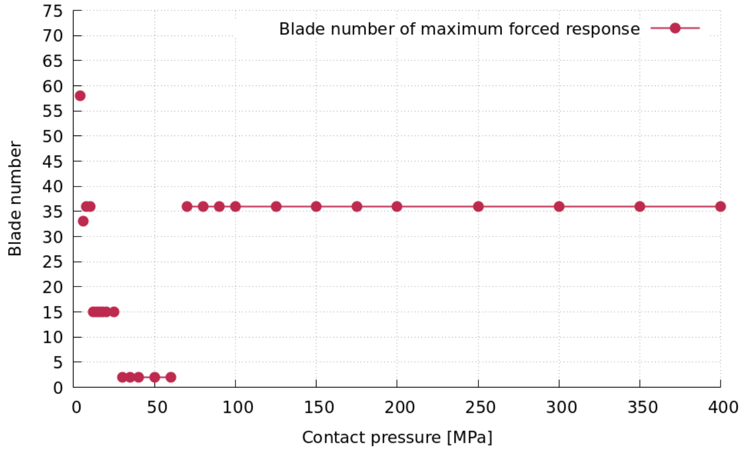

Figure 8.14: Blade number of the maximum forced response for mistuned bladed disk with varying contact pressure on blade outer shrouds

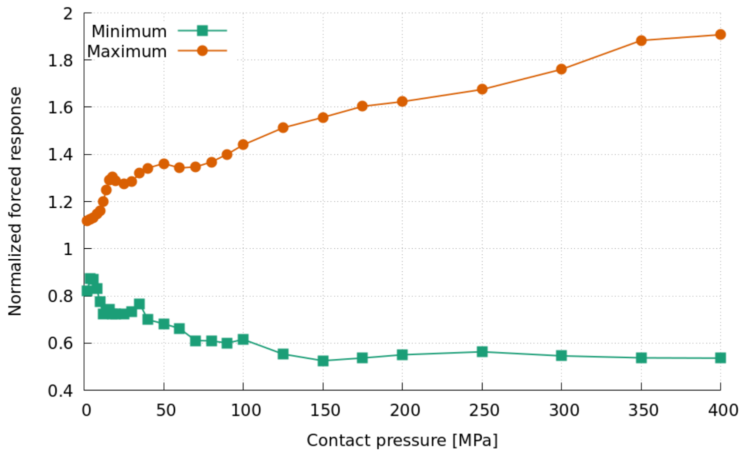

Figure 8.15: Minimum and maximum value of forced response over all blades in mistuned bladed disk for varying contact pressures on blade shrouds

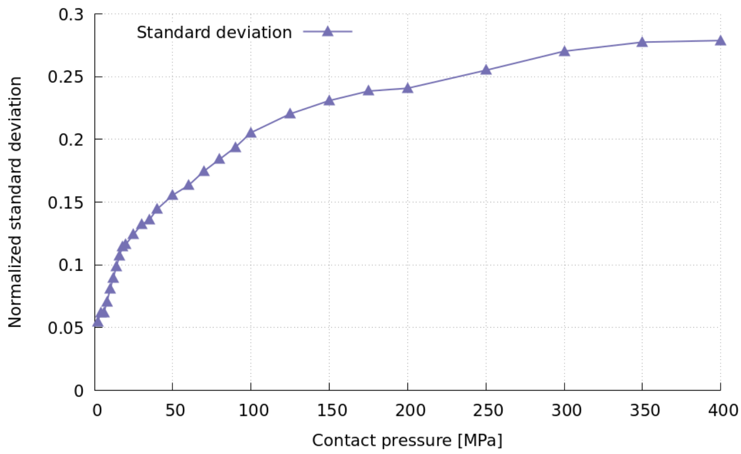

Figure 8.16: Standard deviation of the forced response amplitudes along the circumference of the mistuned bladed disk

respective calculation. The results plotted in Fig. 8.15, show that the difference between the minimum and the maximum forced response increases as the contact pressure increases. It is worth noting that the up to 150 MPa, the difference of minimum and maximum value from the mean value (1.0) is symmetric. The figure shows that the minimum forced response amplitude normalized by the mean amplitude levels off above 200 MPa, leading to an asymmetry when considering the difference of minimum and maximum forced response amplitudes from the mean value. The maximum forced response monotonously increasing until 400 MPa, at which point all blades are fully stuck and the forced response is linear.

For the maximum amplitudes of the 75 blades over the frequency range under consideration, the standard deviation normalized by the mean value for each forced response calculation has been obtained. The standard deviation plotted over the contact pressure range of [4,400] MPa, in Fig. 8.16, is showing 4.5-fold decrease in standard deviation for the calculation with low contact pressure when the compared for the fully linear analysis. It is also worth noting that the gradient of the standard deviation over the contact pressure curve is the largest for low contact pressure values.

The results show that the lower contact pressure values on the shroud interfaces result in smaller variance of the forced response amplitudes along the circumference of the mistuned bladed disk. This behavior can be explained by considering that the blades with localized, high-energy vibrations get damped and therefore those resonance peaks get significantly reduced. The increase in damping does not only reduce the mean forced response amplitudes, but also reduces the standard deviation of the individual blade amplitudes and the through that the mistuning amplification factors.

8.1.3 Effect of rotation speed on nonlinear forced response of mistuned bladed disks with under-platform dampers

Under-platform dampers have been essential part of the design of turbine bladed disks. The small damper parts are placed under the blade platform and under the centrifugal loading they are pressed again the blade under-platforms. Due to the relative motion between the blades and on the damper cottage roof contact interfaces friction forces appear and kinetic energy is dissipated. The normal forces on the under-platform damper contact interfaces are dependent on the damper geometry, friction coefficient of the rough surfaces and the centrifugal forces, as shown in [79].

The design of the dampers is carefully selected to be the most effective for a certain mode in a certain rotation speed range. The most important design parameters of the damper are its mass, the cottage roof surface angle and the surface area. When the damper parameters are already known, the contact pressures can be calculated for any rotation speed. The contact pressures play an essential role in the onset for the slip-stick transition and in the resulting damping ratio.

In the current work, an already available bladed disk and under-platform damper was used. In this study, it has been studied that how this damper design performs for 1F blade mode with open shrouds and with stuck root contact interfaces. To see how the damper performs for different rotation speeds, the rotation speeds at crossings of EO6 to EO34 and mode 1 has been considered, see the schematic Campbell diagram Fig. 2.1. The 1F mode with open shrouds, see Fig. 8.1, is a great candidate for this study, because the mode is disk dominated nodal diameter 5 and above, therefore the change of operational deflection shape through the disk stiffening can be neglected. The modal properties are calculated for the pre-stress state at the rotation speed of the crossing of EO14 line and mode 1. To save computational efforts, the rotation speed dependency of the modal properties is not included.

First, the forced response of the tuned bladed disk has been calculated with varying engine order excitations. As a reference the linear forced response is calculated without UPD and fully stuck UPD. For the nonlinear forced response calculations the contact pressure values are applied on the 3 contact elements on each side of the UPD. The pressure values are calculated for the respective engine order crossings.

The forced response functions, shown selected EO excitations in Fig. 8.17, are normalized with respect to the maximum forced response amplitude and resonance frequency to EO14 excitation of the bladed disk without UPD. The resonance frequency of the non-

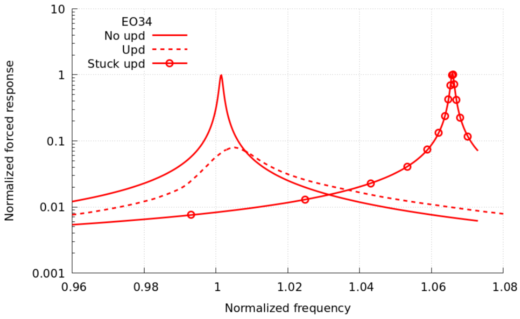

(a) Forced response to EO34

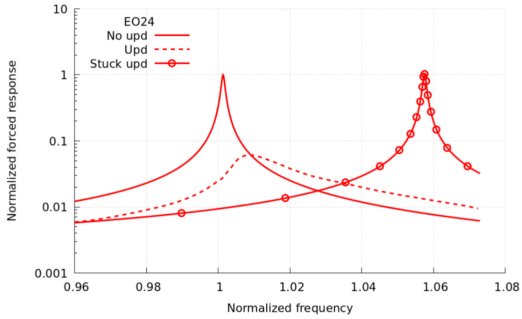

(b) Forced response to EO24

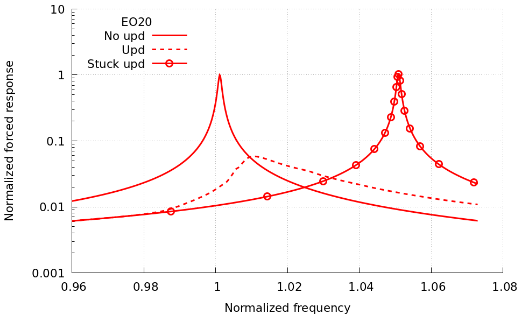

(c) Forced response to EO20

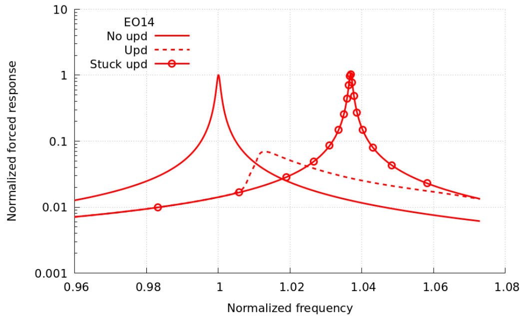

(d) Forced response to EO14

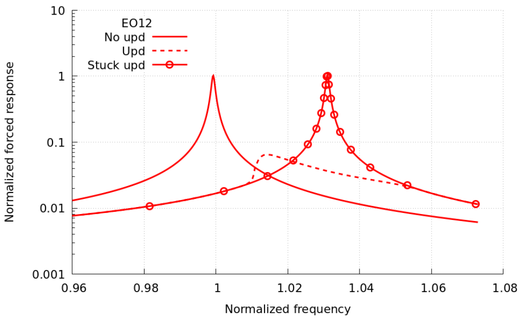

(e) Forced response to EO12

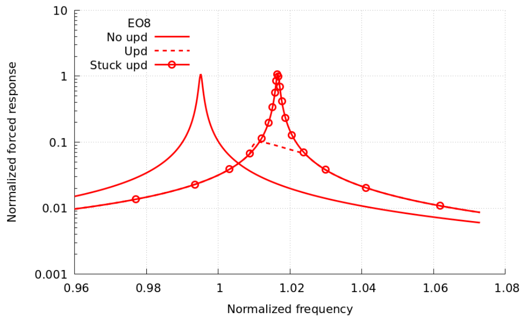

(f) Forced response to EO8

Figure 8.17: Nonlinear forced response of tuned bladed disks with and without UPD showing the damper effectiveness for different centrifugal forces

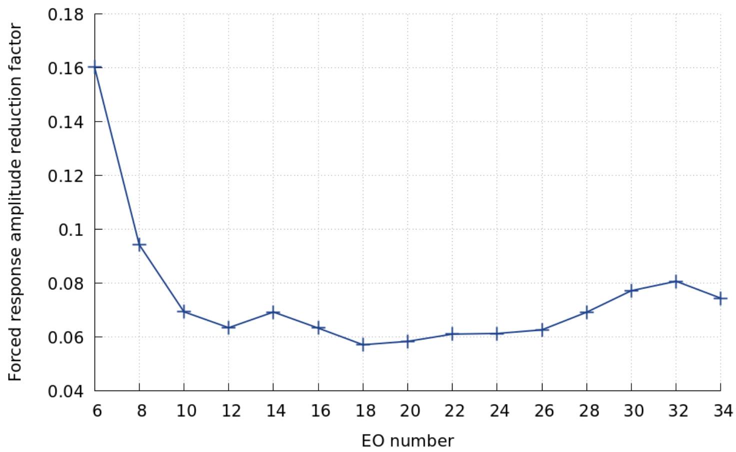

Figure 8.18: Tuned forced response amplitude reduction factors with UPDs for different EO excitations

linear forced responses are between the bladed disk with stuck and without any damper. For lower rotation speed and therefore lower contact pressures, e.g. EO34 in Fig. 8.17a, the forced response function is nearing the solution calculated for the blade disk without UPD. For higher rotation speeds, the resonance frequency increases. For very high contact pressures, as for EO8 in Fig. 8.17f, the resonance frequency approaches the bladed disk with stuck under-platform dampers. For this engine order excitation, the forced response function shows that the slip-stick transition only happens in the narrow frequency band near the resonance frequency of the bladed disk with stuck dampers. On the other hand, for higher engine order excitations the stick-slip motion dominates the forced response on a large frequency band.

The forced response functions in Fig. 8.17 show different damping for the different nonlinear forced responses due to the change in the rotation speed. In order to identify, for which engine order excitation is the damping the most effective, amplitude reduction factors have been calculated. The amplitude reduction factors have been calculated separately for each engine order excitation by dividing the maximum nonlinear forced response amplitude by the maximum forced response amplitude of the linear bladed disk without UPD.

The amplitude reduction factors in Fig. 8.18 show that low EO excitation, the damping is low. On the other hand, for high EO excitation, EO30-EO34, the damping is higher than for EO6 and EO8. For medium engine order excitation values, the reduction factor fluctuates between 0.07 and 0.08. The lowest reduction factor is for EO19.

The forced response has been calculated similarly for a mistuned bladed disk using varying engine order excitations. The forced response for bladed disks without UPD, with

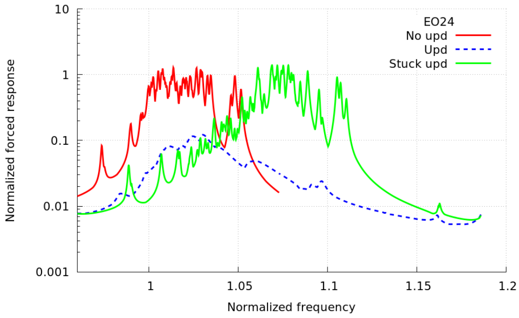

(a) Forced response to EO24

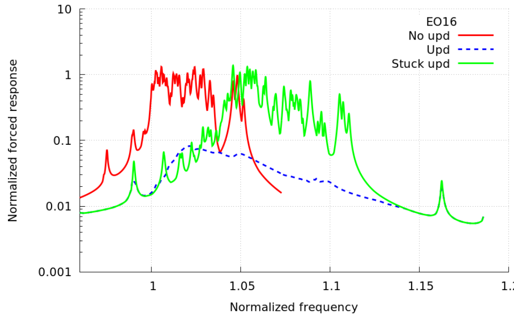

(b) Forced response to EO16

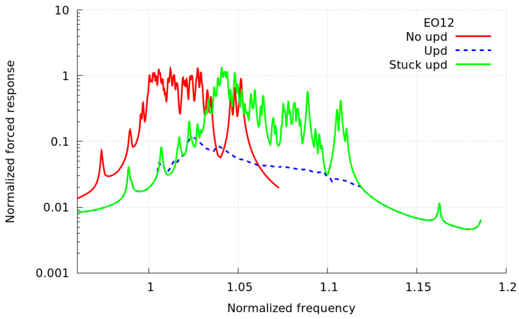

(c) Forced response to EO12

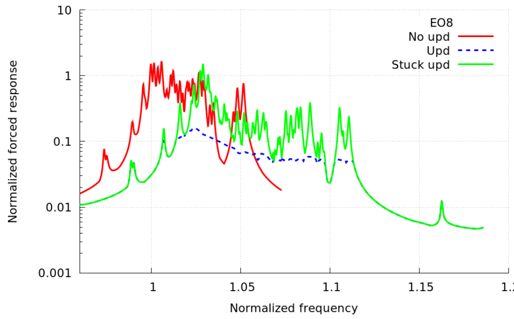

(d) Forced response to EO8

Figure 8.19: Nonlinear forced response of mistuned bladed disks with and without UPD for different EO excitations

stuck and nonlinear UPD has been plotted in Fig. 8.19. The forced response envelopes for the mistuned bladed disks show a similarity with the tuned bladed disks, with respect to the effect of change in engine order excitation. The excitation frequency of the peak amplitudes for the mistuned bladed disk with nonlinear dampers are lower than for the bladed disk with stuck damper and higher than the bladed disk without UPD. Due to the mistuning and the limited coupling between the blades resonance conditions is on a wider frequency range than for the tuned systems.

For mistuned bladed disks, the amplitude reduction factors were calculated similarly as for tuned bladed disks: the ratio of maximum forced response amplitude for bladed disk with nonlinear UPD and maximum forced response of bladed disk without damper. To calculate the ratio, the maximum amplitudes from all blades along the frequency range studied is selected.

By looking at the forced response amplitudes reduction factors over the engine order number, in Fig. 8.20, it shows a significant sensitivity to engine order excitation. The largest forced response amplitude reduction is for EO 14-22. For higher and lower engine order excitations the forced response amplitudes are reduced to a lesser extent for the

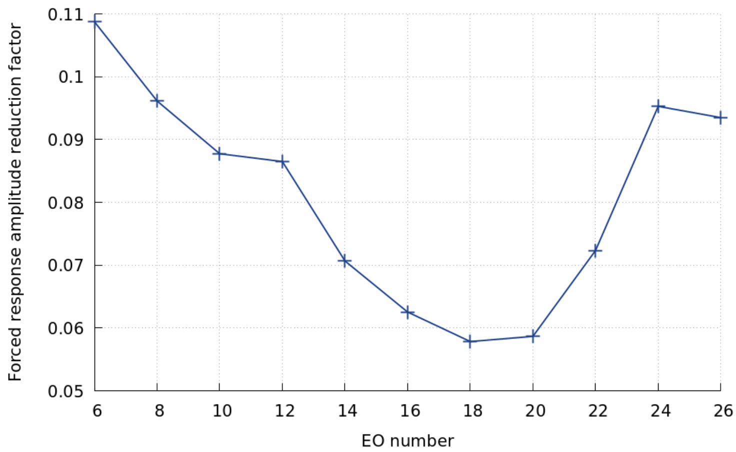

Figure 8.20: Mistuned forced response amplitude reduction factors with UPDs for different EO excitations

nonlinear systems.

It has been studied, how the range of variation of forced response amplitude over the blades is affected by changing the engine order excitations. To this end, the maximum forced response of each blade over the frequency range for the mistuned bladed disk have been stored. The amplitudes for each engine order excitation were normalized by the maximum forced response of the tuned bladed disk with nonlinear UPD and with the respective engine order excitation. For the normalized maximum blade amplitudes, the minimum, maximum and the mean value has been calculated.

The Figure 8.21 shows for engine order 6 to 26 the minimum, maximum and mean values. The mean values are shown with a filled circle symbol and minimum and maximum values are denoted by the two ends of the error bars. The amplification factor (the maximum values) is the highest for EO 24 and 26, but a local maxima can be observed for EO 10 and 12, for which engine orders the amplitude reduction factors showed little damping. On the other hand, forced response amplification factor is the lowest to EO 16 and 18 excitations, for which conditions the under-platform damper proved to performing well. While for the amplification factors a significant variation can be seen, the mean values of forced response vary only on the limited range of 0.8-1.0.

It is also worth noting that with the increased damping the range of amplitude variation defined by the minimum and maximum forced response amplitudes decreases. The same effect has been identified for bladed disks with shroud damping in subsection 8.1.2.

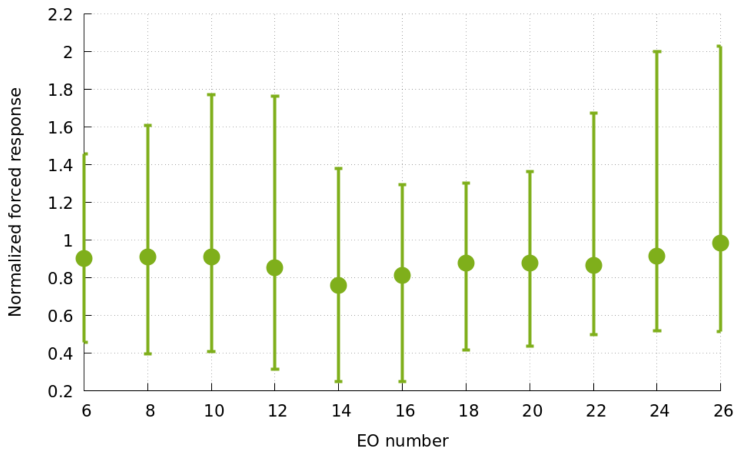

Figure 8.21: Minimum, maximum and mean forced response of mistuned bladed disk with UPDs for different EO excitations

8.2 Nonlinear forced response and its sensitivities with respect to anisotropy orientation angle for mistuned bladed disks

The sensitivities of forced response amplitudes were studied for industrial size bladed disks with friction contact interfaces. The first analyses were done for two-blade structure with stepwise varying anisotropy orientation. As for mistuned bladed disks, structures with (i) blade root damping, (ii) shroud damping and (iii) shroud damping together with UPD were considered.

8.2.1 Sensitivity of forced response of a two-blade structure

The effect of variation of the material anisotropy orientation on the forced response have been studied for the model consisting of two anisotropy mistuned blades, shown in Fig. 8.22. For this analysis the anisotropy angle α of blade 1 (blade on the left-hand side in Fig. 8.22) has been gradually increased from α_1 to α_{10} within the realistic range of this angle variation, while all other anisotropy angles are kept constant. This allows for easily understanding how the change in crystal orientation influences the nonlinear forced response and how that change is reflected in the sensitivities. The nonlinear reduced order model includes 18 contact elements on each root interface and 10 nonlinear nodes on the shroud interfaces, which results in 164 nonlinear nodes applied in total. A small initial gap is set between the two blade shroud interfaces which may close during the vibration period for certain excitation frequencies.

Figure 8.22: FE model of two-blade structure

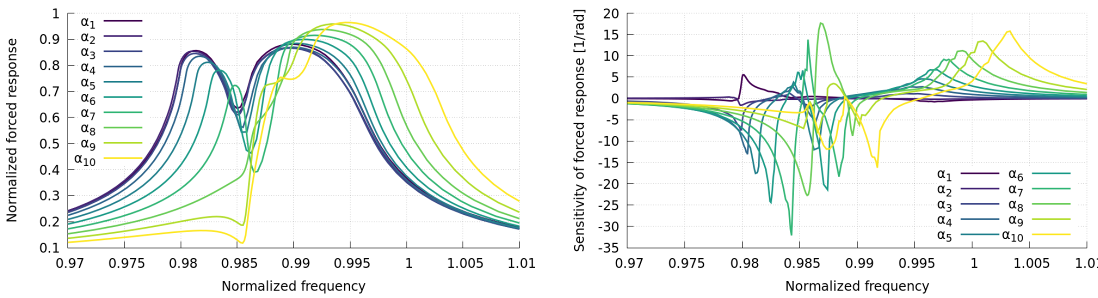

(a) Forced response

(b) Sensitivity of forced response

Figure 8.23: Forced response and its sensitivity of blade 1 with varying α anisotropy angle

The forced response amplitude of blade 1 is obtained at the midspan of the trailing edge and shown in Fig. 8.23a. The response for the primary angle valued at α_1 shows two resonance peaks. By increasing the primary anisotropy angle, the first resonance peak reduces and the second resonance peak increases. The frequency of both resonance peaks increases as higher the value of α increases.

The sensitivity of the forced response amplitude of the first blade is shown in Fig. 8.23b for the different primary anisotropy angle crystal orientations. The reduction of the first resonance peak by increase of α is visualized by the negative sensitivities for α_3-α_8. The sensitivities show the shift of the second resonance peak by the negative sensitivities before and positive sensitivities after the resonance peak. The increase in amplitude for this resonance peak can be seen in the sensitivities as the sensitivity is positive at the frequency of the resonance peak.

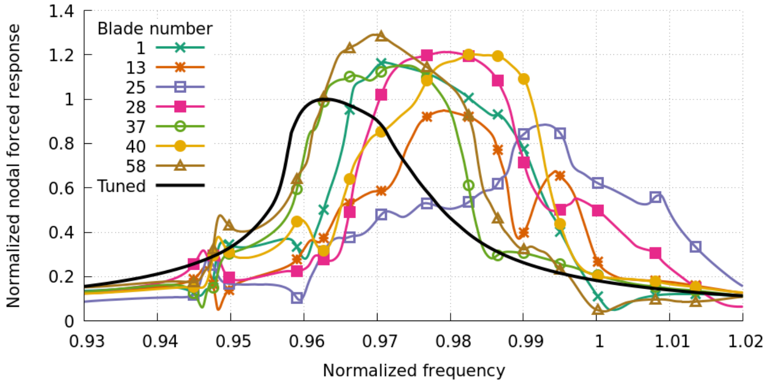

Figure 8.24: Forced response of selected blades for mistuned blade disk for excitation frequency A

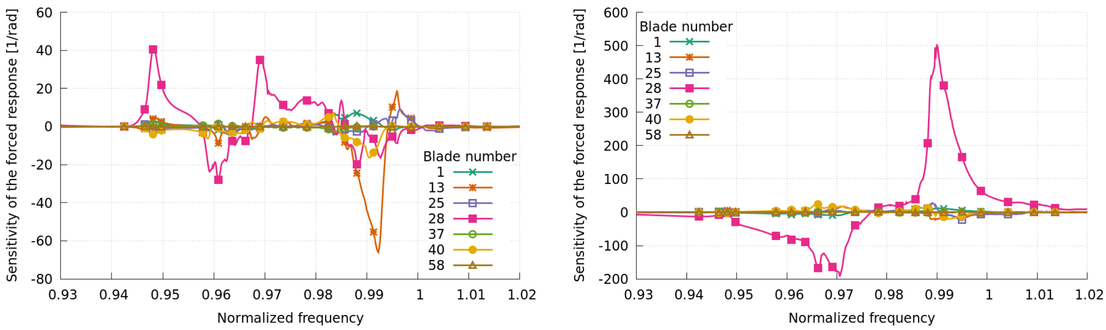

(a) Sensitivity of the forced response of blade 58 (b) Sensitivity of the forced response of blade 28

Figure 8.25: Sensitivity of forced response of two blades with respect to α anisotropy angle of selected blades for excitation frequency A

8.2.2 Sensitivity of forced response of bladed disks with root damping

The sensitivity of the forced response has been calculated for the anisotropy mistuned bladed disk with only root contact, already presented in subsection 8.1.1. Here, the mistuning pattern 1 has been used for the sensitivity analyses and the normalized harmonic excitation level is $||\boldsymbol{p}|| = 1$ with EO8. The forced response of a few selected blades that have high displacement magnitude are shown in Fig. 8.24.

Because the primary anisotropy angles α are the most influential on the forced response, the sensitivities are calculated with respect to the primary anisotropy angles of seven different blades. Five of them have high displacements on this frequency range (blade numbers 1, 28, 37, 40 and 58) and two of them have lower amplification than 1 (blade number 13 and 25). The sensitivities of the forced response are calculated at two blades that have high displacements, these are blade number 58 and 28. In Fig. 8.25a the sensitivities of the displacement at the mid-span of the blade 58 is shown with respect to the primary anisotropy angle α of selected blades. The sensitivities are only significant with respect blade 13 and 28. The sensitivity with respect to the α of blade 28 is large at the frequency of the maximum forced response amplitude of blade 58 at $\omega = 0.97$, therefore the crystal orientation of this blade can influence the maximum amplification factor of the bladed disk. The sensitivity of the forced response of this blade is higher with respect to the α anisotropy angle of blade 13, but at this frequency the response is low.

The sensitivities of the nonlinear forced response of blade 28 with respect to the selected primary anisotropy angles are shown in Fig. 8.25b, that has high amplitudes at $\omega = 0.98$. The sensitivity with respect to this blade show positive value at the $\omega = 0.98$, moreover the sensitivity has the maximum value at 0.99 and the minimum value 0.9. This indicates, that with the increase of α primary angle of blade 28 the frequency of the maximum response displacement will shift to higher frequencies.

8.2.3 Effect of contact pressure level on the sensitivity of forced response of bladed disks with shroud damping

The study for the effect of the contact pressure level on the forced response amplitudes of the anisotropy-mistuned bladed disk with shroud dampers, see subsection 7.2.1, is extended with the analysis of the local sensitivities.

During the calculation of the nonlinear forced response, for every frequency step the sensitivity of the forced response for all blades is calculated with respect to all anisotropy angles. For this bladed disk with 75 blades, the sum of all design parameters is 225.

In general, the interest for the sensitivities lies in the amplitude of the blade which has the highest forced response amplitudes over the frequency range under investigation. In the earlier subsection (subsection 7.2.1), the blade number of the maximum forced response has already been identified. Here, the sensitivity of the forced response for this blade at resonance has been in focus for mistuned bladed disks varying contact pressures on the shrouds. The sensitivities have been normalized with the maximum forced response amplitude of the mistuned bladed disk calculated for the respective shroud contact pressure value.

Fig. 8.26 shows the maximum value of the sensitivity of the forced response amplitude of the blade with the maximum amplitude, broken down to anisotropy angle categories. The figure shows that the sensitivities are largest for all contact pressure values with respect to α angles. The sensitivities with respect to β are the second largest for all contact pressure

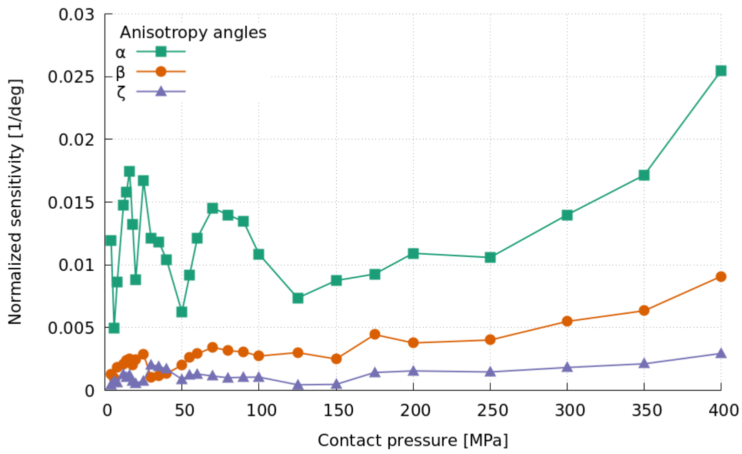

Figure 8.26: Maximum sensitivity value for each anisotropy angle for the maximum forced response of the mistuned bladed disk with varying contact pressure on blade shrouds

values, except for the range of $[20, 40]$ MPa.

In Fig 8.26 a clear tendency can be observed for the maximum sensitivities with the change of contact pressure. The maximum value of the sensitivities is for contact pressure 400 MPa, when all contact interfaces are fully stuck resulting in a fully linear model. This shows that the mistuning for linear bladed disks has the greatest influence on the forced response amplitudes. As the contact pressure decreases, friction forces appear on the contact patches of the blades with large vibration amplitudes. The increased damping for these blades noticeable decreases the sensitivities, as shown in Fig 8.26 on contact pressure range [400:125] MPa. The maximum forced response sensitivity reaches local minimum at 125 MPa, from here by further decreasing the contact pressures to 70 MPa, the sensitivity increases.

In order to draw conclusions from this behavior, it is worth looking at maximum forced response distribution along the bladed disk circumference and especially at the maximum blade number shown in Fig. 8.27.

It can be seen that for contact pressures 70 to 400 MPa, the maximum forced response amplitude is for blade #36. The maximum forced response amplitude distribution, normalized by the mean value of the maximum forced response for each calculation, is shown in 8.28 for contact pressures 70,125,250 and 400 MPa. The distribution of the maximum response amplitudes shows that for contact pressures 350 and 400 MPa, there is significant change of the amplitudes only for blades with large amplitudes, e.g. blade numbers 15, 36, 59 and 63. For the lower contact pressures, the amplitude distribution changes for more blades, e.g. blade numbers 2, 6 and 10.

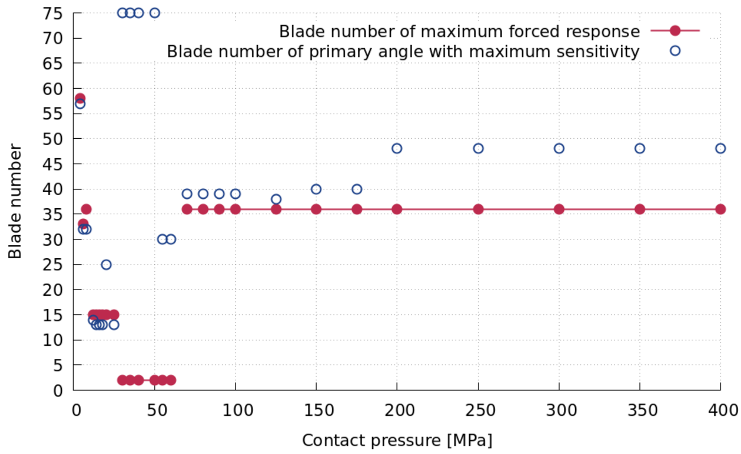

Figure 8.27: Blade number of the maximum forced response and the maximum sensitivity for mistuned bladed disk with varying contact pressure on blade shrouds

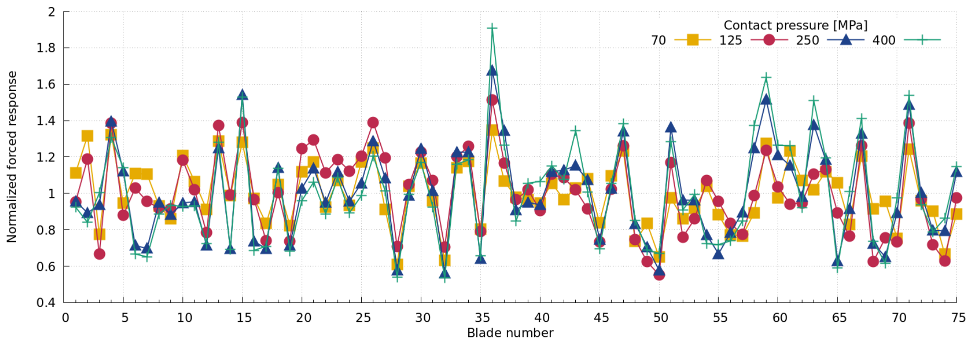

Figure 8.28: Maximum forced response distribution for varying contact pressure on blade shrouds

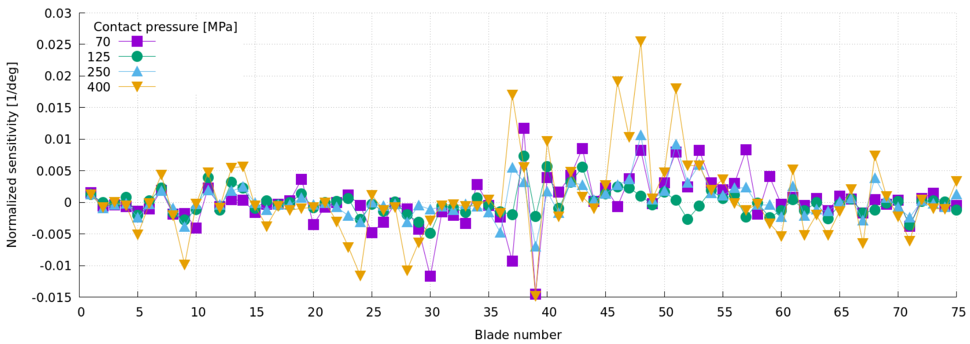

Figure 8.29: Sensitivity of blade #36 with maximum forced response amplitude with respect to α anisotropy angles of all blades with varying contact pressure on blade shrouds

The sensitivities for the forced response amplitude of blade #36 are shown with respect to all α anisotropy angles in Fig. 8.29 for the earlier studied contact pressure values. The sensitivities shown in this figure confirms the trend that for contact pressure 70 and 400 MPa the sensitivities are larger, and for 125 MPa the sensitivities are small with respect to all anisotropy angles. This study shows that for 125 MPa is solution for the forced response amplitudes the most robust, and the amplification factor is the least affected by changes in anisotropy angles.

Observing the maximum values of the sensitivities in Fig. 8.26 and the maximum blade number for each calculation with varying contact pressures in Fig. 8.27 it can be concluded that on a contact pressure range where a certain blade has the maximum forced response amplitude, the sensitivities change in a specific manner. At the middle of the specific contact pressure range, e.g. 50 MPa and 125-250 MPa, the sensitivities are the lowest and pattern of the forced response amplitudes are robust. With the forced response amplitude distribution changing, e.g. on the contact pressure ranges 70-90 MPa and 25-35 MPa.

It is also with noting that the maximum value of the sensitivities is with respect to the anisotropy angle of a blade that is located near the blade of the maximum forced response amplitude.

8.2.4 Sensitivity analysis of the nonlinear forced response of mistuned bladed disks with shroud damping and under-platform dampers

The forced response amplitudes and its sensitivities of the mistuned bladed disks with UPD and shroud damping was studied, see configuration #6 in Table 7. The 1F mode of the bladed disk is excited with high EO excitation. In the Chapter 7, see Fig. 7.27, it has been shown that for this bladed disk at this resonance, the number of contact elements applied do not significantly influence the forced response amplitudes: the difference in forced response amplitudes between using 9 or 12 contact elements on the blade shrouds is negligible. Therefore, it is sufficient to include 9 contact elements for each shroud contact interface for the sensitivity studies. For the forced response function calculation, the first 3 harmonic numbers are included.

The amplitudes for all blades are shown in Fig. 8.30, which shows that the maximum forced response amplitude is achieved for this mistuned bladed disk at blade no. 1 at $\omega_1 = 1.067$. The second and third highest bladed disk forced response amplitudes are obtained at blades #81 and #27. The forced response curves have a very wide resonance peaks, which indicates that significant energy is dissipated at the friction contact interface

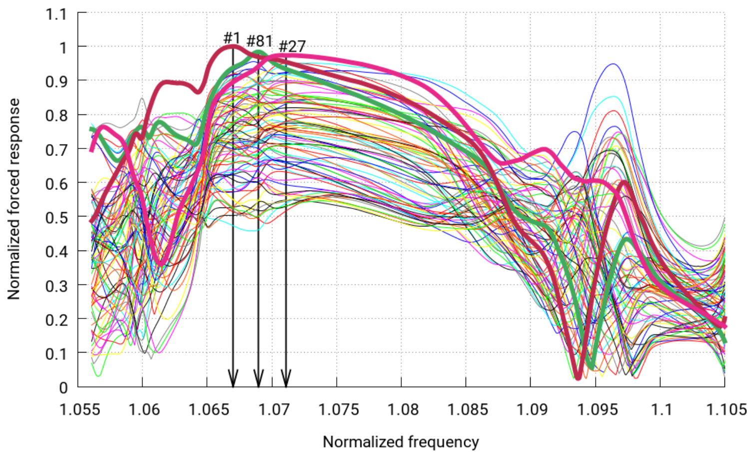

Figure 8.30: Forces response of all blades around the resonance for mistuned bladed disk with shroud and under-platform damping

of the under-platform damper and the blade shrouds. The second high resonance peak at $\omega = 1.097$ is a resonance of a low nodal diameter mode shapes.

The blade maximum amplitude distribution searched over the whole excitation frequency range is shown in Fig. 8.31. The obtained blade amplitude distribution is typical for cases of excitation by high EO travelling wave loads. The operational deflection shape localized for limited number of blades, moreover there is significant variation in the amplitudes of the neighboring blades. The blade #1 and #81 can be considered to be part of the same localization and blade #27 is in another localized range. The forced response amplitudes at blades #1,#27 and #81 are shown with larger filled circle symbols in Fig. 8.31.

A clear correspondence between the value of the primary angles and the nonlinear forced response amplitudes, see Fig. 8.32, cannot be found for this anisotropy mistuned bladed disk. The primary anisotropy angle of the blade with the maximum forces response is at 78% of the maximum allowable range. The primary anisotropy angle of the for blades #27 and #81 are significantly lower at 46% and 19%. The lack of correspondence between amplitudes and primary angles is assumed to be due to the strong dynamic coupling between the blades through shrouds, the disk and under-platform dampers, which overcomes the effects of the primary anisotropy scatter.

Because the maximum forced response amplitude is found for blade no. 1, the sensitivities have been studied with respect to the nodal forced response amplitude of this blade. The sensitivities of the amplitude of blade #1 around the resonance peak have been calculated with respect to all anisotropy angles. The sensitivities are normalized with respect to

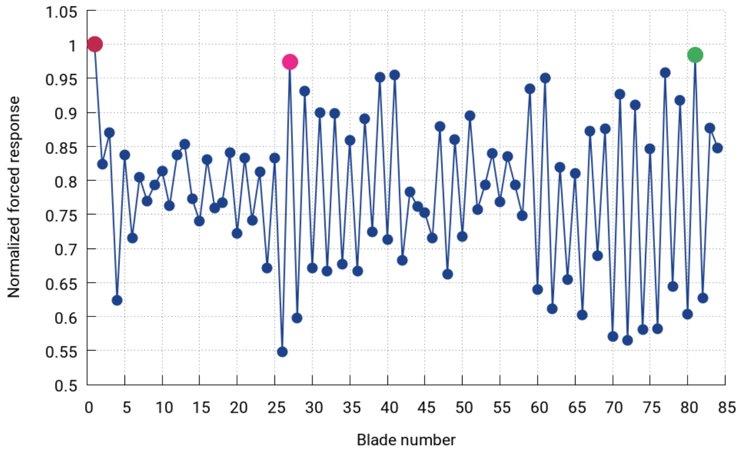

Figure 8.31: Maximum forced response for all blades around the resonance, with the highest three amplitudes denoted with colored circles

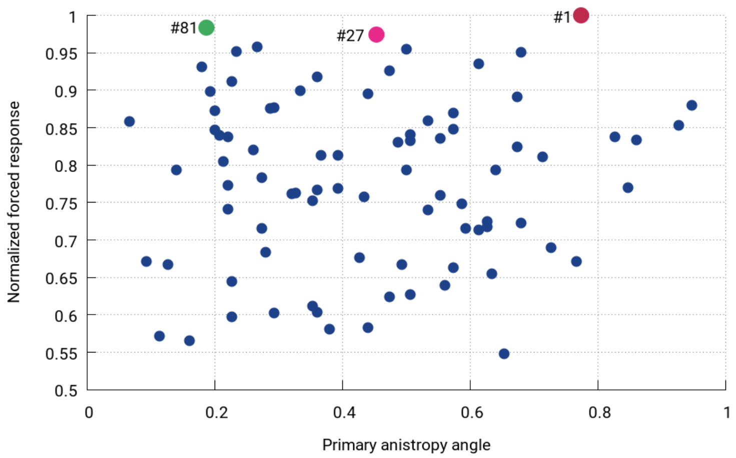

Figure 8.32: Maximum forced response for all blades as the function of primary anisotropy angle, with the highest three amplitudes denoted with colored circles

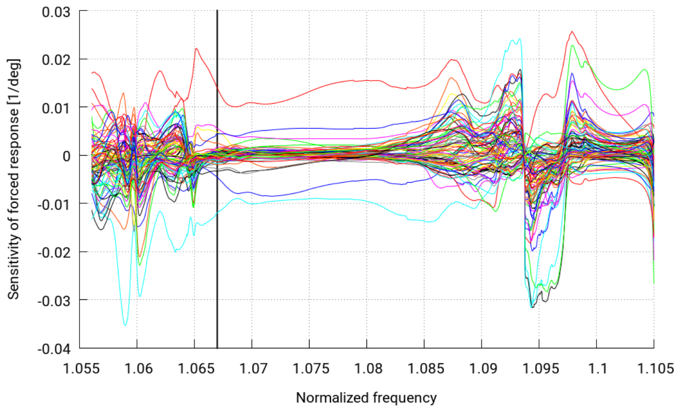

(a) Sensitivity w.r.t. all primary angles

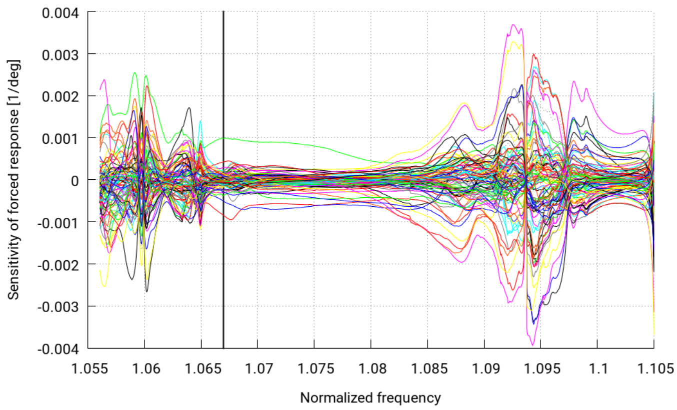

(b) Sensitivity w.r.t. all secondary angles

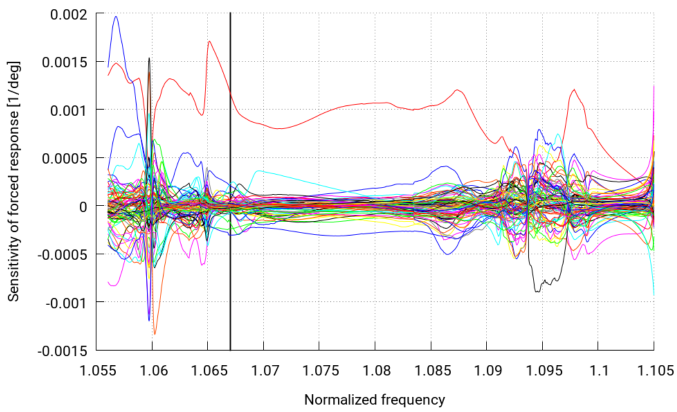

(c) Sensitivity w.r.t. all circular angles

Figure 8.33: Sensitivity of forced response amplitude of blade #1 w.r.t. all anisotropy angles around the resonance

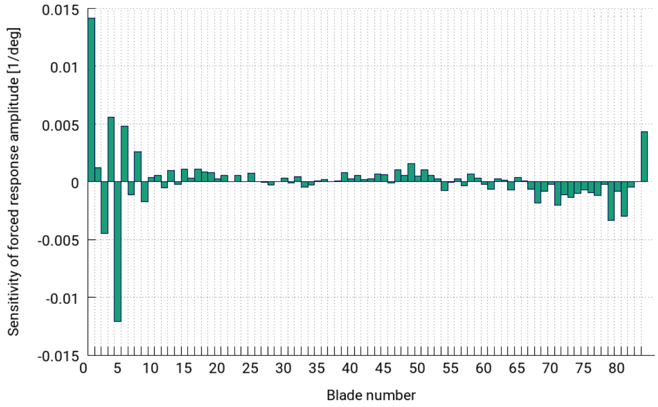

(a) Sensitivity w.r.t. all primary angles

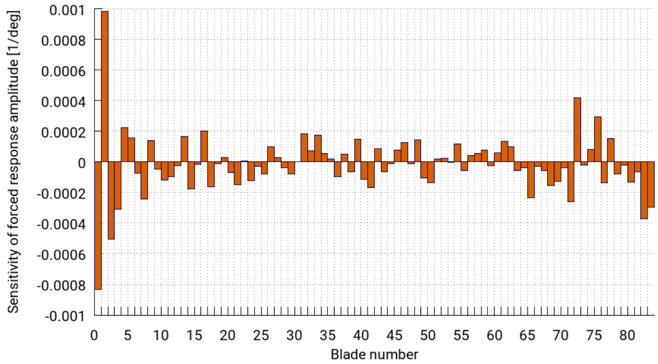

(b) [Sensitivity w.r.t. all secondary angles

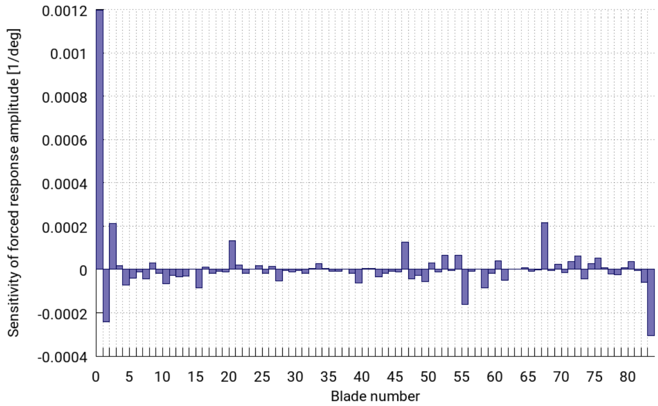

(c) Sensitivity w.r.t. all circular angles

Figure 8.34: Sensitivity of forced response amplitude of blade #1 w.r.t. all anisotropy angles at $\omega_1 = 1.067$

the peak amplitude of blade #1 and the anisotropy angles are measured for the sensitivity calculations in degrees. The sensitivities for the whole considered range are shown in Fig. 8.33. The local sensitivities with respect to α are an order of magnitude higher than for β and ζ. It is worth noting that the sensitivities are particularly high with respect to a few blades. The values of the sensitivities are large for the whole frequency range of interest, but not the largest at the excitation frequency where blade no.1 has the maximum forced response, shown with a vertical line for all plots in Fig. 8.33.

For the structural engineer, the maximum forced response amplitudes of the mistuned bladed disks are of interest. Therefore, the sensitivities of the maximum forced response are studied at excitation frequency where the maximum forced response is obtained. Figs. in 8.34, show the sensitivity of the amplification factor with respect to all anisotropy angles. As the earlier studies showed, the sensitivities of the blade with the maximum forced response amplitudes are the largest with respect to the anisotropy angles of the blade itself and the neighboring blades. For this bladed disk system with coupling through the UPDs and the shrouds, the sensitivities are large with respect to up to five neighboring blades. The sensitivities of the forced response amplitudes of blade #1 is largest with respect to its own anisotropy angles α and ζ. It is worth noting that because the anisotropy angle α is large for blade no. 1, the sensitivity with respect to ζ is large too.

8.3 Conclusions

In this chapter, the effect of anisotropy mistuning in combination with the friction damping has been studied. The non-linear relationship between excitation and response has been studied for different excitation levels. The amplification factors have been determined for higher and lower friction damping. In general, it can be stated that higher friction damping reduces the value of amplification factors and the variation of amplitudes around the blades in the bladed disk assembly.

For bladed disks with UPD, the damping effectiveness was studied for different engine order excitations. For mistuned bladed disks, the range of rotation speeds (i.e. EO crossing) where the damper is the most effective was more localized than for tuned bladed disks.

In this chapter, the forced response and its sensitivities have been calculated for a two-blade model for which the anisotropy orientation was gradually changed. The sensitivities could accurately depict the two characteristics changing in the forced response: (i) change in resonance frequency and (ii) change in peak forced response amplitude.

The studies for sensitivities done for mistuned bladed disks came to similar conclusions than for the linear forced response: sensitivities for localized operational deflection shapes are large with respect to blades that have high amplitudes. With increased friction damping, the sensitivities generally tend to decrease, which is in good agreement with the behavior seen for the standard deviation of amplitudes over all blades for changing friction damping.

Chapter 9

Conclusions and outlook

In this work, the dynamics characteristics of anisotropy mistuned bladed disks and their sensitivities were studied. The presented approach uses high-fidelity and direct modeling of the mistuning for the crystal orientation blade-to-blade variation. The developed methodology and implemented framework includes the local sensitivity calculation for the dynamic characteristics. The developed tools allowed for the calculation of the modal properties and the nonlinear forced response for several industrial anisotropy mistuned bladed disks.

1. In this work a new methodology for the calculation of the sensitivity of modal properties have been developed, implemented and validated.

   In cooperation with the CalculiX developers, a semi-analytic formulation for the calculation of the derivative of distinct natural frequencies and the classical modal expansion formula for the calculation of the mode shape sensitivity has been implemented in CalculiX CrunchiX.

   For industrial size FE models of mistuned bladed disks it is computationally expensive to calculate large number of mode shapes. Therefore, the classical modal method for the calculation of mode shape sensitivity cannot be applied. In order to improve on the convergence characteristics of the mode shape sensitivity calculation two different approaches were implemented and studied.

   - The enhanced modal method is an improvement on the classical method using a modal expansion representation. This new formulation accounts for the modal terms that are not included in the series expansion. The effect of the value for λ_0 parameter used in the formulation was studied. The analysis resulted the finding that the $\lambda_0 = (\lambda_j - \lambda_{j-1})/2$, where λ_j is the eigenvalue of the mode j, for which the sensitivity is calculated for. In case of the mistuned bladed disk, the studies have shown that in order to reach convergence for a specific mode, then at least an additional 20 modes need to be included in the series expansion.

- The algebraic method using a bordering algorithm allows for the exact calculation of the sensitivities. For the optimal placement of the regularization coefficient a methodology ideal for bladed disk structures with localization has been found: the regularization coefficient is placed into position on the main diagonal of matrix $\boldsymbol{A}$ where for each mode the DOF with the largest modal displacement is calculated.
- Both methods for the calculation of the mode shape sensitivities have been studied using high-fidelity FE models for comparing them. The major advantage of the new algebraic method is that the mode shape sensitivities are calculated accurately for all modes and no additional modes need to be calculated to achieve accurate mode shape sensitivity values. Moreover, the calculation times for industrial FE models where the sensitivity of many modes are calculated is less for the algebraic method.

The implementation of the calculation for the flexibility matrix and its sensitivity in CalculiX was supported and thoroughly tested.

In CalculiX, the sensitivities are calculated with respect to rotation vector components. In CalculiX, the rotation vector components have been chosen as the parameters describing the anisotropy orientation, because it is a general description and not specific to mistuned bladed disks with single crystal blade materials. The rotation vectors are defined in the global coordinate system of the FE model. The anisotropy orientations, the actual parameter of interest, is defined in the local coordinate system of the individual blades. A method using the equality of the infinitesimal rotations has been implemented for calculating the sensitivity of any parameter of interest (static displacements, stresses, modal properties and flexibility matrix) in the local blade coordinate system with respect to the anisotropy angles used by the manufacturer.

An integrator-interface tool, InterDyn, has been developed to perform all pre- and post-processor operations for interaction between CalculiX and the nonlinear forced response solver, ContaDyn. Among other functions, the tool facilitates the preparation of finite element models of mistuned bladed disks, condensation of the model, application of the nonlinear contact elements, different types of the visualization of the forced response on the full finite element models.

The validation of the sensitivity calculation for natural frequency, mode shapes, flexibility matrix and forced response amplitudes has been done. The sensitivities calculated with the fast sensitivity calculation method have been compared with sensitivities obtained by using finite differences. The discrepancies in the sensitivities have been negligible although theoretically the accuracy of the finite difference method is less than for the new methods. The validation has been done for simple models and for large scale FE models of industrial bladed disks.

2. The developed capabilities have been tested and used in a large scope of studies, where the effect of the anisotropy mistuning on the modal properties and linear, non-linear forced response for realistic anisotropy mistuned bladed disk are considered. The anisotropy angles describing the crystal orientation of the blades are random sampled from their statistic distribution obtained by the industrial partner for production bladed disks from experimental measurements.

   The analysis of modal properties of blades shows that the blade-alone natural frequency variation can reach 14% due to scatter in the blade material crystal orientation. The range of the natural frequency scatter is dependent on the mean value of the blade stacking axis direction. The natural frequencies can be increased or decreased.

   The effect of the anisotropy mistuning on the mode shapes for disk dominated modes are negligible. For blade dominated and localized modes the maximum modal displacement amplitude and its location along the circumference of the bladed disk is strongly dependent on the anisotropy mistuning pattern.

   The sensitivities of the natural frequencies and the mode shapes were studied for disk dominated, blade dominated modes and for transitional modes where disk and blade both contribute significantly to system vibrations. The largest value of sensitivities were observed for blade dominated modes with localization concentrating to 6-7 blades. The sensitivity of the natural frequencies of such modes were large with respect to the anisotropy angles of the few blades where the localization occurs. The sensitivities of the modal properties are the largest with respect to the primary material anisotropy angle and the sensitivities with respect the other two angles characterizing the crystal orientation are significantly smaller.

   The sensitivities of natural frequencies were studied for different boundary conditions on the blade shrouds. The analyses show that the sensitivity of the natural frequencies with respect to the anisotropy parameters increase as the coupling between the neighboring blades is reduces.

The commonly used method for mistuning quantification by blade frequency, which is usually applied through changing the modulus of elasticity of individual blades to match the blade-alone frequencies in the mistuning pattern, cannot be used for anisotropy mistuned bladed disks. The forced response amplitudes of the individual blades obtained in this thesis are significantly different by description of the anisotropic orientation scatters.

The linear forced response of mistuned bladed disks and its sensitivity have been studied for several modes and engine order excitations. The observed amplification factors vary between 1.1 and 2.7, depending on the excited mode and the engine order of the excitation. The study of the sensitivities of the forced response amplitudes for disk dominated modes showed that the change in anisotropy orientation leads primarily to change in resonance frequency and to negligible change in forced response amplitudes. On the other hand, for blade dominated modes the maximum amplitude and the resonance frequency are sensitive to the changes of the anisotropy orientation of the blades. The maximum amplitude in the anisotropy mistuned bladed disks is the most sensitive to the anisotropy orientation variation of its own blade and the neighboring blades.

3. The modeling approaches for the calculation of the nonlinear forced response for tuned and mistuned bladed disks were studied.

   For the nonlinear forced response calculation, the number of nonlinear friction contact elements strongly influences the accuracy of the calculated vibration amplitudes and the computational effort. The studies have showed that at least 10 contact elements are required for each friction contact interface in the bladed disk for capturing the nonlinear interactions accurately enough.

   The nonlinear forced response solver, ContaDyn, offers fast convergence over the number of modes included in the FRF calculation. For bladed disks where through contact-separation strong nonlinear effects appear and energy is transferred to the higher modes, it is recommended to include 10 mode families in the reduced order model of the mistuned bladed disks.

   For bladed disks where the only contact interface is on the blade roots, it is sufficient to include only odd harmonic numbers. The friction contact interfaces that partially or fully separate during the vibration period, it is required to include 0^{th}, odd and even harmonics. The convergence over the number of harmonics is fast, by including the first 6 harmonic coefficients, the forced response amplitudes are obtained with high accuracy.

For some analyses it is beneficial to remove the rigid body modes from the modal basis. In such cases, multi-point-constraints are applied between blades and the disk. For reduced order models with sufficiently large number of contact elements on the blade root friction joints, the multi-point-constraints do not influence the forced response amplitudes.

The calculated forced response amplitudes are sensitive to the value of the friction coefficient. By decreasing the value of the friction coefficient for the applications in stick-slip state, the slip threshold amplitudes decrease resulting in increased damping.

When the value of contact stiffness describing the elasticity of the contact of the rough surfaces is varied in its realistic range, the forced response amplitudes show negligible changes.

The static pre-stress state of the friction contact elements significantly influences the forced response amplitudes. For mistuned bladed disks it is recommended to calculate the contact pressure on the shroud contact interfaces with high accuracy when both modal and static mistuning is included in the nonlinear forced response analysis.

4. The nonlinear forced response has been successfully validated for tuned and mistuned bladed disk. The validation campaign was done for bladed disks with (i) only root damping, (ii) root and shroud damping and (iii) for bladed disks with nonlinear friction contact on blade roots, shrouds and under-platform dampers. The calculated forced response amplitudes for all modes, when the variation of the friction coefficient value was considered, were obtained within maximum and minimum measured forced response amplitudes.

   The tip-timing measurements allowed the comparison of the calculated and measured forced response amplitude distribution along the circumference of the bladed disk. The range of the blade amplitudes scatter is larger for the measured bladed disks, which meets the expectation as the calculated mistuned forced response only included anisotropy mistuning. For the measured and for the calculated amplitudes similar characteristics can be observed: (i) for low engine order excitation the forced response amplitude distribution takes a sinusoidal wave with low nodal diameter (ii) for high engine order excitation the amplitude distribution shows two to three localizations.

Studies included the range of scatter for forced response amplitudes and resonance frequencies of mistuned bladed disks for varying levels of forced response excitation.

For bladed disks with under-platform damper, studies were done considering the contact pressure variation due to the change of engine order excitation and thereby the change of rotation speed of the resonance crossing. The engine order crossing for which the UPD the optimal damping efficiency has had been identified for tuned and mistuned bladed disks.

The sensitivities with respect to anisotropy orientations has been studied for mistuned bladed disks with only root damping and with shroud damping and under-platform damper. For mistuned bladed disks with friction contact interfaces, blade dominated modes were studied. The maximum nonlinear forced response amplitudes are sensitive to anisotropy parameters of the neighboring blades.

5. The developed capabilities offer a large scope of possibilities for further studies. The capabilities for the calculation of linear forced response sensitivities have been exploited in this project in the work of R. Rajasekharan Nair in [63]. The gradient information for the forced response amplitudes allowed for implementing the gradient based chaos expansion for uncertainty and global sensitivity studies. For the possible future research the following directions can be suggested:

    - Applying the methodology of gradient based polynomial chaos for bladed disks with nonlinear friction contact interfaces could be of interest.
    - Extending the analyses by modeling other sources of mistuning, e.g. blade-to-blade variation in geometry, static and contact parameters would allow the calculation of the forced response of mistuned bladed disks more comprehensively.
    - The developed capabilities offer a foundation to facilitate the sensitivity calculation of the nonlinear forced response with respect to additional parameters. When the sensitivities with respect to many parameters are available, then it allows for effective robustness study and in assessing which parameters have the largest influence on the forced response amplitudes. Additionally, by finding the most important mistuning parameters, an efficient optimization tools can be developed based on the calculated gradient information.

Bibliography

[1] *The Effects of Blade Mistuning on Vibration Response - A Survey*, 1991. 8, 9

[2] H.M. Adelman and R.T. Haftka. Sensitivity analysis of discrete structural systems. *AIAA Journal*, 24(5):823–832, 1986. 17, 29

[3] S. Adhikari and M.I. Friswell. Eigenderivative analysis of asymmetric non-conservative systems. *International Journal for Numerical Methods in Engineering*, 51(6):709–733, 2001. 17

[4] M. Allara. A model for the characterization of friction contacts in turbine blades. *Journal of Sound and Vibration*, 320(3):527 – 544, 2009. 12

[5] José Luis Amorós, Martin J. Buerger, and Marisa Canut de Amorós. *The Laue Method*. Academic Press, New York, 1975. 24

[6] N. K. Arakere and G. Swanson. Effect of crystal orientation on fatigue failure of single crystal nickel base turbine blade superalloys. *Journal of Engineering for Gas Turbines and Power-Transactions of the Asme*, 124(1):161–176, January 2002. 13

[7] Seunghun Baek and Bogdan Epureanu. Reduced-Order Modeling of Bladed Disks With Friction Ring Dampers. *Journal of Vibration and Acoustics*, 139(6), 08 2017. 061011. 11

[8] P. Basu and J.H. Griffin. Effect of Limiting Aerodynamic and Structural Coupling in Models of Mistuned Bladed Disk Vibration. *Journal of vibration, acoustics, stress, and reliability in design*, 108(2):132–139, 1986. 18

[9] Bernd Beirow, Thomas Giersch, Arnold Kühhorn, and Jens Nipkau. Optimization-Aided Forced Response Analysis of a Mistuned Compressor Blisk. *Journal of Engineering for Gas Turbines and Power*, 137(1):012504–012504–10, August 2014. 12, 19

[10] Y. Bhartiya and A. Sinha. Reduced order model of a bladed rotor with geometric mistuning: Comparison between modified modal domain analysis and frequency mistuning approach. In *Proceedings of the ASME Turbo Expo*, volume 6, pages 981–992, 2011. 10

[11] E. Capiez-Lernout, C. Soize, and M. Mbaye. Computational geometrically nonlinear vibration analysis of uncertain mistuned bladed disks. In *Proceedings of the ASME Turbo Expo*, volume 7B, 2014. 18

[12] A. Cardona and M. Geradin. A beam finite element non-linear theory with finite rotations. *International Journal for Numerical Methods in Engineering*, 26(11):2403–2438, 1988. 40

[13] Pierre Caron and Tasadduq Khan. Evolution of Ni-based superalloys for single crystal gas turbine blade applications. *Aerospace Science and Technology*, 3(8):513–523, December 1999. 13

[14] M. P. Castanier, G. Óttarsson, and C. Pierre. A Reduced Order Modeling Technique for Mistuned Bladed Disks. *Journal of Vibration and Acoustics*, 119(3):439–447, July 1997. 10

[15] M.P. Castanier and C. Pierre. Modeling and analysis of mistuned bladed disk vibration: Status and emerging directions. *Journal of Propulsion and Power*, 22(2):384–396, 2006. 9

[16] A.D. Celel and D.N. Duhl. *Second-generation nickel-base single crystal superalloy.* The Metallurgical Society Inc, United States, 1988. 13

[17] D. Charleux, C. Gibert, F. Thouverez, and J. Dupeux. Numerical and experimental study of friction damping blade attachments of rotating bladed disks. *International Journal of Rotating Machinery*, 2006, 2006. 12

[18] Guido Dhondt. *Linear Mechanical Applications*, chapter 2, pages 63–142. John Wiley & Sons, Ltd, 2004. 26

[19] Guido Dhondt. *CalculiX CrunchiX USER'S MANUAL version 2.12*, 2017. 15

[20] D. J. Ewins. Vibration modes of mistuned bladed disks. *Journal of Engineering for Power*, 15:165–173, 1973. 6

[21] D. J. Ewins. Vibration characteristics of bladed disc assemblies. *Journal of Mechanical Engineering Science*, 114:349–355, 1975. 6, 7, 8

[22] D.J. Ewins. The effects of detuning upon the forced vibrations of bladed disks. *Journal of Sound and Vibration*, 9(1):65–79, January 1969. 8, 18

[23] D.J. Ewins and Z.S. Han. Resonant Vibration Levels of a Mistuned Bladed Disk. *Journal of Vibration, Acoustics, Stress, and Reliability in Design*, 106(2):211–217, 1984. 18

[24] D. M. Feiner and J. H. Griffin. A Fundamental Model of Mistuning for a Single Family of Modes. *Journal of Turbomachinery*, 124(4):597–605, November 2002. 10, 12, 15

[25] Christian Firrone and I. Bertino. Experimental investigation on the damping effectiveness of blade root joints. *Experimental Mechanics*, 55:981–988, 06 2015. 12

[26] C.M. Firrone, S. Zucca, and M.M. Gola. The effect of underplatform dampers on the forced response of bladed disks by a coupled static/dynamic harmonic balance method. *International Journal of Non-Linear Mechanics*, 46(2):363–375, 2011. 9

[27] R.L. Fox and M.P. Kapoor. Rates of change of eigenvalues and eigenvectors. *AIAA Journal*, 6(12):2426–2429, 1968. 16, 28

[28] J.H. Griffin. A Review of Friction Damping of Turbine Blade Vibration. *International Journal of Turbo and Jet Engines*, 7(3-4):297–308, 1990. 20

[29] Najeh Guedria, Hichem Smaoui, and Mnaouar Chouchane. A direct algebraic method for eigensolution sensitivity computation of damped asymmetric systems. *International Journal for Numerical Methods in Engineering*, 68(6):674–689, November 2006. 17

[30] J Han. Identifikation der elastischen kennwerte anisotroper hochtemperaturlegierungen mittels resonanzmessungen und finite-elemente-simulation, 1995. 13, 23

[31] A. Hartung and H.-P. Hackenberg. A practical approach for evaluation of equivalent linear damping from measurements of mistuned and/or non-linear stages and forced response validation. In *Proceedings of the ASME Turbo Expo*, volume 7A-2016, 2016. 17, 99, 118

[32] A. Hartung, H.-P. Hackenberg, M. Krack, J. Gross, T. Heinze, and L.P.-V. Scheidt. Rig and engine validation of the nonlinear forced response analysis performed by the tool oragl. *Journal of Engineering for Gas Turbines and Power*, 141(2), 2019. 12, 118

[33] A. Hartung, U. Retze, and H.-P. Hackenberg. Impulse mistuning of blades and vanes. In *Proceedings of the ASME Turbo Expo*, volume 7A-2016, 2016. 2

[34] Andreas Hartung, Ulrich Retze, and Hans-Peter Hackenberg. Impulse Mistuning of Blades and Vanes. *Journal of Engineering for Gas Turbines and Power*, 139(7), 02 2017. 072502. xviii, 118

[35] Tadashi Hasebe, Masao Sakane, and Masateru Ohnami. High Temperature Low Cycle Fatigue and Cyclic Constitutive Relation of MAR-M247 Directionally Solidified Superalloy. *Journal of Engineering Materials and Technology*, 114(2):162–167, April 1992. 14

[36] A. Hohl, B. Kriegesmann, J. Wallaschek, and L. Panning. The influence of blade properties on the forced response of mistuned bladed disks. In *Proceedings of the ASME Turbo Expo*, volume 6, pages 1159–1170, 2011. 10

[37] Jie Hong, Lulu Chen, Yanhong Ma, and Xin Yang. Design Methods of Friction Damping at Blade-Disk Joints. In *Proceedings of the ASME Turbo Expo*, volume Volume 6: Structures and Dynamics, Parts A and B, pages 315–322, 06 2009. 11

[38] N.X. Hou, W.X. Gou, and Z.F. Yue Z.X. Wen. The influence of crystal orientations on fatigue life of single crystal cooled turbine blades. *Materials Science and Engineering A*, 492:413–418, 2008. 13

[39] H. Irretier. Spectral Analysis of Mistuned Bladed Disk Assemblies by Component Mode Synthesis. In *ASME, New York, NY, USA, Design Engineering Div*, pages 115–125, 1983. 10

[40] P. Jean, C. Gibert, C. Dupont, and J.-P. Lombard. Test-Model Correlation of Dry-Friction Damping Phenomena in Aero-Engines. In *Proceedings of the ASME Turbo Expo*, volume Volume 5: Structures and Dynamics, Parts A and B, pages 481–491, 06 2008. 12

[41] A.G.S. Joshi and B.I. Epureanu. Reduced order models for blade-to-blade damping

variability in mistuned blisks. In *Proceedings of the ASME Turbo Expo*, volume 6, pages 1033–1045, 2011. 10, 12

[42] Y. Kaneko. Study on vibration characteristics of single crystal blade and directionally solidified blade. In *Proceedings of the ASME Turbo Expo*, volume 6, pages 931–940, 2011. 14

[43] Y. Kaneko, K. Mori, and H. Ooyama. Resonant response and random response analysis of mistuned bladed disk consisting of directionally solidified blade. In *Proceedings of the ASME Turbo Expo*, volume 7B, 2015. 15, 20

[44] Y. Kaneko, H. Yamashita, K. Mori, and K. Sato. Analysis of variation of natural frequency and resonant stress of blade. In *Proceedings of the ASME Turbo Expo*, volume 5 PART B, pages 801–807, 2006. 15

[45] Herbert B. Keller. The bordering algorithm and path following near singular points of higher nullity. *SIAM J. Sci. Stat. Comput.*, 4(4):573–582, December 1983. 31

[46] A. Koscso. Extension of capabilities of the finite element software calculix for analysis of anisotropic bladed disks. Master thesis, Technische Universität München, Munich, Germany, 2016. xiv, 7, 39, 43, 52

[47] A. Koscso and E.P. Petrov. Sensitivity and Forced Response Analysis of Anisotropy-Mistuned Bladed Disks With Nonlinear Contact Interfaces. *Journal of Engineering for Gas Turbines and Power*, 141(10), 09 2019. 101025. 11

[48] M. Krack, L. Panning, J. Wallaschek, C. Siewert, and A. Hartung. Robust design of friction interfaces of bladed disks with respect to parameter uncertainties. In *Proceedings of the ASME Turbo Expo*, volume 7, pages 1193–1204, 2012. 20

[49] M. Krack, L. Salles, and F. Thouverez. Vibration prediction of bladed disks coupled by friction joints. *Archives of Computational Methods in Engineering*, 24(3):589–636, 2017. 9

[50] Krzysztof Kubiak, Dariusz Szeliga, Jan Sieniawski, and Arkadiusz Onyszko. 11 - the unidirectional crystallization of metals and alloys (turbine blades). In Peter Rudolph, editor, *Handbook of Crystal Growth (Second Edition)*, Handbook of Crystal Growth, pages 413–457. Elsevier, Boston, second edition edition, 2015. 24

[51] D. Laxalde, F. Thouverez, J.-J. Sinou, and J.-P. Lombard. Qualitative analysis of forced response of blisks with friction ring dampers. *European Journal of Mechanics - A/Solids*, 26(4):676–687, July 2007. 9

[52] I.-W. Lee and G.-H. Jung. An efficient algebraic method for the computation of natural frequency and mode shape sensitivities - Part I. Distinct natural frequencies. *Computers and Structures*, 62(3):429–435, 1997. 17

[53] I.-W. Lee and G.-H. Jung. An efficient algebraic method for the computation of natural frequency and mode shape sensitivities - Part II. Multiple natural frequencies. *Computers and Structures*, 62(3):437–443, 1997. 17

[54] Li Li, Yujin Hu, Xuelin Wang, and Ling Ling. Eigensensitivity analysis of damped systems with distinct and repeated eigenvalues. *Finite Elements in Analysis and Design*, 72:21–34, September 2013. 17

[55] Z. Li, S.K. Lai, and B. Wu. A new method for computation of eigenvector derivatives with distinct and repeated eigenvalues in structural dynamic analysis. *Mechanical Systems and Signal Processing*, 107:78–92, 2018. 17

[56] Z.-S. Liu, S.-H. Chen, M. Yu, and Y.-Q. Zhao. Contribution of the truncated modes to eigenvector derivatives. *AIAA Journal*, 32(7):1551–1553, 1994. 16

[57] M. Manetti, I. Giovannetti, N. Pieroni, H. Horculescu, G. Peano, G. Zonfrillo, and M. Giannozzi. The dynamic influence of crystal orientation on a second generation single crystal material for turbine buckets. In *Proceedings of the ASME Turbo Expo*, volume 6, pages 125–133, 2009. 14

[58] J.G. Marshall and M. Imregun. A review of aeroelasticity methods with emphasis on turbomachinery applications. *Journal of Fluids and Structures*, 10(3):237 – 267, 1996. 7

[59] Larry A. Moss and Todd E. Smith. Ssme single crystal turbine blade dynamics, 1987. 14

[60] M. Myhre, F. Moyroud, and T.H. Fransson. Numerical investigation of the sensitivity of forced response characteristics of bladed disks to mistuning. In *American Society of Mechanical Engineers, International Gas Turbine Institute, Turbo Expo (Publication) IGTI*, volume 4, pages 171–182, 2003. 12, 17

[61] L. Méric, P. Poubanne, and G. Cailletaud. Single Crystal Modeling for Structural Calculations: Part 1—Model Presentation. *Journal of Engineering Materials and Technology*, 113(1):162–170, January 1991. 13

[62] R. Mücke and P. Woratat. A cyclic life prediction approach for directionally solidified nickel superalloys. *Journal of Engineering for Gas Turbines and Power*, 132(5), 2010. 14

[63] Rahul Rajasekharan Nair. *Uncertainty and sensitivity analysis for bladed disks with random blade anisotropy orientations.* PhD thesis, University of Sussex, August 2019. 4, 195

[64] R.B. Nelson. Simplified calculation of eigenvector derivatives. *AIAA Journal*, 14(9):1201–1205, 1976. 16, 63

[65] I. U. Ojalvo. Efficient computation of mode-shape derivatives for large dynamic systems. *AIAA Journal*, 25(10):1386–1390, 1987. 17

[66] I.U. Ojalvo. Efficient computation of modal sensitivities for systems with repeated frequencies. *AIAA Journal*, 26(3):361–366, 1988. 17

[67] L. Pesaresi, J. Armand, C.W. Schwingshackl, L. Salles, and C. Wong. An advanced underplatform damper modelling approach based on a microslip contact model. *Journal of Sound and Vibration*, 436:327 – 340, 2018. 11

[68] E. Petrov and M. Geradin. Finite element theory for curved and twisted beams based on exact solutions for three-dimensional solids. Part 1: Beam concept and geometrically exact nonlinear formulation. *Computer Methods in Applied Mechanics and Engineering*, 165(1-4):43–92, 1998. 40

[69] E. P. Petrov. A Method for Use of Cyclic Symmetry Properties in Analysis of Nonlinear Multiharmonic Vibrations of Bladed Disks . *Journal of Turbomachinery*, 126(1):175–183, 03 2004. 32

[70] E. P. Petrov. A Method for Use of Cyclic Symmetry Properties in Analysis of Nonlinear Multiharmonic Vibrations of Bladed Disks. *Journal of Turbomachinery*, 126(1):175–183, March 2004. 36

[71] E. P. Petrov. Method for Sensitivity Analysis of Resonance Forced Response of Bladed Disks With Nonlinear Contact Interfaces. *Journal of Engineering for Gas Turbines and Power*, 131(2):022510–022510–9, December 2008. 20, 21

[72] E. P. Petrov. A Sensitivity-Based Method for Direct Stochastic Analysis of Nonlinear Forced Response for Bladed Disks With Friction Interfaces. *Journal of Engineering for Gas Turbines and Power*, 130(2):022503–022503–9, February 2008. 12, 17

[73] E. P. Petrov. Reduction of Forced Response Levels for Bladed Disks by Mistuning: Overview of the Phenomenon. *Journal of Engineering for Gas Turbines and Power*, 133(7):072501–072501–10, March 2011. 19, 138

[74] E. P. Petrov. Analytical Formulation of Friction Contact Elements for Frequency-Domain Analysis of Nonlinear Vibrations of Structures With High-Energy Rubs. *Journal of Engineering for Gas Turbines and Power*, 141(12), 11 2019. 121006. 33

[75] E. P. Petrov and D. J. Ewins. Analysis of the Worst Mistuning Patterns in Bladed Disk Assemblies. *Journal of Turbomachinery*, 125(4):623–631, December 2003. 19

[76] E. P. Petrov and D. J. Ewins. Analytical Formulation of Friction Interface Elements for Analysis of Nonlinear Multi-Harmonic Vibrations of Bladed Disks. *Journal of Turbomachinery*, 125(2):364–371, April 2003. 9, 20, 21, 32, 33, 35

[77] E. P. Petrov and D. J. Ewins. Effects of Damping and Varying Contact Area at Blade-Disk Joints in Forced Response Analysis of Bladed Disk Assemblies. *Journal of Turbomachinery*, 128(2):403–410, 09 2005. 11

[78] E. P. Petrov and D. J. Ewins. Method for Analysis of Nonlinear Multiharmonic Vibrations of Mistuned Bladed Disks With Scatter of Contact Interface Characteristics. *Journal of Turbomachinery*, 127(1):128–136, February 2005. 10, 32

[79] E. P. Petrov and D. J. Ewins. Advanced Modeling of Underplatform Friction Dampers for Analysis of Bladed Disk Vibration. *Journal of Turbomachinery*, 129(1):143–150, February 2006. 172

[80] E. P. Petrov, K. Y. Sanliturk, and D. J. Ewins. A New Method for Dynamic Analysis of Mistuned Bladed Disks Based on the Exact Relationship Between Tuned and Mistuned Systems. *Journal of Engineering for Gas Turbines and Power*, 124(3):586–597, June 2002. 10, 12

[81] E P Petrov, R Vitali, and R T Haftka. Optimization of mistuned bladed discs using gradient-based response surface approximations. In *41st Structures, Structural Dynamics, and Materials Conference and Exhibit*, pages 1129–1139, 2000. Atlanta, GA, USA. 18

[82] E.P. Petrov. personal communication. 29, 47, 78

[83] E.P. Petrov. personal communication. 30, 47, 78

[84] E.P. Petrov. Method for sensitivity analysis of resonance forced response of bladed disks with nonlinear contact interfaces. *Journal of Engineering for Gas Turbines and Power*, 131(2), 2009. 20

[85] E.P. Petrov. A high-accuracy model reduction for analysis of nonlinear vibrations in structures with contact interfaces. *Journal of Engineering for Gas Turbines and Power*, 133(10), 2011. 21, 32, 34, 35

[86] William H. Press, Saul A. Teukolsky, William T. Vetterling, and Brian P. Flannery. *Numerical Recipes: The Art of Scientific Computing.* Cambridge University Press, Cambridge, UK, third edition edition, 2007. 52

[87] Rahul Rajasekharan and Evgeny Petrov. Uncertainty and global sensitivity analysis of bladed disk statics with material anisotropy and root geometry variations. *Engineering Reports*, 1(3):e12043, 2019. e12043 eng2.12043. 12

[88] V. Ramamurti and P. Seshu. On the principle of cyclic symmetry in machine dynamics. *Communications in Applied Numerical Methods*, 6(4):259–268, May 1990.

[89] Rolls-Royce. *The Jet Engine.* John Wiley & Sons, Chichester, England, UK, 5th edition edition, 2015. 12

[90] C.S. Rudisill and Y.-Y. Chu. Numerical methods for evaluating the derivatives of eigenvalues and eigenvectors. *AIAA Journal*, 13(6):834–837, 1975. 17

[91] Michael W. R. Savage. The Influence of Crystal Orientation on the Elastic Stresses of a Single Crystal Nickel-Based Turbine Blade. *Journal of Engineering for Gas Turbines and Power*, 134(1):012501–012501–7, October 2011. 15

[92] H. Schoenenborn, M. Junge, and U. Retze. Contribution to Free and Forced Vibration Analysis of an Intentionally Mistuned Blisk. In *Turbo Expo: Power for Land, Sea, and Air*, volume Volume 7: Structures and Dynamics, Parts A and B, pages 1111–1120, 06 2012. 26

[93] C. W. Schwingshackl and E. P. Petrov. Modeling of flange joints for the nonlinear dynamic analysis of gas turbine engine casings. *Journal of Engineering for Gas Turbines and Power*, 134(12), 10 2012. 122504. 12

[94] C. W. Schwingshackl, E. P. Petrov, and D. J. Ewins. Effects of Contact Interface Parameters on Vibration of Turbine Bladed Disks With Underplatform Dampers. *Journal of Engineering for Gas Turbines and Power*, 134(3), 01 2012. 032507. 11

[95] A. V. Srinivasan. Flutter and Resonant Vibration Characteristics of Engine Blades. *Journal of Engineering for Gas Turbines and Power*, 119(4):742–775, 10 1997. 7

[96] Yuanqiu Tan, Chaoping Zang, and E.P. Petrov. Mistuning sensitivity and optimization for bladed disks using high-fidelity models. *Mechanical Systems and Signal Processing*, 124:502–523, 2019. 19

[97] N. A. Valero and O. O. Bendiksen. Vibration Characteristics of Mistuned Shrouded Blade Assemblies. *Journal of Engineering for Gas Turbines and Power*, 108(2):293–299, April 1986. 8

[98] B.P. Wang. Improved approximate methods for computing eigenvector derivatives in structural dynamics. *AIAA Journal*, 29(6):1018–1020, 1991. 16, 59, 60

[99] D. S. Whitehead. Effect of Mistuning on the Vibration of Turbo-Machine Blades Induced by Wakes. *Journal of Mechanical Engineering Science*, 8(1):15–21, March 1966. 2, 18

[100] B. Wu, Z. Xu, and Z. Li. A note on computing eigenvector derivatives with distinct and repeated eigenvalues. *Communications in Numerical Methods in Engineering*, 23(3):241–251, 2007. 17

[101] Yutaka Yamashita, Koki Shiohata, and Takeshi Kudo. Analysis of Vibration Characteristics for Last Stage Blade With Friction Contact Surfaces of Steam Turbine. In *Proceedings of the ASME Turbo Expo*, volume Volume 7: Dynamic Systems and Control; Mechatronics and Intelligent Machines, Parts A and B, pages 405–412, 11 2011. 11

[102] M.-T. Yang and J. H. Griffin. A Reduced-Order Model of Mistuning Using a Subset of Nominal System Modes . *Journal of Engineering for Gas Turbines and Power*, 123(4):893–900, 03 1999. 10

[103] Liu Zhong-sheng, Chen Su-huan, and Zhao You-qun. An accurate method for computing eigenvector derivatives for free-free structures. *Computers & Structures*, 52(6):1135 – 1143, 1994. 16

[104] Stefano Zucca, Christian Firrone, and Muzio Gola. Numerical assessment of friction damping at turbine blade root joints by simultaneous calculation of the static and dynamic contact loads. *Nonlinear Dynamics*, 67:1943–1955, 02 2012. 11